Exploring the Synthesis, Structure and Reactivity of a Series of Aluminium Amidinate Complexes

This thesis is submitted in partial fulfilment of the requirements for the Degree of Doctor of Philosophy (Chemistry)

Katie Hobson

Supervised by Professor Claire Carmalt and Dr Clare Bakewell

University College London
Department of Chemistry
October 2021

Declaration

I, Katie Hobson, confirm that the work presented in this thesis is my own. Where information has been derived from other sources, I confirm that this has been indicated in the thesis.

Abstract

The work presented in this thesis relates to the synthesis of sterically encumbered aluminium amidinate complexes and investigating their propensity to catalyse hydroboration reactions or form aluminium-aluminium multiple bonds.

The sterically encumbered 2,6-diphenylmethyl-4-methylphenyl substituent (referred to as Ar*) was employed to synthesise a range of symmetric and asymmetric amidine ligands which, upon complexation to aluminium reagents, yielded a series of aluminium hydride and alkyl amidinate complexes. These compounds were characterised spectroscopically and crystallographically, and any discrepancies between the solid- and solution-state properties have been accounted for.

The propensity of these compounds to catalyse the hydroboration of phenylacetylene using 4,4,5,5-Tetramethyl-1,2,3-dioxaborolane (HBpin) was investigated. The aluminium hydride complexes were found to be active catalysts for this reaction and the alkyl compounds were pre-catalysts. Rates of reaction varied across this series of compounds which can be tentatively linked to the steric encumbrance of the flanking aryl substituents. Where deviations from this trend were observed, they could be rationalised by assessment of the solution-state stability of the complexes. Detailed experimental investigations were conducted to elucidate the mechanism of action. Variation in the observed mechanistic pathways was observed across this seemingly-similar family of compounds, with these pathways being different to previous literature reports of aluminium-catalysed hydroboration reactions.

Finally, these compounds were explored for their viability as precursors to form aluminium-aluminium bonds. Aluminium amidinate and β-diketiminate dihydrides were reacted with a known aluminium(I) reagent to obtain a series of amidinateAl-Al-β-diketiminate and asymmetric β-diketiminateAl-Al-β-diketiminate dialumane complexes with varying steric encumbrance. Preliminary spectroscopic analyses are discussed, with ongoing investigations for complete characterisation and further reactivity.

Impact Statement

The work in this thesis contributes to the field of synthetic inorganic chemistry, with a specific focus on the development of more environmentally benign catalysts as the world strives to move away from precious metal systems. Aluminium was chosen as the target metal in this work, owing to its high Earth abundance, low cost, and low toxicity. Similarly, sustainable aluminium chemistry is currently undergoing a renaissance in interest and is hugely topical in the literature, with huge advances reported in the last five years alone.

Aluminium catalysis has been known since the 1800s, however their capacity to act as transition metal mimics was first realised in 2015. Boron-containing compounds are used as intermediates in many industrially relevant reactions, including in the synthesis of pharmaceuticals and carbon-carbon bond forming reactions. Thus, this work involves the catalytic formation of hydroboration products using a sustainable, Earth abundant metal with huge implications for both the environment and the chemical industry. Aluminium hydroboration catalysts are known, but the research detailed herein presents a new mechanistic pathway for this reaction with divergent reactivity observed across the series. Therefore, this research could advance the field of selective catalysis, by using simple synthetic manipulations to influence reaction outcome. In the chemical industry, greater reaction control can circumvent the formation of unwanted by-products, minimising waste and increasing profits. This would have an enormous, positive impact on the environment.

There are currently only a few reported examples of dialumane and dialumene compounds. This thesis adds to this family of compounds, with new insights into the formation of asymmetric complexes *via* the trapping of reaction intermediates.

Chemists from different disciplines have recognised the impact of this work, and it was awarded the Inorganic section prize for both best poster and best talk at the 2nd year poster and 3rd year talks symposia, respectively, hosted by the Department of Chemistry.

Acknowledgements

Firstly, I'd like to thank my supervisors Professor Claire Carmalt and Dr Clare Bakewell for their guidance and support over the last three years. Claire, for seeing the potential in me as an MSci student and providing me with this opportunity – it has been the best experience. Clare, for showing me what it means to be a great scientist, and for teaching me the importance of always working with integrity and respect. I'd also like to thank Dr Caroline Knapp for taking me under her wing and for always treating me as an equal member of her lab/group.

I'd like to thank Dr Abil Aliev for his assistance with all aspects of my NMR experiments and characterisation. Thanks also to Dr Jeremy Cockcroft for his training, assistance, and useful discussion in X-ray analysis techniques. Thank you to the technical staff who have helped me avert many crises: Tony Field, John Cowley and Tom Bridges.

Thank you to the past and present members of the Bakewell and Knapp groups. Malavika Bhide, Shreya Mrig, Sam Douglas and Kristian Mears – thank you for always being on hand to put out the next literal or metaphorical fire (depending on what kind of day we were all having!), with special thanks to Sam for lots of useful aluminium-based discussion. Kam, Martha and honorary lab 309 members Megan and Molly – your friendship is the best thing to come out of my time in the lab. Megan, lunchtimes without you won't be the same.

I'd like to give a special thank you to my friend Alex and my long-suffering flatmates Emily and Phoebe. You have all been on this wild journey with me and I'm grateful that you always celebrate my successes, commiserate my failures and (most importantly) entertain my gossip.

I'd like to thank my boyfriend Ed for his (endless) patience with me, and for keeping my ego in-check with the perfect balance of belief in my abilities and disbelief at my stupidity. Thank you for making me laugh every day. Finally, thank you to my mam for never doubting me, always believing that I can achieve anything I put my mind to and for always reminding me of this. This thesis is for you. Ed, mam – I love you both very much.

Contents

List of Figures, Schemes and Tables

Chapter 1

Chapter 2

Chapter 3

Chapter 4

Appendix

List of Abbreviations

{^{1}H}	Proton decoupled
Å	Angstrom
Ad	Adamantyl
Ae	Alkaline earth
Am	Amidinate
Anal.	Analysis
Ar§	2,6-diphenylmethyl-4-*iso*-propylphenyl
Ar*	2,6-dimethylphenyl-4-methylphenyl
Ar†	2,6-diphenylmethyl-4-*tert*-butylphenyl
Ave.	Average
BDI	β-diketiminate
br	broad (NMR)
cAAC	Cyclic(alkyl)(amino)carbene
Calc.	Calculated
COSY	COrrelated SpectroscopY
Cp*	1,2,3,5,4-Pentamethylcyclopentadiene
Cp$^{3t\mathrm{Bu}}$	1,3,5-Tri-*tert*-butylcyclopentadienyl
Cy	Cyclohexyl
d	deuterated
d	doublet (NMR)
DCM	Dichloromethane
dep	2,6-diethylphenyl
DFT	Density functional theory
dipp	2,6-Di-*iso*-propylphenyl
DMAP	4-Dimethylaminopyridine
DMS	Dimethylsulfide
FLP	Frustrated Lewis pair
HBpin	4,4,5,5-Tetramethyl-1,3,2-dioxaborolane
HMBC	Heteronuclear Multiple Bond Correlation
HOMO	Highest occupied molecular orbital
*i*Pr	isopropyl

IR	Infrared
J	Coupling constant
K	Kelvin
KHMDS	Potassium *bis*-trimethylsilyl amide
LUMO	Lowest unoccupied molecular orbital
m	multiplet (NMR)
MeLi	Methyllithium
mes	2,4,6-Trimethylphenyl
MHz	Megahertz
NBO	Natural Bond Orbital
NEt_3	Triethylamine
NHC	*N*-Heterocyclic carbene
NMR	Nuclear magnetic resonance
Ph	Phenyl
ppm	Parts per milliom
q	quartet (NMR)
QTAIM	Quantum Theory of Atoms in Molecules
rac	Racemic
ROP	Ring opening polymerisation
SCXRD	Single crystal X-ray diffraction
sept	septet (NMR)
t	triplet (NMR)
^{t}Bu	*tert*-butyl
TMAA	Trimethylamine alane
TMEDA	*N,N,N',N'*-Tetramethylethylenediamine
VSEPR	Valence shell electron pair repulsion
VT	Variable temperature
WBI	Wiberg Bond Index
ΔE_{S-T}	Singlet-triplet energy gap
δ	Chemical shift

Publications

This thesis has resulted in the following publications:

1. *Recent advances in low oxidation state aluminium chemistry*
   Katie Hobson, Claire J. Carmalt and Clare Bakewell*
   Chemical Science, 2020, **11**, 6942

2. *Aluminum amidinates: new insights into alkyne hydroboration*
   Katie Hobson, Claire J. Carmalt* and Clare Bakewell*
   Inorganic Chemistry, 2021, **60**, 10958

Chapter 1:

Introduction

1.1 Catalysis in a 21st Century World

To give an elementary definition, catalysts are classified as anything that increases the rate of a chemical reaction without itself being consumed, generally by providing an alternative reaction pathway. Catalytic reactions can be homogenous or heterogenous and from a practical standpoint (e.g., energy input, reaction time) many reactions either do not proceed or are not economically viable in the absence of a catalyst. It is currently estimated that more than 90% of industrial chemical processes employ the use of catalysts, ranging from fine chemical to bulk commodity synthesis, as well as plastics production and in the automotive industry. Thus, catalysts and catalytic processes form an essential part of modern life and have undoubtedly facilitated many chemical and industrial advancements over the last century.[1]

1.2 Transition Metal Catalysis

Transition metal catalysts are the most extensively researched and developed family of catalysts.[2] They are employed in a vast range of industrial chemical processes with select examples including iron-catalysed ammonia production (Haber process), nickel-catalysed synthesis gas production ("syngas", CO_2/H_2), and palladium-catalysed cross-coupling reactions, used in carbon-carbon and carbon-heteroatom bond forming reactions.[3–5] Transition metals have closely spaced d-orbitals that are partially occupied and their propensity to break strong σ-bonds is attributed to the small energy gap between these orbitals, which allows for facile access to a range of variable oxidation states at the metal centre through the acceptance and back-donation of electron density. Mechanistically, transition metal catalysis is dominated by oxidative addition and reductive elimination processes, and these will be described herein using the palladium-catalysed Suzuki reaction as a representative example (**Figure 1.1**). In a Suzuki reaction, the cross-coupling partners are a boronic acid and an organohalide and in this instance have been used to form a carbon-carbon bond.[6] Palladium(0) metal has the electronic configuration $[Kr]4d^{10}$ and whilst this formally does not warrant transition metal classification (instead this is classified as a d-block element) it still proceeds *via* the same mechanism as formally classified transition metals. The first step in mid-late transition metal-catalysed processes is oxidative addition, whereby two anionic ligands are transferred to a metal centre with concomitant increase in both oxidation state and electron count at the metal centre. This process requires a vacant coordination site at the metal centre and occurs *via* the transfer of electrons from the metal centre to the σ* orbital of the substrate, resulting in the breaking of the σ-bond and the formation of two new metal-ligand bonds. Oxidation state and valence

electron counts increase by 2 during this process, but single electron transfer processes are known and are favoured by first row transition metals.[7] In the example shown in **Figure 1.1**, the alkyl halide R-X (R = alkyl, X = halogen) is added across the palladium(0) centre to form palladium(II), with the electronic configuration [Kr]4d^8. Mechanistically, oxidative addition processes can proceed *via* two different pathways: asynchronous concerted addition or S_N2-type stepwise addition, with the latter mechanism likely to be favoured by a polarised alkyl halide. The second step in the Suzuki reaction is transmetallation, though this is not a feature of all catalytic processes. This involves the transfer (or 'switching') of ligands at the transition metal centre with no change in oxidation state, and in this example is demonstrated by the substitution of halide 'X' for the alkyl species R_1 facilitated by the use of a generic base. The final step in the catalytic cycle is reductive elimination. This is the microscopic reverse of oxidative addition, whereby a product is liberated from the catalyst *via* the formation of a covalent bond and the oxidation state and coordination number at the metal centre decrease (again, this is generally by two). In this example, palladium returns to its original zero oxidation state from palladium(II).[8,9]

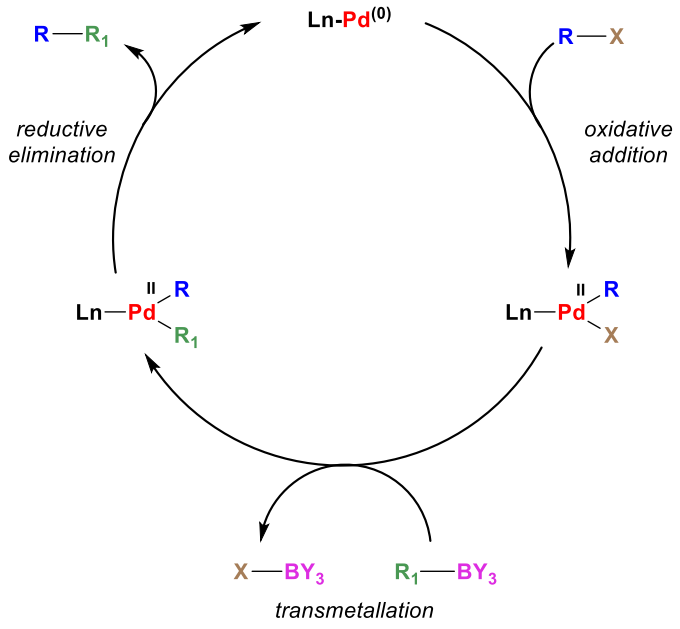

Figure 1.1: Palladium-catalysed Suzuki reaction.

Palladium-catalysed cross coupling reactions have transformed many areas of synthetic chemistry and catalysis in the decades since their discovery. This was proven when, in 2010, Richard Heck, Ei-ichi Negishi and Akira Suzuki were jointly awarded the Nobel Prize for their

respective contributions to this field.[10] Similarly, Nobel Prizes for transition metal catalysis were also awarded in 2001 and 2005, for the discoveries of ruthenium-/osmium-catalysed asymmetric hydrogenation/oxidation reactions and ruthenium-/molybdenum-catalysed olefin metathesis reactions, respectively.[7] However, these landmark discoveries come at a cost.

1.3 Sustainable Chemistry

Many elements in the periodic table are classified as 'precious metals', so called owing to their high economic value and their inherent scarcity in the Earth's crust.[11] Palladium, ruthenium and osmium are all examples of precious metals, with additional examples including platinum, iridium, silver and gold. This has significant ramifications for their cost and supply. For example, demand for palladium has exceeded supply since 2012, resulting in significant price increases and a diminishing finite supply. In 2019, Bloomberg published that palladium is the most expensive of the precious metals, and further reports by the Royal Society of Chemistry highlighted an additional six elements (silver, gallium, ytrrium, indium, arsenic and tantalum) whose global supply is expected to diminish over the next century.[12,13] As part of the International Year of the Periodic Table (2019), the European Chemical Society produced the 'Periodic Table of Scarcity' (**Figure 1.2**)*. The focus of this was to highlight the scarcity of specific elements used in technological devices, but otherwise provides a striking visual aid for the diminishing supply of many elements used in industrially relevant catalytic processes.

As scientific and technological discoveries advance in conjunction with a growing global population, the demand for the Earth's natural resources has never been greater. European and American countries rely on imports of these precious metals, which are often mined in regions of geopolitical instability and can lead to disruption in regular supply chains. Mining and refinement of lower-grade metal ores is one possible solution, but this requires an increase in fossil fuel consumption and CO_2 production. Therefore, alternative mining sources or reaction pathways must be developed if twenty-first century living standards are to be maintained, with a specific focus on minimising the impact on the environment.

* Figure obtained from the European Chemical Society, https://www.euchems.eu/euchems-periodic-table/, accessed 21st September 2021.

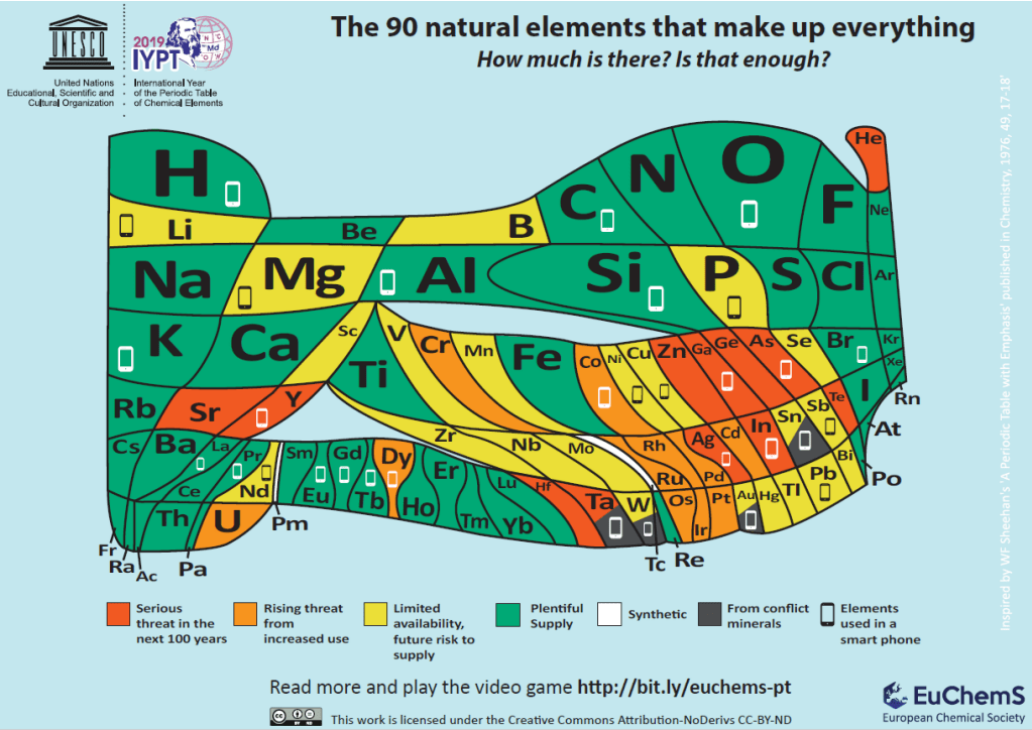

Figure 1.2: Periodic Table of Scarcity produced by the European Chemical Society.

Upon visual inspection of **Figure 1.2**, the high Earth abundance of many main group elements contrasts starkly to their transition metal counterparts. Similarly, their low cost and often low toxicity makes many main group elements attractive targets to focus on the development of more environmentally benign catalysts. The next sections of this chapter will focus on developments specifically pertaining to main group complexes with transition metal-like properties, followed by a summary of main group catalysis.

1.4 Main Group Elements as Transition Metals

1.4.1 Introduction

If main group compounds are to exhibit the same rich chemistry (and catalysis) as transition metals several key challenges must be addressed. Firstly, stable main group complexes with low oxidation states and open coordination sites must be targeted. These must also be able to react with small molecules, and be able to liberate a functionalised product with concomitant regeneration of the active catalyst.[14] Archaic orbital descriptions incorrectly stated that both light (boron, carbon, nitrogen and oxygen) and heavy (heavy in this instance refers to all elements after fluorine) main group elements exhibit the same bonding properties. Their

bonding profiles were said to be comprised of either fully occupied or fully empty s- or p-orbitals, with a large energy gap between the highest occupied molecular orbital (HOMO) and lowest unoccupied molecular orbital (LUMO). This formed the basis of the so-called double bond rule, which stated that elements with a principal quantum number greater than 2 for their valence electrons (aluminium onwards) tend not to form multiple bonds with themselves or other elements.[15] Thus, this description, the large (>4 eV) HOMO-LUMO gap and the absence of any main group compounds with open coordination sites suggests that this precludes their use as compounds that exhibit transition metal-like redox properties.

Key developments in the late 1970s and early 1980s disproved this double bond rule, with the synthesis and characterisation of the first examples of compounds containing Si=Si and P=P double bonds, reported by West and Yoshifuji, respectively (**1A** and **1B**, **Figure 1.3**).[16,17] The isolation of these compounds was facilitated by the use of sterically encumbered supporting ligands, which 'shield' the metal centre and prevent the oligomerisation or polymerisation of the heavier element multiple bonded species, as well as preventing attack by nucleophiles or electrophiles.[18] Huge advances have been made in this field, and many low oxidation state compounds (both mononuclear and dinuclear) are now commonplace in the literature. Select examples of these compounds from across the periodic table are shown in **Figure 1.4**.[19–23]

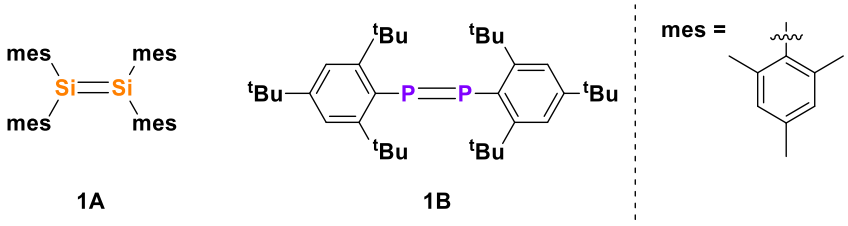

Figure 1.3: The structure of the first compounds containing Si=Si and P=P multiple bonds.

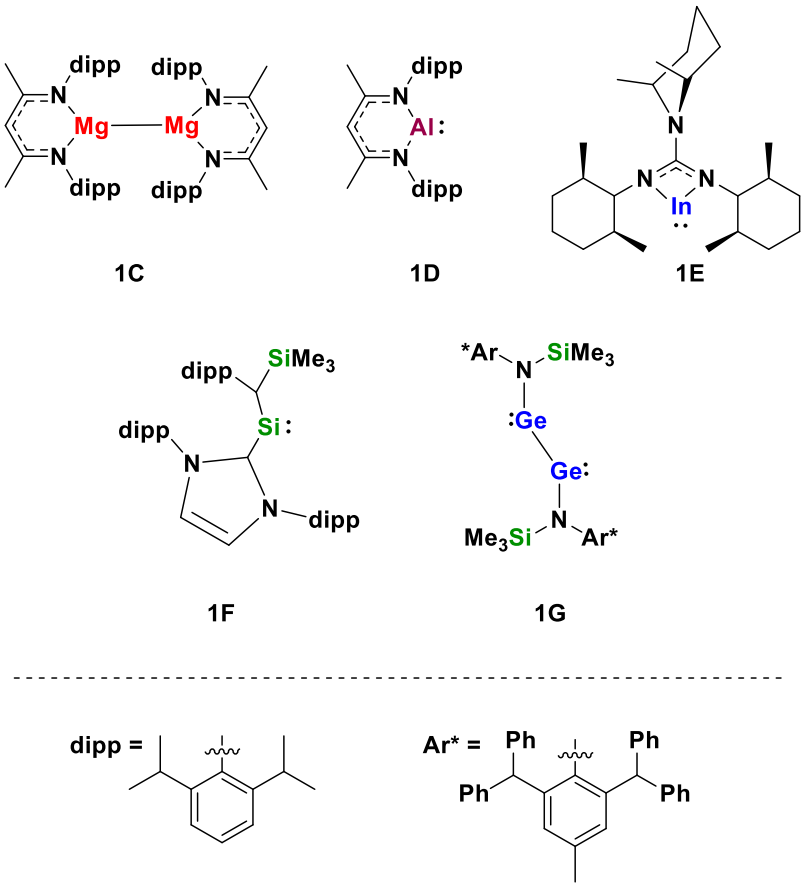

Figure 1.4: Representative examples of low oxidation state and multiple bonded main group compounds.

Considering the isolation of **1A** and **1B**, the initial bonding description of heavier main group elements is no longer applicable to these systems and therefore must be updated. The Si=Si double bond of **1A** was ~2.16 Å, with an almost planar core and it was structurally analogous to ethylene. Descending the periodic table, the increase in covalent radii (C, 0.77 Å; Si, 1.17 Å) results in double bond character that does not match the conventional σ- and π-bond description of a carbon-carbon double bond. Instead, this is best described as two non-bonded lone pairs, comprised of one metal centre with an electron pair (donor) and one electron deficient metal centre. This results in the simultaneous existence of both electron richness and partial unsaturation at each metal centre and is attributed to incomplete electron sharing in the multiple bond.[15,24] Similarly, the formation of σ-bonds is favoured over π-bonds in heavier main group compounds, as reduced orbital overlap results in a weaker bond overall (with an expected increase in reactivity of these compounds).[25] To that effect, the bonding profile in heavier main group elements can be more closely compared to transition metals rather than the

lighter main group congeners, owing to the fact they possess frontier molecular orbitals with small energy separations

1.4.2 Small Molecule Activation at Low Oxidation State Main Group Compounds

In the decades since the realisation that the double bond rule could be broken, the boundaries of main group chemistry have been continually redefined.[26] Now, multiple bonds for most of the p-block have been isolated, including homodiatomic triple bonds for all of group 14 (select examples **1H**-**1M**, **Figure 1.5**).[27–30]

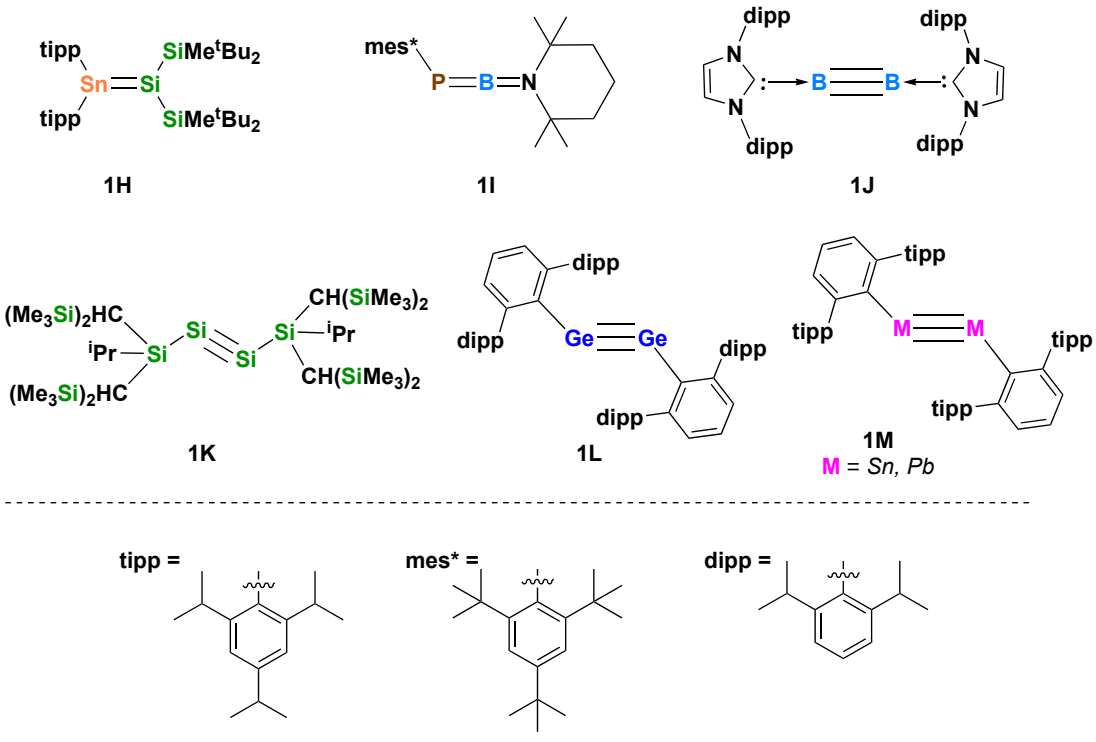

Figure 1.5: Multiple bonds and group 14 homodiatomic triple bonds.

Single crystal X-ray analysis of the group 14 ‘alkyne’ compounds revealed that they adopt *trans*-bent planar geometries (unlike the linear structures of alkynes) with distortion increasing down the group, but otherwise exhibit similar structural properties to alkynes. This distortion was attributed to an increased degree of non-bonded electron localisation at one metal centre with concomitant electron deficiency at the second metal centre, owing to the incomplete

electron sharing of the metal-metal bond. Described in terms of molecular orbital theory, this is a second order Jahn-Teller effect. Second order Jahn-Teller effects arise from the intramolecular mixing of unoccupied non-bonding or anti-bonding orbitals with the HOMO, resulting in the formation of non-bonding, lone pair character in the HOMO and a distortion in the geometry of the molecule.[15,27]

With examples of main group multiple bonded species now commonplace in the literature, research efforts have focussed on investigating their propensity to cleave strong σ-bonds and exhibit transition metal-like properties. Oxidative addition and reductive elimination are key steps in transition metal catalysis (section 1.2), with the simplest example of an oxidative addition reaction involving the addition of dihydrogen across a metal centre. The first example of main group activation of H_2 was reported by Power and co-workers in 2005, when the "digermyne" compound **1L** (**Figure 1.5**) was shown to react with hydrogen under ambient conditions.[31] The reaction produced a mixture of the corresponding hydrogenated germane and digermane products, and the ratios in which they formed were dependent on the stoichiometry of hydrogen. Mechanistically, the initial step of this reaction was calculated to proceed *via* the synergic interaction of the hydrogen and germanium orbitals. Electrons were donated from the σ-orbital of dihydrogen into the LUMO of **1L** (a symmetric n_+ non-bonding combination) with concomitant electron donation from the π-HOMO of **1L** into the σ* orbital of dihydrogen (**Figure 1.6**). The H-H bond was cleaved and added across the metal centres in a formal oxidative addition process, mechanistically similar to transition metal oxidative addition processes.[31]

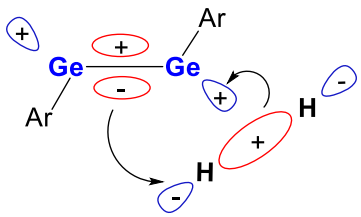

Figure 1.6: Initial interaction of dihydrogen with the frontier orbitals of digermyne **1L**.

Many main group compounds are now known to cleave dihydrogen σ-bonds. For example, the cyclic (alkyl)(amino) carbene (cAAC)-supported diboracumulene compound **1N** was found to activate dihydrogen and yield the 1,2-dihydroborene **1O** (**Scheme 1.1**) and probing the mechanism *via* DFT calculations revealed an overall exothermic process (-20.6 kcal mol^{-1}).

Mechanistically this was said to proceed *via* the binding of H_2 to a vacant p-orbital at one of the boron centres, the formation of a hydride-bridged intermediate and then rearrangement to form **1O**.[32] Select examples of the mechanisms of σ-bond cleavage will be described to give an overview of oxidative addition at main group metal centres.

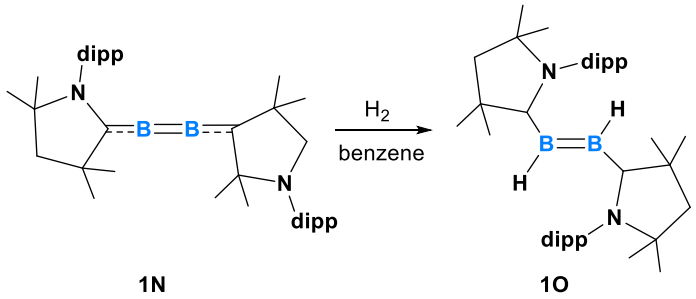

Scheme 1.1: Activation of dihydrogen using **1N**.

The β-diketiminate (BDI) aluminium(I) reagent **1D** (**Figure 1.4**, see Chapter 4 for further discussion) was shown to activate a range of H-X bonds, where X = H, Si, C, B, or N. For example, addition of dihydrogen across the aluminium centre yielded the aluminium dihydride [AlH_2(^{dipp}BDI)], and further investigations using $PhSiH_3$, Cp*H (Cp* = pentamethylcyclopentadiene), pinacolborane (HBpin) or H_2NPh all cleanly formed the products of formal oxidative addition at the aluminium(I) centre. Compound **1D** is isoelectronic to carbenes, and as such features an aluminium-based lone pair with an energetically accessible 3p orbital. These features mirror the reactivity at transition metal centres and thus can account for the facile oxidative addition of strong H-heteroatom bonds.[33]

Similarly, precedent for the activation of O-H bonds was demonstrated by the catalytic reaction of the diaryl germylene (aryl = terphenyl) **1P** with water or methanol at room temperature to yield **1Q** (R = H or Me, **Scheme 1.2**). Mechanistically, the oxygen lone pair was donated into the vacant p-orbital of the germanium centre, while a second molecule of water/methanol solvated the complexed substrate *via* an intermolecular O-H--O interaction.[34] This same mechanism was also said to be in operation for the N-H bond activation of ammonia at **1P**.[35]

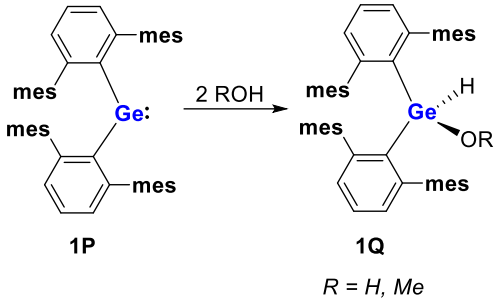

Scheme 1.2: Activation of O-H bonds with **1P**.

Further examples of bond activation at main group metal centres include the breaking of C-X bonds, where X = F, Cl, Br and I. In 2007, Jones *et al.* reported the synthesis of the stable magnesium(I) dimer **1C** (**Figure 1.4**), with a three-coordinate metal centre and a magnesium-magnesium covalent bond (2.060 Å) with high s-character. The HOMO and LUMO/LUMO+1 were the metal-metal σ-bonding and metal-metal π-bonding orbitals, respectively. At the time of publication, the use of **1C** as a reducing agent was predicted.[19] One such example of this includes the remarkable addition of C-F bonds from polyfluorinated arenes across the Mg-Mg bond of **1C** and through a series of experimental investigations, a mechanism involving the formation of a radical intermediate was ruled out. Thus, this process was described as a concerted 2-electron reduction of the C-F bond by **1C**, whose reactivity was akin to a magnesium Grignard reagent.[36] Later work also expanded the substrate scope of C-F bond activation to include primary and secondary C(sp^3)-F bonds using the aluminium reagent **1D**.[37,38]

These examples highlight a fraction of the oxidative addition processes that are now known at main group metal centres and includes a discussion of their different mechanisms of action. These examples are not exhaustive, and further examples of oxidative addition at main group centres include E-H (E = Al, Si, Ge, Sn, P, As), C-X (X = Cl, Br, I), and C-O bond activation.[39–41] Finally, it is not just single-bonded diatomic molecules that can undergo oxidative addition at main group centres. Cleavage of C=O, C=N, and C=S bonds is also known, as well as oxidative addition of alkenes, alkynes, CO_2, NO_2, and CS_2 (this list is not exhaustive).[42–44] Oxidative addition processes at main group centres are highly thermodynamically favourable, owing to the resultant increase in oxidation state at the metal centre and the high stability of the products formed. Many review articles have been written on this subject, with the most comprehensive in recent years written by Nikonov *et al.*[42] Chapter 4 will highlight the specific

advances in low oxidation state aluminium chemistry, whilst the next section will describe the progress made in reductive elimination at main group centres.

1.4.3 Reductive Elimination at Main Group Centres

With oxidative addition at main group metal centres firmly established, reductive elimination reactions must also be explored if main group metals are to exhibit like-for-like transition metal reactivity. This process is facile in transition metal compounds as their partially filled valence orbitals can both accept and release electrons throughout the catalytic cycle but is more challenging for main group metals. Whilst the challenges in isolating low oxidation state main group compounds can be circumvented by using sterically encumbered or stabilising ligands, the need for harsh reducing agents, vacant orbitals, and the aforementioned stability of oxidative addition products often precludes reductive elimination processes at main group metal centres, however, developments in this area have been made.[42] The first example of reductive elimination at aluminium was reported by Fischer *et al.* by showing that Cp^*_2AlH eliminates Cp*H and 0.25 equivalents of the tetramer $(Cp^*Al)_4$.[45] The mechanism of reductive elimination was later probed by Cowley and co-workers, who found the overall process to be endothermic, and that increasing the coordination number and electron density (through the use of strong σ-donors) at the aluminium centre prevented reductive elimination *via* stabilisation of the higher oxidation state centre.[46] Further examples of reductive elimination at aluminium centres are discussed in Chapter 4.

The organotin trihydride compound **1R** underwent dihydrogen elimination *via* a formal reductive elimination process in the presence of a catalytic amount of 4-dimethylaminopyridine (DMAP) to yield the distannane species **1S** (**Scheme 1.3a**). Mechanistic calculations revealed this pathway to proceed *via* the stepwise deprotonation of **1R** using DMAP, and the resultant ammonium salt undergoes hydride abstraction to liberate **1S** (+15.8 kcal mol^{-1}).[47] The dipp-substituted analogue of distannyne **1M** (**Figure 1.5**) was shown to react reversibly with ethylene under ambient conditions (toluene, 298 K); exposure of **1M**-*dipp* to two equivalents of ethylene yielded the resultant distannacyclobutane **1T** (**Scheme 1.3b**). The *cis* arrangement of the aryl-substituents in the solid-state induced considerable strain at the tin centres and resulted in the formation of weak carbon-tin bonds and, as such, ethylene was found to reversibly dissociate from **1T** under reduced pressure.[48] In group 15, pincer-supported antimony and bismuth dichlorides **1U** undergo reductive elimination in the presence of

K[HB(^{i}Bu)$_3$] to yield the monomeric antimony(I) and bismuth(I) compounds **1V** (**Scheme 1.3c**). This was driven by the formation of hydrogen gas (KCl and B^{i}Bu$_3$ by-products also form) liberated from an unstable MH_2 intermediate.[49]

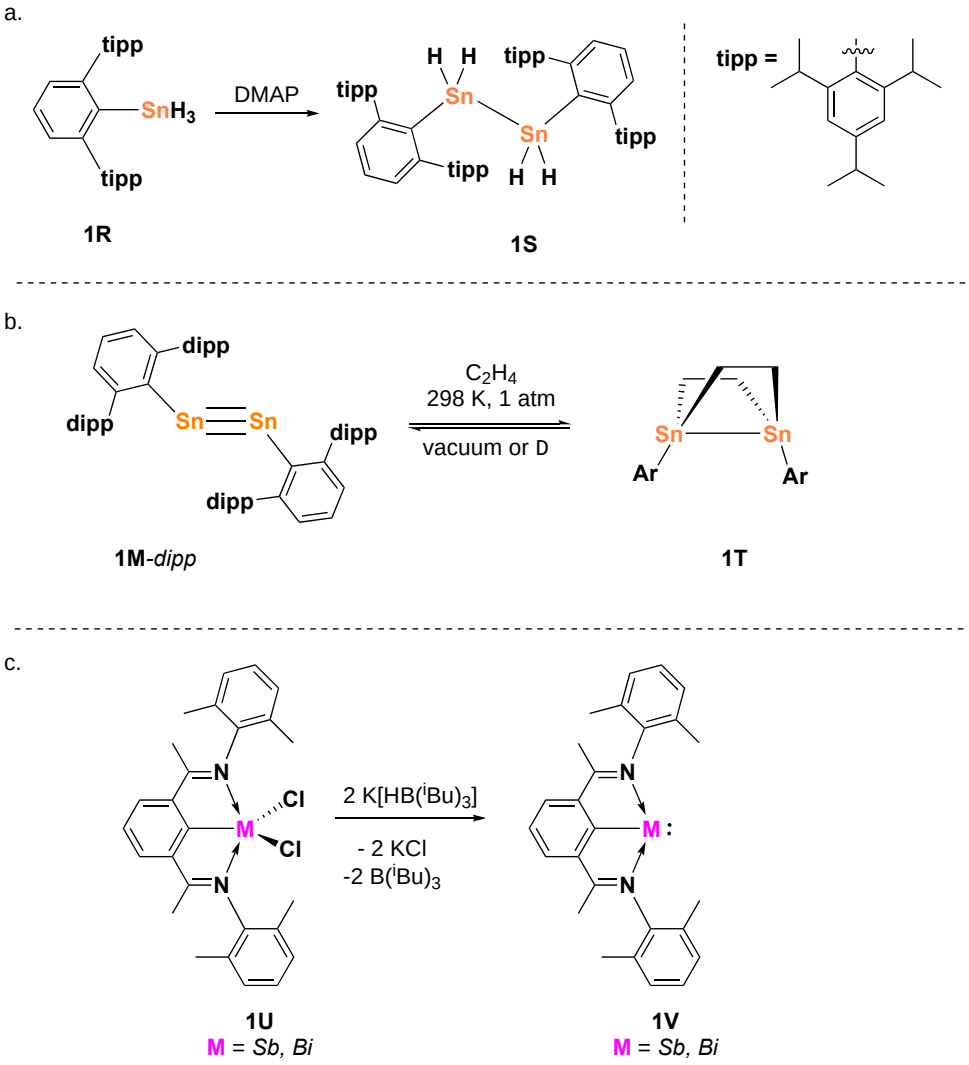

Scheme 1.3: Reductive elimination of hydrogen from **1R**, reversible binding of ethylene from **1T** and reductive elimination of chlorine from **1U**.

To return to the criteria required for main group catalysts to behave analogously to transition metals (section 1.4.1: isolation of stable low oxidation state compounds with vacant coordination sites that can undergo oxidative addition and reductive elimination) examples of all of these compounds or processes are now known. This is a remarkable feat considering the early literature that once deemed these complexes 'impossible' to synthesise. Each step involves significant challenges, but reductive elimination still remains the greatest challenge. The examples of known reductive elimination processes generally involve weak bonds (e.g. C-

Al, Bi-C), but with a field still in its infancy, and the impressive breadth of chemistry discovered in recent years, the future of main group redox processes looks bright.

1.5 Main Group Catalysed Reactions

To date, there are only two examples of main group catalysed reactions that are mechanistically identical to transition metal catalysts, owing to the difficulties in facilitating reductive elimination in main group compounds.[50] The first example involves the use of the digermyne (germanium-germanium triple bond) catalyst **1W** (**Figure 1.7**) for the cyclotrimerisation of terminal alkynes. This was facilitated by the *trans*-bent geometry of this structure, which induced a low-lying LUMO with the in plane π* orbital, as well as the simultaneous σ-/π-donation and π-back-donation from the carbon-carbon triple bond.[51] The second example involved the use of **1X** as a catalyst for the reduction of carbon dioxide and the syntheses of these compounds from a low oxidation state aluminium species are discussed further in Chapter 4 (section 4.1.5.2). Combined computational and experimental investigations were used to elucidate the mechanism of action. This was said to proceed *via* the initial coordination of HBpin to the exocylic carbonate oxygen of **1X**, followed by an endergonic hydride step (rate determining step) which was energetically offset by the formation of the reduced carbonate species. Coordination of CO_2 facilitated the reformation of **1X** and liberation of the CO_2 reduction product (**Figure 1.8**). Compound **1X'** was also catalytically active towards this reaction and it was found that substitution of the $SiMe^tBu_2$ group for the bulkier 'tipp' group (tipp = 1,3,5-tri-*iso*-propylphenyl) invoked increased reactivity into the metal centre. As such, the reduction of CO_2 with **1X'** produced a complex mixture of products and the ratios in which they formed varied with temperature.

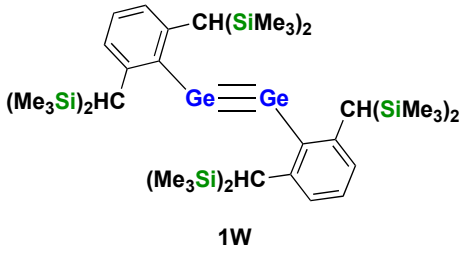

1W

Figure 1.7: Digermyne catalyst **1W**.

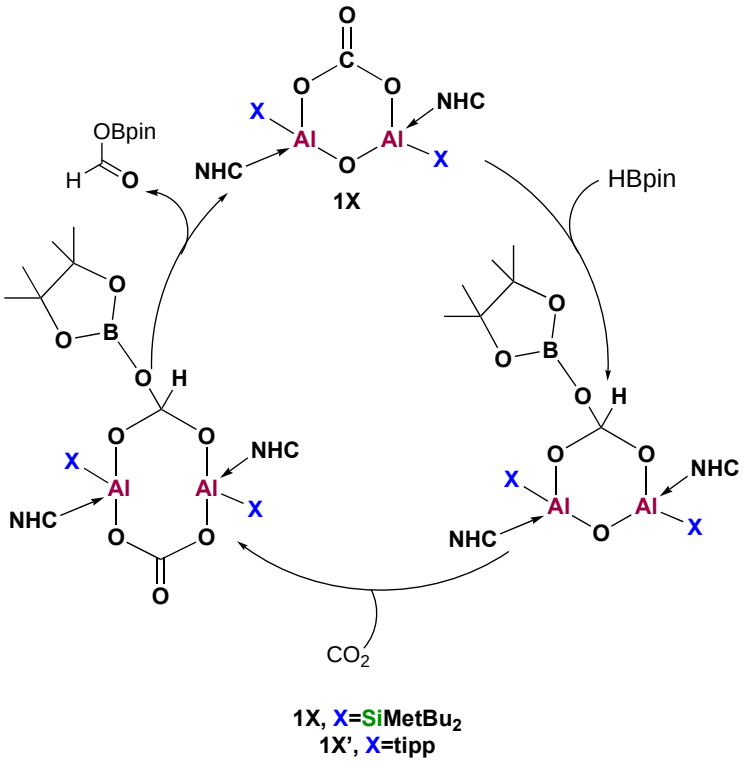

Figure 1.8: Catalytic hydroboration of CO_2 using with **1X**.

Despite the difficulties in mimicking like-for-like transition metal reactivity, main group catalysis has flourished in recent years. A comprehensive review by Hill and co-workers on the use of alkaline earth compounds as catalysts described the lanthanide analogy of Ae^{2+} (Ae = alkaline earth) compounds.[52] Trivalent lanthanide complexes in the +3 oxidation state are redox inactive but exhibit catalytic activity through a series of σ-bond metathesis and polarised insertion reactions which negate the need for a formal change in oxidation state.[53] These reactions involve E-H bonds, where H can be protic (E = N, O, P, S) or hydridic (E = B, Si, Al) and this mode of reactivity extends across the main group (**Figure 1.9**).[52]

The σ-bond metathesis and polarised insertion reactions in **Figure 1.9** can be combined to form catalytic cycles which differ based on the polarity of the E-H bonds. For example, M-E bonds form *via* the protonolysis of protic E-H bonds and undergo polarised insertion reactions with unsaturated molecules. These react with a further equivalent of the E-H substrate to form the anti-Markovnikov product and an additional M-E fragment. Conversely, hydridic E-H bonds form M-H bonds *via* σ-bond metathesis reactions which were active towards insertion into the unsaturated bond. This further reacts with the E-H fragment (σ-bond metathesis) to yield the

Markovnikov addition product and a further equivalent of M-H. This divergent reactivity is summarised in **Figure 1.10**.[52]

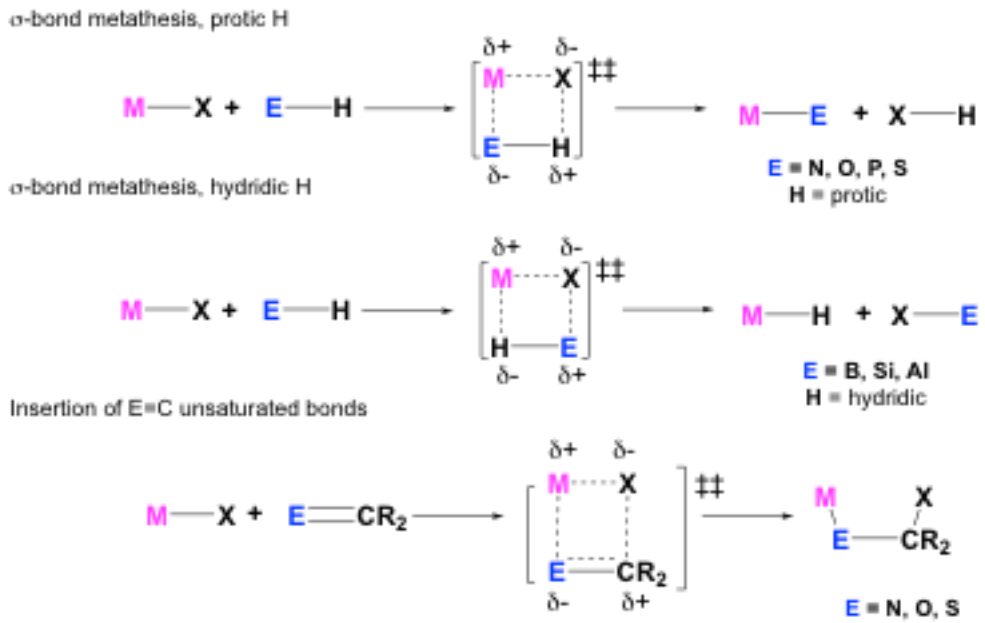

Figure 1.9: Schematic representation of σ-bond metathesis and polarised insertion reactions at main group metal centres.

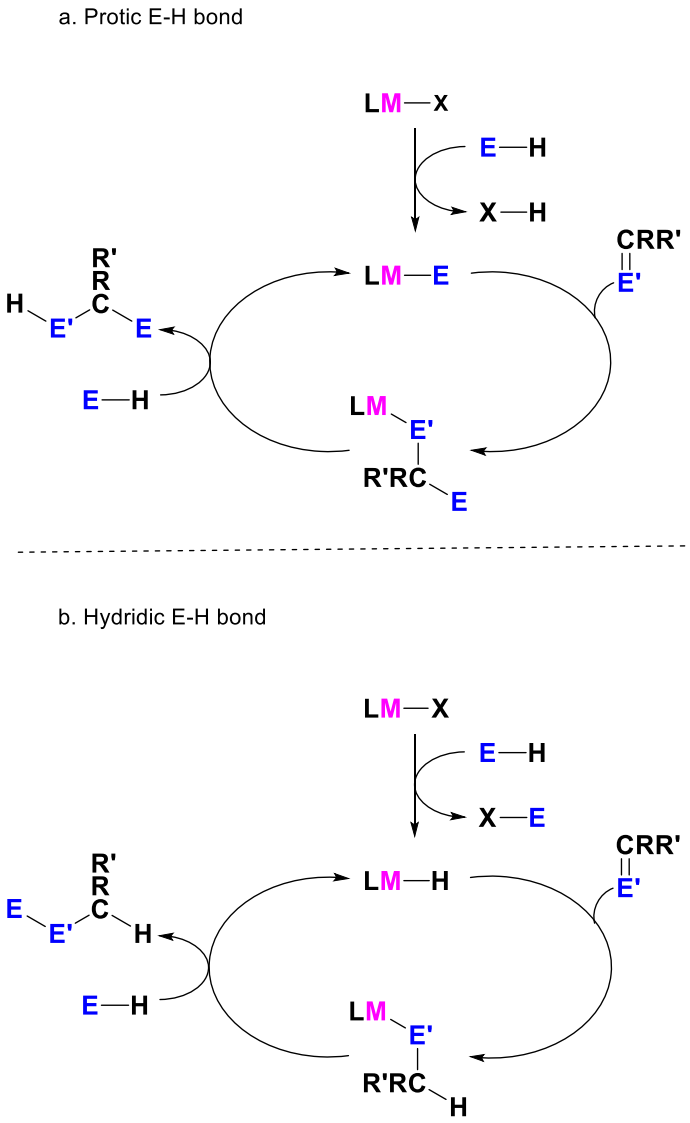

Figure 1.10: Catalytic cycles summarising σ-bond metathesis and polarised insertion reactions for protic and hydridic E-H bonds with an unsaturated substrate.

Examples of many synthetically useful transformations (hydroamination, hydroboration, hydrosilylation) including enantioselective reactions (e.g. Mannich reaction, 1,4-addition reactions), catalysed by main group compounds are now widely known.[54] The first reported example of a group 2 metal-catalysed reaction was reported by Hill and co-workers in 2005, when **1Y** (**Figure 1.11**) was found to catalyse the intramolecular hydroamination of aminoalkenes and alkynes under ambient conditions. The reaction of **1Y** with 1-aminohex-4-ene yielded the cyclisation product **1Z** in 30 minutes and was formed in accordance with

Baldwin's rules.† The initial step in the catalytic cycle involved the formation of a four-membered transition state (and liberation of $HN(SiMe_3)_2$) *via* a polarised insertion reaction (rate determining step) followed by ring closure and resultant regeneration of **1Y** (**Figure 1.11**)[55] Group 13 hydroamination catalysts are also known, for example the gallium catalyst **1AA** (**Figure 1.11**) was reported for the intermolecular hydroamination of terminal alkynes, whilst $[Al(NMe_2)_3]_2$ was shown to catalyse the synthesis of guanidine ligands *via* the hydroamination of the parent aluminium guanidinate complex.[56,57]

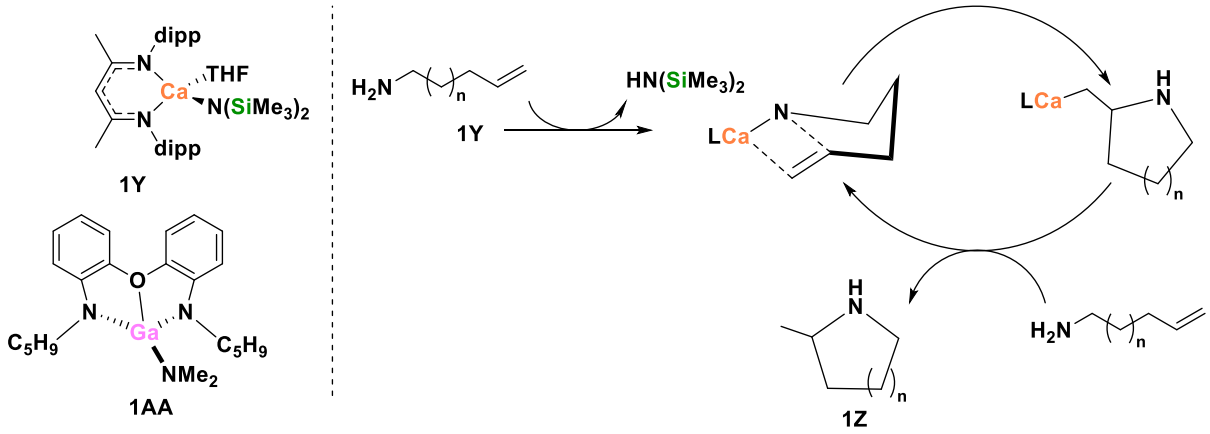

Figure 1.11: Catalysts **1Y** and **1AA**, and the catalytic cycle for the hydroamination of alkynes using catalyst **1Z**.

Hydroboration (addition of B-H bonds across a saturated system) catalysts are again known from across the main group and are active towards a broad range of substrates including alkenes, alkynes, nitriles, and carbonyls.[58] A range of structurally diverse catalysts (**1AB-1AD**, **Figure 1.12**), including the metal-free catalyst **1AD**, were found to catalyse the hydroboration of carbonyl compounds. Independent mechanistic analyses revealed these reactions to proceed *via* the same initial step, with insertion of the metal hydrides into the C=O carbonyl bond to form the resultant alkoxide. A generic cycle is shown in **Figure 1.13**. The alkoxide species then undergoes σ-bond metathesis with the boron-containing substrate (for example, pinacolborane) *via* the formation of a four-membered transition state and this was calculated to be the rate determining step.[59–61]

† Baldwin's rules predict the outcome of ring closure reactions which are governed by the size of the ring and the hybridisation of the orbitals involved.

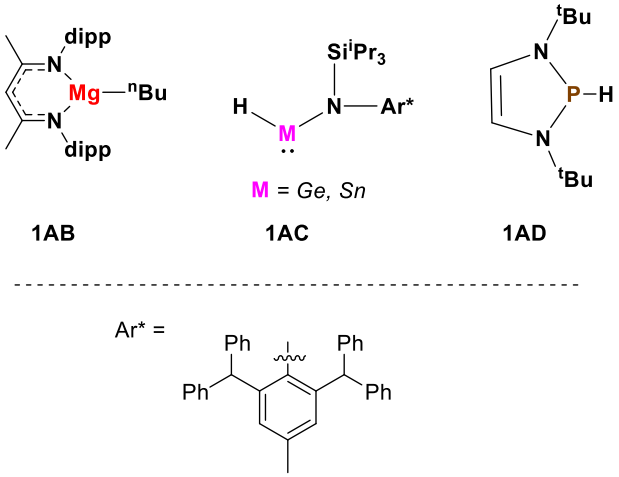

Figure 1.12: Structure of catalysts **1AB**-**1AD**.

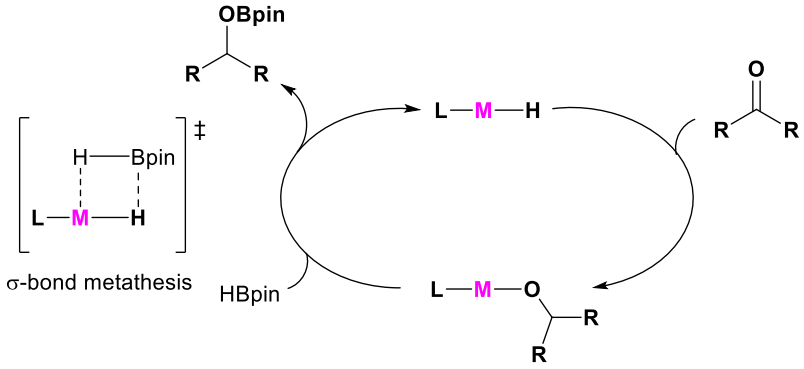

Figure 1.13: Generic catalytic cycle to show the hydroboration of carbonyl compounds.

In addition to hydroamination and hydroboration reactions, main group-catalysed hydrosilyation, hydrophosphination and hydroalkoxylation reactions are also known. These reactions all proceed *via* the σ-bond metathesis and polarised insertion pathways described herein (*vide supra*) and thus further mechanistic details will not be described. Main group catalysed dehydrocoupling reactions have also been reported and proceed *via* the same mechanistic pathways; these reactions involve the elimination of hydrogen from E-H bonds to yield the resultant element-element bonded species, such as B-N, B-P, Si-O, and Si-C bonds. These mechanisms broadly follow two main pathways and are either catalysed by Lewis acids or basic s- and p-block elements.[62] For example, the aluminium hydride catalyst **1AE** (**Figure 1.14)** was reported as a catalyst for the reaction of the dehydrocoupling of boranes with amines,

phenols and thiols, with the dehydrocoupling reaction of *p*-fluorophenol with HBpin described as a representative example. Mechanistically this proceeded *via* consecutive σ-bond metathesis reactions where each Al-H bond was added across the O-H bond of two molecules of *p*-fluorophenol, followed by the cycloaddition of the H-B bond of HBpin to yield a four-membered Al-O-B-H ring as an intermediate. The final step in the cycle involves the simultaneous hydride transfer to aluminium and cleavage of the Al-O bond to yield the dehydrocoupling product **1AF** and regeneration of the aluminium catalyst (**Figure 1.14**).[63]

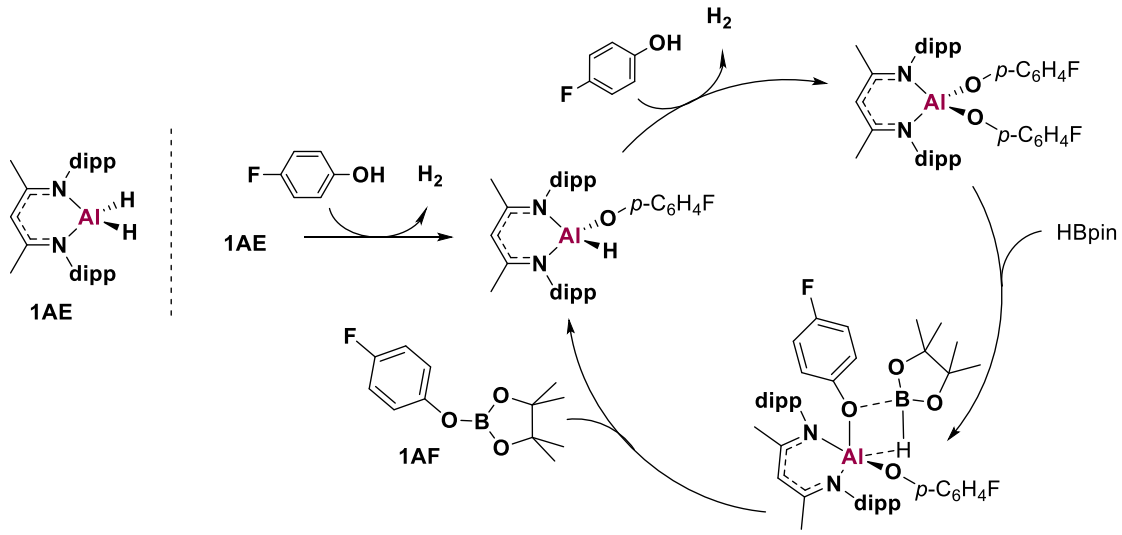

Figure 1.14: Catalyst **1AE** and the mechanism of dehydrocoupling.

The final class of main group catalyst to be discussed herein are frustrated Lewis pairs (FLPs) which contain both Lewis acidic and Lewis basic components with sufficiently bulky supporting ligands to prevent the formation of a class Lewis acid-base adduct. Thus, these compounds work synergistically to exploit the known Lewis acidic/basic properties of group 13 and 15 elements, respectively. In 2006, Stephan and co-workers reported the reversible activation of dihydrogen using the metal-free FLP **1AG** with the related structures **1AH** and **1AI** reported soon after (**Figure 1.15**).[64–66] By inhibiting the formation of the acid-base adduct the individual components can accept and donate electron density, respectively, and thus in this example, cleave the dihydrogen σ-bond. Since then, the breadth of FLP chemistry has expanded drastically, and examples of metal-free catalysts are now known for C=C, C=N and C-O hydrogenation reactions, as well as for examples of small molecule activation (CO_2, PR_3).[67,68]

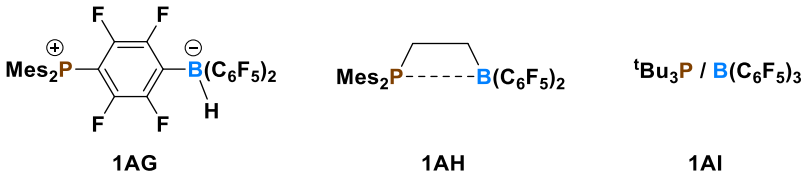

Figure 1.15: Early frustrated Lewis pair catalysts **1AG-1AI**.

Whilst a general introduction to main group catalysis has been given, the work in this thesis exclusively explores the use of aluminium compounds as hydroboration catalysts and for the synthesis of new low oxidation state aluminium compounds. As such, a brief discussion of aluminium chemistry is included, with more detailed introductions given within each chapter.

1.6 Aluminium Chemistry

Aluminium is the most abundant metal in the Earth's crust (8.1%) and is most commonly extracted from bauxite or cryolite (Na_3AlF_6) ores using the Bayer process. This process yields alumina (Al_2O_3) which aggregates in the solid state owing to its highly ionic character induced by the large difference in electronegativity of its constituent atoms (Al, 1.61; O, 3.44). As a result of this, alumina is extremely inert with high thermal and electrical resistance which has facilitated its use in ceramics and in a range of cosmetic processes.[69,70] Alumina is used in a number of industrially relevant chemical reactions including the dehydrogenation of alcohols, isomerisation and alkylation reactions.[71] However, these properties also preclude its widespread commercial use. Instead, ~90% of extracted alumina is converted to aluminium metal *via* the smelting process and benefits from an unrivalled versatility. It has a very low density, allowing for its use in large scale (aerospace, construction industries) and small scale (cooking equipment, furniture) applications.[72] Aluminium(0) has the electronic configuration [Ne] $3s^2 3p^1$, and its intrinsic Lewis acidity can be accounted for by considering the closed-shell stability of aluminium +3 (empty 3p orbitals), which has long been exploited in catalysis. Triethylaluminium [$Al(C_2H_5)_3$] is used as a co-catalyst in the Aufbau reaction (polymerisation of alkyne monomers), and later developments expanded this reactivity to include the synthesis of alcohols.[73,74] These same properties also permit the use of trialkyl aluminium reagents as catalysts in Friedel-Craft reactions, and developments in the field of aluminium chemistry (both catalytic and low oxidation state) have been numerous. Hence, aluminium was chosen as a suitable target to explore its reactivity with a focus on environmental sustainability.

1.7 Summary and Aims and Objectives

The need to progress away from the use of transition metals in industrially relevant catalytic processes is apparent when considering their relative Earth abundance, which is highlighted in **Figure 1.2**. Abundant, low cost, and low toxic main group compounds are the obvious alternative, but their fundamental properties had previously always precluded their use as catalysts, owing to the presence of large HOMO-LUMO gaps and an absence of vacant molecular orbitals/coordination sites. However, huge advances have been made in this field. Main group compounds that exhibit transition metal-like properties, as well as main group catalysed reactions *via* different mechanistic pathways, are now widely established and could one day replace the transition metal industry standards, though further developments are needed in this area.

Aluminium chemistry has seen a renaissance in recent years. Its high abundance, low cost and low toxicity make it an attractive target in the search for main group compounds that exhibit transition metal-like reactivity, with many of these advances achieved in the last decade alone (Chapters 3 and 4). This thesis focuses on the synthesis of aluminium amidinate compounds and investigates their use as hydroboration catalysts, as well as for the synthesis and isolation of low oxidation state compounds. Specifically, the sterically encumbered 2,6-diphenylmethyl-4-methylphenyl (Ar*) ligand was employed to investigate the influence of sterics on the catalytic hydroboration of phenylacetylene, and to ascertain if this ligand would be sufficiently bulky to stabilise a highly strained four-membered monomeric aluminium(I) complex. The following chapter will detail the synthesis and characterisation of these compounds.

Chapter 2:

Synthesis and Characterisation of Aluminium Amidinate Hydride and Alkyl Complexes

2.1 Introduction

2.1.1 Amidine Pro-Ligands

Amidine pro-ligands have the general formula [(R_1)NC(R_2)NH(R_3)] where R_x groups can be either aromatic or aliphatic; related guanidine pro-ligands possess a C-N substituent in the R_2 position (**Figure 2.1**). Amidines are named after the acid or amide obtained upon hydrolysis of the ligand, for example $CH_3C(=NH)NH_2$ is acetamidine. The two nitrogen atoms are referred to as *N* and *N'*, though this does not distinguish between the imino and amino nitrogen atoms. If the substituents in the R_1 and R_3 positions are hydrogen (NH_2), the amidine ligand is classed as unsubstituted. To that effect, amidines can therefore be classed as monosubstituted, symmetrical disubstituted or unsymmetrical disubstituted based on the substituents in the R_1 and R_3 positions.[75] For further details on the chemistry of amidine pro-ligands, a comprehensive review was written by Kilner and Barker.[76]

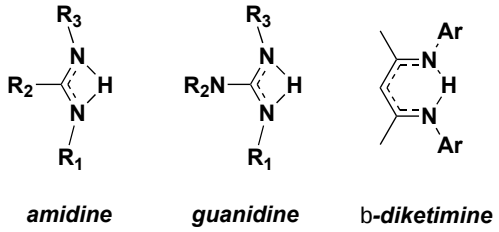

Figure 2.1: General structure of amidine (left), guanidine (centre) and β-diketimine (right) ligands.

2.1.2 Metal Amidinate Complexes

2.1.2.1 Synthesis of Metal Amidinate Complexes

Upon complexation of the amidine ligand to a metal, a four-membered chelate is formed, with a narrow N-M-N bite angle. This four-membered ring is highly strained (compared to five- or six-membered rings), leaving the coordinated metal centre exposed and thus limiting their use in the coordination of highly reactive metal species compared to the more widely employed *β*-diketimine ligand, for example (**Figure 2.1**). Employing sterically demanding substituents in the R_1 and R_3 positions can shield the metal centre, and these are easily incorporated into the framework due to the modular synthesis of these ligands. Three main pathways are used to obtain metal amidinate complexes, and these are described in **Scheme 2.1**. The first pathway (**Scheme 2.1**, bottom) involves the reaction of alkyl-/aryl-metal complexes with *N,N'*-disubstituted carbodiimides. The reaction proceeds *via* the nucleophilic attack of the central carbodiimide carbon by the carbon of the alkyl-/aryl- metal reagent, and this is said to be the

driving force for the reaction.[77] Amidinate complexes can also be synthesised *via* the reaction of carbonitriles with *N,N'*-disubstituted metal amides (**Scheme 2.1**, left). As with the carbodiimide pathway, this process is driven by the nucleophilic attack of the nitrile carbon by the metal amide carbon, before undergoing an *in situ* rearrangement to form the target amidinate complex.[4] Replacing the alkyl groups with a cyclic substituent could prevent this rearrangement. Generally, these reactions form alkali metal amidinates which can be further reacted to obtain the desired metal complex, though these can also be directly targeted from the starting ligands with an appropriate metal precursor.[80]

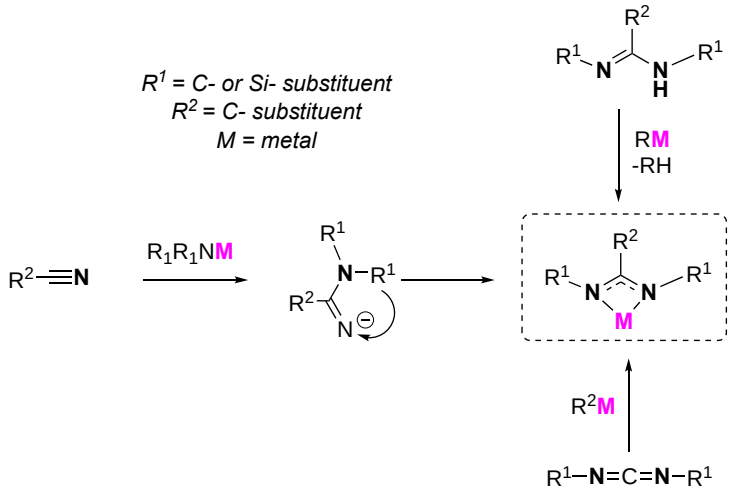

Scheme 2.1: Main reaction pathways for the preparation of amidinate complexes.

2.1.2.2 Bonding Modes in Metal Amidinate Complexes

The five main bonding modes of amidinate complexes have been uncovered through single crystal X-ray analysis and are summarised in **Figure 2.2**. Firstly, **A** highlights a monodentate mononuclear binding mode, whereby one nitrogen atom is σ-bonded to the metal, whilst the other nitrogen is double bonded to the backbone carbon atom and remains unattached. The first example of a species exhibiting this binding mode was reported in 1986, when van Koten *et al.* synthesised the platinum species **2A** (**Figure 2.3**) and characterised it crystallographically. Compound **2A** crystallised in the $P2_1/n$ space group, with four molecules in the unit cell and an approximately square planar platinum centre. Three of the four coordination sites were occupied by the terdentate C_6H_3-*2,6*-$(CH_2NMe_2)_2$ ligand, whilst the fourth site was occupied by the amidine ligand backbone. The monodentate Pt-N bond length was found to be 2.132(6) Å.[81]

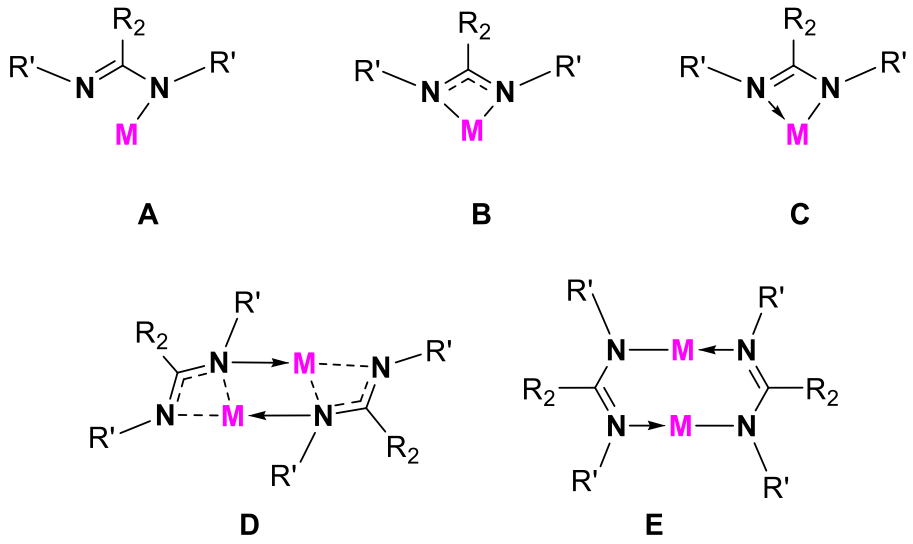

Figure 2.2: Bonding modes in amidinate complexes.

Structures **B** and **C** demonstrate chelated bonding modes, where both nitrogen atoms are bonded to the central metal atom. In the case of **B**, electron density is delocalised across the N-C-N backbone and is classed as an isobidentate mononuclear complex, with σ,σ-symmetrical bonding. In contrast, **C** is considered an anisobidentate mononuclear complex, with σ,σ-unsymmetrical bonding. It is these bonding modes that introduce the aforementioned strain into the four-membered chelate and results in a distortion of the valence angles. Structures of this type are the most common form of amidinate complex, and include monomeric, dimeric and *bis*-ligated complexes. Some generic examples, **2B**-**2D**, are shown in **Figure 2.3**.[82–84] Amidine ligands and related amidinate complexes can be easily modified. The desired electron density or steric hindrance around the metal centre can be fine-tuned through differing N- or C-backbone substituents. Substitutions made at the nitrogen atoms that interact with the metal atom (E.g. N-, or O-containing species) are called peripheral substituents. These destabilise isobidentate bonding modes, forcing the structure to exhibit anisobidentate or even monodentate bonding instead. Select examples are shown in **Figure 2.3**, **2E**-**2G**.[85–87]

Finally, structures **D** and **E** represent examples of isobidentate and anisobidentate dinuclear bonding, respectively. Isobidentate dinuclear complexes often form as centrosymmetric dimers. One such example of an isobidentate dinuclear complex is **2H** (**Figure 2.3**) which was synthesised *via* the reaction of a dimeric lithium silylamide with two equivalents of benzonitrile in THF at 253 K. The dimeric structure of **2H** was confirmed by X-ray crystallography. The lithium atoms were bonded to the amidinate backbone nitrogen atoms, with additional coordination interactions from the oxygen atom of the ether substituent. In this complex,

lithium has a formal coordination number of four, with three sites occupied by nitrogen atoms and the fourth occupied by the oxygen atom of the ether group. The structure of **2H** was highly distorted, as evidenced by the lithium-nitrogen bond lengths: Li(1)-N(1), 1.693(3) Å; Li(2)-N(1'), 1.973(2) Å; Li(1)-N(2), 2.401(3) Å, Li(2)-N(2'), 2.025(2) Å. Interestingly, **2H** did not contain any coordinated solvent molecules despite being synthesised in THF. When reacted with two equivalents of yttrium trichloride in THF, the resultant structure (dimeric, with μ_2 bridged chlorine atoms) differed from **2H** in that it contained coordinated THF molecules at the yttrium centre, and the oxygen substituent of the ether group was no longer coordinated to the metal centre.[88]

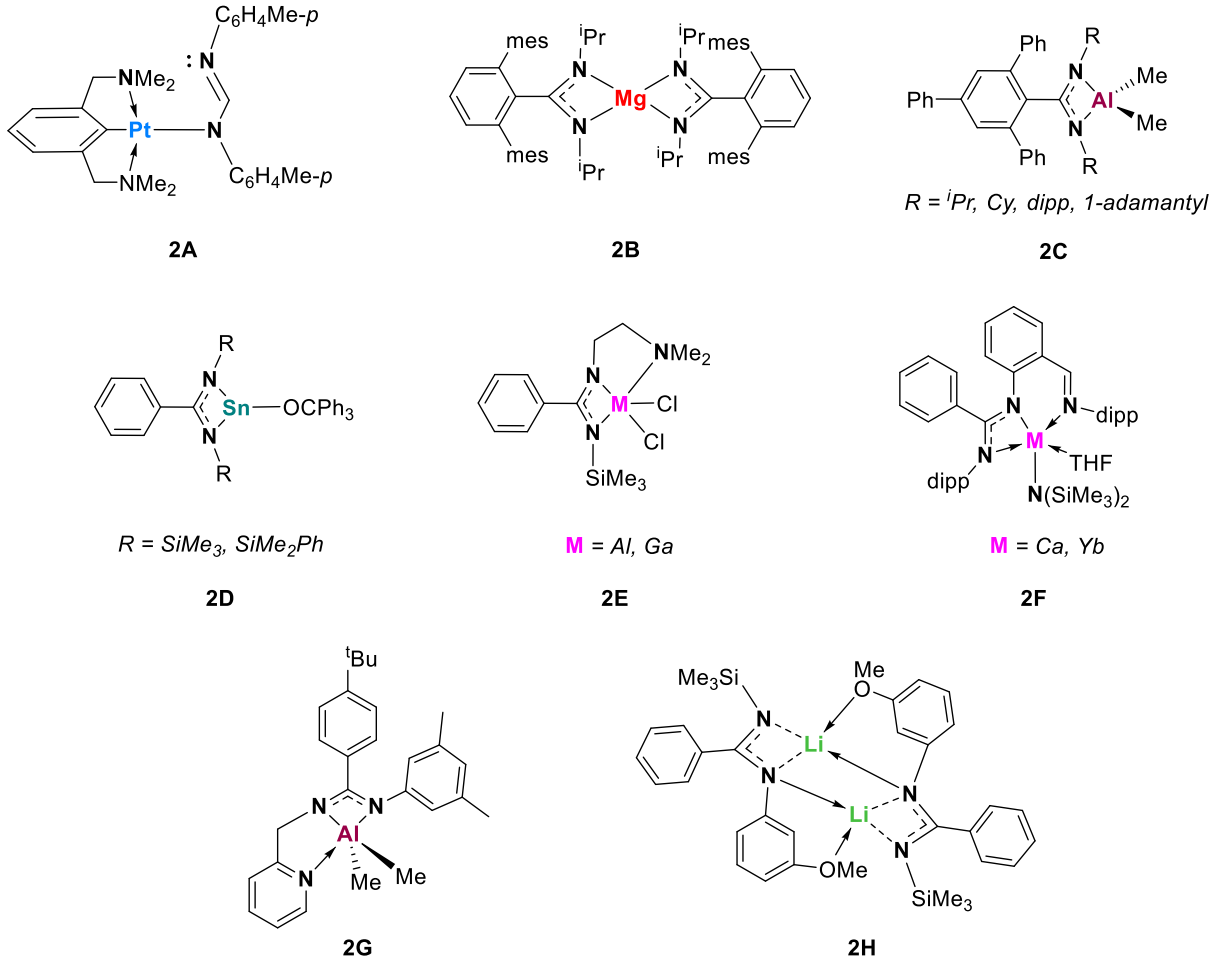

Figure 2.3: Structures of amidinate complexes **2A-2H**.

With the coordination modes of amidinate complexes established, the synthesis, characterisation, and applications of aluminium amidinate complexes will be reviewed.

2.1.2.3 Aluminium Amidinate Complexes

Aluminium amidinate complexes first emerged in the literature between the late 1980s and early 1990s, with some of the earliest examples (**2I**-**2I'**, **Figure 2.4**) reported by Weidlein *et al*..[89,90] The dimethyl aluminium amidinate **2I** was synthesised *via* the reaction of the parent carbodiimide with methyllithium (MeLi) to obtain the lithium amidinate species, before being reacted with dimethylaluminium chloride to obtain **2I**. In contrast, **2I'** was obtained directly *via* the reaction of the parent sulfurdiimide ligand with trimethyl aluminium. Through spectroscopic analyses (NMR, infrared (IR), and Raman), **2I** and **2I'** were found to adopt distorted tetrahedral aluminium centres, as well as exhibit C_{2v} symmetry.[89,90]

Later examples of aluminium amidinate complexes (**2J**-**2K**) were reported by Jordan and co-workers and were additionally characterised in the solid-state.[83] The aluminium alkyl complex **2J** (Cy = cyclohexyl) was targeted directly *via* the reaction of the parent carbodiimide with trimethyl aluminium, whilst **2J'** was synthesised by reacting the ligand with *tert*-butyllithium to obtain the lithium amidinate, before further reacting with dimethylaluminium chloride. The dichloride complexes **2K** and **2K'** were both synthesised *via* the lithium amidinate route and reacted with aluminium trichloride. As with **2I**/**2I'**, spectroscopic analyses indicated C_{2v} symmetry, and a symmetric bidentate coordination of the N-C-N amidinate moiety. All complexes were characterised crystallographically and found to adopt distorted tetrahedral aluminium centres. The Al-N bond angles in **2J** were essentially equal (1.923(2) *versus* 1.926(2) Å), whilst a degree of asymmetry was observed in **2J'** (1.927(2) *versus* 1.9124(14) Å). The Al-N bonds in **2K** were identical (1.879(2) Å), whilst in **2K'** they were 1.872(3) and 1.863(3) Å. The N-C bond lengths for all complexes existed in the range 1.325(2)-1.343(5) Å; **2J** had the shortest bond lengths (1.325(2), 1.329(3) Å), whilst **2J'** had the longest (1.339(2)-1.343(2) Å). The shorter Al-N bond lengths of **2K**/**2K'** (**2K**: 1.336(3)-1.339(3) Å; **2K'**: 1.335(5)-1.340(5) Å) were attributed to the increased polarisation of the Al-Cl bond. The average N-Al-N angle was rather acute for both the alkyl and chloride complexes (**2J**-**2J'**: 68.74°; **2K**-**2K'** 70.91°). The Cl-Al-Cl bond angle average was a nearly perfect tetrahedral at 110.61° (109.47° for perfect tetrahedral), whereas the C-Al-C average bond length was much larger in comparison (117.42°). The smaller angle of **2K**/**2K'** was rationalised through simple valence-shell electron-pair repulsion (VSEPR) concepts, in that the higher electronegativity of Al-Cl *versus* Al-C results in a smaller electron bonding pair.[83]

Further developments in the late 1990s helped elucidate the catalytic capabilities of aluminium amidinate complexes. The related aluminium amidinate **2L** was synthesised *via* the reaction of the analogous aluminium alkyl amidinate with *tris*-(pentafluorophenyl)borane ($B(C_6F_5)_3$) and **2L** was classified as a base-free ion pair. ^1H NMR analysis of **2L** indicated that the anionic moiety binds to the aluminium centre by a B-Me-Al bridge and rotation about this bridging unit is slow due to steric congestion. Efforts to isolate **2L** in the solid-state were unsuccessful, but further investigations revealed that **2L** was a successful ethylene polymerisation catalyst, and the increased activity was attributed to the coordination of the anionic component.[91] Thus, by the turn of the century, the spectroscopic and crystallographic characterisation of *mono*-aluminium amidinate complexes was well established, and early investigations into their functionality were starting to emerge.

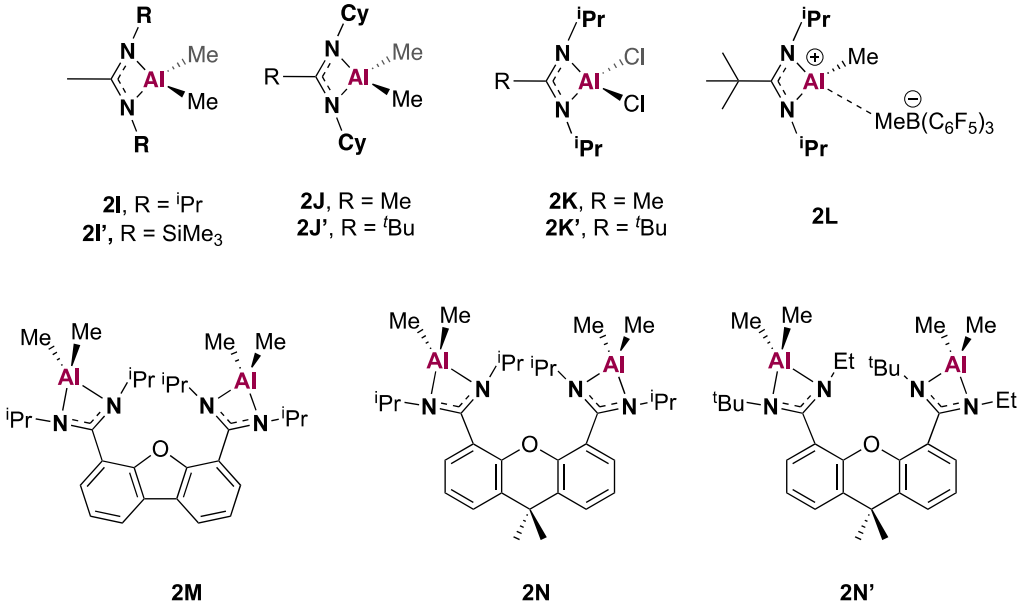

Figure 2.4: Structure of aluminium catalysts **2I**-**2N'**.

The synthesis and characterisation of aluminium *bis*-amidinate complexes is also well developed. Compared to their *mono*-amidinate counterparts, *bis*-amidinate complexes adopt trigonal bypyramidal structures and are often synthesised in a 2:1 ratio of ligand:metal reagent. One such example of this was the synthesis of *bis*-amidinate complexes **2M** and **2N** (**Figure 2.4)** *via* the reaction of the corresponding amidine ligand with trimethyl aluminium. These structures differ by their backbone linker unit: dibenzofuran (**2M**) or 9,9-dimethylxanthane (**2N**). X-ray analysis revealed both structures possessed two pseudotetrahedral aluminium centres with bidentate binding modes ($Al\text{-}N_{ave}$ 1.93 Å) and a pair of methyl group donors ($Al\text{-}Me_{ave}$ 1.95 Å). The intermetal separations in **2M** and **2N** were heavily influenced by the

backbone ligand framework, with Al-Al distances of 6.505(9) and 5.930(9) Å, respectively. The related asymmetric complex **2N'** (**Figure 2.4**), with variation at the N-substituent, was synthesised to explore whether rotational diastereomers existed in solution. At room temperature, the reaction mixture revealed the presence of **2N'**-C_2 and **2N'**-C_s, present in a 1:0.9 ratio, and this did not change after 24 hours at room temperature. However, heating to 343 K overnight shifted this equilibrium and each diastereomer was present in a 1:1 ratio.[92]

Further examples of bridging aluminium *bis*-amidinate complexes have been synthesised and tested for their capacity to catalyse the ring-opening polymerisation (ROP) of ε-caprolactone. Complexes **2O** and **2P** feature phenyl and cyclohexane bridging units, respectively, whilst the monomeric counterparts **2Q** and **2R** were synthesised to ascertain whether the bimetallic complexes exhibited increased catalytic activity (**Figure 2.5**). All complexes were synthesised from the relevant pro-ligand with 0.5 (**2O**-**2P**) or 1 equivalent(s) (**2Q**-**2R**) of trimethyl aluminium. Complexes **2O**, **2P**, **2Q** and **2R** were recrystallised in THF and characterised crystallographically. In all instances, the complexes were solvent free, and each aluminium centre was four-coordinate with two methyl substituents and bidentate nitrogen binding modes. The methyl groups lie above and below the plane of the molecule to minimise interactions with the N-C-N-Al moiety. Complex **2O** was described as a representative example of **2O**-**2R**, with Al-Me bond lengths between 1.933(4)-1.946(5) Å and Al-N bond lengths between 1.934(3)-1.952(3) Å. The N-Al-N bond angles in **2O** were nearly identical, at 68.33(11) and 68.43(11)°. The amidinate core was nearly planar (< 1.72 ° torsion angle) and the bonding mode was said to be delocalised across the N-C-N-Al core. Interestingly, the intermetal separations of **2O** and **2P** were far greater than for **2M**/**2N**, at 10.49 and 10.58 Å, respectively. All catalysts were active towards the ROP of ε-caprolactone, however there was no increase in activity observed for the bimetallic complexes compared to their monometallic counterparts. This was attributed to the opposing orientations and large intermetal separations of the aluminium centres.[93] The structurally related aluminium amidinate complex (**2S**, **Figure 2.5**) exhibited similar properties (delocalised N-C-N, planar core) and was found to catalyse the ROP of *rac*-lactide.[94]

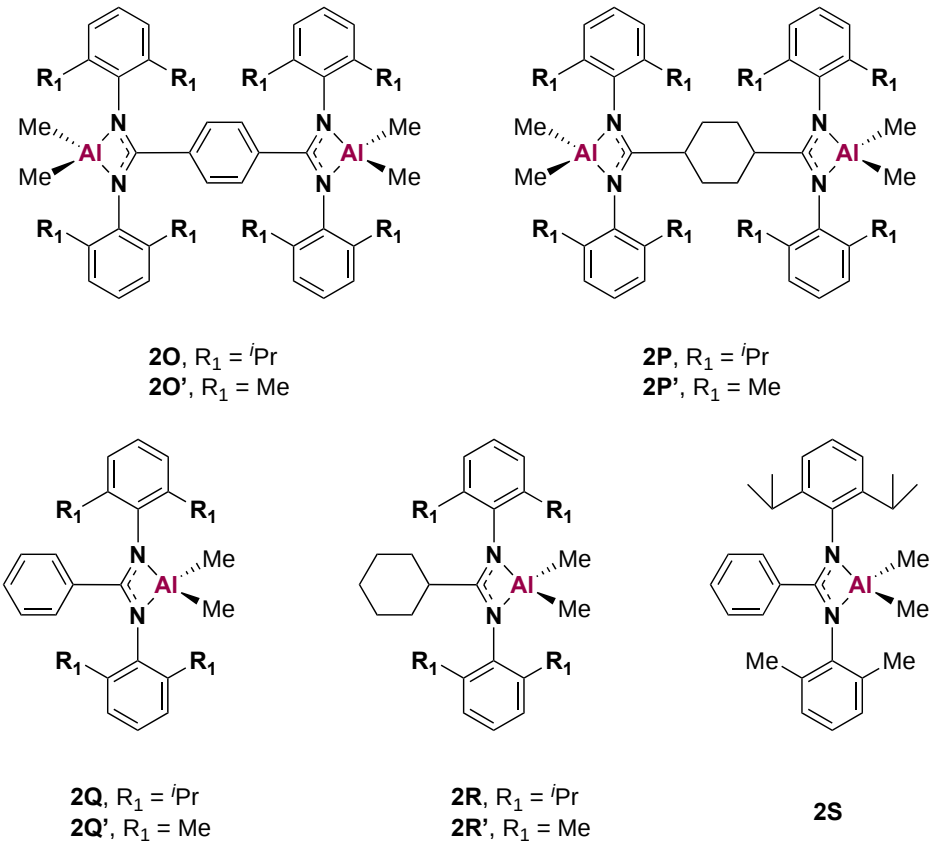

Figure 2.5: Structure of catalysts **2O**-**2S**.

Expanding on this work, Kretschmer and co-workers synthesised a series of bridging aluminium *bis*-amidinate and guanidinate complexes and systematically altered the length of the linker unit to study the effect of intermetal separation on the catalytic activity (ROP of ε-caprolactone and *L*-lactide). To that effect, the amidinate and guanidinate complexes **2T** and **2U** were synthesised with ethylene propylene, butylene, or 1,3-xylylene linker units (**Figure 2.6**). The complexes were synthesised from the relevant pro-ligand with trimethyl aluminium and characterised spectroscopically. Complexes **2T**-*ethyl*, **2T**-*butyl*, **2U**-*ethyl*, **2U**-*propyl* and **2U**-*butyl* were characterised crystallographically. The Al-Me bond lengths of all complexes ranged between 1.951(14)-1.969(16) Å, and were in good agreement with related amidinate, *bis*-amidinate and guanidinate complexes. As for **2O**-**2R**, the C-N bond lengths of **2T**-**2U** were almost equal, indicative of effective electron delocalisation across the N-C-N backbone and a delocalised bidentate binding mode; the *bis*-amidinate C-N bond lengths were slightly shorter than in the *bis*-guanidinate complexes (amidinate: 1.338(15)-1.348(15) Å, guanidinate: 1.342(18)-1.370(17) Å). Unsurprisingly, the intermetal separation increased in line with the number of carbon atoms in the linker chain. For example, the intermetal separation in **2T**-*ethyl*

was 6.291(7) Å, increasing to 8.209(6) Å in **2T**-*butyl*. The distance of **2T**-*ethyl* lies in a similar range to **2M**, whilst both distances are much shorter than for **2O** and **2P**.[95]

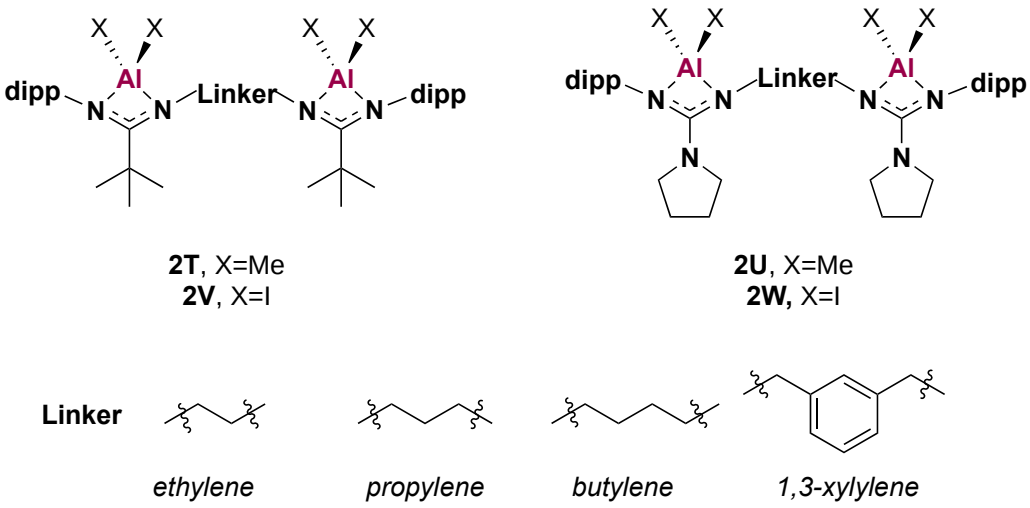

Figure 2.6: Structure of catalysts **2T**-**2W**.

Iodisation reactions were attempted for **2T** and **2U** to obtain the related *bis*-amidinate and guanidinate diiodide complexes **2V** and **2W** (**Figure 2.6**). All amidinate complexes were isolated and characterised crystallographically, whereas only **2W**-*propyl* was isolated for the guanidinate family. Very few changes were noted in the ^{1}H NMR spectra of the iodide complexes, except for the disappearance of the methyl resonances below 0 ppm. For the amidinate complexes, the Al-I bond lengths were found to lie in the range of 2.475(15)-2.523(2) Å, which were slightly longer than for a previously reported mononuclear complex (Al-I: 2.438(3), 2.481(3) Å).[96] The Al-I distances were slightly longer in **2W**-*propyl* (2.503(6), 2.508 Å) compared to the amidinate distances, but were said to be in good agreement with previously reported guanidinate complexes.[97,98] The increased polarisation of the iodine substituent compared to methyl resulted in a contraction of the Al-N bond lengths (amidinate: 1.868(4)-1.896(3) Å, **2W**-*propyl*: 1.870(16)-1.876(2) Å) and an increase in the N-Al-N bond angles (amidinate: 70.21(17)-71.2(2)°, **2W**-*propyl*: 72.21(7)°). Whilst these catalysts were active towards the ROP of ε-caprolactone and *L*-lactide, it was not possible to discern any trends relating to carbon chain length of the linker unit and catalytic activity (although, in general, chains with >2 carbons exhibited better activity).[95]

Further examples of aluminium amidinate complexes examined for their catalytic activity are shown in **Figure 2.7** (**2X**-**2Z**). In this instance, the bimetallic catalysts **2X** and **2Y** displayed increased activity in the ROP of ε-caprolactone compared to the analogous monometallic species **2Z**, demonstrating that cooperative effects were in operation (in contrast to **2O**-**2R**). However, the complexes were characterised only by ^{1}H NMR spectroscopy and in the absence of crystallographic data further links between structure and catalytic activity cannot be made.[99] More recently, however, these complexes were shown to facilitate the fixation of carbon dioxide into cyclic carbonates, expanding the applications of the aluminium amidinate family.[100]

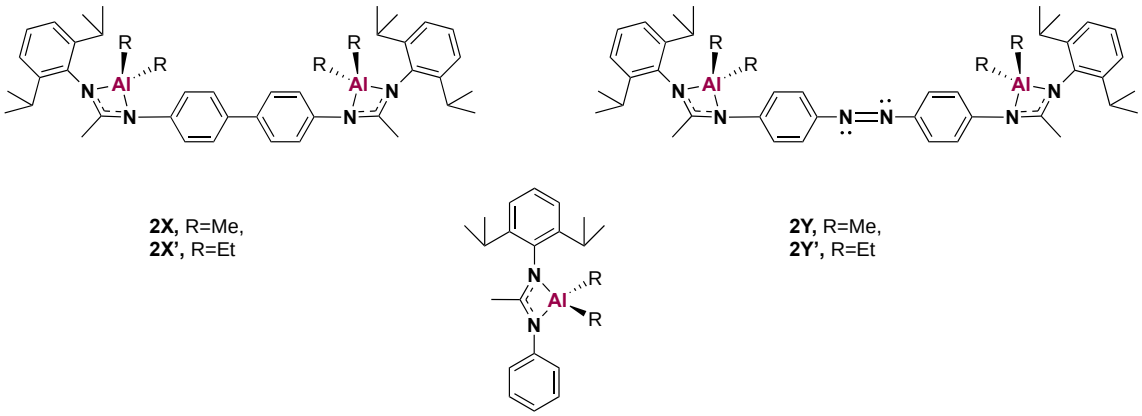

Figure 2.7: Structure of catalysts 2X-2Z.

2.1.2.4 Amidinate and Guanidinate Complexes Bearing "Super-Bulky" Ligands

Whilst the uses of amidinate complexes in catalysis have been described herein, it is pertinent to note that they have not exhibited the same rich chemistry and versatility as related β-diketiminate complexes. Low oxidation state BDI complexes were reported as early as 2000, whereas the literature pertaining to amidinate complexes is less well developed. Attempts to synthesise the low valent analogues of **2T** and **2U** *via* the reduction of **2U** and **2W** (using magnesium powder, cobaltocene or potassium mirrors) were all unsuccessful, attributed to the increased strain and decreased stability of the four-membered chelate. In recent years, select examples of amidinate and guanidinate complexes have emerged in the literature bearing "super-bulky" N-atom substituents. Namely, complexes bearing 2,6-diphenylmethyl-4-*tert*-butylphenyl ("Ar†") and 2,6-diphenylmethyl-4-*iso*-propylphenyl ("Ar§") ligands (**Figure 2.8a**) have been used to isolate group 1 and group 2 guanidinate and amidinate complexes,

respectively (**2AA**-**2AB**, **Figure 2.8b**).[101–103] The amide ligand (Ar†NH$_2$)CO) was dehydrated in the presence of phosphorus pentoxide/aluminium oxide (P_2O_5/Al_2O_3) to yield the carbodiimide (Ar†NH$_2$)C which was treated with LiN=C^{t}Bu$_2$ to yield the guanidinate lithium salt (**2AA**). The analogous guanidine ligand was synthesised *via* deprotonation of the lithium salt with lutidinium chloride, which was easily derivatised to obtain the potassium and caesium analogues. The structures of **2AA** (M = Li, K, Cs) were characterised crystallographically. The N^{Ar†}-C bond lengths existed in the range 1.302(2)-1.334(2) Å (shortest, M = Li, longest, M = Cs) and indicate charge delocalisation across the N-C-N moiety, whilst the N-C-N bond angles were said to be in good agreement with related guanidinate species.[101] Most importantly, the complexes did not aggregate in solution and each metal centre was found to be free of coordinating solvent (formally two-coordinate metal ions). The increased steric encumbrance of the Ar† ligand circumvented the aggregation of these complexes by encapsulating the metal within a 'coordination pocket', which was defined by three (M = Li, K) or four (M = Cs) encircling phenyl rings.[101]

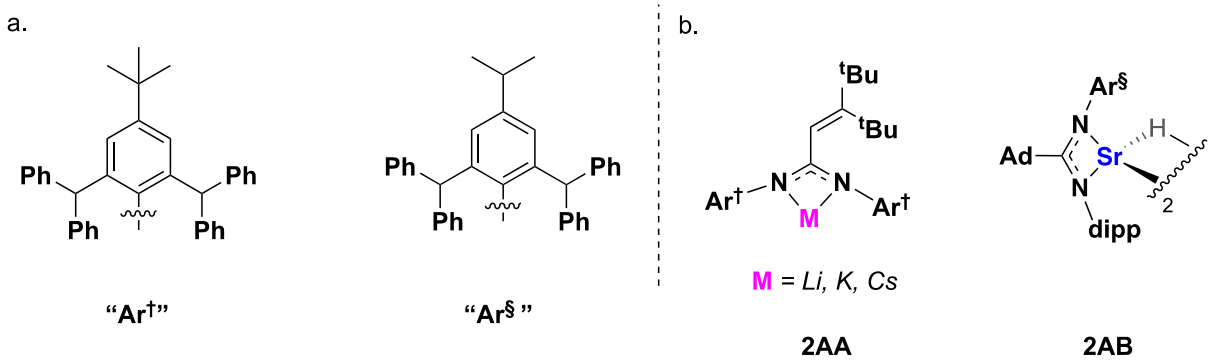

Figure 2.8: a. "Super-bulky" ligands Ar† and Ar§; b. guanidinate complex **2AA** and amidinate complex **2AB**.

In a similar fashion, the super-bulky amidinate complex **2AB** was synthesised *via* the reaction of the parent strontium *bis*-(trimethylsilyl)amide complex with phenylsilane in hexane at 298 K. In the solid-state, **2AB** was found to be a hydride-bridged dimer, with a delocalised N-C-N central moiety. The large covalent radius of strontium (1.95 Å) facilitated the formation of high-coordinate strontium metal centres which both have strong interactions with one phenyl group of the amidine ligand.[103] The isolation of both complexes **2AA**-**2AB** was facilitated by increased kinetic stabilisation at the metal centres, arising from the increased steric encumbrance of the super-bulky ligands. The applications of these complexes are beyond the

scope of this discussion but have been included to highlight that highly strained four-coordinate complexes can be isolated when an appropriately sized ligand is used. With this in mind, it was hypothesised that using the super-bulky 2,6-diphenylmethyl-4-methylphenyl substituent would facilitate the isolation of a series of fundamentally interesting amidinate complexes. As such, their synthesis and characterisation will be discussed in this chapter.

2.2 Synthesis of Amidine Pro-Ligands

The following notation system has been implemented in this thesis: 'mes' refers to a 2,4,6-trimethylphenyl substituent, 'dipp' refers to 2,6-diisopropylphenyl and the 2,6-diphenylmethyl-4-methylphenyl substituent has been abbreviated to 'Ar*'.

A series of known (**2.2**, **Scheme 2.2**) and novel (**2.5-2.7**, **Scheme 2.3**) symmetric and asymmetric amidine ligands bearing varied *N*,*N*'-substituents was synthesised according to modified literature procedures.[104,105] The sterically demanding 2,6-diphenylmethyl-4-methylphenyl "Ar*" ligand was chosen as the R_1 substituent for complexes **2.5-2.7** to kinetically stabilise the metal centre, whilst the 4-methylphenyl backbone was chosen to aid compound solubility during ligand synthesis.

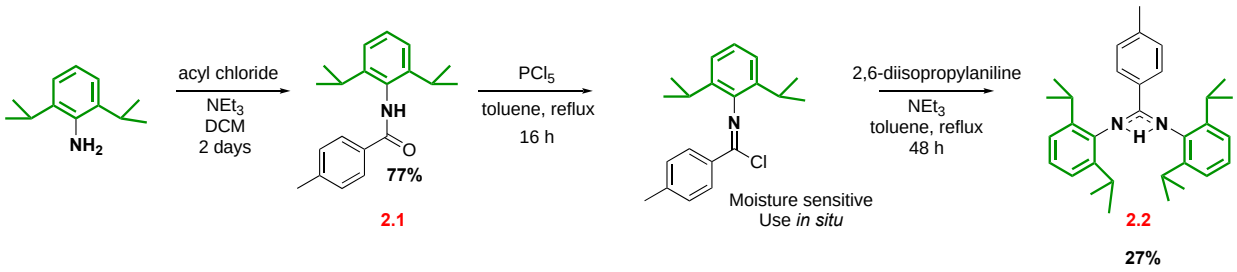

Scheme 2.2: Synthesis of amidine ligand **2.2**.

One equivalent of aniline "dippNH$_2$" (**2.2**) or "Ar*NH$_2$" (**2.5-2.7**) was reacted with one equivalent of *para*-toluoyl chloride in dichloromethane (DCM) to obtain the amide compounds **2.1** and **2.4.** The resultant amides were reacted with phosphorus pentachloride (PCl_5) under inert conditions to yield the imidoyl chloride, and heating at reflux in the presence of a second equivalent of aniline and triethylamine (NEt_3) in toluene afforded the crude amidine ligand as a viscous brown oil. Pure ligand samples were isolated after recrystallisation in different solvent systems (**2.2**: hot ethanol, **2.5-2.6**: hot methanol, **2.7**: methanol/DCM) and in varying yields between 27% - 65%.‡

‡ See experimental section for full details.

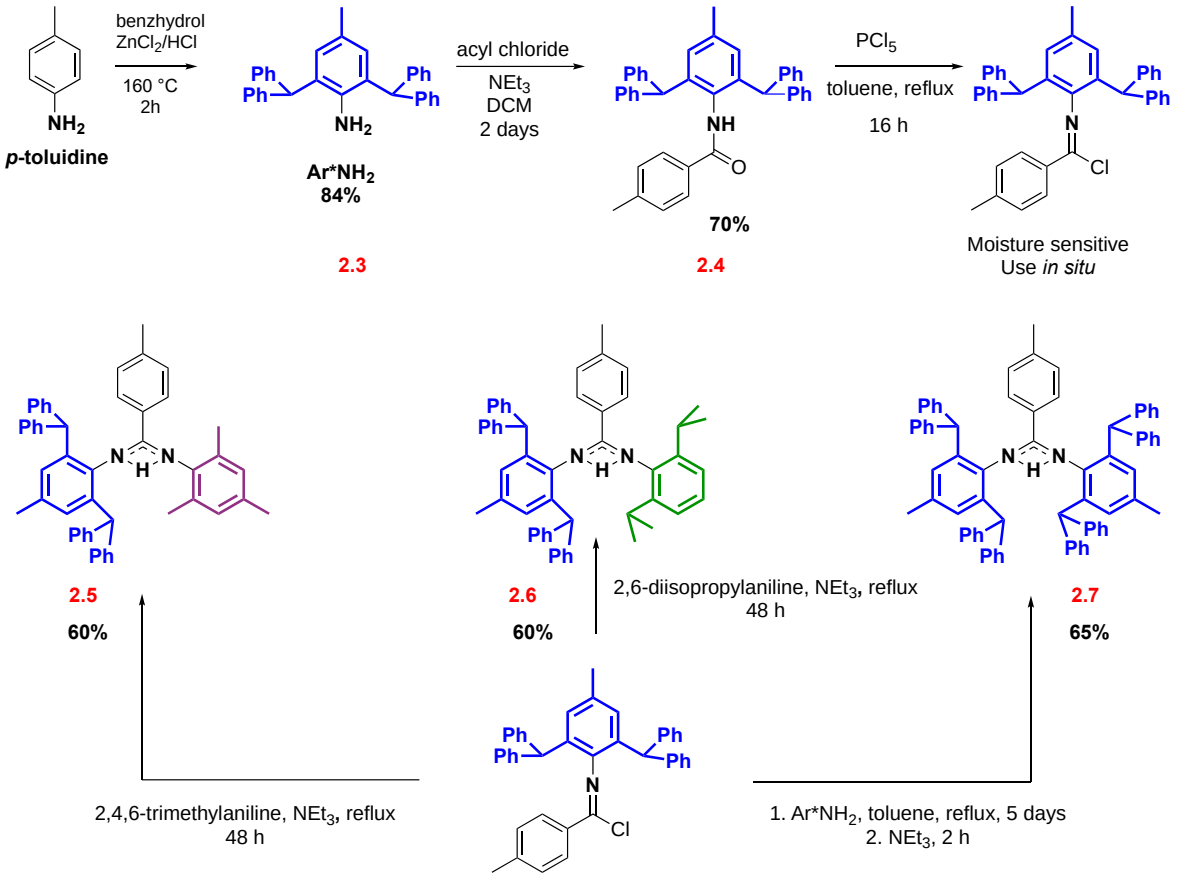

Scheme 2.3: Synthesis of amidine ligands **2.5**-**2.7**.

The bulkiest amidine ligand in the series, **2.7**, required more forcing conditions to couple the second Ar* substituent. The system was heated at reflux for 5 days (*versus* 2 days), with subsequent addition of NEt_3 and heating for a further two hours. The ^{1}H NMR spectra of compounds **2.2**, **2.5**-**2.7** exhibited a distinctive singlet peak in the range 4.78-5.66 ppm (**2.2**: 5.66 in $CDCl_3$, **2.5**: 4.78 in $CDCl_3$, **2.6**: 5.25 in $CDCl_3$, **2.7**: 5.06 in C_6D_6) corresponding to an amine (N**H**) proton, indicating the desired amidine had formed. The ^{1}H NMR spectrum of compound **2.2** was more complex; in $CDCl_3$ (**Figure 2.9**) it exhibited four doublets in the range 0.84-1.32 ppm corresponding to four diastereotopic diisopropyl C**H**$_3$ groups and two distinctive pairs of multiplets (3.12-3.20/3.21-3.28 ppm). These correspond to the methine protons and occur in an approximate ratio of 3:1. In order to establish if all of these signals corresponded to one species, or a number of different species, several NMR experiments (**Figure 2.9**) were undertaken. Heating the sample saw the methine resonances coalesce into one broad signal, which occurred with broadening of the rest of the spectrum. Running the sample in benzene-

d6 saw the ratios of the C**H** and C**H**$_3$ protons change indicating that the multiple peaks were the result of a single product showing dynamically exchanging species. This was supported by elemental analysis. The improved resolution of the spectrum in chloroform-*d* (compared to benzene-*d6*) indicated a degree of stabilisation from the acidic carbon-deuterium bond.

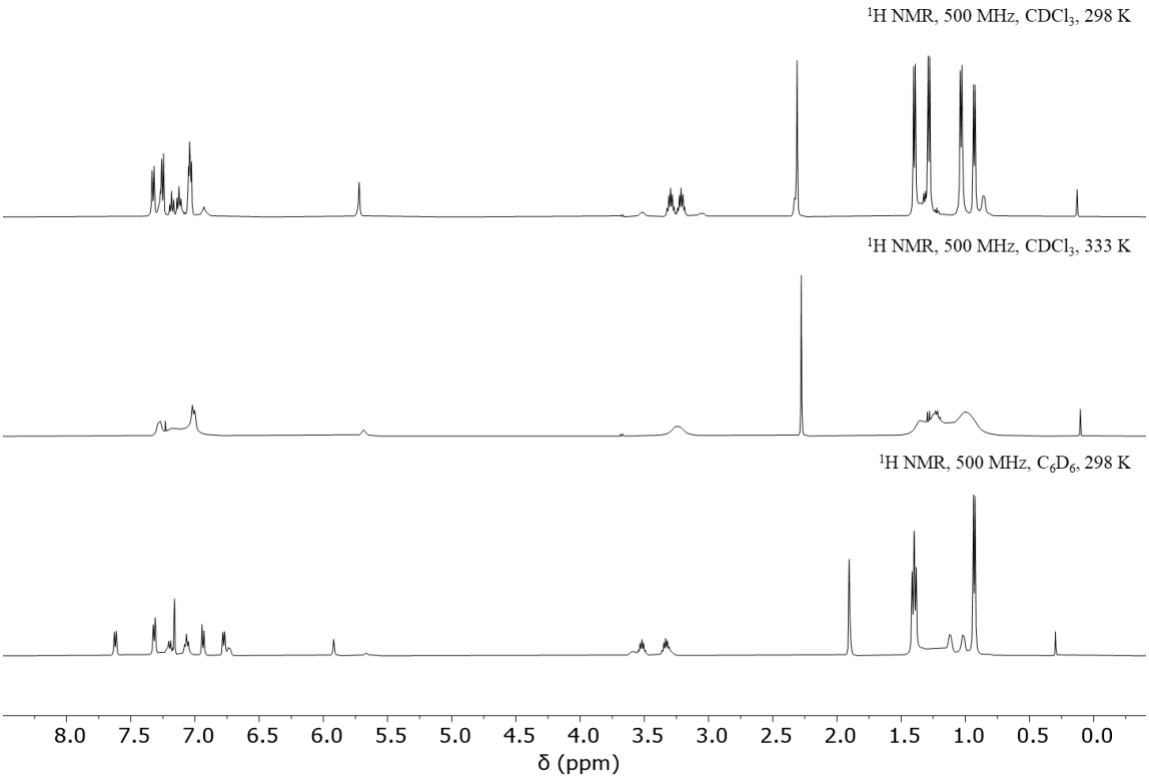

Figure 2.9: ^{1}H NMR spectra of ligand **2.2** in $CDCl_3$ (top), $CDCl_3$ at 333 K (middle) and C_6D_6 (bottom).

2.3 Synthesis of Aluminium Hydride Complexes

The aluminium hydride complexes **2.8**-**2.10** were synthesised by the addition of one equivalent of the respective pro-ligand (**2.2**, **2.6**, **2.7**) to 1.2 equivalents of trimethylamine alane (TMAA) in toluene at 195 K (prep scale) or in benzene-*d6* at 298 K (analytical scale) (**Scheme 2.4**). Hydrogen gas was seen to evolve immediately upon addition and monitoring by ^{1}H NMR spectroscopy revealed complete consumption of the ligand starting material in less than 15 minutes. Products were isolated by extraction into toluene and washing the residual precipitate with hexane (**2.8**), or by the removal of the solvent *in vacuo* before washing with hexane (**2.9**, **2.10**). Further removal of the solvent *in vacuo* yielded all products as white powders.

The ^{1}H NMR spectra of all complexes exhibited similar features. Firstly, the disappearance of the amidine N**H** resonance suggested the initial ligand had undergone complexation. In

conjunction with a broad resonance integrating to two protons between 3.6-5.1 ppm in C_6D_6, which is characteristic of an aluminium hydride signal (Al**H**$_2$: **2.8** 5.06 ppm, **2.9** 4.77 ppm, **2.10** 3.63 ppm), this strongly indicated the formation of a mono-ligated aluminium dihydride species. Reaction yields varied across the series; **2.10** was isolated in a 70% yield, whilst compounds **2.8** and **2.9** were isolated in yields of 42% and 36%, respectively.

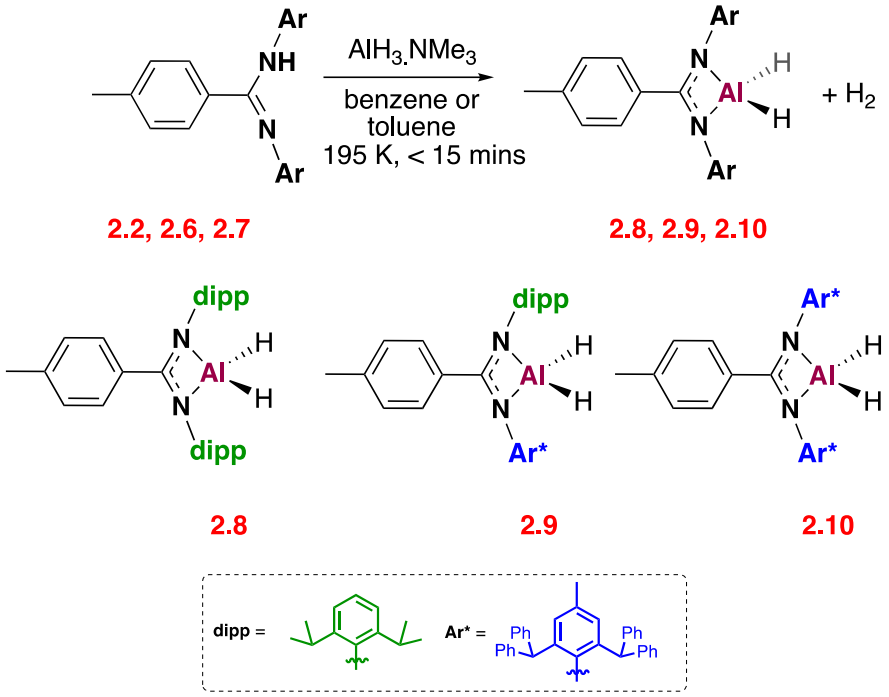

Scheme 2.4: General synthesis of aluminium hydride compounds **2.8**-**2.10**.

The ^{1}H NMR spectra of purified **2.2** and crude **2.8** were broad, throwing into doubt the purity of the starting ligand. However, ligand purity could be verified upon complexation to a bulky, monomeric magnesium species, or by extraction of crude **2.8** into toluene (**Figure 2.10**). Both reactions yielded clean NMR spectra, with only one species present in solution.

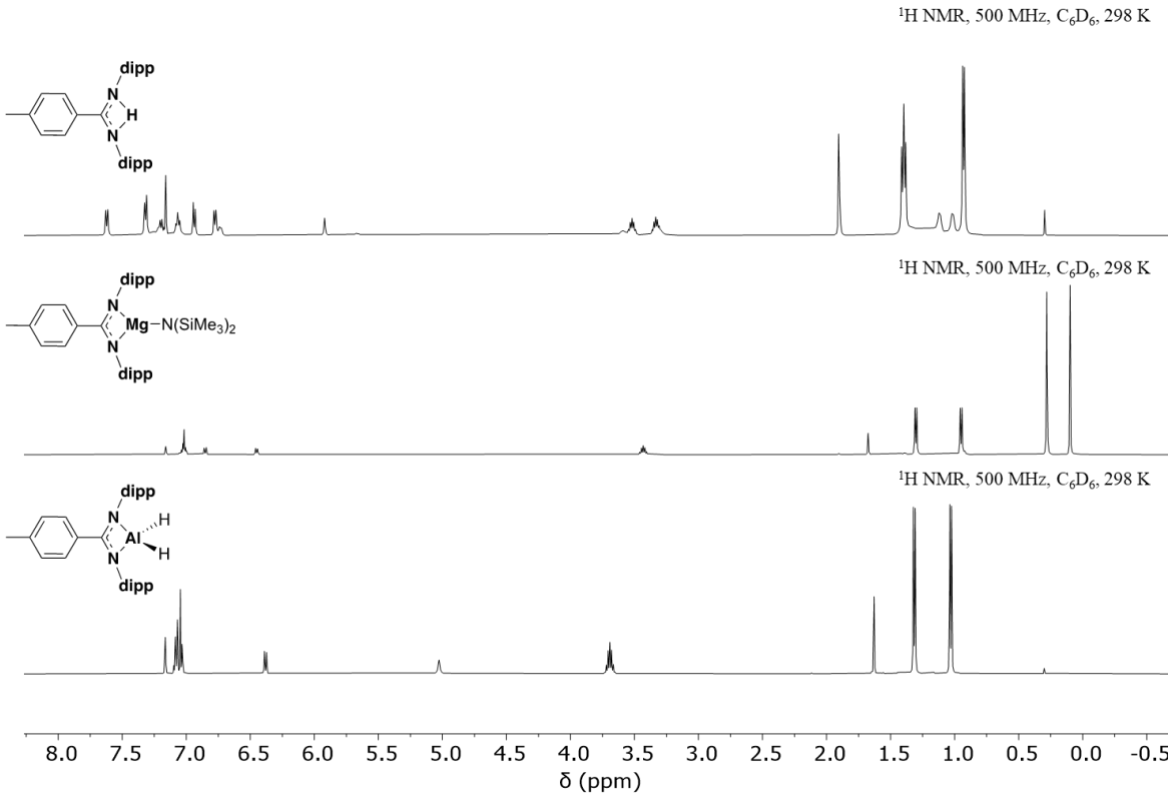

Figure 2.10: ^{1}H NMR spectra of **2.2** (top), bulky magnesium complex (middle) and **2.8** (bottom); all spectra recorded in benzene-d_6.

2.3.1 X-ray Crystal Structures of 2.9 and 2.10

Crystals of **2.9** suitable for X-ray diffraction were grown from a saturated solution of benzene-*d*$_6$. Complex **2.9** crystallised as a hydride bridged dimer in an orthorhombic Aea2 space group with two molecules of benzene in the unit cell (**Figure 2.11**). The hydride bridged dimer has two five-coordinate aluminium centres adopting square pyramidal geometries (τ=0.04) and is structurally similar to related bridged aluminium hydride compounds.[106,107] The Al-HA and Al-H bonds lie in the same plane but with a slight asymmetry, as is reflected in both the bond lengths (Al1-HA 1.64 Å, Al1-H 1.75 Å) and bond angles (Al1-HA-Al1 107.24°, Al1-H-Al1 97.75°). One phenyl group from each Ar* substituent lies in plane with the Al-H-Al-H bridged moiety but, with distances >4 Å, these are unlikely to afford any additional stabilisation to the complex. Selected key bond lengths and bond angles are shown in **Table 2.1**.

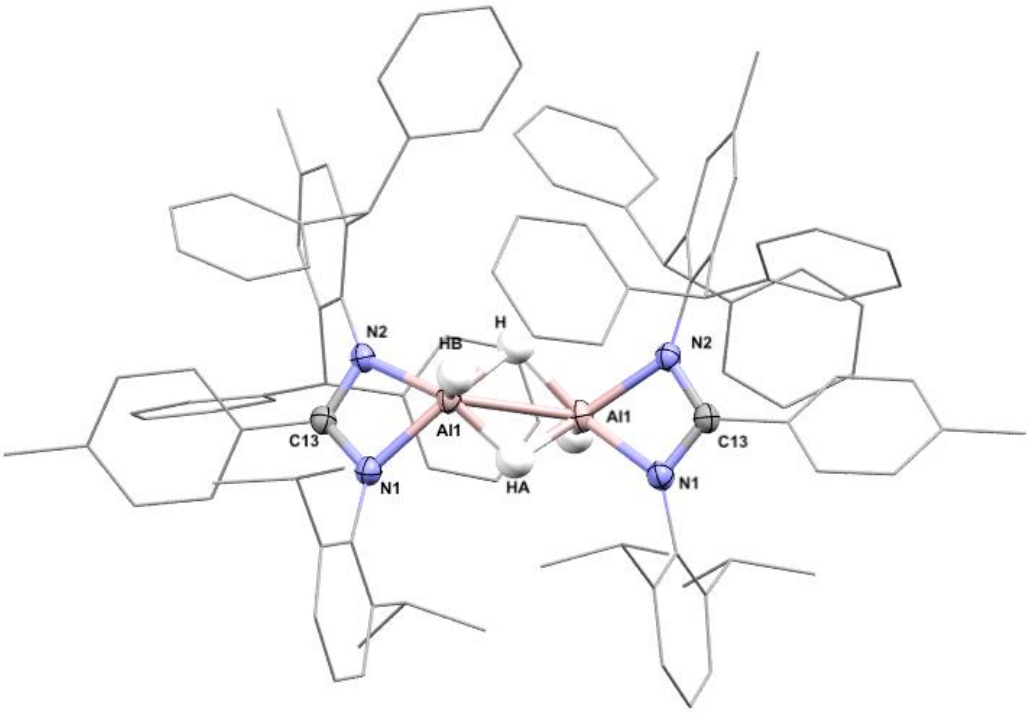

Figure 2.11: The X-ray crystal structure of **2.9**; some hydrogen atoms omitted for clarity.

Table 2.1: Selected bond lengths (Å) and angles (°) for complex **2.9**.

Bond Length		Bond Length		Bond Length	
Al1-N2	1.941(1)	Al1-HA	1.64	Al1-H	1.75
Al1-N1	1.961(2)	Al1-HB	1.43(2)		

Bond Angle	
HB-Al1-N1	109.0(1)
HB-Al1-N2	115.0(1)
Al1-HA-Al1	107.0
Al1-H-Al1	98.0
H-Al1-HA	107.0
HB-Al1-H	106.0

Complex **2.10** crystallised from a concentrated solution of benzene-d_6/hexane with a distorted tetrahedral geometry and in the $P\bar{1}$ space group (Z=2, **Figure 2.12**). The increased steric encumbrance of the bulky Ar* ligand allowed for the isolation of **2.10** as an unsupported monomer and is the first reported example of a monomeric aluminium dihydride bearing an amidinate ligand. The terminal Al–H bonds were found to be identical in length (1.46(2) Å), whilst the Al–N bonds were nearly identical in length (1.943(9)/1.939(9) Å), in direct contrast to the asymmetry of **2.9**. A stabilising interaction between the aluminium hydrides and two phenyl groups was observed, with through space phenyl…hydride interactions of ~ 3 Å

(**Figure 2.13**). Selected key bond lengths and bond angles are shown in **Table 2.2**. In the absence of crystallographic data for **2.8**, it is proposed this would dimerise in the solid state in a similar manner to **2.9**, owing to the smaller size of the ligand.

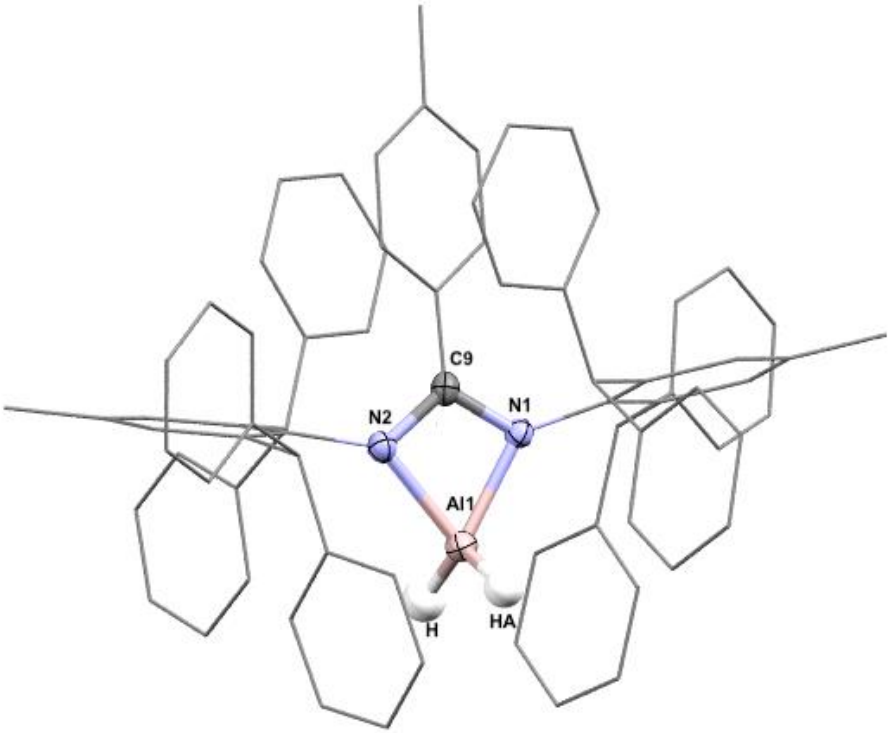

Figure 2.12: The X-ray structure of 2.10; hydrogen atoms omitted for clarity.

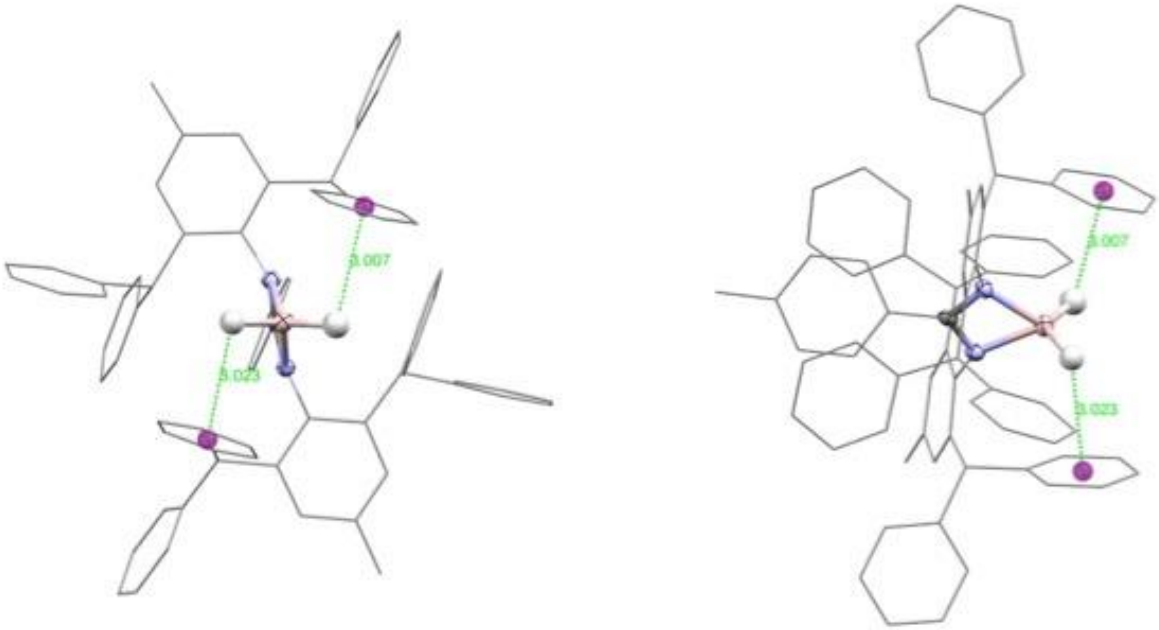

Figure 2.13: Through space phenyl...hydride interactions in 2.10.

Table 2.2: Selected bond lengths (Å) and angles (°) for complex 2.10.

Bond Length		Bond Length	
Al1-N2	1.939(9)	Al1-HA	1.46(2)
Al1-N3	1.943(9)	Al1-H	1.46(2)

Bond Angle	
N2-Al1-N3	68.4(4)
N2-Al1-H	108.0(7)
H-Al1-HA	121.0(1)
N3-Al1-HA	108.4(7)

2.4 Synthesis of Aluminium Hydride Complexes Bearing the 2,4,6-Trimethylphenyl Substituent

The reaction of ligands **2.2**, **2.6** and **2.7** with TMAA each resulted in the formation of a single aluminium dihydride compound (**2.8**-**2.10**, *vide supra*) with no further species isolated or identified. In contrast, preparative scale reactions of **2.5** with trimethylamine alane in toluene at room temperature repeatedly formed mixtures of aluminium hydride compounds that could not be separated through work up or recrystallisation techniques alone. Careful manipulation of the reaction conditions led to the isolation of compounds **2.11**-**2.13** (**Scheme 2.5**).

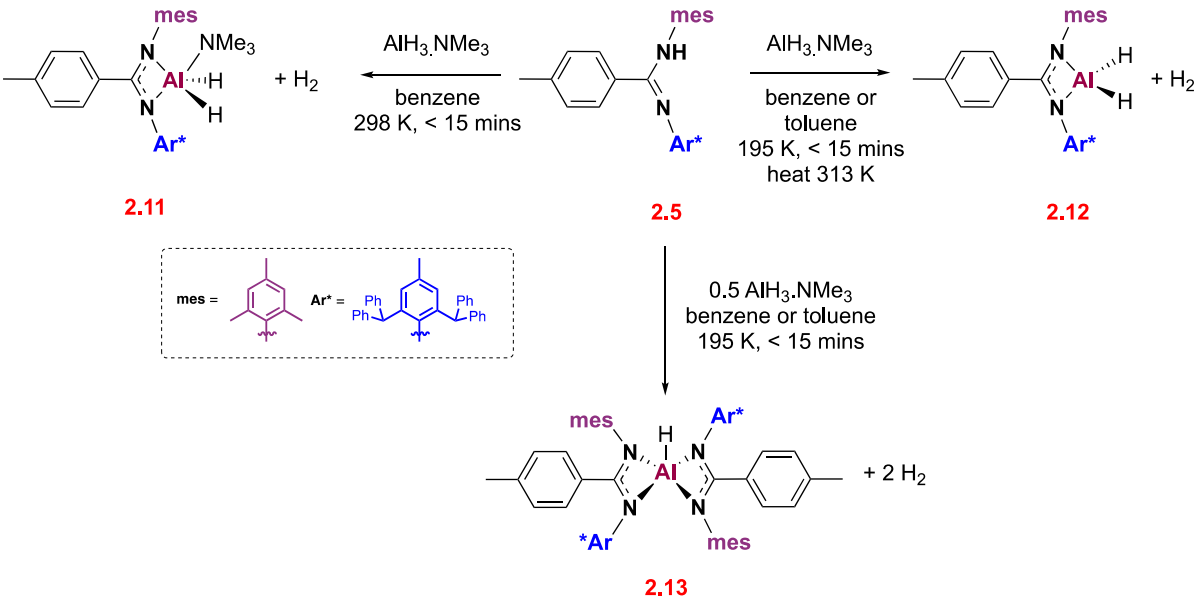

Scheme 2.5: Synthetic routes to structurally varied mes aluminium dihydride complexes **2.11**, **2.12** and **2.13**.

2.4.1 Synthesis and Characterisation of 2.11-2.13

On an NMR scale, one equivalent of **2.5** was added to 1.2 equivalents of trimethylamine alane in benzene-d_6 and transferred to a J Young NMR tube. Hydrogen gas was seen to evolve immediately. The crude ^{1}H NMR spectra showed both sharp (major product) and broad (minor product) singlets in the alkyl region (1.60-2.32 ppm), as well as sharp doublets and broad singlets in the aromatic region (5.91-6.34 ppm), suggesting that a mixture of structurally related products had formed. Owing to the broad nature of the spectrum, and the unidentified mixture of products, it was not possible to determine the ratios in which each compound had formed. Excess trimethylamine was observed at 2.01 ppm.

Recrystallisation in benzene-d_6/hexane and drying *in vacuo* yielded a clean NMR spectrum showing a single product only. A broad singlet at 4.54 ppm integrating to two protons was assigned as Al**H**$_2$. There were five singlets in the region 1.60-2.30 ppm; the singlet at 1.93 ppm integrating to nine protons indicates the presence of trimethylamine, and this upfield shift in resonance after recrystallisation indicates a degree of bonding to the Lewis acidic aluminium centre. The remaining singlets can all be assigned to alkyl groups on the ligand, with the singlet at 2.28 ppm (six protons) assigned to the *ortho* protons of the mes substituent.

Single crystal X-ray analysis was needed to fully elucidate the structure. Single crystals suitable for X-ray analysis were grown from a concentrated solution of benzene-d_6/hexane. It revealed **2.11** to be a monomeric aluminium dihydride that crystallised in the P-*1* space group (Z=2) with one molecule of trimethylamine datively bound to the aluminium centre, as is consistent with the ^{1}H NMR spectrum (**Figure Figure 2.14**). The NMe_3 group coordinates in the same plane as the amidinate nitrogen atom bearing the Ar* substituent (N1-Al1-N3 = 164.2(4)°) and lies almost orthogonal to the nitrogen atom of the mesityl substituent (N2-Al1-N3 = 98.5(4)°). Upon comparison to monomeric **2.10**, the Al-H bonds are elongated (Al-HA 1.47(2), Al-H 1.54(2) and this is attributed to the asymmetry induced by the trimethylamine group. The nitrogen atom of the amine substituent adopts a tetrahedral geometry, with all three C-N3-C bond angles falling in the range 107.1(1) - 109.1(1)°. Despite its larger ligand size, the dimeric solid-state structure of **2.9** suggests that the dative bonding of the trimethylamine group undoubtedly facilitates the formation of **2.11** as a monomeric species.

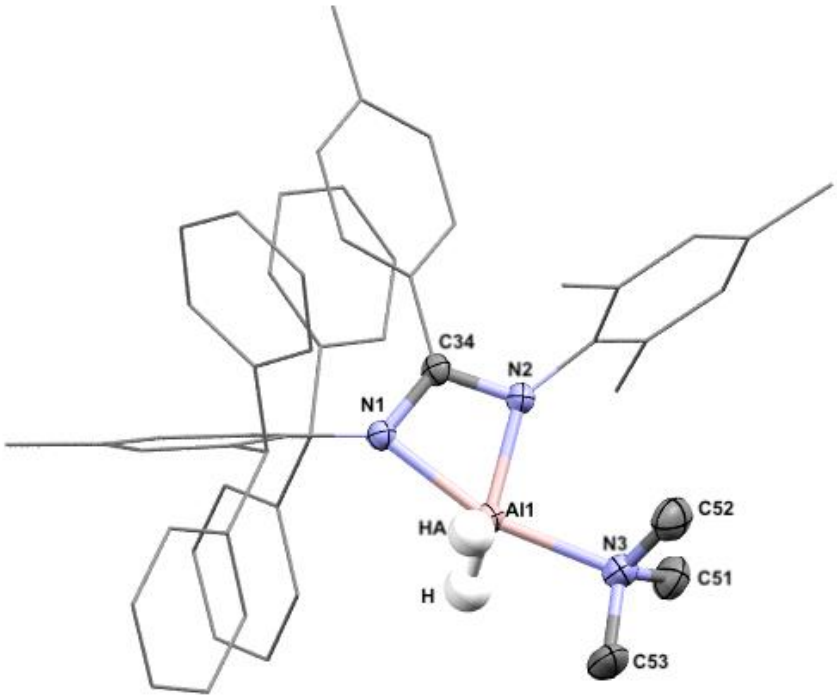

Figure 2.14: The X-ray structure of **2.11**; hydrogen atoms omitted for clarity.

To scale up the synthesis of **2.11**, multiple reaction conditions were tested. Variation of solvents, reagent stoichiometries, temperatures and recrystallisation conditions were all unsuccessful in isolating **2.11** as a single product and instead largely produced mixtures containing previously unidentified products. Trimethylamine resonances were not observed in any ^{1}H NMR spectra in the synthesis of **2.8**-**2.10**.

The amine-free analogue of the mes aluminium dihydride could be directly targeted by modifying the synthetic procedure. Compound **2.12** was synthesised by dropwise addition of a toluene solution of **2.5** at 195 K to a toluene solution of trimethylamine alane at 195 K. After removal of solvent, the crude reaction mixture was heated under vacuum at 313 K for 4 hours to eliminate the trimethylamine group and isolate **2.12** as a single product. In contrast to **2.11**, a shift in the Al**H**$_2$ resonance was observed (5.02 ppm) and only four singlets were present in the alkyl region of the ^{1}H NMR spectrum. The absence of a peak corresponding to the NMe$_3$ protons and all expected ligand resonances, in conjunction with X-ray crystallography, confirmed the synthesis of the amine-free analogue.

Single crystals of **2.12** were grown from benzene-d_6/hexane. Compound **2.12** crystallised as a hydride bridged dimer in the *C2/c* space group (**Figure 2.15**), with the C_2 axis lying between the two aluminium centres. The structure of **2.12** exhibited disorder and the mesityl group was found to be split over two positions which both had major (78.8%) and minor (21.2%) occupancy. Both terminal hydrides of **2.12** face in the same direction, in direct contrast to **2.9** and other structurally similar bridged aluminium hydride compounds.[97] The aluminium centres adopt square pyramidal geometries (τ=0.24) with highly contorted amidinate ligands (N2-Al1-HA 105.3(8)°, N1-Al1-H 122.0(8)°) on the opposite face to the terminal hydrides. The asymmetry of the bridging Al1-H bonds in **2.9** is also observed in **2.12**, but to a greater extent (Al-H 1.91(2) Å, 1.54(2) Å). The bond angles of the N^{Ar}-Al1-HB (**2.9,** Ar = Ar*, dipp) and N^{Ar}-Al1-HA (**2.12**, Ar = Ar*, mes) substituents are similar, and all angles are obtuse (**2.9**: N1-Al1-HB 109.0(1)°, N2-Al1-HB 115.1(1)°, **2.12**: see above). It is unsurprising that **2.12** crystallises as a dimer, owing to the smaller ligand size of the mes substituent and the reduced kinetic stabilisation afforded to the molecule in the absence of the trimethylamine moiety.

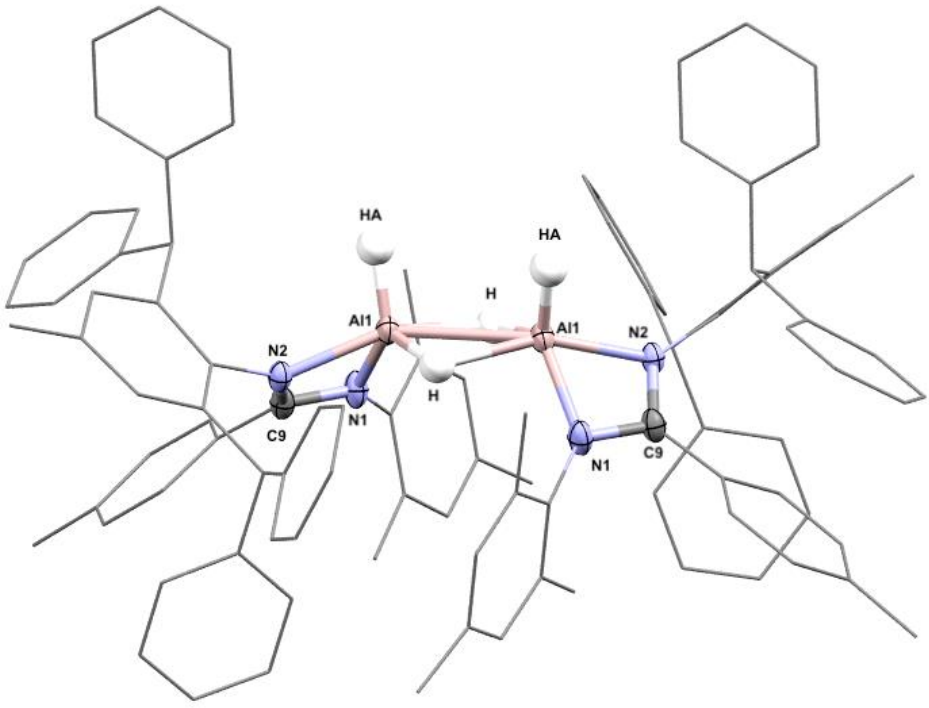

Figure 2.15: The X-ray structure of **2.12**.

A third species was also observed to be forming in the original NMR scale reactions and the targeted isolation of **2.12** did not account for the second product observed in the crude reaction mixture of **2.11**. This prompted the proposal that more than one ligand could be bound to the

aluminium centre as the formation of **2.11** gave some precedence for this. To explore this possibility, two equivalents of **2.5** (toluene, 195 K) were added dropwise to one equivalent of trimethylamine alane in toluene at 195 K. The solvent was removed *in vacuo* before washing with hexane and isolating the product as a white powder. The resultant ^{1}H NMR spectrum was broad, and all resonances were in good agreement with the minor product present in the crude reaction mixture of **2.11**. **Figure 2.16** shows a plot of the ^{1}H NMR spectra conducted at 298 K and 343 K. The broad nature of the spectrum at 298 K indicated the formation of a *bis*-ligated monomer, as this could be attributed to the steric crowding of the mes and Ar* substituents in close proximity around one aluminium centre. In contrast to compounds **2.8**-**2.12**, no Al**H** resonances were observed, however this was also noted for related *bis*-ligated aluminium hydride species.[108–110] Conducting the NMR at 343 K enhanced the resolution of the spectrum, and five singlets integrating to six protons each are observed. This suggests the ortho protons on the mes substituent were no longer chemically equivalent, owing to the strained and crowded nature of the proposed *bis*-ligated monomer.

As with **2.11**, X-ray analysis was required for full structure elucidation. Single crystals were grown from a concentrated solution of benzene-d_6/hexane and revealed the formation of **2.13** as a *bis*-ligated monomer. Compound **2.13** crystallised in the *C2/c* space group (Z=4), with the with the C_2 axis bisecting the Al-**H** bond (**Figure 2.17**). In contrast to **2.12**, **2.13** adopts a severely distorted trigonal pyramidal geometry (τ=0.68) as is observed with related *bis*-amidinate and guanidinate complexes.[108,111] The nitrogen atom bearing the Ar* substituent lies nearly orthogonal to the aluminium centre (H-Al1-N2 96.9°), whilst the mes-substituted nitrogen sits at a more obtuse angle (H-Al1-N1 117.3°) due to the distortion at the aluminium centre. The Al-N^{mes} and Al-N^{Ar*} bond lengths were also unsymmetrical, measuring 1.89(9) and 2.13(9) Å respectively. The terminal Al-H bond was freely located and measured and, at 1.46(2) Å, is the shortest Al-H bond of the mes-substituted compounds **2.11**-**2.13.** Selected bond lengths and angles of **2.11**-**2.13** are shown in **Table 2.3**.

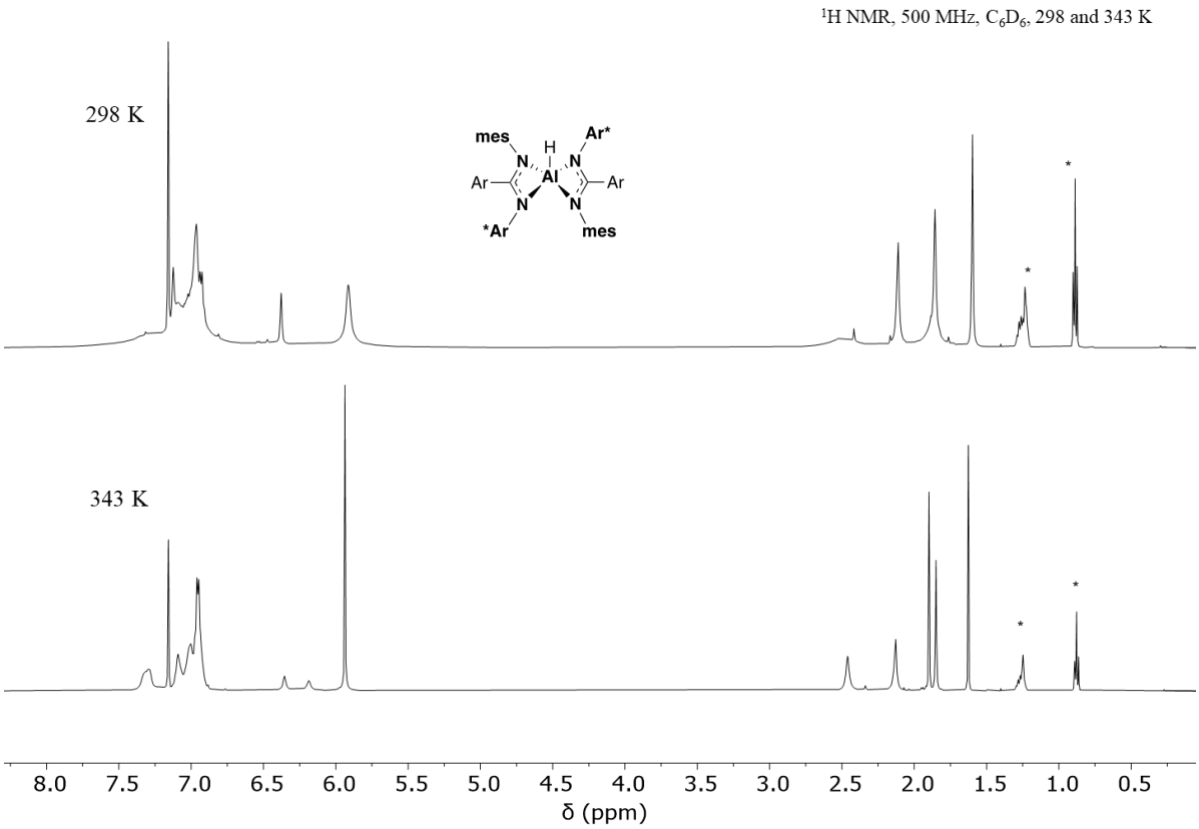

Figure 2.16: ^{1}H NMR spectrum of **2.13** at 298 K (top) and 343 K (bottom).

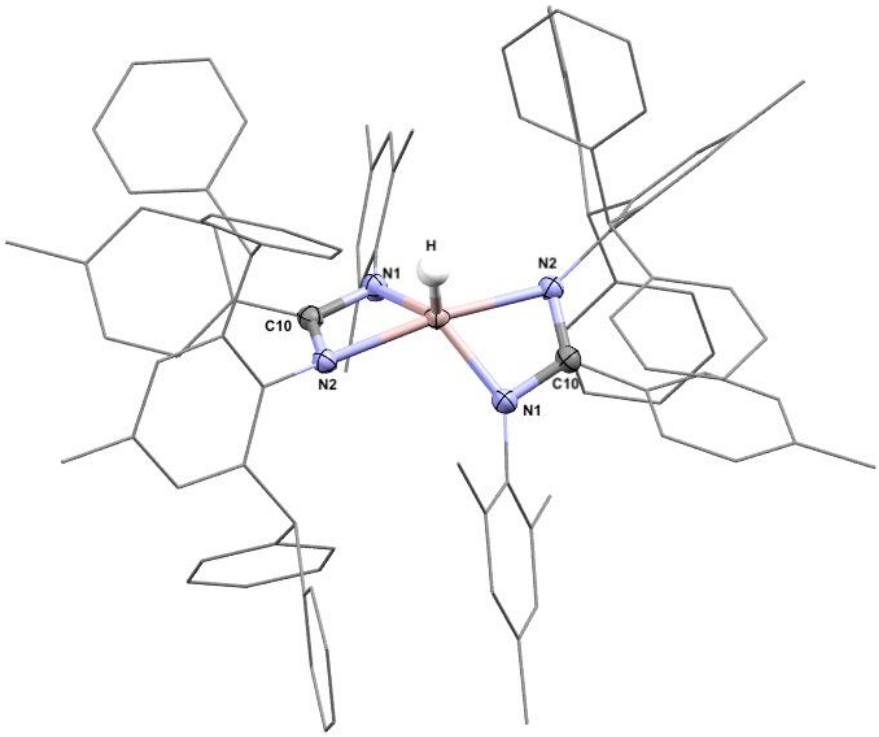

Figure 2.17: The X-ray structure of **2.13**; hydrogen atoms omitted for clarity.

Whilst *bis*- and even *tris*-amidinate complexes have been previously reported, the steric demands of the Ar* substituent are far greater than those reported in the literature.[112,113] Analogous complexes for ligands **2.6** and **2.7** were not observed. The smaller size of **2.5** afforded the formation of aluminium hydride derivates (**2.11**, **2.13**) that were not observed for ligands **2.6** and **2.7**. Reaction work-up conditions for **2.12** had to be manipulated to promote single product formation, whilst the increased size of **2.6** and **2.7** facilitated the formation of single products without competing reaction pathways.

The synthesis of a monomer, a dimer, and a *bis*-ligated monomer from the same starting ligand (**2.5**) highlights the variation in structures that can be isolated from an appropriately sized ligand and carefully selected reaction conditions. The isolation of pure samples of **2.11**-**2.13** was, in general, more difficult compared to **2.8**-**2.10**. Multiple attempts were often needed to isolate the products, and it was not possible to synthesise **2.11** on a preparative scale. Many reactions conducted at room temperature produced mixtures of **2.12**-**2.13** and, over time, the solution equilibrium shifted to favour the *bis*-ligated monomer; this indicates a degree of solution instability that was not observed for compounds **2.8**-**2.10**.

Table 2.3: Selected bond lengths (Å) and angles (°) for compounds **2.11**-**2.13**.

	2.11	**2.12**	**2.13**
Al1-N1	2.081(10)	1.894(13)	1.899(9)
Al1-N2	1.950(10)	1.987(12)	2.126(9)
Al1-N3	2.154(11)	-	-
Al1-H	1.54(2)	1.54(2)/1.90(2)	1.46
Al1-HA	1.47(2)	1.44(2)	-
N-C-N	110.1(1)	108.4(12)	111.2(9)
N-Al-N	65.66(4)	68.1(5)	66.25
H-Al-H	123.0(1)	75.0(1)	-

2.5 Synthesis of Alkyl Complexes 2.14-2.15

Expanding the scope of aluminium amidinate compounds, it was possible to synthesise the aluminium dimethyl compounds **2.14** and **2.15** *via* the reaction of amidine ligands **2.6** and **2.7** with 1.2 equivalents of trimethyl aluminium (**Scheme 2.6**) at 195 K.

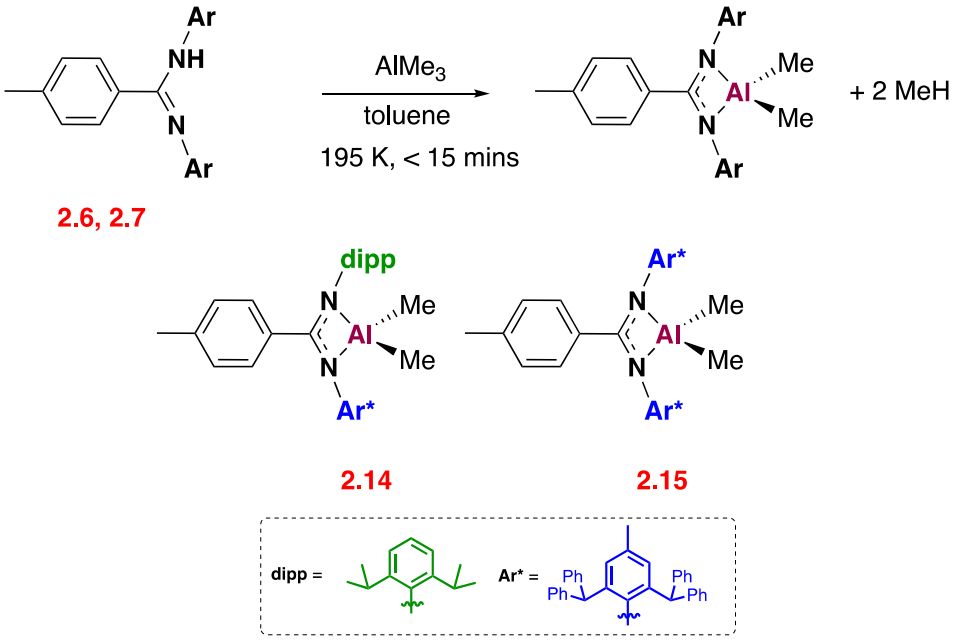

Scheme 2.6: General synthesis of aluminium dimethyl compounds 2.14 and 2.15.

Trimethyl aluminium was added dropwise to a solution of the relevant amidine ligand dissolved in toluene. Methane gas was seen to evolve, and the reaction was allowed to warm to room temperature before overnight stirring. Both compounds were isolated as white powders after washing with hexane. The ^{1}H NMR spectra of **2.14** and **2.15** revealed deprotonation of the starting ligand, in conjunction with a characteristic singlet below 0 ppm (six protons, **2.14**: -0.28 ppm, **2.15**: -0.88 ppm) indicative of coordination to a Lewis acidic aluminium centre. Attempts to synthesise an aluminium alkyl compound from **2.5** were unsuccessful. Multiple resonances were observed below 0 ppm and suggest that, as with the aluminium hydride compounds, a mixture of products had formed, and it was not possible to isolate a single product.

Single crystals suitable for X-ray diffraction were grown from hexane at 255 K. Compound **2.14** crystallised in the $P\bar{1}$ space group with one molecule of hexane in the unit cell. The aluminium centre adopts a distorted tetrahedral geometry. There was an asymmetry in the complex; the Al-N^{dipp} bond was shorter (1.943(1) Å) than the Al-N^{Ar*} bond (1.961(1) Å) whilst the Al-C^{Me} bonds were also asymmetric (Al1-C55 1.960(2) Å, Al1-C54 1.942(2) Å). Compared to the series of aluminium amidinate hydride compounds, the structure of **2.14** is fairly unremarkable and the bond lengths are in good agreement with reported literature structures.[114] Selected bond lengths and angles are shown in **Table 2.4**. In the absence of crystallographic data, it is anticipated **2.15** would be monomeric in the solid state.

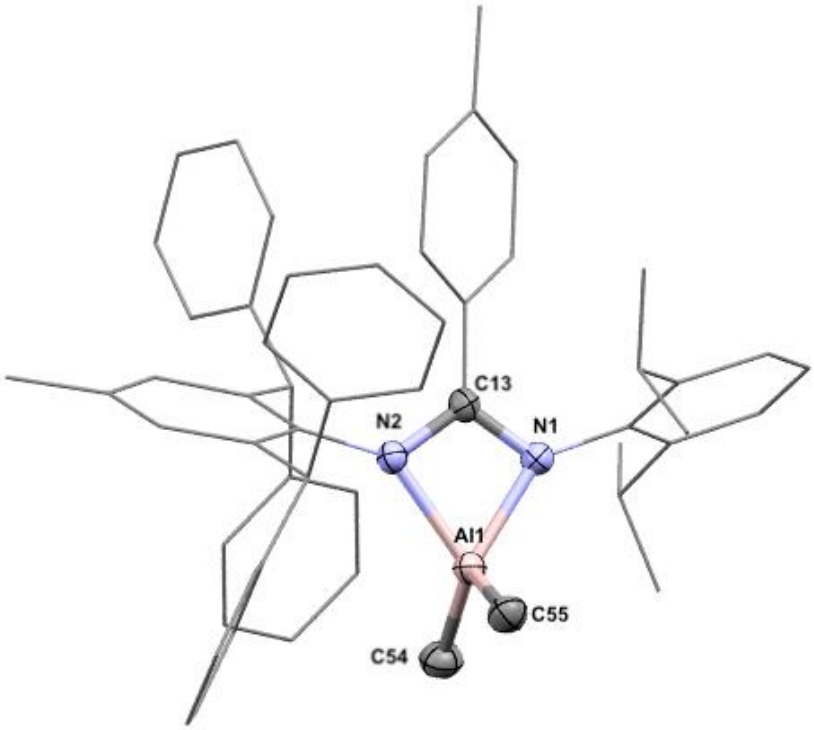

Figure 2.18: The X-ray structure of **2.14**; hydrogen atoms and hexane molecule omitted for clarity.

Table 2.4: Selected bond lengths (Å) and angles (°) for **2.14**.

Bond Length		Bond Length		Bond Length	
Al1-N1	1.943(1)	Al1-C54	1.942(2)	N1-C1	1.429(2)
Al1-N2	1.961(1)	Al1-C55	1.960(2)	N2-C21	1.424(2)

Bond Angle	
N1-Al1-N2	68.3(5)
N1-Al1-C55	112.6(7)
N2-Al1-C54	118.0(7)
C54-Al1-C55	117.0(8)

2.6 Solid State versus Solution State Characterisation

The synthesis of aluminium hydride and alkyl complexes **2.8**-**2.15** has demonstrated the versatility of this amidine ligand series, in particular a range of structural variation has been observed in solid state. However, the *in situ* reactivity of these complexes is governed by their solution state properties, and thus this has also be investigated. Upon inspection of the ^{1}H NMR spectra of **2.8**-**2.12**, it was not possible to draw any meaningful conclusions linking the structure of the complex to the resonance of the Al**H**$_2$ signal.

In order to better understand the nature of these complexes in solution we measured their molecular dimensions by diffusion-ordered NMR spectroscopy (DOSY). Molecules in solution not only tumble but diffuse/translate laterally over time. The rate constant for diffusion, also known as the self-diffusion coefficient (D) can be understood for a spherical molecule of hydrodynamic radius r_s, using the Stokes-Einstein relation:

$$D = \frac{k\mathrm{T}}{6\pi\eta r_s}$$

Where T is the absolute temperature and η is the viscosity of the solvent.

The DOSY technique is a two-dimensional NMR experiment that uses pulsed field gradients to label molecules at a different location in the tube. A second gradient pulse, that is applied after a variable time delay, generates a spin echo used to make visible those molecules that have not moved from their original location. Thus molecular diffusion results in progressive exponential attenuation of the signal as the variable delay is increased The output of the experiment is the normal 1D–^{1}H spectrum in the f2 direction and the log D along f1. The output of the experiment is a pseudo-2D spectrum with chemical shift on f2 axis and the log D along "f1".

Table 2.5 shows the calculated hydrodynamic radii for the species. It is assumed here that the molecules show similar departure from a sphere and that they have similar solvation shells allowing us to make direct comparisons of their relative dimensions.[115]

The monomeric dimethyl complexes **2.14** and **2.15** have hydrodynamic radii of 5.8 and 6.8 Å respectively. The stark increase in radius size between **2.14** and **2.15** highlights the large solution volume of the Ar* substituent compared to the dipp substituent and is also observed upon inspection of the calculated assumed spherical volumes: 820 Å^3 (**2.14**) and 1320 Å^3 (**2.15**). The hydrodynamic radii of these aluminium alkyl complexes are in good agreement with related literature compounds.[105,116,117]

Table 2.5: Comparison of AlH ^{1}H NMR resonances, diffusion coefficients, calculated hydrodynamic radii and calculated volume assuming a sphere for complexes **2.8**-**2.15**.

Compound	Al–H ^{1}H NMR shift	Diffusion Coefficient	Hydrodynamic Radius (Å)	Volume (Å)
2.8	5.06	7.3	5.0	520
2.9	4.77	5.6	6.5	1150
2.10	3.63	4.9	7.4	1700
2.11	4.54	5.4	6.7	1250
2.12	5.01	4.8	7.6	1840
2.14	-	6.3	5.8	820
2.15	-	5.3	6.8	1320

The aluminium dihydride complexes **2.9** and **2.10** are both larger than their monomeric aluminium alkyl counterparts, with hydrodynamic radii of 6.5 Å and 7.4 Å respectively. At 1.4x (**2.9**) and 1.3x (**2.10**) larger, this indicates a monomer-dimer equilibrium in solution that predominantly favours a monomeric structure but possesses a degree of dimerisation. The larger volume and radius of **2.11** (1250 Å^3, 6.7 Å) compared to **2.9** is attributed to the additional trimethylamine moiety, rather than exhibiting any dimeric character in solution (the trimethylamine group makes dimerisation unfavourable). Unsurprisingly, complex **2.8** was found to have the smallest radius across this series (5.0 Å) due to the absence of any sterically demanding Ar* substituents.

Interestingly, however, complex **2.12** was found to have the largest radius (7.6 Å) across the series despite the small size of the mes substituent and the absence of any trimethylamine groups, suggesting that it retains a greater degree of dimeric character in solution. DFT calculations were used to further probe the solution state stability of complexes **2.11** and **2.12** as a result of this preference to retain dimeric character in solution.[§] The calculated Gibbs free energies of **2.11**, **2.12** and **2.12-mono** support experimental observations and revealed it is most thermodynamically stable for **2.12** to exist in its dimeric form in solution (**Figure 2.19**).[**]

§ DFT calculations were performed by Dr Clare Bakewell.
** The calculations were performed by Dr Clare Bakewell at a C H N (6-31G**)/Al (SDDAll), ωB97X level of theory. Basis set and functional were benchmarked by comparison to the solid-state structure of **2.10**.

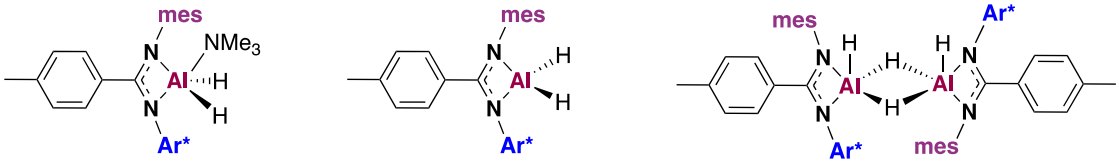

ΔG (kcal mol^{-1}):	-7.7	0	-13.5
	2.11	**2.12-mono**	**2.12**

Figure 2.19: Gibbs free energies of 2.11, 2.12-mono and 2.12.

2.7 Summary and Outlook

2.7.1 Summary

A series of amidine pro-ligands with variation in the R_1 and R_3 positions has been isolated and fully characterised. Upon reaction with aluminium reagents (trimethylamine alane, trimethyl aluminium) a series of novel aluminium hydride and alkyl complexes bearing amidine ligand backbones was synthesised. Compounds **2.8**-**2.15** were isolated and fully characterised, with both the solid- and solution-state structures investigated. Complexes **2.10**-**2.11** and **2.13**-**2.14** were isolated as monomers in the solid-state, whilst **2.9** and **2.12** existed as hydride bridged dimers. Where crystallographic data was unavailable, the solid-state structure was predicted based on observations across the rest of the series. As such, it is anticipated that **2.8** would crystallise as a hydride bridged dimer akin to **2.9**/**2.12**, whereas **2.15** would crystallise as a monomer in the solid state, similar to **2.10**/**2.14**. Investigations into the solution-state properties of **2.8**-**2.15** revealed a general link between the size of the pro-ligand and the resultant complex in solution. Where complexes were found to deviate from this trend, DFT calculations were used to attribute this to the increased stability of dimeric (*versus* monomeric) structures in solution.

2.7.2 Outlook

Complexes **2.9**, **2.11** and **2.12** are the first examples of aluminium hydride complexes bearing asymmetric amidine ligands. Investigations into the solid- and solution-state properties of this rare series of structurally distinct aluminium complexes present interesting findings and can be used selectively when investigating any potential applications of these complexes. In this thesis, these applications are for catalytic processes and for the synthesis of low oxidation state aluminium complexes.

The remainder of this thesis will focus on the reactivity and applications of this series of complexes. It has been widely established in recent years that aluminium hydride and alkyl complexes are proficient catalysts for a number of synthetically useful reactions. As such, investigations into the catalytic activity of **2.8**-**2.15** (excluding **2.11** and **2.13**) for the reaction of the hydroboration of phenylacetylene were conducted (see Chapter 3). The mechanistic activity of this novel series of complexes was compared to literature aluminium catalysts through detailed kinetic investigations and exploration of their stoichiometric reactivity.

This family of complexes could easily be expanded by altering groups in the R_1 and R_3 positions with both smaller and larger aryl substituents, prompting further investigation into their solid and solution state properties.

2.8 Chapter 2 Experimental Section

2.8.1 General Materials and Methods for All Chapters

Ligand synthesis was carried out using standard organic chemistry techniques. All other reactions were carried out using standard Schlenk techniques under an argon atmosphere or using a nitrogen filled glovebox. All reagents were obtained from commercial sources. Benzhydrol, 2,6-diisopropylaniline, trimethyl aluminium (2M in toluene) and lithium aluminium hydride (4M in ether) were obtained from Sigma. *Para*-toluoyl chloride and 2,4,6-trimethylaniline were obtained from Fischer Scientific Ltd. Benzaldehyde and phenylacetylene were purchased from Sigma and distilled using CaH_2. 4,4,5,5,-Tetramethyl-1,3,2-dioxaborolane (HBpin) was purchased from Sigma and used without further purification.

Dry solvents were obtained from a Grubbs solvent purification system and stored under nitrogen over activated 3/4 Å molecular sieves. Benzene-d_6 was obtained from Sigma, dried and degassed and stored under nitrogen over activated 3/4 Å molecular sieves. NMR-scale reactions were conducted in J Young NMR tubes and were prepared in a glovebox; all heating of NMR tubes was done in a DrySyn NMR tube heating block at the temperature stated.

Nuclear magnetic resonance (NMR) spectra were recorded on a Bruker Avance 500 spectrometer operating at 500 MHz for ^{1}H NMR and 125 MHz for $^{13}C\{^{1}H\}$ spectra. Solvent peaks were used as internal references for ^{1}H and ^{13}C chemical shifts ppm. When required, spectra were recorded on Bruker Avance III 300, 400 or 600 MHz spectrometers. Spectra were processed and analysed using Mestrenova software. Elemental analyses were determined Elemental Microanalysis Ltd, Hameldown Road, Okehampton Business Park, Exeter Road, Devon, EX20 1UB.

Pro-ligand synthesis:

In the experimental and NMR data below, the following notations correspond to the following ligand moieties: Am = amidinate backbone, BDI = β-diketiminate backbone, L = *p*-toluidine backbone, *mes* = 2,4,6-trimethylphenyl substituent, *dipp* = 2,6-diisopropylphenyl substituent, *Ar** = 2,6-diphenylmethyl-4-methylphenyl substituent, *dep* = 2,6-diethylphenyl, *Ph* = aromatic protons. Italicised *o*, *m*, *p* refers to ortho, meta and para positions, respectively.

2.8.2 Synthesis of $Ar^{dipp}NH(CO)L$ (2.1)

2,6-Diisopropylaniline (13.6 mmol, 2.5 mL), *para*-toluoyl chloride (13.6 mmol, 2.11 g) and NEt_3 (11.0 mmol, 1.55 mL) were dissolved in DCM and stirred at 298 K for 48 h. The product

was washed with Na_2CO_3 (3 x 100 mL) and dried ($MgSO_4$). The solvent was removed *in vacuo* and the resultant amide was isolated as a white powder. Recrystallised in DCM. (2.94 g, 77%).

^{1}H NMR (500 MHz, $CDCl_3$, 298K) δ ppm: 1.20 (d, 12H, $CH(C\mathbf{H}_3)_2$, $^3J_{HH}$ = 6.9 Hz), 2.44 (s, 3H, $^L C\mathbf{H}_3$), 3.14 (sept, 4H, $C\mathbf{H}(CH_3)_2$, $^3J_{HH}$ = 6.9 Hz), 7.22 (d, 2H, ^{dipp}*m*-C**H**, $^3J_{HH}$ = 7.7 Hz), 7.27 (d, 2H ^{L}*o*-C**H**, $^3J_{HH}$ = 7.6 Hz), 7.35 (m, 1H, ^{dipp}*p*-C**H**,), 7.81 (d, 2H, ^{L}*m*-C**H**, $^3J_{HH}$ = 6.5 Hz); $^{13}C\{^1H\}$ NMR (125 MHz, $CDCl_3$, 298K) δ ppm: 21.6 (**C**H_3), 23.8 (**C**H_3), 29.1 (**C**H_3), 123.6 (^{dipp}*m*-**C**H), 127.4 (^{L}*m*-**C**H), 128.5 (^{dipp}*p*-**C**H), 129.5 (^{L}*o*-**C**H), 131.5 (**C**^{IV}), 131.8 (**C**^{IV}), 142.3 (**C**^{IV}), 146.6 (**C**^{IV}), 167.0 (**C**^{IV}).

2.8.3 Synthesis of $Ar^{dipp}Ar^{dipp}AmH$ (2.2)

$Ar^{dipp}NH(CO)L$ (**2.1**, 6.78 mmol, 2.0 g) and PCl_5 (8.13 mmol, 1.69 g) were dissolved in toluene under an inert atmosphere and heated at reflux overnight. The solvent was removed *in vacuo* and the reaction mixture was heated at 423 K for 1 hour. The r2100esultant imidoyl chloride was dissolved in toluene, 2,6-diisopropylaniline (6.78 mmol, 1.27 mL) and NEt_3 (8.08 mmol, 1.22 mL) were added and heated at reflux for 48 h. The product was extracted with toluene/ether, washed (1 x $NaHCO_3$, 2 x H_2O), dried ($MgSO_4$) and the solvent removed *in vacuo*. Recrystallised in ethanol. (0.84 g, 27 %). ^{1}H NMR data matched that reported in the literature.[105]

^{1}H NMR (400 MHz, $CDCl_3$, 298K) δ ppm: 0.84 (d, 6H, $CH(CH_3)_2$, $^3J_{HH}$ = 6.4 Hz), 0.95 (d, 6H, $CH(C\mathbf{H}_3)_2$, $^3J_{HH}$ = 6.4 Hz), 1.19 (d, 6H, $CH(C\mathbf{H}_3)_2$, $^3J_{HH}$ = 6.8 Hz), 1.31 (d, 6H, $CH(C\mathbf{H}_3)_2$, $^3J_{HH}$ = 7.2 Hz), 2.24 (s, 3H, $^L CH_3$), 3.17 (m, 4H, $CH(CH_3)_2$), 5.63 (s, 1H, NH), 6.95 – 7.25 (m, 10H, ^{Ph}CH). Anal. Calc. ($C_{32}H_{42}N_2$): C, 84.53; H, 9.31; N, 6.16. Found: C, 83.70; H, 9.30; and N, 6.11.

2.8.4 Synthesis of Ar^*NH_2 (2.3)

Para-toluidine (40 mmol, 4.36 g) and benzhydrol (80 mmol, 15.0 g) were heated to a melt (150 °C). A solution of $ZnCl_2$ (20 mmol, 2.71 g) in hydrochloric acid (12 M, 3 mL) was added dropwise and the reaction was heated at reflux (433 K) for 3 h, then allowed to cool to 298 K. The product was dissolved in DCM and washed with ammonium chloride (NH_4Cl) solution and then brine. The product was dried ($NaHCO_3$, silica gel), filtered and the solvent removed

in vacuo, before washing with minimum amounts of ethyl acetate, to yield the product as a white powder. (9.0 g, 59%). ^{1}H NMR data matched that reported in the literature.[118]
^{1}H NMR: (400 MHz, CDCl3, 298K) δ ppm: 2.04 (s, 3H, C**H**$_3$), 3.29 (s, 2H, C**H**(Ph)$_2$), 5.47 (s, 2H, N**H**2), 6.40 (s, 2H, C**H**(Ph)$_2$), 7.11-7.32 (m, 20H, ^{Ph}C**H**).

2.8.5 Synthesis of Ar*NH(CO)L (2.4)

Ar*NH$_2$ (**2.3** 13.6 mmol, 6.0 g), *para*-toluoyl chloride (13.6 mmol, 2.11 g) and NEt$_3$ (11.0 mmol, 1.55 mL) were dissolved in DCM and stirred at 298 K for 48 h. The product was washed with Na$_2$CO$_3$ (3 x 100 mL) and dried (MgSO$_4$). The solvent was removed *in vacuo* and the resultant amide was isolated as a white powder. (6.46 g, 84 %).

^{1}H NMR: (500 MHz, CDCl$_3$, 298K) δ ppm: 2.15 (s, 3H, ^{Ar*}C**H**$_3$), 2.36 (s, 3H, ^{L}C**H**$_3$), 5.62 (s, 2H, ^{Ar*}C**H**), 6.39, (s, 1H, N**H**), 6.59 (s, 2H, C**H**(Ph)$_2$), 7.01-7.28 (m, 24H, ^{Ph}C**H**); ^{13}C{^{1}H} NMR (125 MHz, CDCl$_3$, 298K) δ ppm: 21.5 (^{L}**C**CH$_3$), 21.8 (^{Ar*}C**H**$_3$), 52.7 (^{Ar*}**C**H), 126.5 (^{Ph}**C**H), 126.8 (^{Ph}**C**H), 128.4 (^{Ph}**C**H), 129.2 (^{Ph}**C**H), 129.5 (**C**^{IV}), 137.2 (**C**^{IV}), 142.2 (**C**^{IV}), 142.4 (**C**^{IV}), 143.2 (**C**^{IV}).

2.8.6 Synthesis of Ar*Ar^{mes}AmH (2.5)

Ar*NH(CO)L (**2.4**, 4.48 mmol, 2.50 g) and PCl$_5$ (5.38 mmol, 1.12 g) were dissolved in toluene under an inert atmosphere and heated at reflux overnight. The solvent was removed *in vacuo* and the reaction mixture was heated at 423 K for 1 hour. The resultant imidoyl chloride was dissolved in toluene, 2,4,6-trimethylaniline (4.48 mmol, 0.63 mL) and NEt$_3$ (5.82 mmol, 0.80 mL) were added and heated at reflux for 48 h. The product was extracted with toluene/ether, washed (1 x NaHCO$_3$, 2 x H$_2$O), dried (MgSO$_4$) and the solvent removed *in vacuo*. Recrystallised in hot methanol. (1.30 g, 44 %).

^{1}H NMR (500 MHz, CDCl$_3$, 298K) δ ppm: 2.13 – 2.20 (m, 15H, C**H**$_3$), 4.75 (s, 1H, N**H**), 6.06 (s, 2H, C**H**(Ph)$_2$), 6.56 (s, 2H, ^{mes}*m*-C**H**), 6.69 (s, 2H, ^{Ph}C**H**), 6.73 (d, 2H, ^{L}*m*-C**H**, $^{3}J_{HH}$ = 7.5 Hz), 6.82 (d, 2H, C^{B}**H**, $^{3}J_{HH}$ = 7 Hz), 6.97 (br s, 4H, ^{Ph}C**H**), 7.15 (br s, 14H, ^{Ph}C**H**); ^{1}H NMR (125 MHz, CDCl$_3$, 333K): 2.22 (s, 6H, ^{mes}*m*-C**H**$_3$) 2.28 (s, 3H, ^{L}C**H**$_3$), 2.34 (s, 3H, C**H**$_3$), 2.46 (s, 3H, ^{Ph}C**H**$_3$), 4.84 (s, 1H, N**H**), 6.08 (s, 2H, C**H**(Ph)$_2$), 6.89 (s, 2H, ^{mes}*m*-C**H**), 6.77 – 7.28 (m, 25H, ^{Ph}C**H**); ^{13}C{1H} NMR (500 MHz, CDCl$_3$, 298K) δ ppm: 19.6 (**C**H$_3$), 20.8 (**C**H$_3$), 21.4 (**C**H$_3$), 21.9 (^{Ph}**C**H$_3$), 52.6 (**C**H(Ph)$_2$), 126.3 (^{Ph}**C**H), 126.8 (^{Ph}**C**H), 128.3 (^{Ph}**C**H), 128.8

(^{Ph}**C**H), 129.0 (^{Ph}**C**H), 129.5 (^{Ph}**C**H), 130.1 (^{Ph}**C**H), 134.3 (C^{IV}), 136.6 (C^{IV}), 139.1 (C^{IV}), 143.3 (C^{IV}), 143.6 (C^{IV}), 143.9 (C^{IV}), 146.1 (C^{IV}). Anal. Calc. ($C_{50}H_{46}N_2$): C, 88.98; H, 6.87; N, 4.15. Found: C, 88.30; H, 6.89; and N, 4.16.

2.8.7 Synthesis of Ar*Ar^{dipp}AmH (2.6)

Ar*NH(CO)L (**2.4**, 8.96 mmol, 5.0 g) and PCl_5 (10.75 mmol, 2.24 g) were dissolved in toluene under an inert atmosphere and heated at reflux overnight. The solvent was removed *in vacuo* and the reaction mixture was heated at 423 K for 1 h. The resultant imidoyl chloride was dissolved in toluene, 2,6-diisopropylaniline (8.96 mmol, 1.6 mL) and NEt_3 (11.65 mmol, 1.6 mL) were added and heated at reflux for 48 h. The product was extracted with toluene/ether, washed (1 x $NaHCO_3$, 2 x H_2O), dried ($MgSO_4$) and the solvent removed *in vacuo*. Recrystallised in hot methanol. (4.21 g. 62%).

^{1}H NMR (500 MHz, $CDCl_3$, 298K) δ ppm: 0.81 (d, 6H, CH(C**H**$_3$)$_2$, $^3J_{HH}$ = 6.5 Hz), 1.11 (d, 6H, CH(C**H**$_3$)$_2$, $^3J_{HH}$ = 6.5 Hz), 2.15 (s, 3H, ^{Ar*}C**H**$_3$), 2.19 (s, 3H, ^{L}C**H**$_3$), 3.30 (sept, 2H, C**H**(CH$_3$)$_2$, $^3J_{HH}$ = 6 Hz), 4.75 (s, 1H, N**H**), 5.92 (s, 2H, C**H**(Ph)$_2$), 6.50 (d, 2H, ^{L}*o*-C**H**, $^3J_{HH}$ = 7 Hz), 6.55 (s, 2H, ^{Ar*}*m*-C**H**), 6.79 (d, 2H, ^{L}*m*-C**H**, $^3J_{HH}$ = 7 Hz), 6.93– 7.15 (m, 21H, ^{Ph}C**H**); ^{13}C{1H} NMR (125 MHz, $CDCl_3$, 298K) δ ppm: 21.3 (^{L}**C**H$_3$), 21.8 (^{Ar*}**C**H$_3$), 22.9 (CH(**C**H$_3$)$_2$), 24.6 (CH(**C**H$_3$)$_2$), 28.5 (**C**H(CH$_3$)$_2$), 52.8 (**C**H(Ph)$_2$), 122.1 (C^{IV}), 122.9 (^{Ph}**C**H), 126.3 (C^{IV}), 127.6 (C^{IV}), 128.2 (^{L}*o*-**C**H), 128.5 (^{L}*m*-**C**H), 128.7 (^{Ph}**C**H), 129.0 (^{Ar*}*mes*-**C**H), 129.4 (C^{IV}), 130.1 (C^{IV}), 134.8 (C^{IV}), 136.3 (C^{IV}), 143.2 (C^{IV}), 143.5 (C^{IV}), 143.8 (C^{IV}). Anal. Calc. ($C_{53}H_{52}N_2$): C, 88.78; H, 7.31; N, 3.91. Found: C, 87.24; H, 7.31; and N, 3.92.

2.8.8 Synthesis of Ar*Ar*AmH (2.7)

Ar*NH(CO)L (**2.4**, 6.7 mmol, 3.5 g) and PCl_5 (8.0 mmol, 1.67 g) were dissolved in toluene under an inert atmosphere and heated at reflux overnight. The solvent was removed *in vacuo* and the reaction mixture was heated at 423 K for 1 hour. The resultant imidoyl chloride was dissolved in toluene and Ar*NH_2 (**2.3**, 6.0 mmol, 2.64 g) was added. The reaction was heated at reflux for 96 h. NEt_3 (8.7 mmol, 1.21 mL) was added and heated at reflux for a further 2 h. The product was solubilised in toluene, washed (1 x $NaHCO_3$, 2 x H_2O), dried ($MgSO_4$) and the solvent was removed *in vacuo.* Recrystallised from methanol/DCM. (3.35 g, 51%).

^{1}H NMR (500 MHz, C_6D_6, 298 K) δ (ppm): 1.88 (s, 6H, ^{Ar*}C**H**$_3$), 1.91 (s, 3H, C**H**$_3$), 5.25 (s, 1H, N**H**), 6.20 (d, 2H, ^{L}*o*-C**H**, $^{3}J_{HH}$ = 7 Hz), 6.36 (d, 4H, ^{Ph}*o*-C**H**, $^{3}J_{HH}$ = 22 Hz), 6.67 (d, 2H, ^{L}*m*-C**H**, $^{3}J_{HH}$ = 4.5 Hz); ^{13}C{^{1}H} NMR (125 MHz, C_6D_6, 298 K) δ ppm: 21.2 (^{Ar*}**C**H), 51.7 (^{Ph}**C**H), 53.5 (^{Ph}**C**H), 125.7 (^{Ph}**C**H), 126.4 (^{Ph}**C**H), 128.9 (^{L}*o*-**C**H), 127.1 (^{L}*m*-**C**H), 129.3 (^{Ph}**C**H), 129.8 (^{Ph}**C**H), 130.1 (**C**^{IV}), 130.4 (**C**^{IV}), 134.7 (**C**^{IV}), 138.4 (**C**^{IV}), 143.1 (**C**^{IV}), 143.7 (**C**^{IV}), 144.1 (**C**^{IV}), 145.9 (**C**^{IV}). Anal. Calc. ($C_{74}H_{62}N_2$): C, 90.76; H, 6.38; N, 2.86. Found: C, 89.51L H, 6.43; and N, 2.88.

2.8.9 Synthesis of [AlH$_2$(Ar^{dipp}Ar^{dipp}Am)] (2.8)

A solution of Ar^{dipp}Ar^{dipp}AmH (**2.2**, 0.4 mmol, 200 mg) dissolved in toluene (7 mL) was added dropwise at -78 °C to a solution of trimethylamine alane (57 mmol, 51 mg) in toluene (7 mL) at -78 °C. Hydrogen gas was seen to evolve, and the reaction was stirred for 1 hour at 298 K. The solvent was removed *in vacuo* before the product was extracted into hexane (2 x 10 mL) and filtered. The solvent was removed *in vacuo* and the product isolated as a white solid (94 mg, 42 %).

^{1}H NMR (500 MHz, C_6D_6, 298 K) δ ppm: 1.03 (d, 12H, CH(C**H**$_3$)$_2$, $^{3}J_{HH}$ = 6.5 Hz), 1.31 (d. 6H, CH(C**H**$_3$)$_2$, $^{3}J_{HH}$ = 7.0 Hz), 1.63 (s, 3H, ^{L}C**H**$_3$), 3.67 (sept, 4H, C**H**(CH$_3$)$_2$, $^{3}J_{HH}$ = 7.0 Hz), 5.06 (s, 2H, Al**H**$_2$), 6.38 (d, 2H, ^{L}*o*-CH, $^{3}J_{HH}$ = 8.5 Hz), 7.03 - 7.08 (m, 8H, ^{Ph}C**H**); ^{13}C{^{1}H} NMR (125 MHz, C_6D_6, 298 K) δ ppm: 21.2 (^{L}**C**H$_3$), 22.4 (CH(**C**H$_3$)$_2$), 25.9 (CH(**C**H$_3$)$_2$), 29.3 (**C**H(CH$_3$)$_2$), 123.4 (^{Ph}**C**H), 123.9 (^{Ph}**C**H), 126.0 (^{Ph}**C**H), 128.6 (^{L}*o*-**C**H), 129.9 (^{Ph}**C**H), 138.7 (**C**^{IV}), 141.3 (**C**^{IV}), 143.5 (**C**^{IV}). Anal. Calc. ($C_{32}H_{43}N_2Al$): C, 79.63; H, 8.98; and N, 5.80. Found: C, 79.57; H, 9.08; and N, 5.85.

2.8.10 Synthesis of [AlH$_2$(Ar*Ar^{dipp}Am)] (2.9)

NMR Scale: To a solution of trimethylamine alane (0.0279 mmol, 2.5 mg) dissolved in benzene-*d*$_6$, Ar*Ar^{dipp}AmH (**2.6**, 0.0279 mmol, 20 mg) was added and the solution was transferred to a J Young NMR tube. H_2 gas was seen to evolve.

Preparative Scale: A solution of Ar*Ar^{dipp}AmH (**2.6**, 0.279 mmol, 200 mg) dissolved in toluene (7 mL) was added dropwise at 195 K to a solution of trimethylamine alane (0.297 mmol, 25 mg) in toluene (7 mL) at 195 K. Hydrogen gas was seen to evolve, and the reaction was stirred for 1 hour at 298 K. The solvent was removed *in vacuo* and single crystals suitable for X-ray analysis were grown from benzene-*d*$_6$ at 298 K. (75 mg, 36%).

^{1}H NMR (500 MHz, C_6D_6, 298 K) δ ppm: 0.79 (d, 6H, CH(C**H**$_3$)$_2$, $^{3}J_{HH}$ = 6.5 Hz), 1.26 (d, 6H, CH(C**H**$_3$)$_2$, $^{3}J_{HH}$ = 6.5 Hz), 1.69 (s, 3H, ^{L}C**H**$_3$), 1.86 (s, 3H, ^{Ar*}C**H**$_3$), 3.52 (sept, 2H, C**H**(CH$_3$)$_2$, $^{3}J_{HH}$ = 6.5 Hz), 6.13 (d, 2H, ^{L}*o*-C**H**, $^{3}J_{HH}$ = 8 Hz), 6.53 (d, 2H, ^{L}*m*-C**H**, $^{3}J_{HH}$ = 7.5 Hz), 6.79 (s, 2H, C**H**(Ph)$_2$), 6.98 – 7.14 (m, 21 H, ^{Ph}C**H**), 7.47 (d, 4H, ^{Ph}C**H**, $^{3}J_{HH}$ = 7.5 Hz); ^{13}C{^{1}H} NMR (125 MHz, C_6D_6, 298 K) δ ppm: 21.3 (^{Ar*}**C**H$_3$), 21.6 (^{L}**C**H$_3$), 23.7 (CH(**C**H$_3$)$_2$), 25.4 (CH(**C**H-$_3$)$_2$), 28.1 (**C**H(CH$_3$)$_2$), 51.5 (**C**H(Ph)$_2$), 124.6 (^{Ph}**C**H), 128.4 (^{L}*o*-**C**H), 128.5 (^{Ph}**C**H), 128.8 (^{Ph}**C**H), 129.7 (^{Ph}**C**H), 129.8 (^{L}*m*-**C**H), 130.8 (^{Ph}**C**H), 130.0 (**C**^{IV}), 130.2 (**C**^{IV}), 133.2 (**C**^{IV}), 138.9 (**C**^{IV}), 143.6 (**C**^{IV}), 144.3 (**C**^{IV}), 146.1 (**C**^{IV}). Anal. Calc. ($C_{53}H_{53}N_2Al$): C, 84.42; H, 7.53; and N,4.10. Found: C, 83.67; H, 7.07; and N, 3.76.

2.8.11 Synthesis of [AlH$_2$(Ar*Ar*Am)] (2.10)

NMR Scale: To a solution of trimethylamine alane (0.0279 mmol, 2.5 mg) dissolved in benzene-*d*$_6$, Ar*Ar*AmH (**2.7** 0.0279 mmol, 27 mg) was added, and the solution was transferred to a J Young NMR tube. Hydrogen gas was seen to evolve.

Preparative Scale: A solution of Ar*Ar*AmH (**2.7**, 0.204 mmol, 200 mg) dissolved in toluene (7 mL) was added dropwise at 195 K to a solution of trimethylamine alane (0.204 mmol, 18 mg) in toluene (7 mL) at 195 K. Hydrogen gas was seen to evolve, and the reaction was stirred for 1 hour at 298 K. The solvent was removed *in vacuo* and single crystals suitable for X-ray analysis were grown from benzene-*d*$_6$/hexane at 298 K. (145 mg, 70%).

^{1}H NMR (500 MHz, C6D6, 298 K) δ ppm: 1.72 (s, 6H, ^{Ar*}C**H**3), 1.83 (s, 3H, ^{L}C**H**3), 3.64 (s, 2H, Al**H**$_2$), 5.87 (d, 2H, ^{L}*o*-C**H**, $^{3}J_{HH}$ = 8 Hz), 6.36 (s, 4H, C**H**(Ph$_2$)), 6.80 (d, 2H, ^{L}*m*-C**H**, $^{3}J_{HH}$ = 8 Hz), 6.90 (s, 4H, ^{Ar*}C**H**), 7.00 – 7.07 (m, 25H, ^{Ph}C**H**), 7.14 (t, 11H, ^{Ph}C**H**, $^{3}J_{HH}$ = 7.5 Hz), 7.29 (d, 8H, ^{Ph}*o*-C**H**, $^{3}J_{HH}$ = 7.5 Hz); 13C{1H} NMR (125 MHz, C6D6, 298 K) δ ppm: 21.0 (^{L}**C**H3), 21.2 (^{Ar*}**C**H3), 52.1 (**C**H(Ph$_2$)), 125.9 (^{Ph}**C**H), 126.8 (^{Ph}**C**H), 128.5 (^{L}*o*-**C**H), 128.8 (^{Ph}**C**H), 129.5 (^{L}*m*-**C**H), 129.7 (^{Ph}*o*-**C**H), 130.1 (^{Ph}**C**H), 130.7 (^{Ph}**C**H), 134.4 (**C**^{IV}), 138.7 (**C**^{IV}), 139.1 (**C**^{IV}), 140.3 (**C**^{IV}), 144.2 (**C**^{IV}), 145.7·Anal. Calc. ($C_{74}H_{63}N_2Al$): C, 87.68; H, 6.50; and N, 2.96. Found: C, 86.94; H, 6.18; and N, 2.74.

2.8.12 Synthesis of [AlH_2•NMe_3(Ar*Ar^{mes}Am)] (2.11)

NMR Scale: To a solution of trimethylamine alane (0.0279 mmol, 2.5 mg) dissolved in benzene-d_6, Ar*Ar^{mes}AmH (**2.5**, 0.0279 mmol, 18 mg) was added and the solution was transferred to a J Young NMR tube. H_2 gas was seen to evolve.

^{1}H NMR (500 MHz, C_6D_6, 298 K) δ ppm: 1.67 (s, 3H, ^{L}C**H**$_3$), 1.82 (s, 3H, ^{Ar*}C**H**$_3$), 1.99 (s, 18H, N(C**H**$_3$)$_3$), 2.00 (s, 3H, ^{mes}*p*-C**H**$_3$), 2.31 (s, 6H, ^{mes}*o*-C**H**$_3$), 4.10 (s, 4H, Al**H**$_2$), 5.91 (s, 2H, C**H**(Ph)$_2$), 6.07 (d, 2H, ^{L}*o*-C**H**, $^3J_{HH}$ = 8.0 Hz), 6.30 (d, 2H, ^{L}*m*-C**H**, $^3J_{HH}$ = 8.0 Hz), 6.61 (s, 2H, ^{mes}*m*- C**H**), 7.03 – 7.20 (m, 12H, C**H**), 7.33 (d, 4H, ^{Ar}*o*-C**H**, $^3J_{HH}$ = 7.5 Hz), 7.62 (d, 4H, ^{Ar}*o*-C**H**, $^3J_{HH}$ = 7.5 Hz); ^{13}C{^{1}H} NMR (125 MHz, C_6D_6, 298 K) δ ppm: 18.5 (^{L}**C**H$_3$), 19.6 (^{mes}*o*-**C**H$_3$), 20.5 (^{mes}*p*-**C**H$_3$), 22.0 (^{Ar*}**C**H$_3$), 50.5 (^{Ph}**C**H), 125.7 (**C**^{IV}), 125.9 (^{Ph}**C**H), 128.5 (^{L}*m*-**C**H$_3$), 128.8 (^{mes}*m*-**C**H), 129.1 (**C**^{IV}), 129.5 (**C**^{IV}), 130.0 (^{Ph}*o*-**C**H), 130.5 (^{Ph}*o*-**C**H), 132.5 (**C**^{IV}), 133.9 (**C**^{IV}), 134.9 (**C**^{IV}), 138.7 (**C**^{IV}), 143.7 (**C**^{IV}), 147.4 (**C**^{IV}).

2.8.13 Synthesis of [AlH_2(Ar*Ar^{mes}Am)] (2.12)

A solution of Ar*Ar^{mes}AmH (**2.5**, 0.31 mmol, 210 mg) dissolved in toluene (7 mL) was added dropwise at 195 K to a solution of trimethylamine alane (0.37 mmol, 33 mg) in toluene (7 mL) at 195 K. Hydrogen gas was seen to evolve, and the reaction was stirred for 1 hour at 298 K. The solvent was removed *in vacuo* and the resultant mixture was heated to 313 K for 4 hours, before washing with hexane and filtering. Single crystals suitable for X-ray analysis were grown from toluene/hexane at 298 K. (49 mg, 24%)

^{1}H NMR (600 MHz, C_6D_6, 298 K) δ ppm: 1.63 (s, 3H, ^{L}C**H**$_3$), 1.78 (^{Ar*}C**H**$_3$), 2.00 (s, 3H, ^{mes}*p*-C**H**$_3$), 2.10 (s, 6H, ^{mes}*o*-C**H**$_3$), 5.02 (s, 2H, Al**H**$_2$), 6.02 (d, 2H, ^{L}*o*-C**H**, $^3J_{HH}$ = 7.8 Hz), 6.22 (br d, 2H, ^{L}*m*-C**H**,) 6.39 (s, 2H, C**H**(Ph$_2$)) 6.51 (s, 2H, ^{mes}*m*-C**H**), 6.87 - 7.19 (m, ^{Ph}C**H**), 6.95 (^{Ar*}*m*-C**H**), 7.37 (d, 4H, ^{Ph}*o*-C**H**, $^3J_{HH}$ = 7.8 Hz); ^{13}C{^{1}H} NMR (150 MHz, C_6D_6, 298 K) δ ppm: 20.4 (^{mes}*m*-**C**H$_3$), 21.0 (^{L}**C**H$_3$), 21.0 (^{Ar*}**C**H$_3$), 21.1 (^{mes}*p*-**C**H$_3$), 21.4 (**C**^{IV}), 53.5 (**C**H(Ph$_2$)), 123.5 (^{Ph}**C**H), 126.0 (^{Ph}**C**H), 126.4 (^{Ph}**C**H), 128.5, 128.6 (^{Ph}**C**H), 128.7 (^{Ph}**C**H), 129.0 (^{Ph}**C**H), 129.3 (^{L}*m*-**C**H), 129.6 (^{mes}*m*-**C**H), 130.1 (^{L}*o*-**C**H), 130.1 (^{Ph}*o*-**C**H), 130.5 (^{Ph}**C**H), 133.9 (**C**^{IV}), 134.5 (**C**^{IV}), 137.4 (**C**^{IV}), 139.1 (**C**^{IV}), 142.2 (**C**^{IV}), 143.0 (**C**^{IV}), 143.8 (**C**^{IV}), 146.1 (**C**^{IV}).

2.8.14 Synthesis of [AlH(Ar*Ar^{mes}Am)$_2$] (2.13)

A solution of of Ar*Ar^{mes}AmH (**2.5**, 0.31 mmol, 210 mg) dissolved in toluene (7 mL) was added dropwise at 195 K to a solution of trimethylamine alane (0.37 mmol, 33 mg) in toluene (7 mL) at 195 K. hydrogen gas was seen to evolve, and the reaction mixture was stirred for 1 hour at 298 K. The solvent was removed *in vacuo* and the crude product was washed with hexane, filtered, and isolated. Single crystals suitable for X-ray analysis were grown from toluene/hexane. (166 mg, 41%).

^{1}H NMR (600 MHz, C_6D_6, 298 K) δ ppm: 1.63 (s, 3H, ^{L}C**H**$_3$), 1.78 (^{Ar*}C**H**$_3$), 2.00 (s, 3H, ^{mes}*p*-C**H**$_3$), 2.10 (s, 6H, ^{mes}*o*-C**H**$_3$), 5.02 (s, 2H, Al**H**$_2$), 6.02 (d, 2H, ^{L}*o*-C**H**, $^3J_{HH}$ = 7.8 Hz), 6.22 (br d, 2H, ^{L}*m*-C**H**,) 6.39 (s, 2H, C**H**(Ph$_2$)) 6.51 (s, 2H, ^{mes}*m*-C**H**), 6.87 - 7.19 (m, ^{Ph}C**H**), 6.95 (^{Ar*}*m*-C**H**), 7.37 (d, 4H, ^{Ph}*o*-C**H**, $^3J_{HH}$ = 7.8 Hz); ^{13}C{^{1}H} NMR (150 MHz, C_6D_6, 298 K) δ ppm: 20.4 (^{mes}*m*-**C**H$_3$), 21.0 (^{L}**C**H$_3$), 21.0 (^{Ar*}**C**H$_3$), 21.1 (^{mes}*p*-**C**H$_3$), 21.4 (**C**^{IV}), 53.5 (**C**H(Ph$_2$)), 123.5 (^{Ph}**C**H), 126.0 (^{Ph}**C**H), 126.4 (^{Ph}**C**H), 128.5, 128.6 (^{Ph}**C**H), 128.7 (^{Ph}**C**H), 129.0 (^{Ph}**C**H), 129.3 (^{L}*m*-**C**H), 129.6 (^{mes}*m*-**C**H), 130.1 (^{L}*o*-**C**H), 130.1 (^{Ph}*o*-**C**H), 130.5 (^{Ph}**C**H), 133.9 (**C**^{IV}), 134.5 (**C**^{IV}), 137.4 (**C**^{IV}), 139.1 (**C**^{IV}), 142.2 (**C**^{IV}), 143.0 (**C**^{IV}), 143.8 (**C**^{IV}), 146.1 (**C**^{IV}).

2.8.15 Synthesis of [AlMe$_2$(Ar*Ar^{dipp}Am)] (2.14)

Ar*Ar^{dipp}AmH (**2.6**, 0.28 mmol, 200 mg) was dried under vacuum for 1 hour, dissolved in toluene (10 mL) and cooled to 195 K. Trimethyl aluminium (0.34 mmol, 0.17 mL) was added dropwise, methane gas was seen to evolve, and the reaction was stirred at 298 K overnight. The solvent was removed *in vacuo* and recrystallised in hot hexane. (160 mg, 74%).

^{1}H NMR (500 MHz, C_6D_6, 298 K) δ ppm: -0.035 (s, 6H, Al(C**H**$_3$)$_2$), 0.77 (d, 6H, CH(C**H**$_3$)$_2$, $^3J_{HH}$ = 7.0 Hz), 1.23 (d, 6H, CH(C**H**$_3$)$_2$, $^3J_{HH}$ = 6.5 Hz), 1.72 (s, 3H, ^{L}C**H**$_3$), 1.81 (s, 3H, ^{Ar*}*p*-C**H**$_3$), 3.43 (sept, 2H, C**H**(CH$_3$)$_2$, $^3J_{HH}$ = 7.0 Hz), 6.21 (d, 2H, ^{L}*o*-C**H**, $^3J_{HH}$ = 8.5 Hz), 6.49 (s, 2H, C**H**(Ph)$_2$), 6.65 (d, 2H, ^{L}*m*-C**H**, $^3J_{HH}$ = 8.5 Hz), 6.95 – 7.28 (m, 25H, ^{Ph}C**H**);^{13}C{^{1}H} NMR (500 MHz, C_6D_6, 298K) δ ppm: -9.6 (Al(**C**H$_3$)$_2$), 21.2 (^{L}**C**H$_3$), 21.2 (^{Ar*}**C**H$_3$), 23.2 (CH(**C**H$_3$)$_2$), 25.7 (CH(**C**H$_3$)$_2$), 28.3 (**C**H(CH$_3$)$_2$), 51.6 (C**H**(Ph)$_2$), 128.8 (^{L}*o*-**C**H), 129.7 (^{L}*m*-**C**H), 124.1 (^{Ph}**C**H), 125.9 (^{Ph}C), 126.1 (^{Ph}C), 128.5 (^{Ph}C), 128.6 (^{Ph}C), 129.4 (^{Ph}C), 129.6 (^{Ph}C), 130.1 (C^{IV}), 130.2 (C^{IV}), 131.4 (C^{IV}), 134.0 (C^{IV}), 139.1 (C^{IV}), 140.6 (C^{IV}), 143.5 (C^{IV}), 143.9 (C^{IV}), 145.2 (C^{IV}). Anal. Calc. ($C_{55}H_{57}N_2Al$): C, 84.47; H, 7.80; and N, 3.94. Found: C, 84.84; H, 7.34; and N, 3.58.

2.8.16 Synthesis of [AlMe$_2$(Ar*Ar*Am)] (2.15)

Ar*Ar*AmH (**2.7**, 0.20 mmol, 200 mg) was dried under vacuum for 1 h, dissolved in toluene (10 mL) and cooled to 195 K. Trimethyl aluminium (0.26 mmol, 0.13 mL) was added dropwise, methane gas was seen to evolve, and the reaction was stirred at 298 K overnight. The solvent was removed *in vacuo* and the resultant product was washed with hexane to yield a white solid after filtration (93 mg, 44%).

^{1}H NMR (500 MHz, C_6D_6, 298 K) δ ppm: -0.88 (s, 6H, Al(C**H**$_3$)$_2$), 1.73 (s, 6H, ^{Ar*}C**H**$_3$), 1.82 (s, 3H, ^{L}C**H**$_3$), 6.06 (d, 2H, ^{L}*o*-C**H**, $^3J_{HH}$ = 8.5 Hz), 6.43 (s, 4H, C**H**(Ph)$_2$), 6.96 - 7.11 (m, 38H, ^{Ph}C**H**), 7.23 (d, 8H, ^{Ph}*o*-C**H**, $^3J_{HH}$ = 8 Hz); ^{13}C{^{1}H} NMR (500 MHz, C_6D_6, 298K) δ ppm: 21.5 (^{Ar*}**C**H$_3$), 51.2 (**C**H(Ph)$_2$), 126.0 (^{Ph}**C**H), 126.5 (^{Ph}**C**H), 128.2 (^{L}*m*-**C**H), 129.0 (^{L}*o*-**C**H), 129.4 (^{Ph}*o*-**C**H), 130.3 (^{Ph}**C**H), 131.5 (**C**^{IV}), 134.4 (**C**^{IV}), 138.9 (**C**^{IV}), 139.5 (**C**^{IV}), 144.2 (**C**^{IV}), 145.2 (**C**^{IV}). Anal. Calc. ($C_{76}H_{65}N_2Al$): C, 88.17; H, 6.52; and N, 2.71. Found: C, 87.78; H, 6.56; and N, 2.72

2.8.17 Trimethylamine alane

Trimethylamine hydrochloride (115 mmol, 11.0 g) was dried in a Schlenk flask overnight. Ether (100 mL) was added, and the reaction mixture cooled to 195 K. Lithium aluminium hydride (4 M in ether, 138 mmol, 34.5 mL) was added dropwise to the reaction mixture and stirred vigorously. The reaction was stirred at 195 K for 30 mins, then warmed to 295 K and stirred overnight. The reaction was filtered, and the solvent was removed *in vacuo* using an ice/water/sodium chloride water bath (approx. 268 K) and a secondary trap. The resultant white powder was purified by sublimation.

^{1}H NMR (500 MHz, C_6D_6, 298 K) δ ppm: 1.84 (s, 9H, C**H**$_3$), 4.13 (s, 3H, Al**H**$_3$).

Chapter 3:

Aluminium Amidinate Hydride and Alkyl Complexes as Catalysts for the Hydroboration of Phenylacetylene

3.1 Introduction

3.1.1 Hydroboration Reactions

Hydroboration reactions are defined as the addition of a hydrogen-boron bond from an organoborane compound across the double or triple bond of an unsaturated compound (alkenes, alkynes, carbonyl, nitrile). Owing to the reversed polarity of the hydrogen-boron bond ($H^{\delta-}$-$B^{\delta+}$), this reaction proceeds *via* Anti-Markovnikov addition and both components are added suprafacially across the unsaturated bond (**Scheme 3.1**).[119]

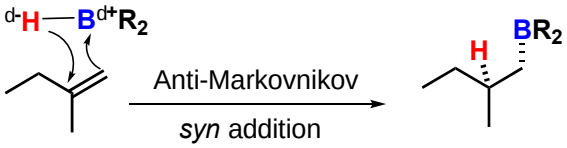

Scheme 3.1: Mechanistic example of a hydroboration reaction across an alkene double bond.

These compounds are versatile and are therefore widely exploited in organic synthesis. Most commonly, they are used as coupling reagents or intermediates in a range of palladium-catalysed cross coupling reactions for the formation of C-C, C-N and C-O bonds.[6] Some examples of the most common types of boron reagents used include 9-BBN (9-BBN = 9-Borabicyclo-[3.3.1]-nonane), catechol boronic esters and pinacol boronic esters.[120] They are also susceptible to oxidation and, as such, are used to introduce new functional groups into a molecule (or as intermediates in a multi-step synthesis).[121] These compounds play a crucial role in organic synthesis, and recent research efforts have focused on the development of more sustainable routes to synthesise organoboron compounds.

3.1.2 Aluminium-Catalysed Hydroboration Reactions

The first reports of aluminium-catalysed hydroboration reactions emerged in the literature in 2015, when Roesky *et al.* reported that the aluminium triflate species **3A** (**Figure 3.1**) was catalytically active towards the hydroboration of organic carbonyl compounds. Compound **3A** was synthesised *via* the reaction of the parent aluminium dihydride complex with methyl trifluoromethanesulfonate (‘methyl triflate’) in toluene at 273 K and occurred with concomitant formation of methane gas. The structure of **3A** was confirmed spectroscopically and crystallographically, and the presence of a single aluminium-hydrogen bond was confirmed by IR spectroscopy (1791 cm^{-1}). The addition of the triflate moiety resulted in a contraction of the Al-N bond length of (**LAlH$_2$** (L = ^{dipp}BDI): 1.8989 Å, **3A**: 1.8764 Å) and indicated an increase

in positive charge at the aluminium centre; this was confirmed by natural bond orbital (NBO) analysis (q**LAlH$_2$**: 1.41 *e*, q**3A**: 1.81 *e*) and increased the Lewis acidity at the aluminium centre.

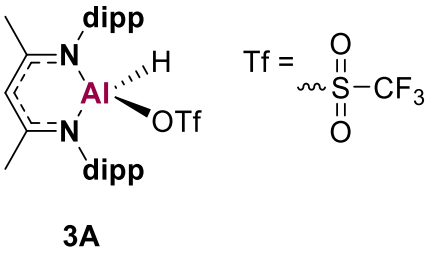

3A

Figure 3.1: The structure of the aluminium triflate catalyst **3A**.

The hydroboration of a range of aldehydes and ketones was investigated using pinacolborane (HBpin) and catalyst **3A** (1-2 mol%) at room temperature in benzene-d_6. It was found to be active towards a range of substrates, with reaction times and yields varying across the series (benzaldehyde: 1 mol%, 99% conversion in 1 hour; acetophenone: 2 mol%, 51% conversion in 6 hours).

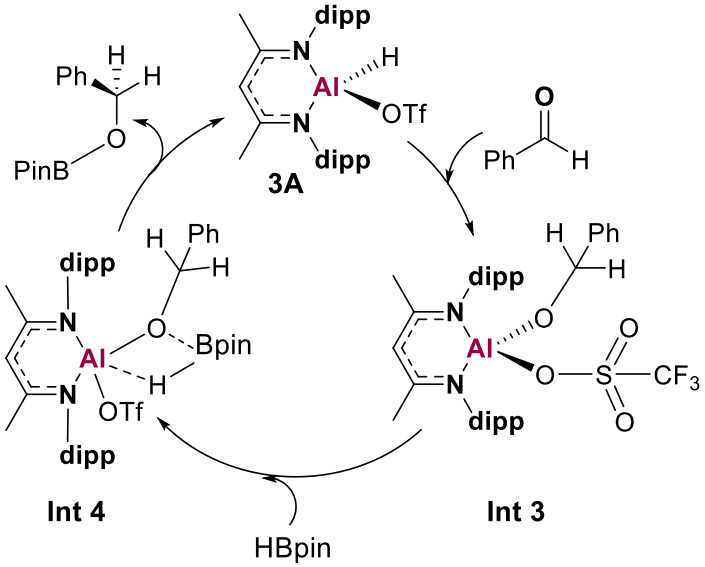

Figure 3.2: Catalytic cycle to show the hydroboration of benzaldehyde.

The mechanism of action was probed computationally and is shown in **Figure 3.2** using benzaldehyde as a representative carbonyl compound. Initially, the benzaldehyde molecule coordinates to the tetrahedral aluminium centre through the oxygen atom and undergoes a series of intramolecular rearrangements to form the tetrahedral aluminium-benzyloxide compound **Int 3**. The aluminium centre acts as a hydride donor to the carbonyl carbon and the kinetic barrier associated with this step is very high and is said to be the rate determining step.

The B-H bond of HBpin adds across the Al-O bond of **Int 3** to form **Int 4** with a four membered Al-O-B-H ring, which undergoes rapid ring opening to generate the hydroboration product and **3A** *via* the addition of a hydride from the HBpin substrate.[122]

In the years since **3A** was first reported, a range of structurally diverse aluminium catalysts have emerged in the literature that are susceptible towards a range of alkene, alkyne, carbonyl and nitrile substrates with many examples included in a detailed review by Park *et al.*[123–127] The remainder of this discussion will focus on the literature pertaining to alkene and alkyne substrates.

3.1.2.1 The Hydroboration of Alkenes and Alkynes

Expanding upon the catalytic activity of **3A**, Roesky and co-workers synthesised the aluminium dihydride catalyst **3B** (**Figure 3.3**) and examined its capacity to catalyse the hydroboration of terminal alkynes using pinacolborane. Reactions were conducted at 303 K in chloroform-*d* and monitored for 12 hours in the presence of **3B** (3 mol%), HBpin and a range of terminal alkyne substrates. In general, yields >70% were observed when reacted with propargyl ethers, propargyl aryl- and alkyl-substituted alkynes, as well as for aryl-substituted alkynes bearing both electron-donating (*p*-OMe) and electron-withdrawing (*m*-F) groups. Electron rich alkynes with secondary alkyl substituents were found to be much slower, and aliphatic alkynes were found to react more rapidly compared to analogous aromatic alkyne compounds.

The mechanism of action was probed through a series of stoichiometric and computational experiments and the proposed acetylide pathway is shown in **Figure 3.4**. The first step involves the formation of the aluminium acetylide complex (**Int 1**) *via* the σ-bond metathesis of the terminal alkyne C-H bond across the Al-H bond of **3B** with concomitant formation of dihydrogen. **Int 1** is the catalytically active species, which undergoes *syn*-addition of the HBpin B-H bond across the carbon-carbon triple bond to form the aluminium alkenyl hydride **Int 2**. The highly polarised nature of the Al-C bond in **Int 2** (qAl = 1.65 *e*, qC = -0.89 *e*) facilitated the addition of the Al-C bond to the terminal C-H bond of a second molecule of phenylacetylene (by σ-bond metathesis) to form the product and regenerate **3B**.[63] In 2018, the structurally related aluminium catalysts **3C** and **3D** were reported by Yang *et al.* and proposed to proceed *via* the same mechanism, with liberation of methane (**3C**) or ethane (**3D**) when

forming the active aluminium acetylide species.[128] Reaction conditions were not standardised across this series of compounds and thus direct conclusions about catalyst performance cannot be drawn.

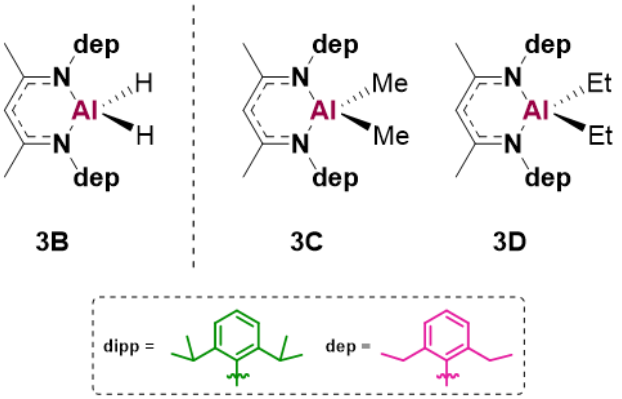

Figure 3.3: Structurally related aluminium catalysts **3B-3D**.

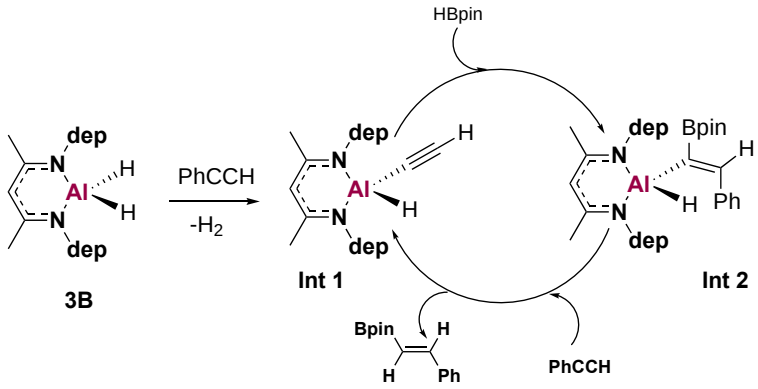

Figure 3.4: Catalytic cycle to show hydroboration of phenylacetylene *via* acetylide pathway.

In 2016, Cowley, Thomas and co-workers reported the first examples of aluminium catalysts capable of catalysing the hydroboration of both terminal and internal alkynes using commercially available reagents. This offered the obvious benefit of commercially available catalysts, as well as expanding the substrate scope to include disubstituted alkynes. The commercially available reagents di-*iso*-butylaluminium hydride (DIBAl-H, **3E**) and Et_3Al•DABCO (DABCO = 1,4-diazabicyclo[2.2.2]octane, **3F**) (10 mol%, **Figure 3.5**) were reacted with a range of alkynes in the presence of HBpin in toluene and heated at 383 K for 2 hours. Terminal aryl- and alkyl-substituted alkynes all underwent hydroboration, and the steric parameters of the alkyl-substituted alkynes did not affect the rate of reaction. Similarly, electron-donating and electron-withdrawing aryl substituents were tolerated equally, as was

observed for catalyst **3B**. Investigations into the hydroboration of internal alkynes were more varied; symmetrical and unsymmetrical alkynes with both aryl- and alkyl-substituents were hydroborated in yields >70% after 2 hours, though yields were better for the terminal alkynes.

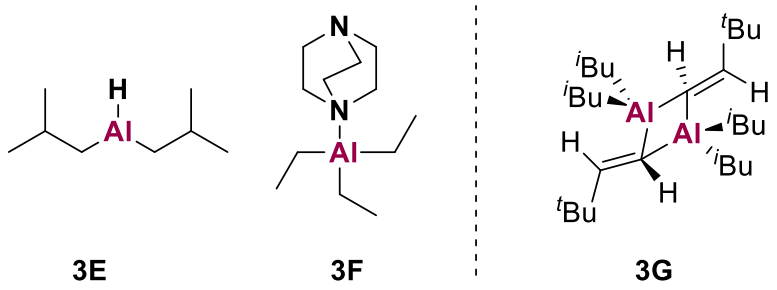

Figure 3.5: Structures of commercially available catalysts **3E** and **3F**. Structure of aluminium-alkenyl species **3G**.

The catalytic activity of **3E** and **3F** was found to be equal, suggesting that a similar mechanism was in operation, and the ability to hydroborate internal alkynes ruled out the aluminium acetylide pathway proposed for **3B.** Instead, the hydroalumination pathway shown in **Figure 3.6** was proposed. The mechanism proceeds *via* alkyne hydroalumination to form an aluminium-vinyl species (**Int 1**) which undergoes σ-bond metathesis with HBpin. Specifically, **Int 1** underwent transmetallation from aluminium to boron, which liberated the product and regenerated the aluminium hydride catalyst.

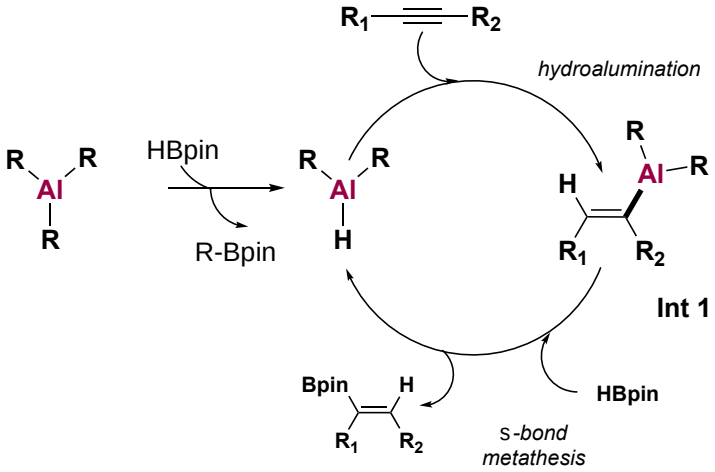

Figure 3.6: Catalytic cycle to show hydroboration of internal and terminal alkynes using **3E** and **3F** via the hydroalumination pathway. The hydride generation step is only required for **3F**.

Experimental verification for this pathway was sought using a previously-reported aluminium alkenyl (**3G**, **Figure 3.5**) that is known to undergo hydroalumination.[129] The formation of an (*E*)-vinylboronate ester from the reaction of the aluminium alkenyl with HBpin verified the transmetallation C-B bond forming step and demonstrated that the hydroalumination step is crucial for the catalytic cycle.[130] Further investigations into the catalytic activity of commercially available aluminium reagents also revealed lithium aluminium hydride ($LiAlH_4$) and *bis*-(2-methyoxyethoxy)aluminium hydride (Red-Al) to be pre-catalysts for the hydroboration of alkene substrates. Ketone, ester, and nitrile functional groups were also tolerated.[131]

In 2018, Mulvey and co-workers reported the first examples of lithium diamido-dihydridoaluminates and lithium mono-amido-monohydrido-dialkylaluminates for the catalytic hydroboration of aldehydes, ketones, and terminal alkynes. These catalytic reactions confirmed the bimetallic nature of this process, through coordination to lithium and hydride transfer from aluminium.[132] Encouraged by this and the reports of the catalytic activity of $LiAlH_4$, this work was expanded to investigate the difference in activity between bimetallic lithium aluminates and their neutral, mononuclear aluminium counterparts (**3H-3J**, **Figure 3.7**). The enhanced reactivity of the lithium aluminate species was readily demonstrated through the hydroboration of carbonyl compounds. For example, the hydroboration of benzophenone went to completion after 30 minutes at room temperature using **3H**-*anionic*, whilst only 94% conversion was achieved with **3H**-*neutral*. This effect was more pronounced for **3I** (*anionic*: 99%, 30 minutes; *neutral*, 69%, 5 hours) and **3J** (*anionic*: 79%, 30 minutes; *neutral*: 17%, 4 hours). Further control reactions with lithium hydride in the presence of benzophenone yielded only 10% product after 4 hours, proving that the enhanced catalytic performance of **3H-3J**-*anionic* is down to the intrinsic functionality of the bimetallic system.

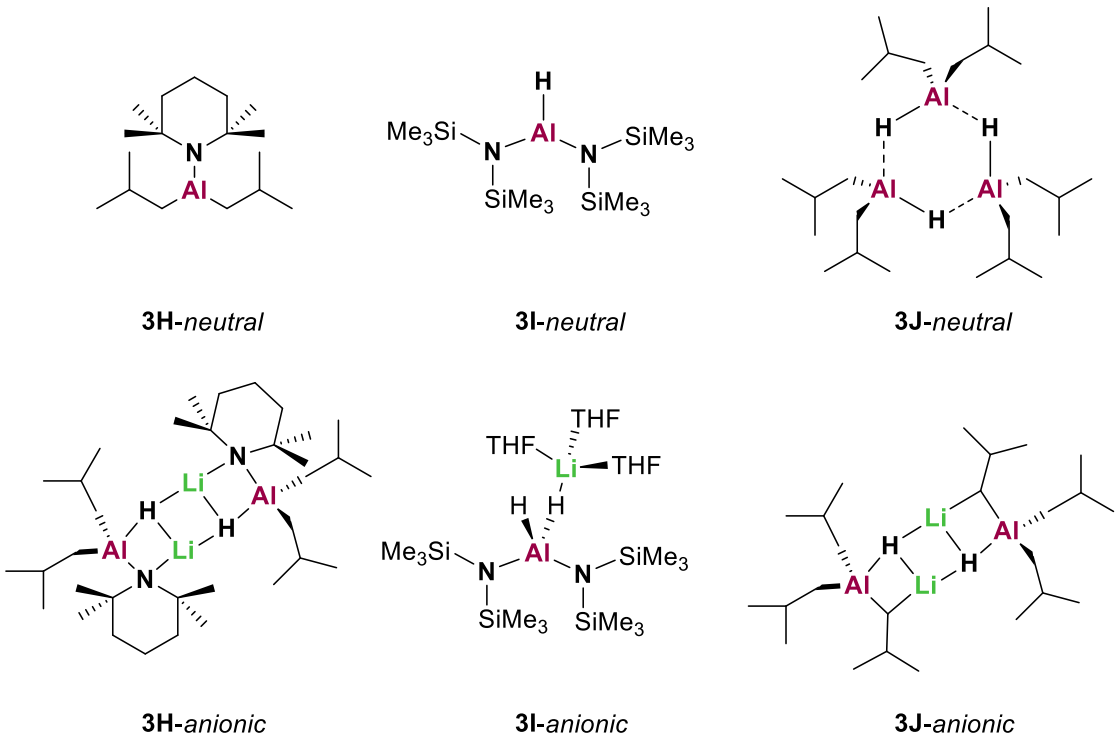

Figure 3.7: Neutral and anionic aluminium complexes **3H**-**3J**.

The reactivity of alkyne substrates was more complex when the hydroboration of phenylacetylene was investigated using **3H** and **3J**. For ease of comparison, conditions were standardised to match that of Cowley *et al.* (10 mol% catalyst, tol-d_8, 383 K). After 2 hours at 383 K, 71% conversion to the hydroboration product was observed in the presence of **3H**-*anionic*. In line with carbonyl catalysis observations, this showed enhanced reactivity compared to **3H**-*neutral*, which was not catalytically active in these conditions (0%, 17 hours). **3J**-*neutral* generated a marginally higher yield than **3J**-*anionic* (83% and 85% after 2 hours, respectively), indicating for the first time that the reactivity with alkynes was more complex, and that the anionic complex was not always catalytically superior. Furthermore, the increased reactivity of **3J**-*anionic* versus **3H**-*anionic* for the same reaction suggests that intrinsic hydride nucleophilicity plays a role in catalytic activity. The complex catalytic profile was further demonstrated when diphenylacetylene was tested under the same conditions (**3J**-*anionic*: 10%, 2 hours; **3J**-*neutral*: 60%, 2 hours), though the reverse was found to be true when 1-phenyl-propyne was used as the alkyne substrate (**3J**-*anionic*: 60%, 2 hours; **3J**-*neutral*: trace). The variation observed across this series of alkyne and carbonyl substrates suggests that catalytic activity is heavily dependent on the nature of the substrate. Thus, having access to a range of mononuclear and heterobimetallic complexes allows catalytic reactions to be refined according to the most suitable combinations of substrate and catalysis.

In 2019, the family of aluminium hydroboration catalysts was expanded by both the groups of Cowley and Panda to include aluminium dihydride complexes supported by amidophosphine ligands (**3K-3L**, **Figure 3.8**).

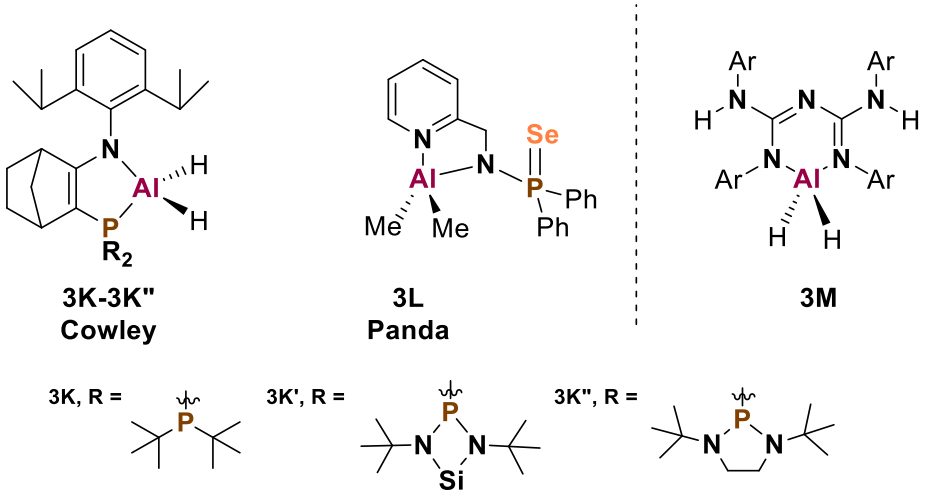

Figure 3.8: Aluminium dihydride catalysts supported by an amidophosphine ligand.

The aluminium *bis*-alkyl complex **3L** was synthesised by the facile reaction of the starting ligand (2-picolylamino-diphenylphosphane selenide) with trimethylaluminium at room temperature. In contrast, **3K-3K"** could not be targeted directly from the parent ligand and instead was synthesised from the lithiated form of the ligand and trimethyl aluminium. Preliminary investigations revealed that **3K-3K"** were active catalysts for the hydroboration of terminal alkynes (3 mol% catalyst, neat conditions, 298 K). Altering the steric bulk of the R group revealed that **3K"** was much slower compared to **3K-3K'**, and was related to the facile accessibility of the κ^2-N,N coordination mode ("ligand slip") in solution.[133] Catalyst optimisation reactions revealed that **3L** was most efficient in neat conditions, at room temperature and for 8 hours. Alkenes bearing electron-donating substituents were found to give the highest yields (>80-90%), though electron-withdrawing alkenes were also converted in good yields. Additional reactions were tested using alicyclic (>80% conversion), long-chain (quantitative yield) and bromo-substituted alkenes (~90% conversion). A range of terminal alkyne substrates were also tolerated, and the chemoselectivity of **3L** was demonstrated when reacted with 4-ethynylphenyl acetate; only the alkyne moiety underwent hydroboration, leaving the carbonyl substituent intact. Mechanistically, this was said to proceed via the hydroalumination pathway shown in **Figure 3.6**, though this was not backed up by

experimental or computational observations.[134] This same chemoselectivity was also reported for **3M**, which was found to be active towards both internal and terminal alkynes with the acetylide and hydroalumination pathways said to be in operation depending on the alkyne substrate.[135]

Developments within this field have advanced rapidly over recent years, and aluminium hydroboration catalysts are now commonplace in the literature. The substrate scope for this family of catalysts is broad, with terminal and internal alkynes, containing electron-donating and electron-withdrawing substituents widely tolerated. Based on this literature, the aluminium hydride and alkyl complexes reported in Chapter 2 were investigated for their capacity to catalyse hydroboration reactions, with the reactions of phenylacetylene with HBpin chosen as a model reaction. These substrates were chosen for their commercial availability, and for ease of comparison to the current literature.

3.2 Catalytic Hydroboration of Phenylacetylene

The aluminium hydride (**2.8**-**2.10**, **2.12)** and alkyl (**2.14**-**2.15**) complexes were tested as catalysts for the reaction of the hydroboration of phenylacetylene using pinacolborane. A reminder of the catalyst structures is shown in **Figure 3.9**. Reactions were conducted at 0.25 M concentration in benzene-d_6 and monitored over time using ^{1}H NMR spectroscopy. An initial test reaction using complex **2.9** was monitored over 12 hours at room temperature, after which point the formation of a hydroboration product was observed in a 38% yield. At elevated temperatures rates were seen to increase dramatically, thus all further reactions were carried out at 353 K.

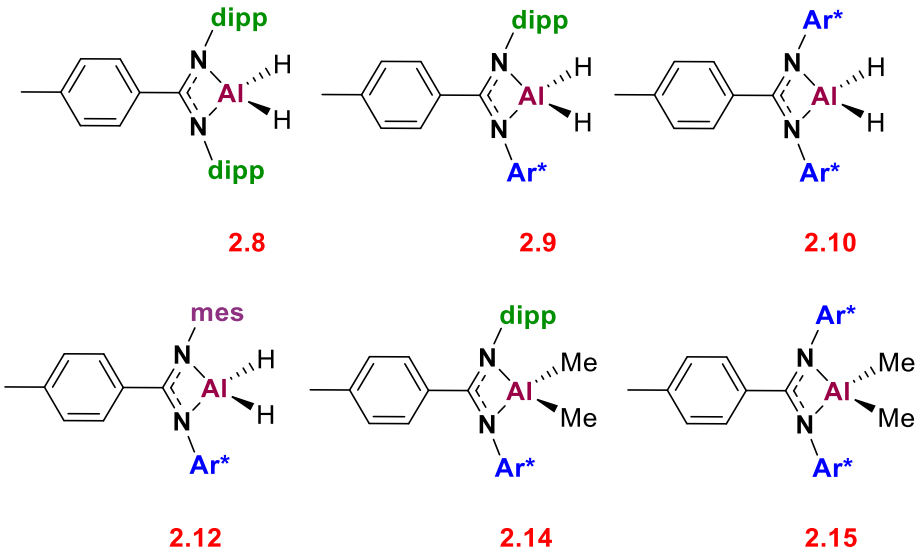

Figure 3.9: The structures of **2.8**-**2.10**, **2.12** and **2.14**-**2.15**

All complexes studied were found to be catalytically active towards the hydroboration of phenylacetylene, with the exclusive formation of the (*E*)-vinylboronate ester **3.1** *via* Anti-Markovnikov addition (**Scheme 3.2**). The catalytic activity of trimethylamine alane was also investigated. After 2 hours, 48% conversion to the (*E*)-vinylboronate ester was observed, however monitoring the reaction for longer time periods revealed almost no further reactivity (13 hours, 54%). This suggests that trimethylamine alane degraded under the reaction conditions and was unsurprising given the temperature-sensitive nature of this compound. A control reaction in the absence of any aluminium species was conducted and revealed no reaction between substrates after 24 hours at 353 K.

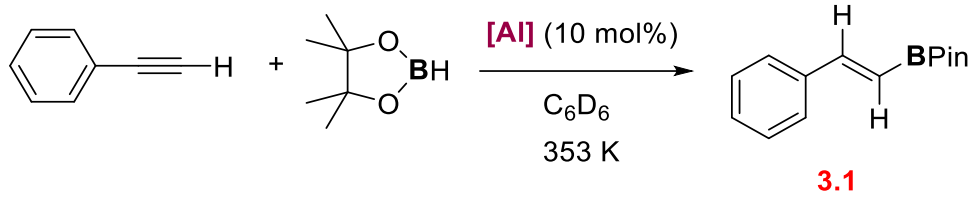

Scheme 3.2: General catalytic conditions for the hydroboration of phenylacetylene.

Key ^{1}H NMR signals were used to probe this reactivity and observe product formation (**Figure 3.10**). For example, the methyl groups of HBpin resonate as a singlet at 0.99 ppm that integrates to twelve protons. These same methyl groups in **3.1** resonate as a singlet at 1.12 ppm and, over the course of the reaction, this singlet intensifies whilst that at 0.99 ppm is consumed. Similarly, **3.1** was identified by two doublets at 6.46 and 7.76 ppm that integrate to one proton each. Each doublet has a calculated 3-bond coupling constant (J) of 18.5 Hz and corresponds to the *trans* alkene coupling protons. The consumption of phenylacetylene was also monitored (singlet, 2.72 ppm, doublet 7.40 ppm) though this is less distinctive than the HBpin or product resonances.

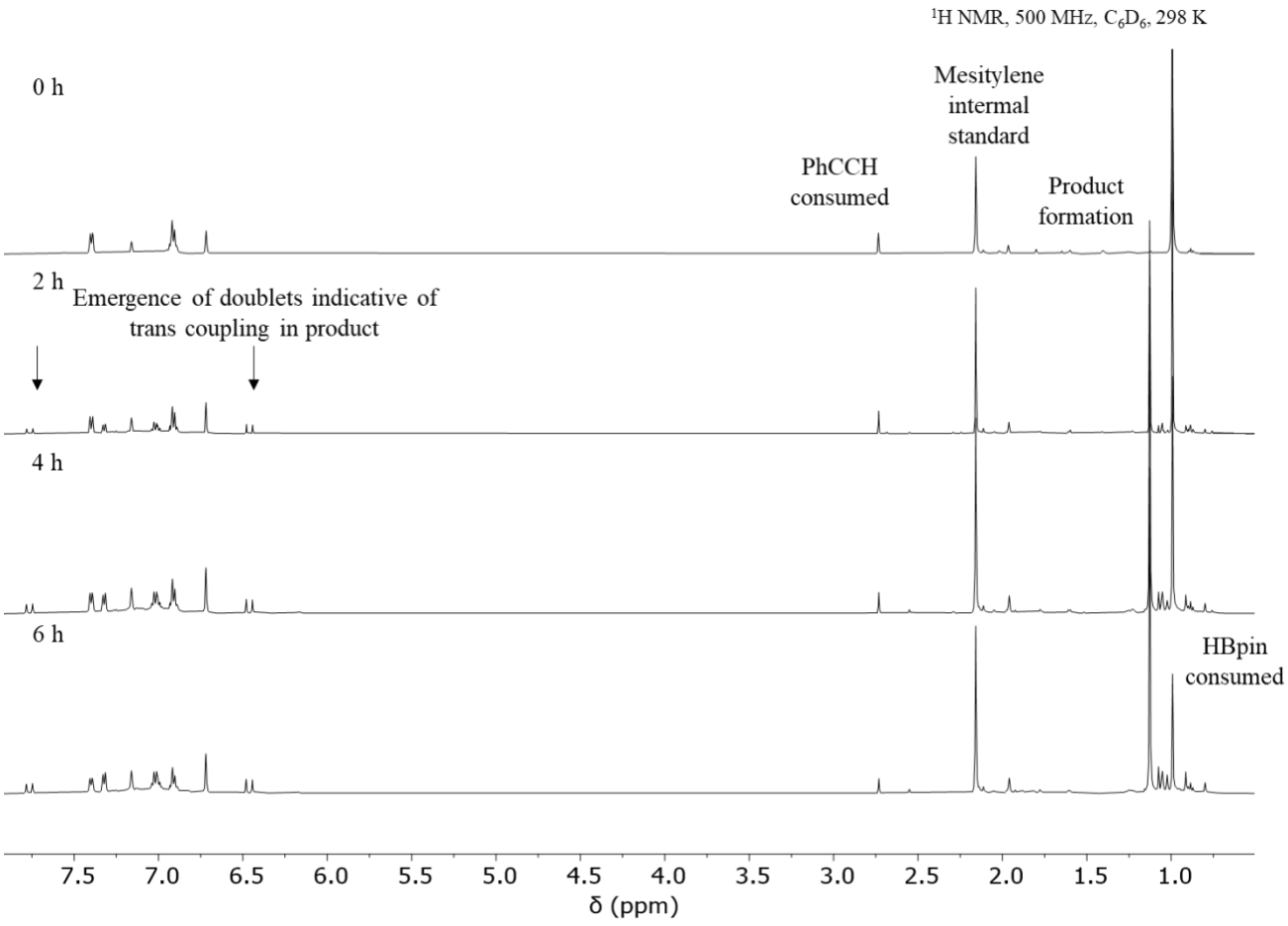

Figure 3.10: Representative ^{1}H NMR stack of the catalytic hydroboration of phenylacetylene.

3.3 Reaction Profiles and Kinetics

Table 3.1 shows the time taken for each catalyst to achieve high conversions (>88%). The reactions took between 6 (**2.8**) and 95 (**2.15**) hours and a general inverse relationship was observed between solution-state volume and reaction time, with some notable exceptions.

Table 3.1: Catalytic hydroboration of phenylacetylene with HBpin. [a] Calculated by ^{1}H NMR.

Catalyst	Time (h)	Conv. (%)[a]	Hydrodynamic Radius (Å)
2.8	6	89	5.0
2.9	11	89	6.7
2.10	56	89	7.4
2.12	22	89	7.6
2.14	12	90	5.8
2.15	95	89	6.8

Examination of the reaction times reveals significant differences across the series of the aluminium hydride compounds with the following trend observed: **2.8** > **2.9** > **2.12** > **2.10.** The smallest catalyst, **2.8**, was the fastest. Of the complexes employing the bulky Ar* substituent, **2.9** proceeded 1.8x faster than **2.12** and 5x faster than **2.10**. The slower rate of **2.12** compared to **2.9** was surprising considering the smaller size of the mes substituent and prompted further investigation (section 3.4.1.3). Of the aluminium alkyl complexes, catalyst **2.14** went to completion in 12 hours, which was 7.6x faster than the required 95 hours for **2.15**; the slower time of **2.15** was attributed to the increased steric encumbrance of the additional phenyl groups.

Figure 3.11 shows plots of product formation (yield) versus time for aluminium hydride and alkyl complexes **2.8**-**2.10, 2.12** and **2.14**-**2.15**. The aluminium hydride complexes displayed similar reaction profiles. At an initial glance it appeared that two kinetic regimes may be in operation; one at lower conversion (up to approx.75% conversion), after which point a second regime becomes dominate which appears to follow zero order kinetics (with respect to HBpin) and continues to high conversion. This is most obvious in the kinetic profiles of **2.10** and **2.12** (**Figure 3.11**) and suggests that an alternative reaction pathway, side-product formation or catalyst degradation occurs at high conversions.

The aluminium alkyl complexes, **2.14** and **2.15**, exhibit different reaction profiles compared to their analogous aluminium hydride counterparts. The hydride and alkyl complexes bearing one dipp substituent (**2.9**/**2.14**) required similar reaction times to reach high conversions (11 versus 12 hours, respectively), whilst **2.15** was significantly slower than **2.10** despite bearing the same Ar* substituent (56 versus 95 hours). The graphs in **Figure 3.11** show that an initial induction period was observed for the alkyl complexes (**2.14**: 1 hour, **2.15**: 7 hours). With catalyst **2.9**, a 37.5% yield was recorded after 1 hour. In contrast, no product was observed after 1 hour using analogous **2.14** and it took a further 2 hours to reach similar conversions (t=3 h, 35.9% yield). No obvious second regime was observed. The same phenomenon was observed for **2.10** and **2.15** but overall reaction times are very different. It took 7 hours to reach 5% conversion using **2.15** (no product formation was observed before this) whereas, at the same time point, 45.7% conversion was recorded using **2.10**.

Through analysing the product *versus* time graphs of the aluminium hydride and alkyl complexes some initial information on reaction mechanism can be obtained. Firstly, the notable differences in the kinetic profiles suggested that the aluminium hydride and alkyl complexes likely proceed *via* different mechanisms. This is further corroborated by the observed induction periods for the alkyl complexes, which led to the hypothesis that the alkyl species are pre-catalysts for the hydroboration of phenylacetylene, and some time is required for the active catalyst to form (and that the length of the induction period is linked to solution-state volume). This is in line with reported examples of aluminium alkyl hydroboration pre-catalysts in the literature, which formed a mixed hydride-alkyl species *in situ* as the active catalyst.[136]

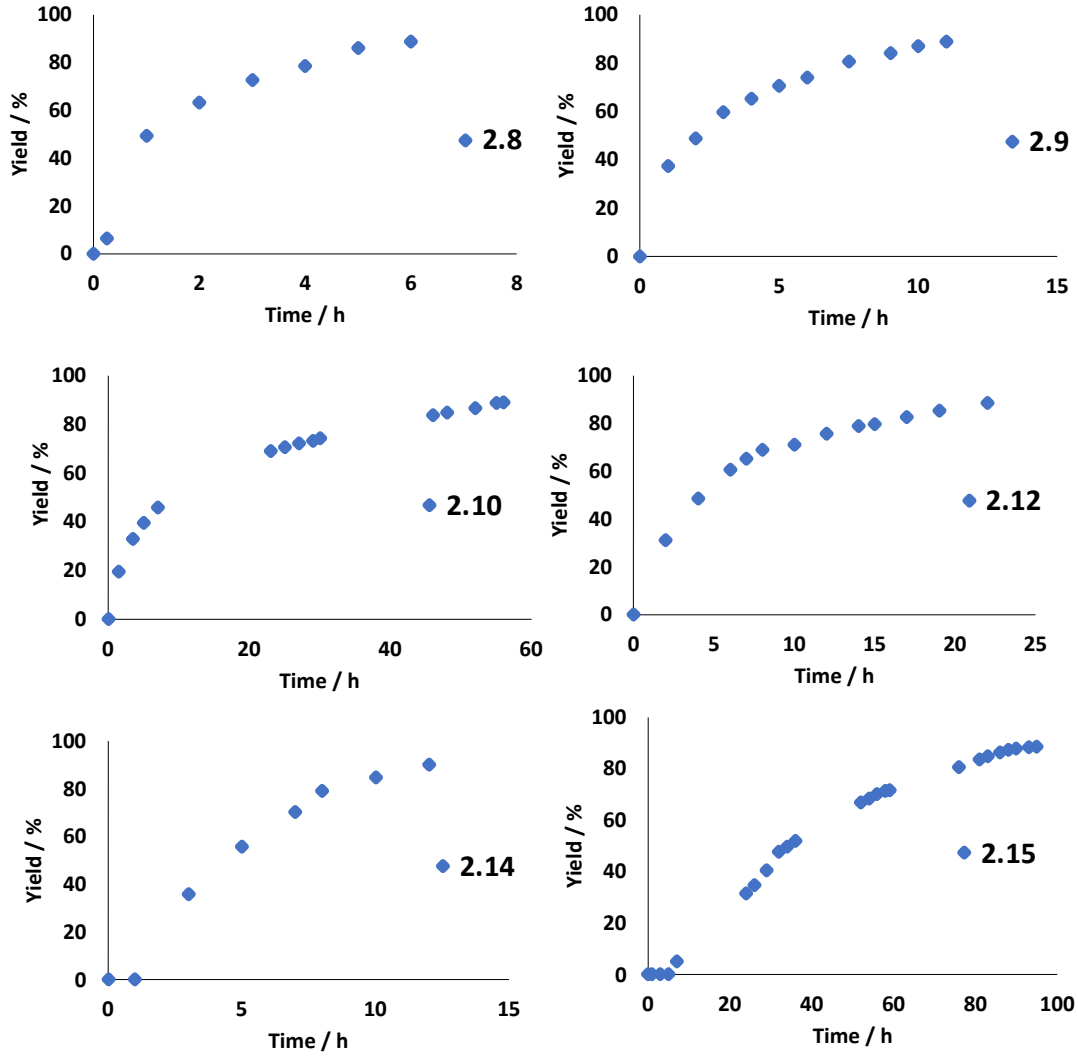

Figure 3.11: Plots of product (yield) versus time graphs for catalysts **2.8-2.10**, **2.12-2.15**.

3.3.1 Modelled Reaction Kinetics

To further probe the possibility of the hydride and alkyl complexes proceeding *via* different mechanistic pathways, both first- and second-order kinetics fits were modelled to examine the profile of catalysis (**Figure 3.12**). This revealed key differences in the kinetic profiles of the hydride and alkyl catalysts. Catalysts **2.8-2.10** and **2.12** exhibited two regimes when modelled as a second-order fit, one up to ~75% conversion, and a second regime at higher conversions. Below 75% conversion, all catalysts exhibited nearly perfect second order kinetics. Above 75% conversion, deviation from this linearity was observed, confirming the previous observation that a second regime becomes dominant (*vide supra*). This suggests that the reaction kinetics are more complex than it initially appears, and that there are potentially multiple reaction pathways occurring simultaneously. This is in contrast to the literature catalysts described in

section 3.1.2, where the kinetics were said to follow the same reaction profile throughout. In contrast, modelling the data for the aluminium alkyl complexes **2.14** and **2.15** revealed a good agreement with a first-order fit (with respect to HBpin) and there was no deviation from the line of best fit at high conversions. These observations reinforce the suggestion that different mechanistic pathways are in operation between the hydride and alkyl complexes.

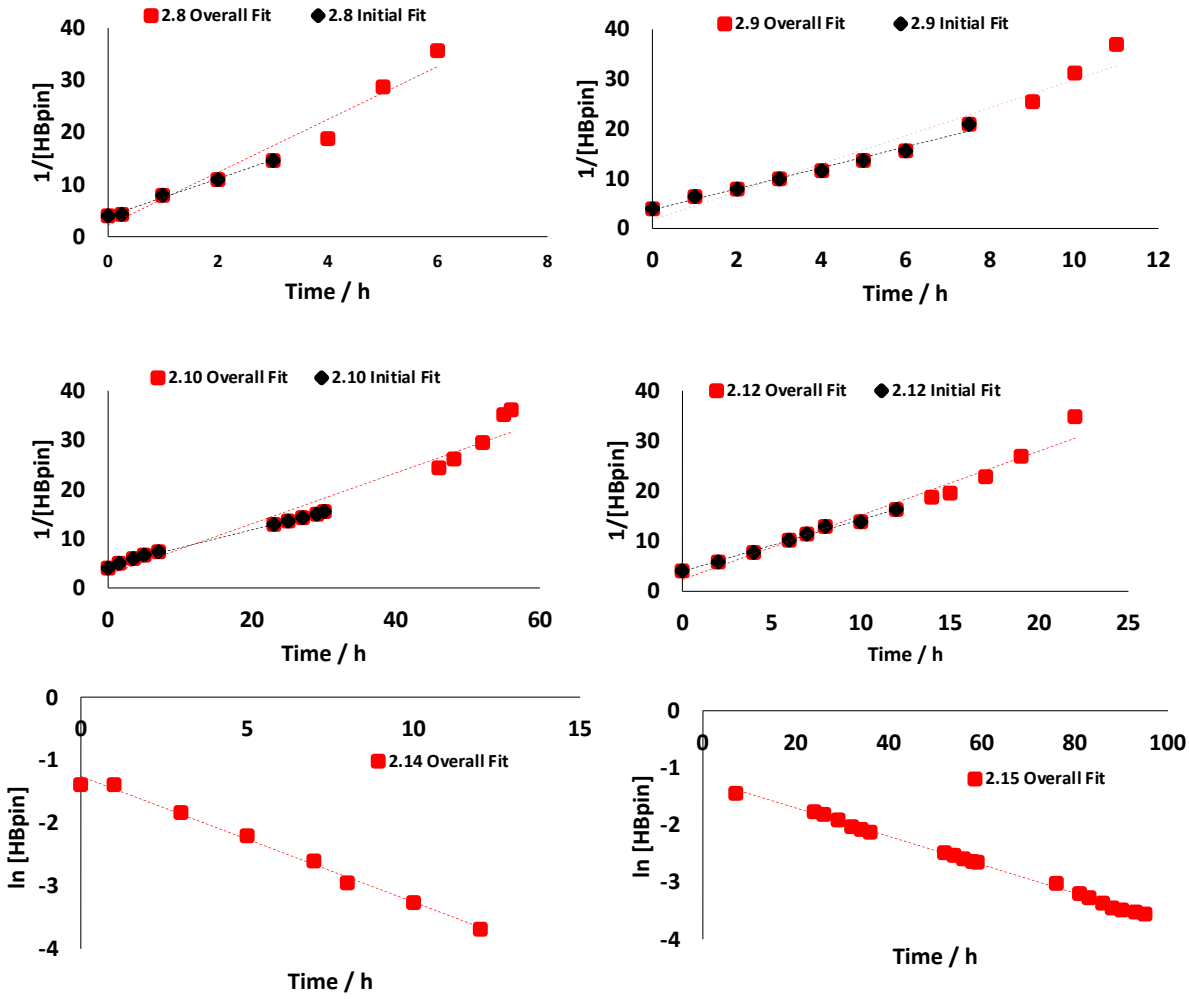

Figure 3.12: Plotted reaction orders for initial and overall reactions for catalysts **2.8**-**2.10**, **2.12** and **2.14**-**2.15**. Aluminium hydride complexes were modelled according to a second-order fit; aluminium alkyl complexes were modelled according to a first-order fit. * The 7-hour induction period was not included in the data for **2.15**

3.4 Elucidating the Mechanism

The kinetic data presented above provided interesting insights into the likelihood of structurally related aluminium amidinate complexes operating *via* different mechanistic pathways. However, further investigations were required to elucidate the mechanism(s) of action.

3.4.1 Stoichiometric Reactions

A series of stoichiometric reactions was conducted to probe the possible hydroalumination or acetylide pathways by reacting each of the aluminium catalysts with one or two equivalents of phenylacetylene or HBpin. The stoichiometric reactions of a known aluminium hydroboration catalyst with phenylacetylene and HBpin have previously been reported by Roesky and co-workers.[63] In this work, they used the β-diketiminate complex [AlH_2(^{dep}BDI)] (dep = 2,6-diethylphenyl, **3.4 Scheme 3.3**) to propose the catalytic mechanism detailed in section 3.1.2.1. Complex **3.4** and a related β-diketiminate complex [AlH_2(^{dipp}BDI)] (**3.5**, **Scheme 3.3**) were synthesised according to literature procedures (from ligands **3.2** and **3.3**, respectively), and their stoichiometric reactivity was examined to benchmark against the novel aluminium amidinate catalysts.[20] The stability of each substrate was first tested; no decomposition was observed when heated at 353 K in benzene-d_6 for 18 hours. All stoichiometric reactions were carried out on an NMR scale.

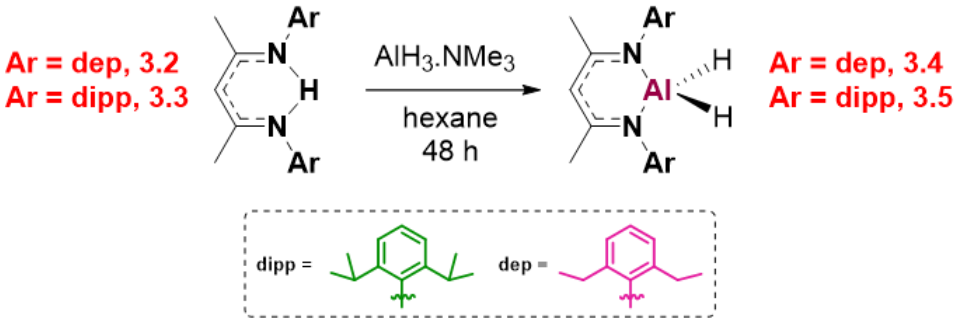

Scheme 3.3: Synthesis of known β-diketiminate complexes **3.4** and **3.5**.

3.4.1.1 Reactions with β-Diketiminate Complexes 3.4-3.5

The seminal work reported by Roesky and co-workers examined the stoichiometric reactivity of **3.4** with one equivalent of phenylacetylene and HBpin in chloroform-*d* at room temperature (296 K). When reacted with one equivalent of phenylacetylene, they reported the formation of a mono-substituted aluminium acetylide complex after 6 hours with concomitant formation of hydrogen gas. For ease of comparison between the literature and the research presented herein, these reactions were repeated in both chloroform-*d* and benzene-d_6. The reactions of **3.4** and **3.5** with phenylacetylene (1:1 and 1:10 ratios) were conducted at room temperature in both NMR solvents (**Scheme 3.4**). In all instances, no reactivity was observed after 6 hours at room temperature and heating the reaction overnight (313.15 K) yielded no product. **Figure 3.13** shows a ^{1}H NMR stack of **3.4** and ten equivalents of phenylacetylene in chloroform-*d*

monitored for the duration of the reaction. Furthermore, conducting the reaction at 353 K in benzene-d_6 in the presence of **3.5** also revealed no reactivity.

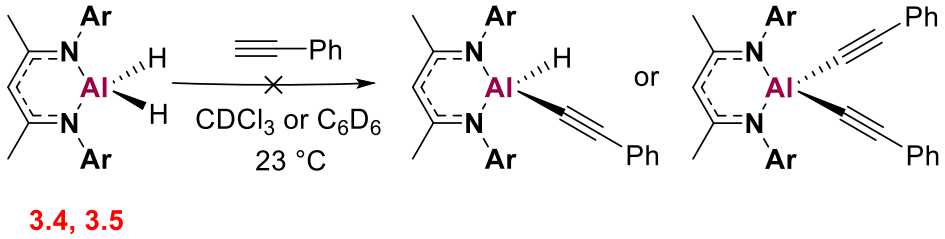

3.4, 3.5

Scheme 3.4: General scheme to show the reactivity of **3.4** and **3.5** with phenylacetylene.

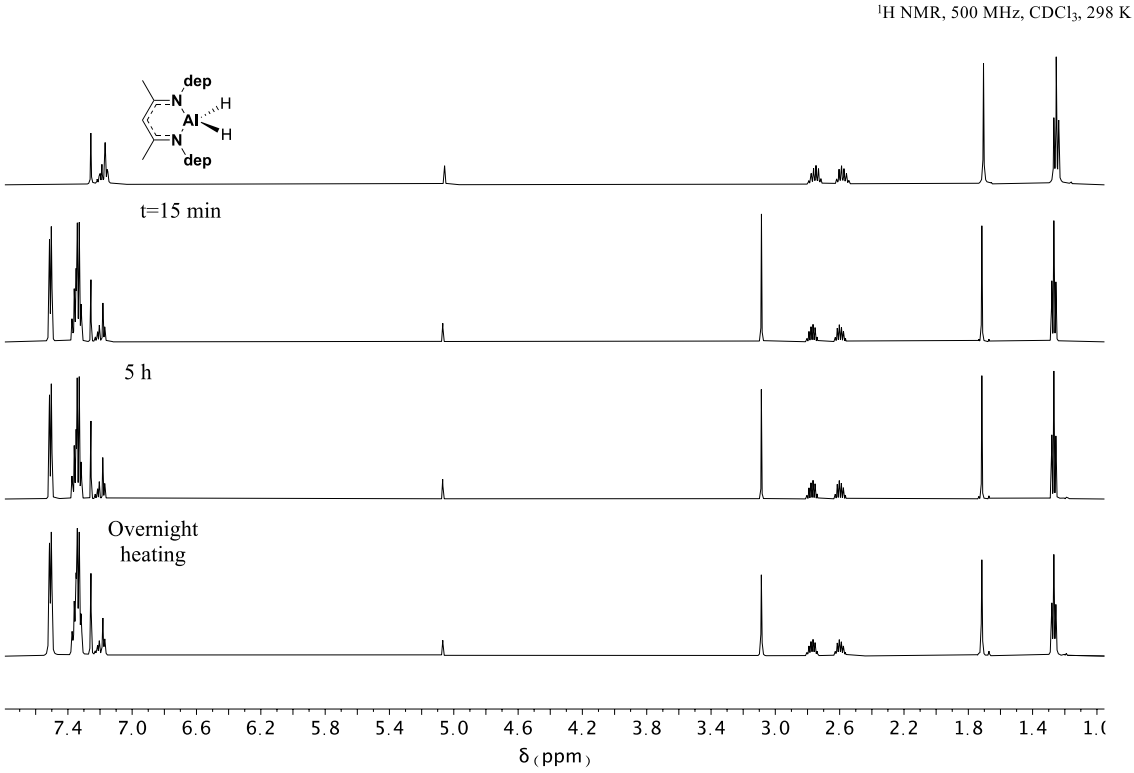

Figure 3.13: ^{1}H NMR plot of **3.4** with ten equivalents of phenylacetylene in chloroform-*d*.

It was also reported that **3.4** did not react with HBpin at room temperature. However, the data presented within the supporting information directly contradicts this claim, and the ^{1}H NMR spectrum provided shows a mixture of products formed, including excess HBpin.[63] Repeating this reaction using 2 equivalents of HBpin and monitoring by ^{1}H NMR spectroscopy (**Figure 3.14**) revealed complete consumption of **3.4** and HBpin in less than 15 minutes. The consumption of HBpin was confirmed by both ^{1}H and ^{11}B NMR spectroscopy and the formation of a mixture of products was observed. The emergence of two singlets (0.33/0.64 ppm) integrating to six protons each suggests that the HBpin methyl substituents were no

longer chemically equivalent, and this upfield shift compared to HBpin (1.26 ppm) indicated that a bond may be formed to the Lewis acidic aluminium centre. ^{11}B NMR spectroscopy showed a resonance at -36 ppm. Multiple methine resonances (of the BDI ligand) were observed further corroborating the formation of multiple products. These experiments contradict the reports in the literature, but further characterisation was not sought. Repeating this reaction in benzene-d_6 revealed the same de-symmetrisation of the HBpin methyl groups (0.52/0.91 ppm) with no starting material remaining.

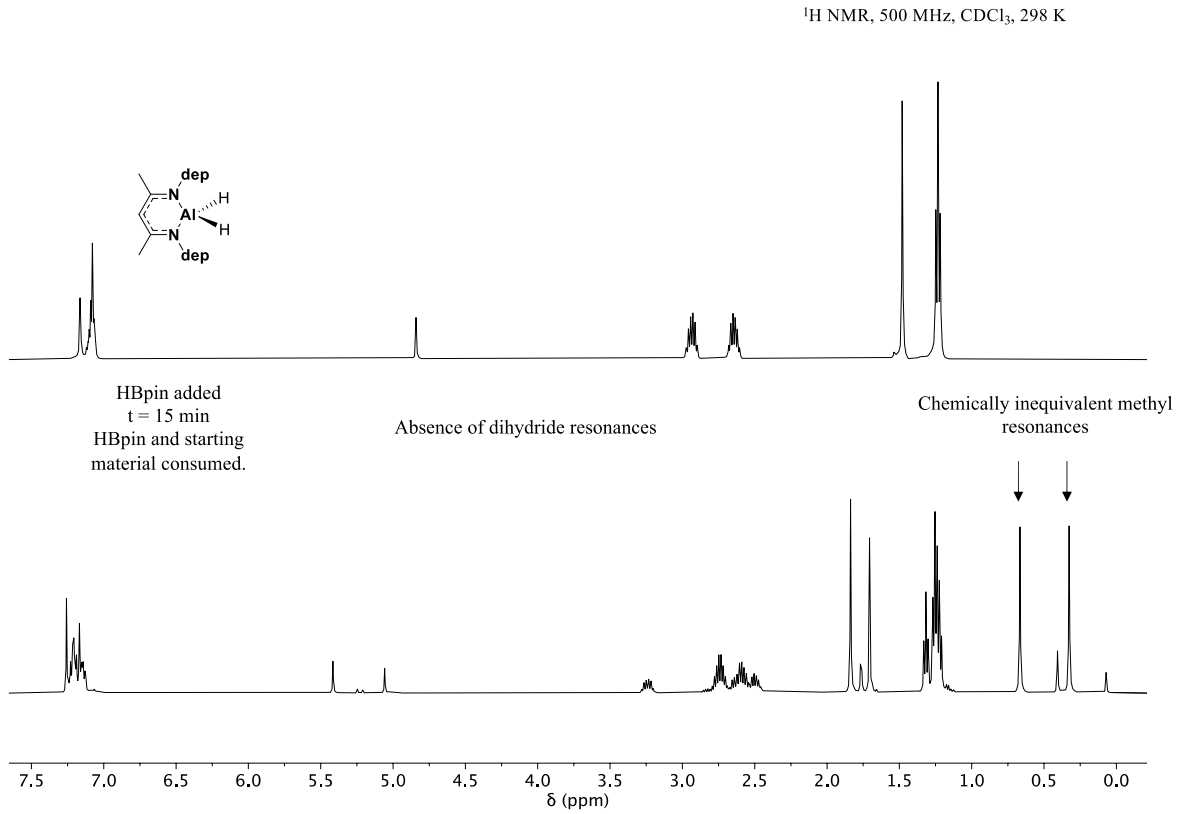

Figure 3.14: ^{1}H NMR of the reaction of **3.4** with HBpin in chloroform-*d*.

The same reactivity was observed for complex **3.5** with HBpin in chloroform-*d*. The reaction was seen to proceed quickly (as was also observed in benzene-d_6). A loss of symmetry was observed at the aluminium centre. Multiple resonances in the alkyl region of the spectra emerged and were then consumed over the course of the reaction suggesting that a mixture of products formed initially, and over time these were consumed to form one major product (and excess HBpin). Analysing the reaction mixture by ^{11}B NMR spectroscopy showed a quintet at -36 ppm, indicative of the formation of a borohydride $[BH_4]^-$ species.

3.4.1.2 Reactions with 2.9-2.10

The aluminium hydride complexes **2.9-2.10** were reacted with phenylacetylene at room temperature and, in all instances, no formation of an aluminium acetylide species akin to that proposed by Roesky *et al.* was observed (**Scheme 3.5**). In contrast to **3.4-3.5**, where no reaction was apparent, small amounts of decomposition were observed when heated at 353 K, with further decomposition and trace formation of hydrogen (**2.9**) produced at longer reaction times. The rate of decomposition varied across the series. For example, **2.9** showed decomposition after 1 hour at 353 K, which increased further upon sequential addition of a second equivalent of phenylacetylene and heating for a further 3 hours. In contrast, reacting **2.10** with two equivalents of phenylacetylene and heating at 353 K showed only traces of decomposition after 6 hours, and longer reaction times (>24 h) were needed to observe further decomposition (**Figure 3.15**).

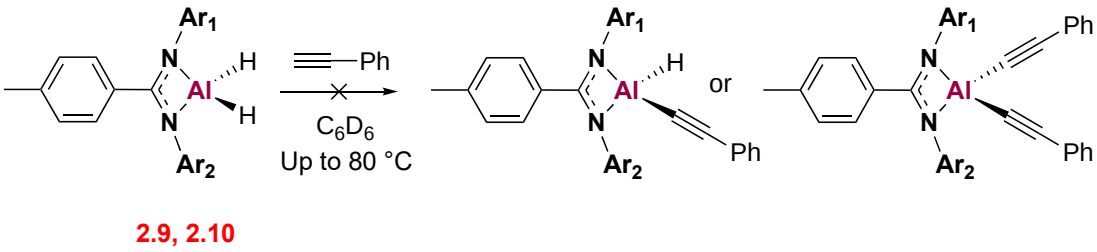

Scheme 3.5: General scheme to show the reactivity of **2.9** and **2.10** with phenylacetylene.

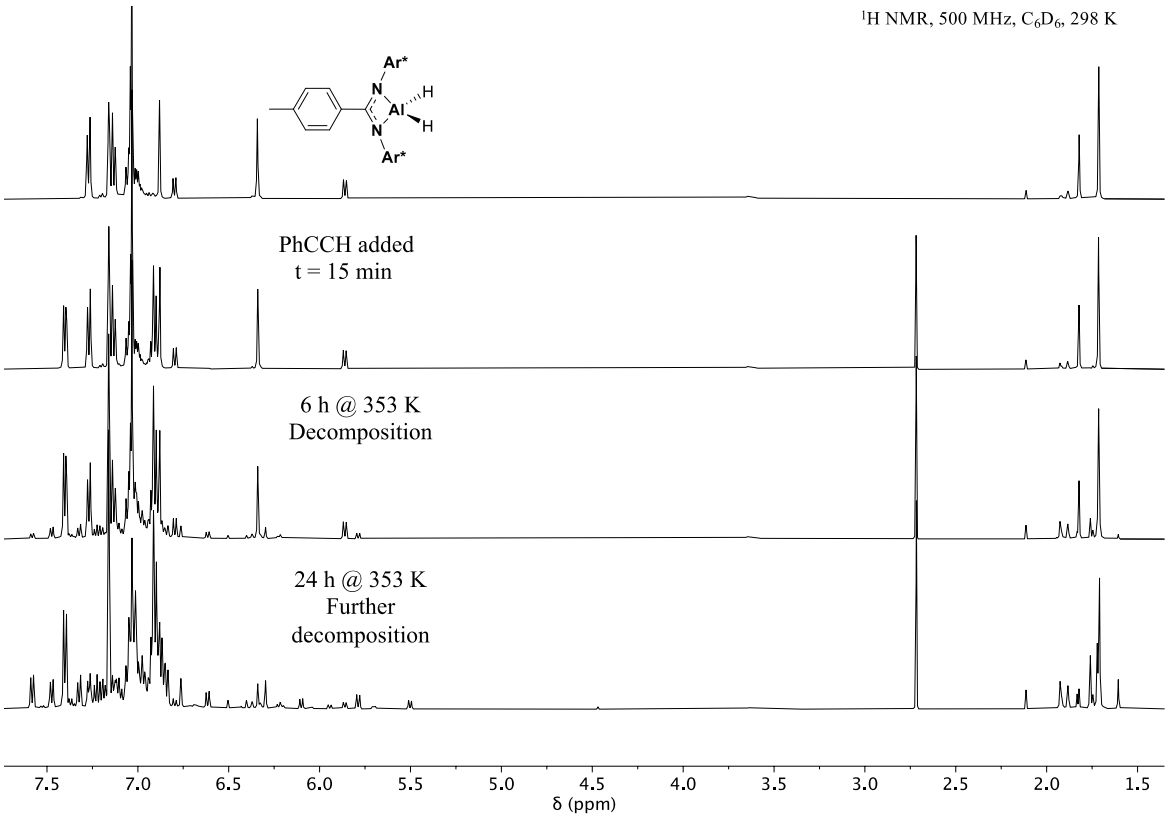

Figure 3.15: ^{1}H NMR stack of **2.10** with phenylacetylene.

The reactivity of **2.9** and **2.10** with two equivalents of HBpin was explored in benzene-*d*$_6$. After 15 minutes at room temperature, complete consumption of the starting aluminium dihydride was observed in both instances, with excess HBpin remaining and a broad resonance (-10 ppm) observed in the ^{11}B NMR spectrum. Sharp singlets at 1.64/1.82 ppm (**2.9**) and 1.20/1.30 ppm (**2.10**) integrating to six protons each were indicative of a loss of symmetry at the HBpin methyl substituents, as was observed for **3.4**-**3.5**. The spectrum for **2.9** was broad, whereas the spectrum for **2.10** was sharp and resolved (**Figure 3.16**). Heating both samples for 30 minutes at 353 K revealed the loss of these singlets (as well as the resonance at -10 ppm in the ^{11}B NMR), and both spectra became sharp and resolved. A broad borohydride resonance emerged in both ^{11}B NMR spectra at -36 ppm. This suggests that an initial asymmetric [LAlH_2•HBpin] adduct was rapidly formed, which was then converted to the final product after heating at 353 K. This reaction was repeated to trap the proposed adduct and elucidate its structure through ^{1}H-^{11}B NMR correlation experiments, however, this species was short lived even at room temperature and these experiments were unsuccessful.

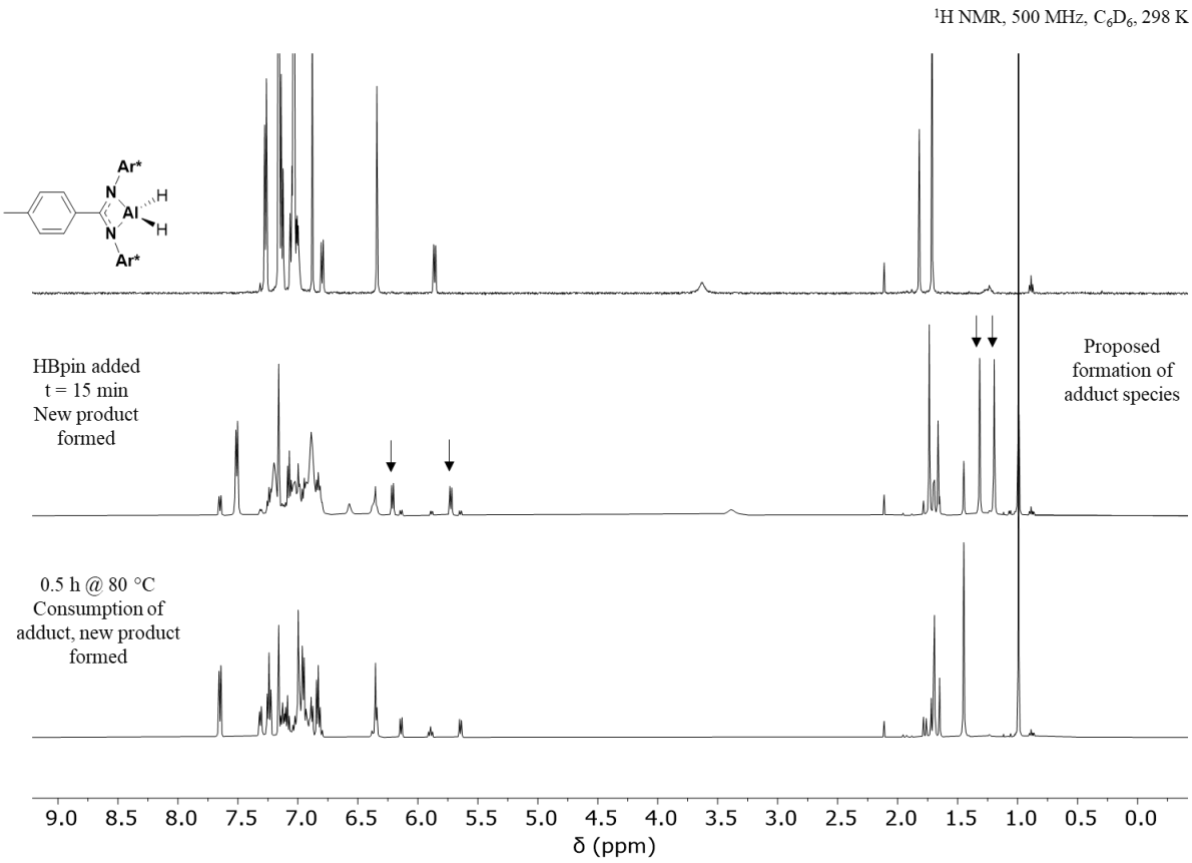

Figure 3.16: ^{1}H NMR stack of the reaction of **2.10** with HBpin.

A preparative scale reaction of **2.10** with HBpin was conducted to isolate the reaction product and aid in elucidating its structure; the reactivity is summarised in **Scheme 3.6**. Compound **2.10** was dissolved in toluene, HBpin was added, and the reaction was heated for 30 minutes at 353 K. The solvent was removed *in vacuo* and the crude product was recrystallised in toluene/hexane.

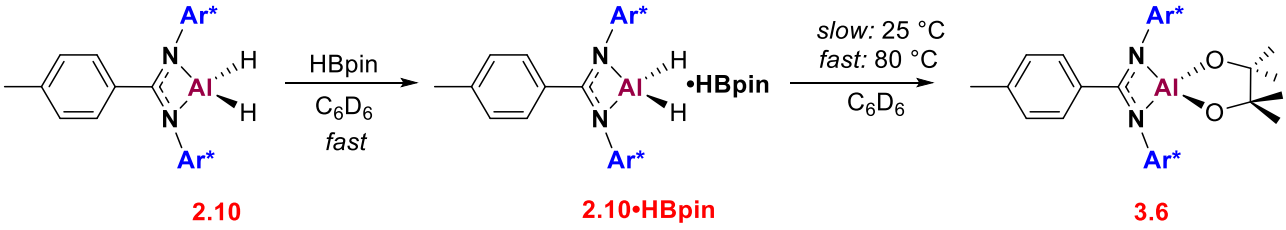

Scheme 3.6: Scheme to show the reaction of **2.10** with two equivalents of HBpin.

Analysis of the ^{1}H NMR spectrum revealed the presence of twelve protons of the pinacolate group that resonate as a singlet at 1.45 ppm, indicating a restoration of symmetry to the final

product. However, inspection of the ^{11}B NMR spectrum showed an absence of any boron-containing compounds after recrystallisation.

Single crystals suitable for analysis were grown from a concentrated solution of benzene-*d*$_6$/hexane and revealed the identity of the product to be the aluminium pinacolate **3.6**. Compound **3.6** crystallised in the P2$_1$/*c* space group with four molecules in the unit cell (**Figure 3.17**). The solid-state structure showed a puckered pinacolate moiety, with roughly equal Al-O bond lengths (1.718(1)/1.721(1) Å) and an O-Al-O angle of 98.5°. A contraction of the Al-N bonds was observed compared to the parent dihydride **2.10** (Al-N **3.6**: 1.897(1)/1.904(1) Å; **2.10**: 1.943(10)/1.939(10) Å). A related β-diketiminate complex revealed nearly identical bond lengths (1.897(1)/1.904(1) Å) but possessed longer Al-O bonds (1.718(1)/1.721(1) Å) and a smaller O-Al-O angle (92.7 °).[137] A summary of key bond lengths and angles is shown in Table 3.2.

The formation of **3.6** must occur with concomitant formation of borane (BH_3), though this was not observed in the ^{11}B NMR spectrum. However, a broad resonance was observed at -35 ppm, (as for **3.4**/**3.5**) attributed to the formation of a borohydride species. The precise identity of this species is unknown, but the isolation of **3.6** must form *via* the further reaction of BH_3.

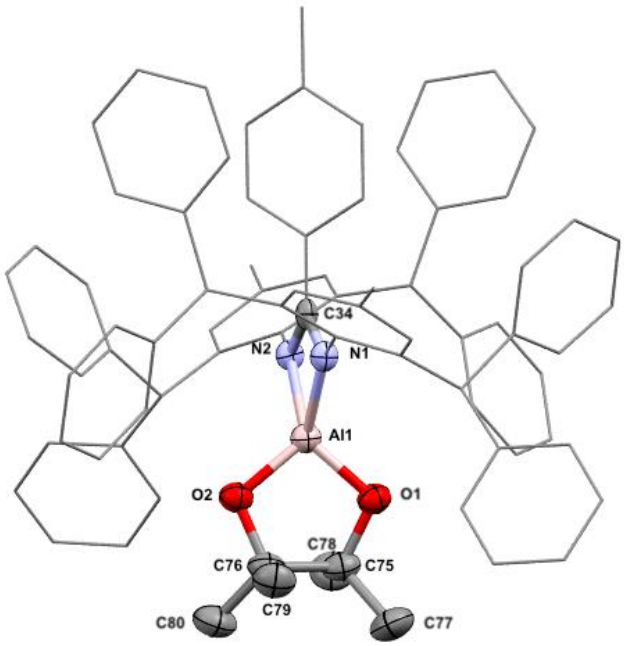

Figure 3.17: The X-ray structure of **3.6**.

Table 3.2: Selected bond lengths (Å) and angles (°) for compound **3.6**.

Bond Length		Bond Length	
Al1-N1	1.904(1)	Al1-O1	1.721(1)
Al1-N2	1.895(1)	Al1-O2	1.718(1)

Bond Angle	
N1-Al1-N2	70.59(6)
N1-C34-N2	109.1(1)
O1-Al1-O2	98.47(6)

Attempts to recrystallise the product formed from the reaction of **2.9** and HBpin were unsuccessful. However, owing to the similarities in the NMR spectra, it seems likely that the reaction of **2.9** would proceed through an analogous asymmetric adduct and proceed to form an aluminium pinacolate structure. Similarly, whilst Roesky and co-workers reported an absence of reactivity between **3.4** and HBpin, repeating these reactions under the same (chloroform-*d*) and different (benzene-d_6) conditions revealed identical reactivity to the amidinate complexes **2.9** and **2.10**, and therefore the formation of a β-diketiminate aluminium pinacolate species is proposed.

3.4.1.3 Reactions with 2.12

The stoichiometric reactivity of **2.12** was investigated in benzene-d_6. When reacted with one equivalent of phenylacetylene, catalyst degradation was observed with trace amounts of hydrogen gas formed after heating for 2 hours at 353 K. Heating for longer reaction times (>6 hours) showed further degradation in the aromatic region of the ^{1}H NMR spectrum, gradual consumption of phenylacetylene and the emergence of a new product. Styrene was also identified in the reaction mixture (doublets at 5.60 ppm ($^{3}J_{HH}$ = 17 Hz) and 5.07 ppm ($^{3}J_{HH}$ = 11 Hz)), demonstrating the divergent reactivity of **2.12** from **2.9**-**2.10** and **3.4**-**3.5**.

When reacted with one equivalent of HBpin, an unidentified product formed, and no new resonances attributed to the pinacolate methyl groups were identified. In contrast to **2.9**-**2.10** and **3.4**-**3.5**, which were found to react cleanly with HBpin, **2.12** showed signs of decomposition after 15 minutes at room temperature which increased when heated at 353 K. Repeating the reaction and monitoring it at room temperature revealed the same decomposition over longer reaction times. Monitoring the reaction by ^{11}B NMR revealed a distinctive quartet

at -7 ppm attributed to the formation of borane (BH_3, **Figure 3.18**) in solution and the absence of a $[BH_4]^-$ species which was noted for complexes **2.9**-**2.10** and **3.4**-**3.5**.

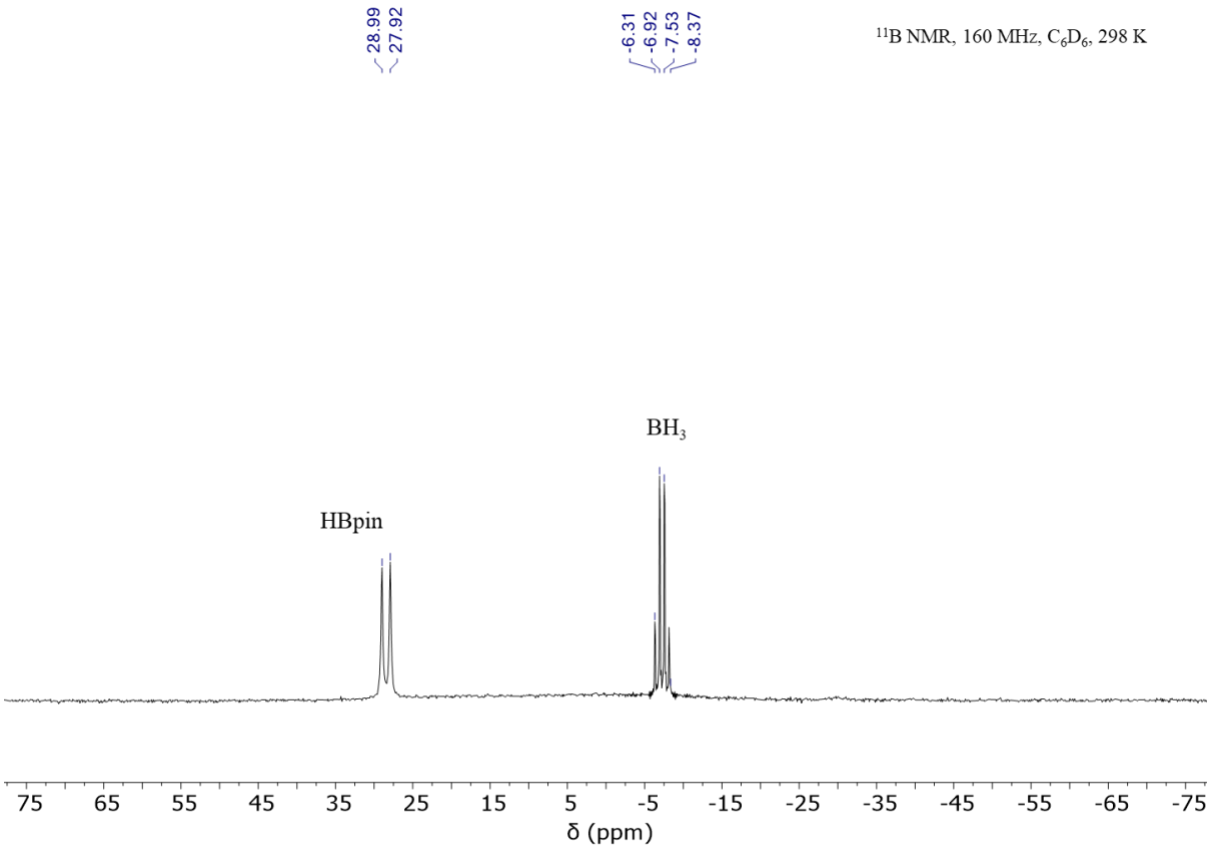

Figure 3.18: ^{11}B NMR spectrum of the reaction of **2.12** with HBpin.

3.4.1.4 Reactions with 2.14-2.15

The difference in catalytic reaction profiles and modelled kinetics data for the aluminium alkyl complexes **2.14**-**2.15** suggested they would exhibit divergent reactivity with phenylacetylene and HBpin compared to the aluminium amidinate and β-diketiminate complexes **2.9**-**2.10**, **2.12,** and **3.4**-**3.5**. In general, these complexes were found to be more stable than their hydride counterparts, being able to withstand heating to elevated temperatures (353 K) in the presence of each substrate.

Reacting **2.14** with one equivalent of phenylacetylene showed no reactivity after 15 minutes at room temperature, or after heating for 2 hours at 353 K. Heating for longer reaction times (up to 48 hours) and monitoring by ^{1}H NMR spectroscopy revealed that two new products had formed (**Figure 3.19**). A resonance below 0 ppm (-0.51 ppm) was observed, indicative of the

formation of a second aluminium alkyl species. The concomitant formation of methane (0.16 ppm) indicated liberation of one alkyl group and the formation of a mono-substituted acetylide species as the major product. After 48 hours, approximately 17% of **2.14** remained in the reaction mixture (singlet, -0.29 ppm; multiplet, 3.63 ppm) and prolonged heating could reduce this further. The ^{1}H NMR spectrum also indicated the formation of trace amounts of a second minor product that has been tentatively assigned as the *bis*-substituted acetylide complex; whilst no signal below 0 ppm would be observed for this, a third product was identified in the mixture at much lower concentration, as evidenced by small doublets at 1.05/1.29 ppm.

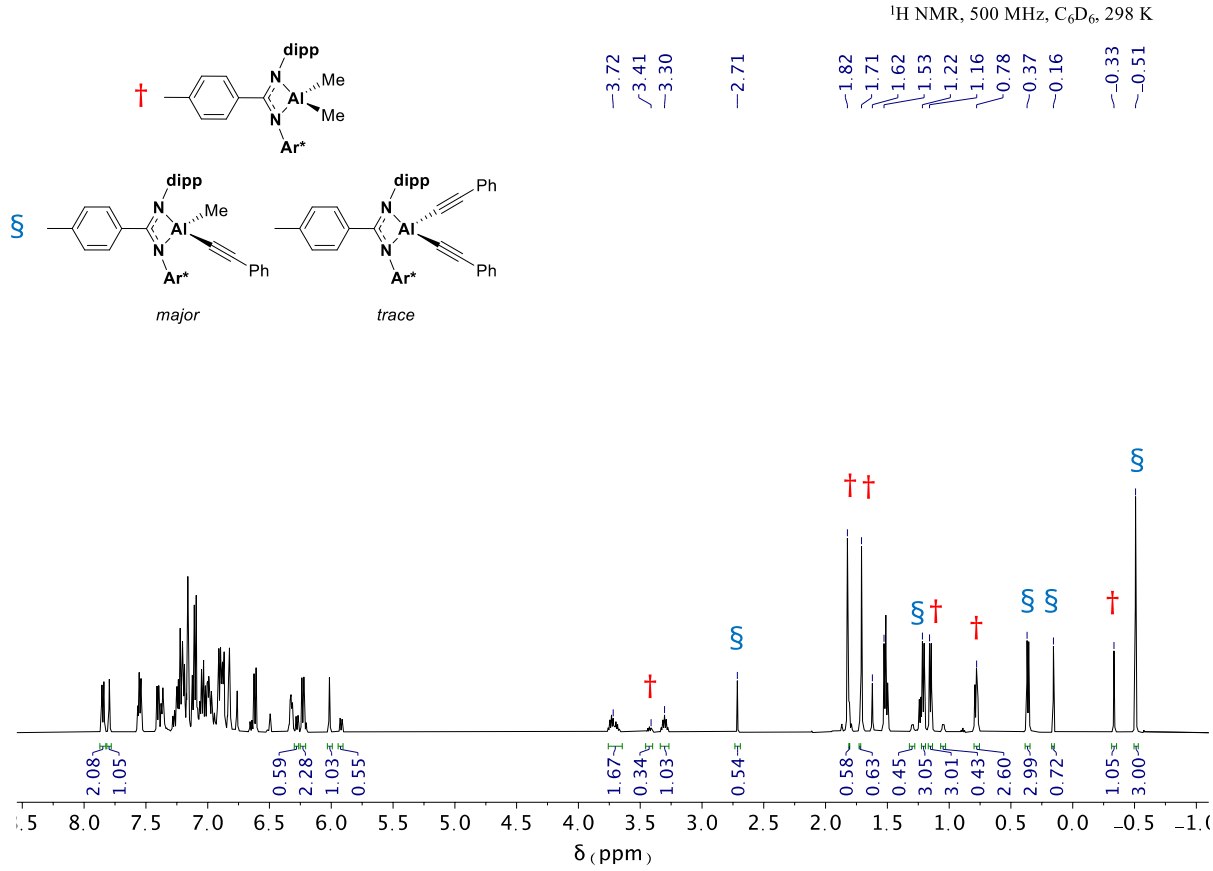

Figure 3.19: ^{1}H NMR spectrum of the reaction of **2.14** with phenylacetylene after 48 hours.

The reaction of **2.15** with phenylacetylene was much slower in comparison. After 5 days at 353 K, the ^{1}H NMR spectrum showed two resonances below 0 ppm (**2.15**: -0.87 ppm, product: -0.92 ppm) again indicative of the formation of a mono-substituted aluminium acetylide complex, though this was only present at approximately 16% conversion. All recrystallisation attempts were unsuccessful.

Catalysts **2.14** and **2.15** were reacted with HBpin, heated at 353 K, and monitored by ^{1}H and ^{11}B NMR spectroscopy. Reacting each catalyst with one equivalent of HBpin and heating for 2 hours at 353 K revealed complete consumption of HBpin and concomitant formation of Me-Bpin; this was confirmed by resonances in the ^{1}H NMR (singlet, 0.40 ppm; singlet, 1.05 ppm) and ^{11}B (singlet, 34 ppm) spectra.[138] To explore the reactivity of these complexes further, **2.15** was reacted with an excess (four equivalents) of HBpin. After 1 hour at 353 K, both H- and Me-Bpin were present in the reaction mixture, with Me-Bpin increasing in intensity when monitored over the course of 7 hours. After this time, near complete consumption of the starting dimethyl resonance (-0.87 ppm) was observed in the ^{1}H NMR spectrum and HBpin/Me-Bpin were observed in the ^{11}B NMR spectrum. Interestingly, the formation of **3.6** was observed after 7 hours and is presumed to proceed *via* **2.10** as an intermediate (**Scheme 3.7**).

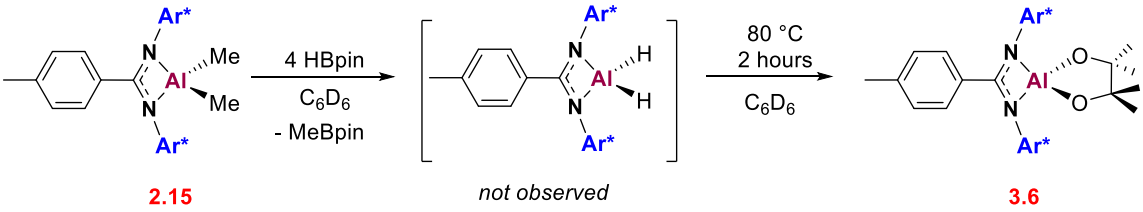

Scheme 3.7: Proposed reactivity of **2.15** with HBpin.

3.4.1.5 Summary of Stoichiometric Reactions

The reactions presented in sections 3.4.1.1 – 3.4.1.4 were conducted to elucidate the mechanistic pathway of the aluminium amidinate complexes and determine if the known acetylide or hydroalumination pathways were applicable to these systems.

Repeating reactions from the literature yielded unexpected results. That is, complexes **3.4**-**3.5** were found not to react with phenylacetylene, whilst they reacted rapidly with HBpin. This pattern of reactivity was true of both complexes (**3.4**-**3.5**), both substrates and in chloroform-*d* and benzene-d_6. The reaction profiles of the β-diketiminate complexes with HBpin were mirrored by the aluminium hydride complexes **2.9**-**2.10** under the same conditions, and the isolation of the aluminium pinacolate structure **3.6** suggests that analogous complexes form across this series. In contrast, the β-diketiminate complexes did not react with phenylacetylene, whilst complexes **2.9**-**2.10** decomposed under the same reaction conditions.

Catalyst **2.12** exhibited reduced solution-state stability in comparison. When reacted with HBpin, divergent reactivity was observed compared to **2.9**-**2.10** and **3.4**-**3.5**: an analogous pinacolate structure was not formed, and the presence of borane, a known decomposition product of HBpin was identified in the ^{11}B NMR spectrum.[139] This reactivity, in conjunction with DOSY NMR and DFT calculations (Chapter 2), offers additional insight into why catalyst **2.12** exhibited longer reaction times (22 hours) compared to **2.9** (11 hours) despite bearing the smaller mes substituent.

The aluminium alkyl complexes **2.14**-**2.15** showed further divergent reactivity. This was less surprising considering the observed differences in the modelled kinetic profiles and provides further evidence that these complexes proceed *via* different mechanistic pathways.

These stoichiometric reactions highlight the individual reactivity of each complex and offer some initial insights into the mechanistic pathways of these catalysts. Firstly, they indicate that the acetylide pathway first proposed by Roesky and co-workers using compound **3.4** was incorrect and could not occur for this catalyst/substate combination. The aluminium acetylide pathway can also be ruled out for the aluminium hydride compounds **2.8**-**2.10** and **2.12** owing to the lack of reactivity and/or decomposition in the presence of phenylacetylene. In the instances when an aluminium acetylide species was formed (**2.14**-**2.15**), these were only observed after heating at elevated temperatures for extended periods of time (>72 hours) and are therefore unlikely to form on the timescale of a catalytic reaction. In contrast, the facile (and rapid) formation of a proposed HBpin adduct indicates that this could be an important species in the catalytic pathway.

The hydroboration of diphenylacetylene was attempted with complexes **2.9**, **2.12** and **2.14** to ascertain whether these catalysts could hydroborate internal alkynes, and determine whether the hydroalumination pathway first proposed by Cowley *et al*. was applicable to these systems. No product formation was observed in all instances, however this did not necessarily rule out this pathway. For example, the diphenylacetylene substrate is large, and this specific reaction may have a large energy barrier. To assess the viability of this pathway, the initial step of the acetylide and hydroalumination reaction pathways was probed by DFT using a simplified aluminium complex. (**Figure 3.20**).[††]

[††] DFT calculations were performed by Dr Clare Bakewell.

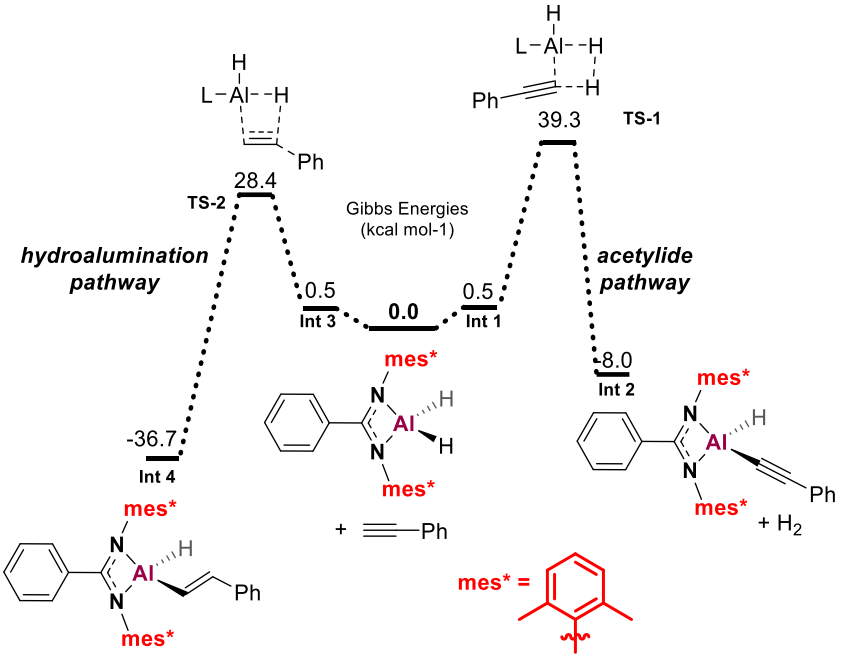

Figure 3.20: Calculated reaction pathways for the initial steps of the hydroalumination (LHS) and acetylide (RHS) pathways.

The hydroalumination pathway had a ΔG of activation of 28.4 kcal mol^{-1} which is both kinetically and thermodynamically favourable however, as this reaction does proceed slowly at room temperature, a lower energy barrier would be expected. The energy barrier for the acetylide pathway was much greater (39.3 kcal mol^{-1}) and is thermodynamically unfavourable and this has previously been noted in the literature.[140] Evidently, neither of these pathways can be applied to the aluminium hydride and alkyl complexes reported herein, and further investigation was required. To gain additional insight into the mechanistic pathway, the time course of each reaction was monitored by ^{11}B NMR spectroscopy.

3.4.2 Monitoring Catalysis by ^{11}B NMR

All catalytic reactions were monitored by ^{11}B NMR spectroscopy to further help elucidate the reaction mechanism. **Figure 3.21** shows the stack of ^{11}B NMR spectra over the course of the reaction using catalyst **2.9** as a representative example for catalysts **2.8**-**2.10**.

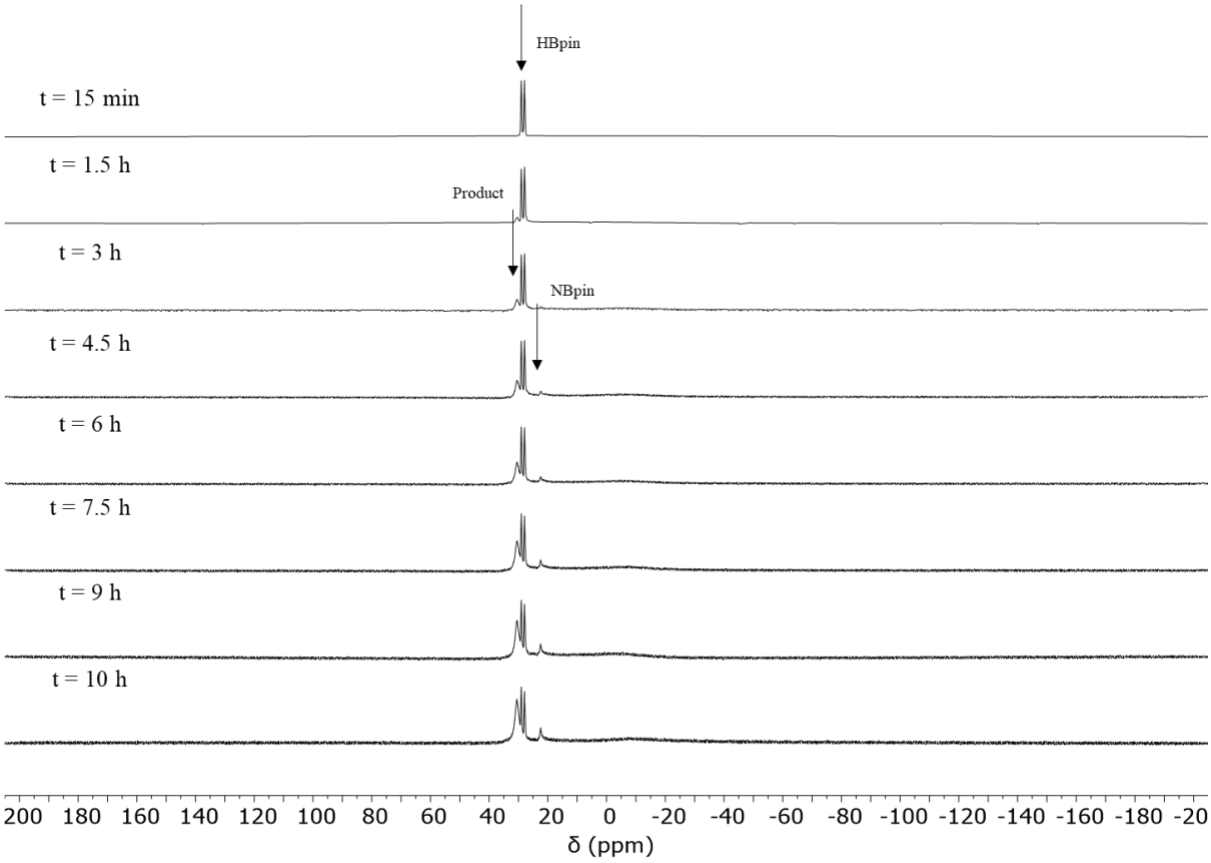

Figure 3.21: ^{11}B NMR stack during aluminium hydride catalysis, using **2.9** as a representative example.

Examining the time course of the reaction for **2.9** (**Figure 3.11**), it can be noted that the kinetics start to become more complex between 6 and 7.5 hours. In addition to HBpin (doublet, 28 ppm) and the hydroboration product (broad singlet, 30 ppm), a third resonance at 22 ppm appeared in the ^{11}B NMR spectrum at very low intensity at 4.5 hours and increased at time points thereafter. This indicated that the complexity of the kinetics may be attributed to the competitive formation of a new boron-containing species. This was also present in the ^{11}B NMR spectra of the non-catalytic reactions using diphenylacetylene, suggesting that it forms independently of catalysis and that competitive formation of this species in catalytic reactions can account for the observed shift in mechanistic regime. It was not possible to elucidate the structure of this species, however, the structure and ^{11}B NMR spectra of complexes containing N-Bpin bonds have previously been reported in this region (21-25 ppm).[141] The borohydride resonances observed ~-35 ppm in the stoichiometric reactions were not identified during catalytic reactions.

Monitoring the catalytic activity of **2.12** by ^{11}B NMR spectroscopy revealed key differences in the NMR spectra despite exhibiting a similar kinetic profile as catalysts **2.8**-**2.10** (**Figure 3.22**). The same peaks were observed as for complexes **2.8**-**2.10** (product, HBpin, proposed N-Bpin compound) with additional resonances at 24 (singlet, unidentified product) and -7 (quartet, BH_3) ppm. The presence of borane in the stoichiometric and catalytic reactions with **2.12**, whilst $[BH_4]^-$ was only observed stoichiometrically for **2.9**-**2.10**, provides further evidence for divergent reactivity between these complexes and the reduced solution-state stability of **2.12**.

The catalytic capabilities of borane have often been overlooked in the literature, but recent reports have emerged detailing its role in hydroboration catalysis.[139,142–145] Thomas and co-workers were able to prove its role in catalysis through a series of catalytic and control reactions. The formation of a borane adduct was observed during catalysis and proposed to be catalytically active; addition of 10 mol% *N,N,N',N'*-Tetramethylethylenediamine (TMEDA) inhibited formation of this and catalytic activity was markedly reduced. For example, in the presence of $LiAlH_4$, the addition of TMEDA reduced the yield of the hydroboration of 4-*tert*-butylstyrene from 81% to 5% under the same reaction conditions. Mechanistically, this is said to proceed *via* a simple hydroboration and transborylation step and was found to be the dominant catalytic process.[139]

This information suggests that the catalytic profile for **2.12** is more complex than initially perceived (and compared to the other catalysts in this series) and that a borane-catalysed pathway may also be in operation. These competing mechanistic pathways, in conjunction with the solution-state properties of **2.12** (increased dimeric character in solution) can account for the observed longer reaction time of **2.12** when compared to **2.9** and **2.14**.

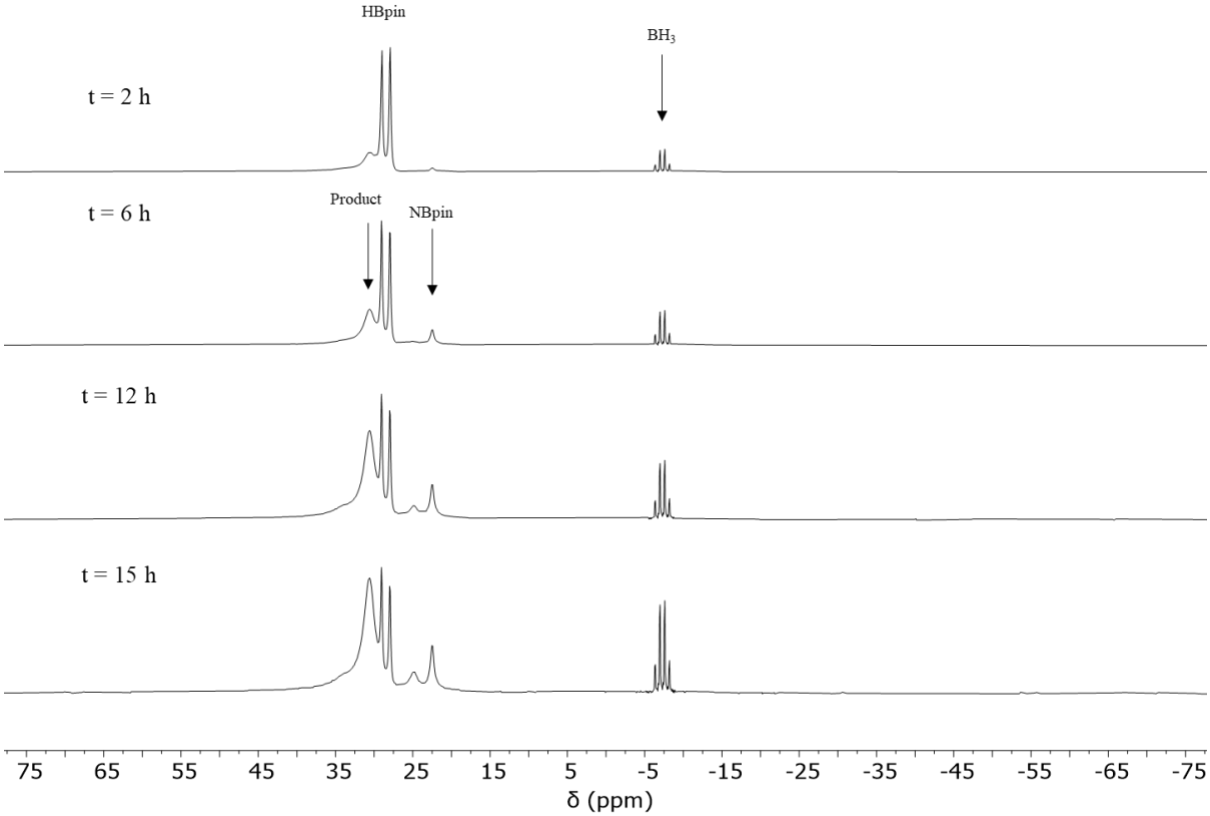

Figure 3.22: ^{11}B NMR stack during aluminium hydride catalysis using **2.12**.

Figure 3.23 shows a representative stack of the ^{11}B NMR spectra for the alkyl catalysts **2.14** and **2.15**. Compared to **2.12**, there was a distinct absence of borane in the spectra, but the same unidentified singlets at 22/24 ppm were observed. There was an additional singlet at 34 ppm assigned to Me-Bpin, further highlighting the different reactivity of the alkyl complexes compared to the hydrides.[138] As with **2.12**, this suggests that the stoichiometric reactions were a better representation of the true catalytic reaction profile, in contrast to **2.9**-**2.10**.

The information presented under all subheadings in section 3.4.1 highlights significant, but reproducible, differences in the reactivity of each series of the aluminium hydride and alkyl complexes. Trends can be explained through tentative links to catalyst size, structure, or stability. The observed differences in reaction kinetics, both within and between each series, suggest that catalyst structure is important, and seems to contravene the idea that a common catalytic species is in operation.

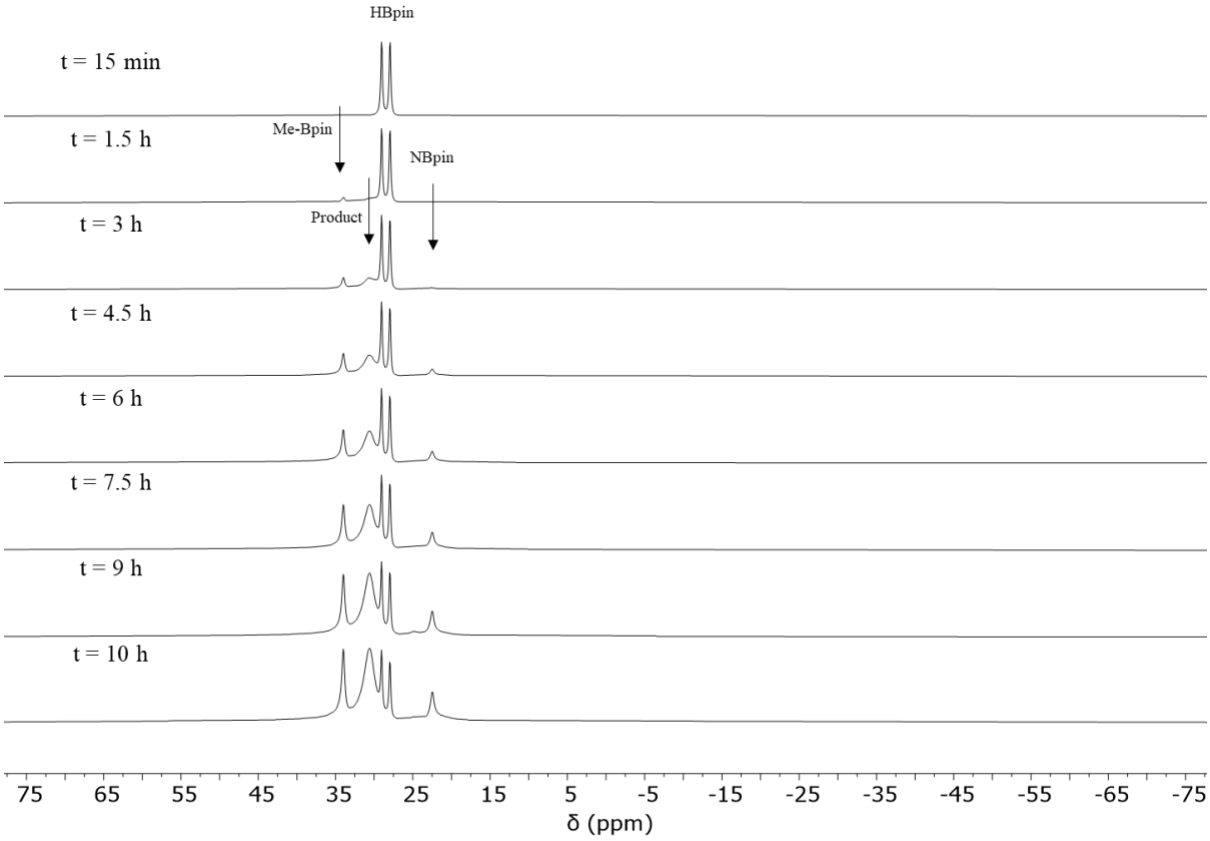

Figure 3.23: ^{11}B NMR stack during aluminium alkyl catalysis, using **2.14** as a representative example.

3.4.3 Proposed Catalytic Cycle

Through a series of catalytic and stoichiometric reactions, the acetylide and hydroalumination pathways first proposed by Roesky and Cowley, respectively, were ruled out for the catalysts presented here. The stoichiometric reactions revealed that the mechanism is likely to proceed *via* the formation of a HBpin adduct. Similarly, the formation of **3.6** or related aluminium pinacolate structures was not observed in the ^{1}H NMR spectrum during catalysis and suggests that this reactivity is only observed in the absence of phenylacetylene. Therefore, further information is required to derive the rate equation.

There exists some literature precedent for catalytic hydroboration reactions proceeding *via* a HBpin adduct. In 2019, Rueping and co-workers proposed that the magnesium-catalysed hydroboration of phenylacetylene proceeds *via* the reaction of $MgBu_2$ with HBpin to form Bu-Mg-H and Bu-Bpin (Bu = butyl). The catalytically active species is Mg-Bu-H with one molecule of HBpin datively bound to the magnesium centre through an oxygen atom, with a calculated activation barrier of 8.9 kcal mol^{-1}. This enters the catalytic cycle where it undergoes

transmetallation with one molecule of phenylacetylene.[146] Based on these reports, and the experimental observations reported herein, a speculative catalytic mechanism is shown in **Figure 3.24a**.

.

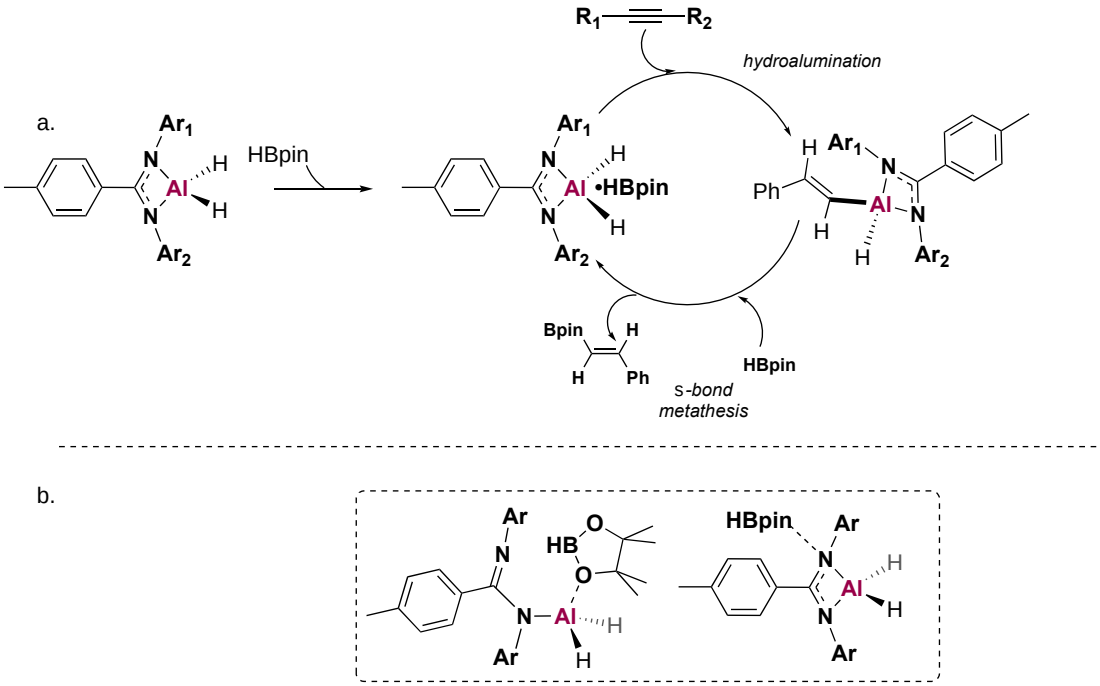

Figure 3.24: a. Proposed catalytic cycle for aluminium catalysed hydroboration of phenylacetylene. b. Proposed strucutres of aluminium-HBpin adduct.

The first step is the formation of a HBpin adduct, which was observed both stoichiometrically and catalytically, but multiple attempts to elucidate the precise structure of this species were unsuccessful. However, the formation of an oxygen-bound Al-HBpin species (identical to that proposed by Rueping *et al.*) was ruled out, owing to the coordinatively saturated nature of this compound that would prohibit catalytic turnover. Instead, two potential adduct species are shown in **Figure 3.24b**. The structure of this species was also probed *via* DFT calculations, but results were inconclusive. It is then proposed that the HBpin adduct undergoes hydroalumination with phenylacetylene to form an aluminium-vinyl species. Hydrogen gas was not seen to evolve during any catalytic reactions (even with **2.12**) supporting the formation of an aluminium-vinyl species and ruling out the formation of an aluminium acetylide complex. Finally, this is proposed to undergo σ-bond metathesis, yielding the (*E*)-vinylboronate ester and regenerating the aluminium catalyst.

Plotting the product (yield) versus time graphs for **2.14-2.15** (section 3.5, **Figure 3.11**) revealed that the aluminium alkyl complexes are pre-catalysts for this reaction, and the active catalytic species forms *in situ* over time. The precise identity of the catalytic structure was investigated using ^{1}H and ^{11}B spectroscopy and the findings are summarised in **Scheme 3.8**.

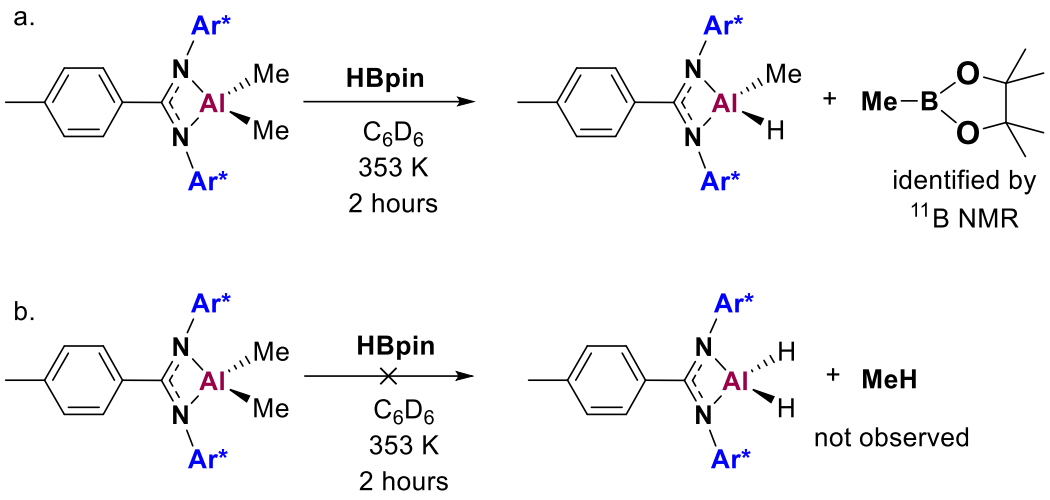

Scheme 3.8: a. Mixed hydride-alkyl species proposed through ^{11}B NMR observations. b. Absence of aluminium hydride and methane formation in ^{1}H NMR used to rule out generation of parent dihydride as active catalyst.

The stoichiometric reactions of **2.14-2.15** with HBpin revealed the formation of Me-Bpin in both the ^{1}H and ^{11}B NMR spectra, and this reactivity was mirrored during catalysis. Additionally, the parent aluminium dihydride compounds (**2.9-2.10**) did not form from **2.14-2.15** during any stoichiometric or catalytic reactions. In conjunction with the absence of methane in the ^{1}H NMR spectrum, this indicates the formation of a mixed hydride-alkyl species. The formation of this mixed species, instead of generating the parent aluminium dihydrides, could also account for the different reaction kinetics observed between the aluminium hydride and alkyl complexes.

3.5 Summary and Outlook

3.5.1 Summary

The aluminium hydride and alkyl complexes **2.8-2.10**, **2.12** and **2.14-2.15** were tested for their capacity to catalyse the hydroboration of phenylacetylene using HBpin. All catalysts were shown to be catalysts or pre-catalysts for the reaction, with reaction times varying between 6 (**2.8**) and 95 hours (**2.15**). The reaction times could be tentatively explained through links to catalyst size, structure, and/or stability. The aluminium hydride complexes showed complex

kinetic profiles, adhering to a second-order regime at low conversions (<75% conversion) whilst a more complex regime became dominant at high conversions. This was attributed to competitive side product formation observed during ^{11}B NMR spectroscopy.

The mechanism of action was probed through a series of stoichiometric reactions. The reactivity of the β-diketiminate complexes **3.4**-**3.5** with phenylacetylene and HBpin was investigated and was found to directly contradict the examples reported in the literature. Complexes **2.9**-**2.10** exhibited similar reactivity with HBpin, and the isolation of **3.6** suggested that aluminium pinacolate species are likely to form across this series. These complexes showed decreased stability in the presence of phenylacetylene compared to the related β-diketiminate complexes, and complex **2.12** exhibited different reactivity altogether, which is attributed to the greater degree of dimeric character in solution. The aluminium alkyl species **2.14**-**2.15** were found to form aluminium acetylide complexes when reacted with phenylacetylene, but the acetylide pathway was ruled out mechanistically owing to the slow rate of formation. When reacted with HBpin, the pinacolate structure **3.6** and Me-Bpin were seen to form.

Monitoring the catalytic reactions by ^{11}B NMR spectroscopy provided additional insight into the reactivity of these complexes and suggests that, except for **2.12**, the reactions are mediated by the aluminium complex and not competitive borane formation. The generation of borane revealed the catalytic profile for **2.12** to be increasingly complex and suggested multiple reaction pathways were in operation. This information was compiled to suggest a catalytic cycle, which proceeds *via* the formation of a HBpin adduct, then transmetallation to form an aluminium-vinyl species, followed by σ-bond metathesis. Through assessment of the ^{1}H and ^{11}B spectra, a mixed hydride-alkyl species was proposed to form as the active catalyst from the aluminium alkyl species **2.14**-**2.15**.

3.5.2 Outlook

The work discussed in this chapter pertains to the catalytic hydroboration of terminal alkynes. This is a seemingly simple transformation and the literature in this area is well developed. However, examination of the reaction kinetics and experimental attempts to elucidate the mechanism revealed that the reactivity is more complex and nuanced than has previously been accounted for in the literature. The catalytic cycle proposed herein is the first example of

aluminium-catalysed hydroboration reactions proceeding *via* a HBpin adduct, though a similar mechanism has previously been proposed for related magnesium-catalysed reactions. The structure of the catalyst was shown to have a profound effect on the catalyst activity and mechanism of action, even across a series of related compounds exhibiting only subtle structural differences. These subtle differences offer the opportunity to access divergent reaction pathways through simple synthetic manipulations, and this family of complexes could easily be expanded for future investigations into this phenomenon.

3.6 Chapter 3 Experimental Section

3.6.1 General Procedure for the Catalytic Hydroboration of Phenylacetylene (3.1)

Phenylacetylene (0.15 mmol, 16.5 μL) was added to a solution of catalyst (0.015 mmol, 10 mol%), 1,3,5- trimethylbenzene (10 μL), and HBpin (0.15 mmol, 21.5 μL) in benzene-d_6 (600 μL) and transferred to a J Young NMR tube. A t=0, ^{1}H NMR spectrum was recorded, and the sample tube was then heated at 80 °C. Each reaction was monitored over time, with ^{1}H NMR spectra recorded at regular time points (usually every hour) until >88% completion was achieved. The yield was determined by ^{1}H NMR spectroscopy using 1,3,5-trimethylbenzene as an internal standard.

^{1}H NMR (500 MHz, C_6D_6, 298 K) δ ppm: 1.13 (s, 12H, C**H**$_3$), 6.46 (d, 1H, C**H**, $^3J_{HH}$ = 18.5 Hz), 6.98−7.04 (m, 3H ^{Ph}C**H**), 7.32 (d, $^3J_{HH}$ = 10.0 Hz), and 7.76 (d, 1H, CH, $^3J_{HH}$ = 18.5 Hz).

3.6.2 General Procedure for Stoichiometric Reactions with Phenylacetylene

Phenylacetylene (0.0276 mmol, 3 μL) was added to a solution of catalyst (0.0276 mmol) in benzene-d_6 (600 μL) and transferred to a J Young NMR tube. A t=0, ^{1}H NMR spectrum was recorded. The sample tube was heated at 353 K and monitored at regular time intervals (^{1}H NMR spectroscopy) over the course of the reaction.

3.6.3 General Procedure for Stoichiometric Reactions with HBpin

HBpin (0.0138 mmol, 2 μL) was added to a solution of catalyst (0.0138 mmol) in benzene-d_6 (600 μL) and transferred to a J Young NMR tube. A t=0, ^{1}H NMR spectrum was recorded. The sample tube was heated at 353 K and monitored (^{1}H and ^{11}B NMR spectroscopy) at regular time intervals over the course of the reaction.

3.6.4 Synthesis of ^{dep}BDIH (3.2)

Concentrated HCl (50 mmol, 4.2 mL) was added to a solution of acetylacetonate (49 mmol, 5 mL) and 2,6-diethylaniline (100 mmol, 15.85 mL) in ethanol. The reaction was heated at reflux for 72 h. The reaction mixture was cooled to room temperature, the solvent was removed *in vacuo* and the residue was neutralised with sodium carbonate/DCM. The product was extracted into DCM (3 x 100 mL), dried ($MgSO_4$) and filtered. The solvent was concentrated *in vacuo*

and precipitated out with methanol. A second recrystallisation from MeOH/DCM was required. (4.42 g, 12.2%). NMR matches that reported in the literature.[147]

^{1}H NMR (500 MHz, C_6D_6, 298 K) δ ppm: 1.17 (t, 12 H, $CH_2C\mathbf{H}_3$, $^{3}J_{HH}$ = 6 Hz), 1.61 (s, 6H, $C\mathbf{H}_3$), 2.48-2.67 (m, 8 H, $C\mathbf{H}_2CH_3$, $^{3}J_{HH}$ = 6 Hz), 4.75 (s, 3H, $C\mathbf{H}_3$), 7.06-7.11 (m, 6H, $^{Ph}C\mathbf{H}$), 12.37 (s, 1H, N**H**).

3.6.5 Synthesis of ^{dipp}BDIH (3.3)

Concentrated HCl (48 mmol, 4 mL) was added to a solution of acetylacetonate (49 mmol, 5 mL) and 2,6-diisopropylaniline (110 mmol, 20.85 mL) in ethanol. The reaction was heated at reflux for 72 h. The reaction mixture was cooled to room temperature, the solvent was removed *in vacuo* and the residue was neutralised with sodium carbonate/DCM. The product was extracted into DCM (3 x 100 mL), dried ($MgSO_4$) and filtered. The solvent was concentrated *in vacuo* and recrystallised from MeOH/DCM (10.5 g, 51.2%). NMR matches that reported in the literature.[148]

^{1}H NMR (500 MHz, $CDCl_3$, 298 K) δ ppm: 1.13 (d, 12 H, $CH(C\mathbf{H}_3)_2$, $^{3}J_{HH}$ = 6.5 Hz), 1.22 (d, 12 H, $CH(C\mathbf{H}_3)_2$, $^{3}J_{HH}$ = 7 Hz), 1.72 (s, 6H, $C\mathbf{H}_3$), 3.13 (sept, 4H, $C\mathbf{H}(CH_3)_2$, $^{3}J_{HH}$ = 7 Hz), 4.89 (s, 1H, C**H**), 7.14 (m, 6H, $^{Ph}C\mathbf{H}$), 12.18 (s, 1H, N**H**).

3.6.6 Synthesis of [AlH_2(^{dep}BDI)] (3.4)

Synthesised according to literature procedures.[149] To a solution of trimethylamine alane (1.194 mmol, 106 mg) dissolved in toluene, ^{dep}BDIH (**3.2**, 1.194 mmol, 500 mg) was added and the solution was stirred for 1 h. The solvent was reduced *in vacuo* and recrystallised from hot hexane at 5 °C (257 mg, 48%). NMR matches that reported in the literature.

^{1}H NMR (300 MHz, C_6D_6, 298 K) δ ppm: 1.18 (d, 12H, $CH(C\mathbf{H}_3)_2$, $^{3}J_{HH}$ = 6.9 Hz), 1.44 (d, 12H, $CH(C\mathbf{H}_3)_2$, $^{3}J_{HH}$ = 6.9 Hz), 1.60 (s, 6H, $C\mathbf{H}_3$), 3.47 (sept, 4H, $C\mathbf{H}(CH_3)_2$, $^{3}J_{HH}$ = 6.9 Hz), 4.54 (br s, 2H, $Al\mathbf{H}_2$), 4.91 (s, 1H, C**H**), 7.13 – 7.22 (m, 6H, $^{Ar}C\mathbf{H}$).

3.6.7 Synthesis of [AlH_2(^{dipp}BDI)] (3.5)

Synthesised according literature procedures.[63] To a solution of trimethylamine alane (0.83 mmol, 70 mg) dissolved in toluene, ^{dipp}BDIH (**3.3**, 0.69 mmol, 250 mg) was added and the

solution was stirred for 1 h. The solvent was reduced *in vacuo* and recrystallised from hot hexane at 5 °C. (160 mg, 59.4%). NMR matches that reported in the literature.

^{1}H NMR (500 MHz, C_6D_6, 298 K) δ ppm: 1.23 (t, 12 H, $CH_2C\mathbf{H}_3$, $^{3}J_{HH}$ = 7.5 Hz), 1.48 (s, 6H, $C\mathbf{H}_3$), 2.60-2.97 (m, 8 H, $C\mathbf{H}_2CH_3$, $^{3}J_{HH}$ = 7.5 Hz), 4.53 (s, 2H, $Al\mathbf{H}_2$) 4.84 (s, 3H, $C\mathbf{H}_3$), 7.06-7.12 (m, 6H, $^{Ph}C\mathbf{H}$).

3.6.8 [Al(OC(CH$_3$)$_2$)$_2$(Ar*Ar*Am)] (3.6)

[AlH_2(Ar*Ar*Am)] (**2.10**, 0.0496 mmol, 50 mg) was dissolved in toluene and HBpin (0.0546 mmol, 8 μL) was added. The reaction was heated for 30 min at 80 °C before the solvent was removed *in vacuo* and recrystallised from toluene/hexane (18 mg, 32.4%).

^{1}H NMR (600 MHz, C_6D_6, 298 K) δ ppm: 1.45 (s, 12H, $C\mathbf{H}_3$), 1.65 (s, 3H, $^{L}C\mathbf{H}_3$), 1.69 (s, 6H, $^{Ar*}C\mathbf{H}_3$), 5.64 (d, 2H, ^{L}*o*-C**H**, $^{3}J_{HH}$ = 8.4 Hz), 6.14 (d, 2H, ^{L}*m*-C**H**, $^{3}J_{HH}$ = 6.0 Hz), 6.36 (s, 4H, C**H**(Ph_2)), 7.00 (s, 4H, ^{Ar*}*m*-C**H**), 6.80 - 7.33 (m, $^{Ph}C\mathbf{H}$), 7.67 (d, 8H, ^{Ph}*o*-C**H**, $^{3}J_{HH}$ = 8.4 Hz); $^{13}C\{^{1}H\}$ NMR (150 MHz, C_6D_6, 298 K) δ ppm: 14.2 (C^{IV}), 20.8 ($^{L}\mathbf{C}H_3$), 22.9 ($^{Ar*}\mathbf{C}H$), 28.0 ($\mathbf{C}H_3$), 31.0 (C^{IV}), 51.2 ($\mathbf{C}H(Ph)_2$), 77.8 (C^{IV}), 125.6 ($^{Ph}\mathbf{C}H$), 126.4 ($^{Ph}\mathbf{C}H$), 128.2 (^{L}*o*-**C**H), 128.2 ($^{Ph}\mathbf{C}H$), 129.4 ($^{Ph}\mathbf{C}H$), 129.9 (^{L}*m*-**C**H), 129.9 (^{Ph}*o*-**C**H), 130.1 (C^{IV}), 130.2 (C^{IV}), 131.2 ($^{Ph}\mathbf{C}H$), 131.3 (C^{IV}), 134.8 (C^{IV}), 136.5 (C^{IV}), 139.1 (C^{IV}), 142.2 (C^{IV}), 146.6 (C^{IV}).

Chapter 4:

Targeting Novel Aluminium(I) Complexes and Complexes with Aluminium-Aluminium Multiple Bonds

4.1 Introduction

The isolation of main group complexes in low oxidation states is now a well-established area of research and a general introduction to the topic, and the modes of bonding/reactivity is given in Chapter 1. The advances specifically relating to low oxidation state and multiple bonded aluminium chemistry have been numerous in recent years and will be discussed herein.

4.1.1 Low Oxidation State Aluminium Complexes

The catalytic capabilities of aluminium have been known since the late 19th century, facilitated by the intrinsic Lewis acidity of aluminium and the polarisation of the reactive substrate ($Al^{\delta+}$-$X^{\delta-}$). These processes exploit aluminium in the +3 oxidation state, and the +1 and +2 oxidation states were said to be inaccessible owing to their thermodynamic instability.

4.1.2 Neutral Aluminium(I) Compounds

The isolation of the ionic cluster $K_2[Al_{12}{}^iBu_{12}]^{2+}$ in 1991 saw the first complex in which the oxidation state of aluminium was approaching +1, and increasing the steric encumbrance with the use of Cp* ligands facilitated the formation of the tetrameric Al(I) cluster **4A** (**Figure 4.1**) which was stable at room temperature.[150,151] The aluminium centre adopted a regular tetrahedral geometry, and each Cp* ligand was η^5-coordinated to aluminium. At room temperature, **4A** generally remained tetrameric in solution but underwent dissociation to the monomeric analogue Cp*Al(I) (which can then go on to react with small molecules) at elevated temperatures.[70]

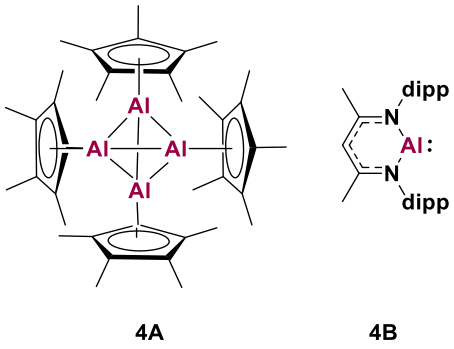

Figure 4.1: Structures of **4A** and **4B**.

In seminal work by Roesky *et al.* the synthesis of the monomeric aluminium(I) compound **4B** (**Figure 4.1**) was reported *via* the reduction of the parent aluminium diiodide with potassium

metal. Compound **4B** was characterised crystallographically to confirm the +1 oxidation state and was said to be analogous to a *N*-heterocyclic carbene, with an aluminium-based lone pair and a vacant 3p orbital on the aluminium centre. Compound **4B** possessed longer Al-N bonds compared to the aluminium(III) dimethyl analogue (1.957(2) *versus* 1.922 Å), as well as a more acute N-Al-N bond angle (**4B**: 89.86°, Al(III): 96.18(9)°) which was indicative of a more covalent bonding profile in **4B** with decreased Lewis acidity at the aluminium centre. At the time of publication, compound **4B** was the first reported example of a formally two-coordinate aluminium centre, and its stability in the solid state was attributed to the kinetic stabilisation provided by the steric bulk and electron-donating nitrogen atoms of the dipp substituents on the aluminium centre and the Al-based lone pair.[20]

The reactivity of **4B** has been extensively explored (**Figure 4.2**) and reviewed in the decades since it was first synthesised, governed by its propensity to undergo facile oxidative addition at the aluminium centre.[152,153] The propensity of **4B** to break strong C-F bonds was highlighted in Chapter 1, and later developments showed that **4B** reacted with 1,3-cyclohexadiene to yield the cycloaddition product **4C**. Carbon monoxide was found to react with **4C** to form the insertion product **4D**, and this reaction was reversible at elevated temperatures (313-373 K).[154] Finally, Nikonov and co-workers reported the oxidative addition of the Al-H bonds of **4E** to **4B** to yield the aluminium dimer **4F**. The formation of **4F** was observed in ca. 50% yield when reacted at 298 K for four hours. The reaction mixture was found to disproportionate back to a mixture of the starting reagents **4B** and **4E** upon heating (323 K), providing evidence for *in situ* reductive elimination at the aluminium centre.[33]

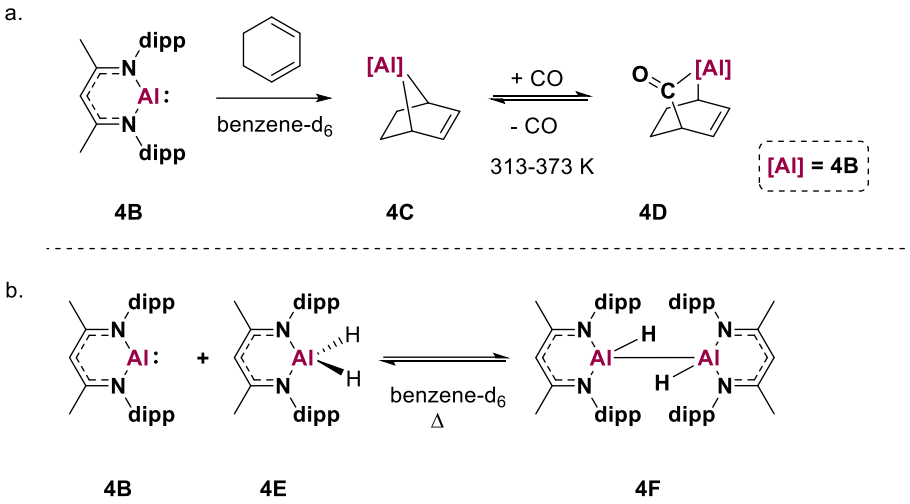

Figure 4.2: Examples of oxidative addition to **4B**.

Until recently, **4A** and **4B** remained the sole reported examples of isolated, neutral aluminium(I) complexes. New complexes of this type are a synthetically challenging target, owing to the high reactivity and small cation size of aluminium, but they are also an attractive synthetic target based on the well-developed reactivity of **4B**. In 2019, Braunschweig and co-workers isolated **4G** (**Figure 4.3**) as the first example of a monomeric Cp-based aluminium(I) compound. This was achieved by increasing the steric encumbrance of the Cp-ligand from Cp*, which favoured formation of the tetrameric species **4A**, to Cp^{3tBu} (1,3,5-tri-*tert*-butylcyclopentadienyl (**Figure 4.3**)). The synthesis of **4G** is shown in **Scheme 4.1**. Compound **4G** was targeted *via* the salt elimination reaction of $Mg(Cp^{3tBu})_2$ with aluminium tribromide ($AlBr_3$) in pentane to yield the analogous bromide species $Cp^{3tBu}AlBr_2$ (**4H**). Compounds **4H** and **4A** were sonicated to obtain the comproportionation product **4I**, and **4G** was liberated upon the addition of a strong Lewis basic cyclic (alkyl)(amino) carbene. Complex **4G** was not characterised crystallographically but its formation was confirmed through combined spectroscopic analyses (^{27}Al and DOSY NMR).

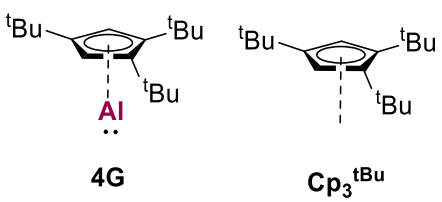

Figure 4.3: Aluminium(I) compound **4G** and the structure of the Cp^{3tBu} ligand.

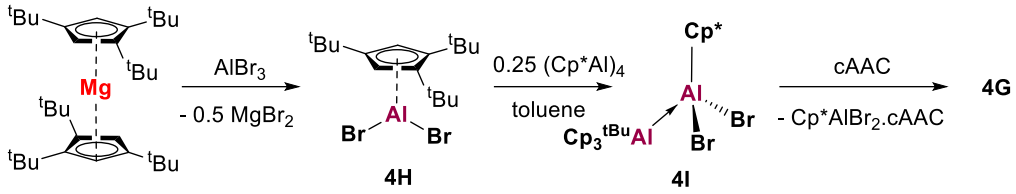

Scheme 4.1: Synthesis of **4G**.

The formation of **4G** as an aluminium(I) compound was further confirmed by examining its propensity to activate small molecules and a summary of its reactivity with haloalanes (right) and nitrogen compounds (left) is shown in **Scheme 4.2**. Reacting **4G** with one molecule of **4H** revealed the existence of valence tautomerism between the aluminium(I)-aluminium(III) product **4J** and the dialumane (aluminium(II)-aluminium(II)) species **4K**. The Al(I)-Al(III) compounds **4L** and **4M** were obtained *via* the reaction of **4G** with $^{t}BuAlCl_2$ and $AlBr_3$, respectively, and the formation of the analogous aluminium(II) dimers was not observed. The 6-membered heterocycle **4N** was synthesised *via* the reaction of **4G** with N_2O and is the formal oligomerisation product of $Cp^{3tBu}Al{=}O$, whilst reaction with phenyl azide yielded the imidoalane **4O**. Analogous complexes of **4J**-**4O** were not obtained when each reagent was reacted with $(Cp^*Al)_4$ which clearly highlights the synthetic advantages of using the Cp^{3tBu} ligand.[155,156]

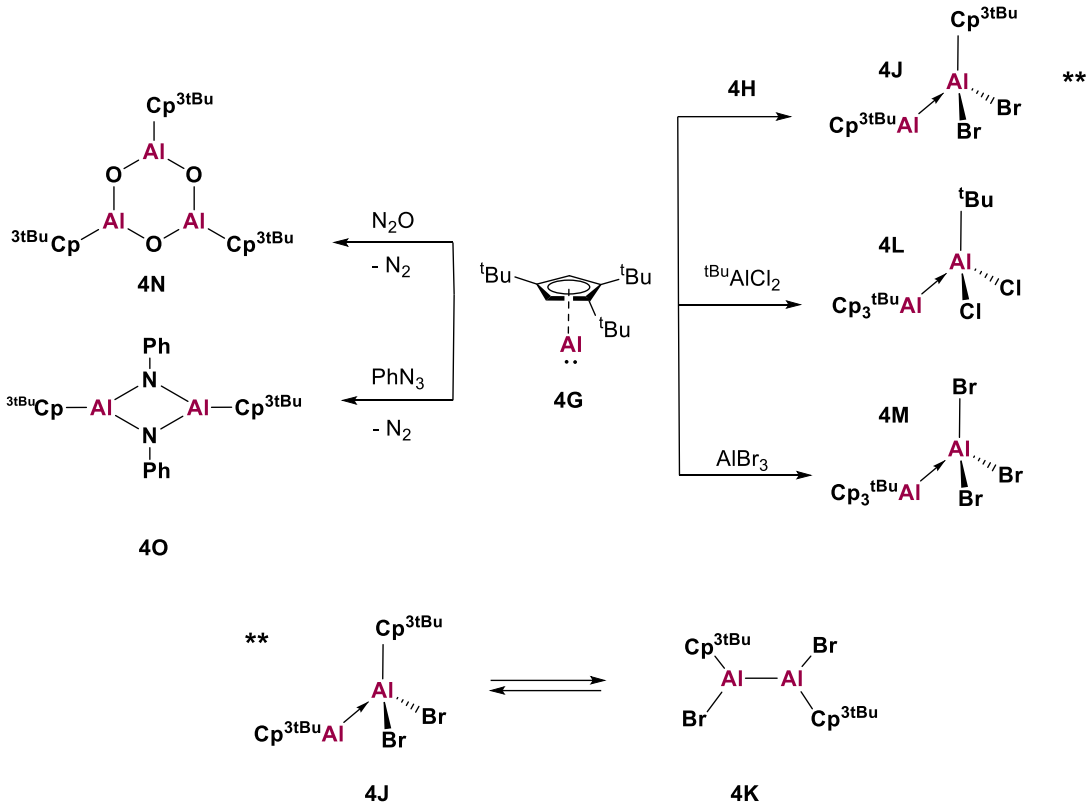

Scheme 4.2: Summary of the reactivity of **4G**.

The family of aluminium(I) compounds was also expanded to include monomeric aluminium(I) hydrides. The first reported example of an aluminium(I) hydride was reported by Jones *et al.* in 2018, whereby the reduction of aluminium(III) BDI compounds with magnesium(I) dimers led to the formation of aluminium(I) hydrides containing Al_6H_6 cluster cores (**4P**, **Figure 4.4**). These clusters were highly insoluble in hydrocarbon solvents and thus precluded their use (and characterisation) in the solution-state.[157] Further developments by Braunschweig and co-workers led to the isolation of the aluminium(I) hydride **4Q** (**Figure 4.4**).

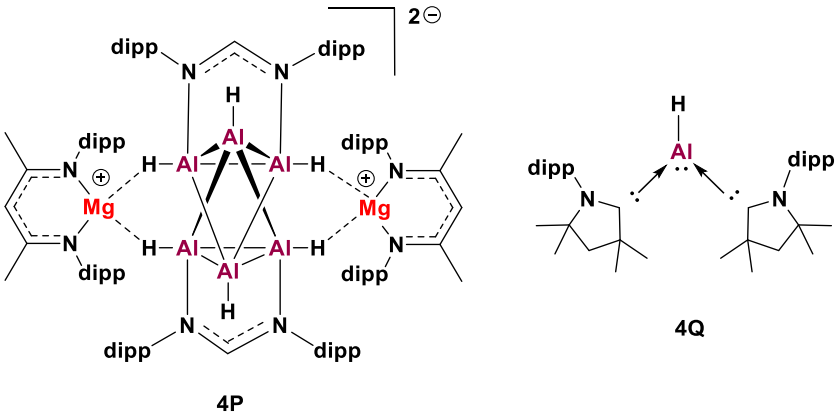

Figure 4.4: Structures of **4P** and **4Q.**

It was proposed that a base-stabilised analogue of Al(I)-H would be isolable *via* the reduction of an appropriately functionalised Al(III) precursor and thus, a cyclic (alkyl)(amino) carbene was used as both the Lewis base and alkyl substituent, owing to their intrinsic excellent σ-donating and π-accepting properties.[158] To that effect, **4Q** was synthesised *via* the reduction of the parent aluminium(III) dichloride under ambient conditions (room temperature) with KC_8, though the desired product was also obtained using milder reducing agents (sodium silanes); the presence of the Al(I)-H bond was confirmed using IR spectroscopy with a characteristic stretching frequency at 1928 cm^{-1}. Additional crystallographic and computational analyses of **4Q** were conducted. Compound **4Q** was centrosymmetric in the solid-state and the Al(I) atom exhibited a trigonal planar geometry with slightly larger C-Al-C bond angles (134.68°) compared to C1-Al-H and C2-Al-H (114.17 and 111.26°, respectively). The hydride was freely located in the difference Fourier map and indicates the presence of an electron rich hydride. The almost equal Al-C bond lengths (Al-C1, 1.930(2) Å; Al-C2, 1.925(2) Å) of **4Q** indicate minimal lone pair delocalisation between the aluminium centre and the empty p-orbitals of the neighbouring cAAC ligands which was also verified computationally. DFT analysis also revealed a reduced degree of π-backbonding compared to the boron analogue, and this was attributed to poor overlap of the aluminium and cAAC p-orbitals.[159] Through a series of complex computational calculations, the electronic structure of **4Q** was described as an Al(I) hydride with ~0.33% contributions from an open shell Al(III) diradical resonance form with singlet open-shell character.[158] The reactivity of **4Q** is summarised in **Scheme 4.3**.

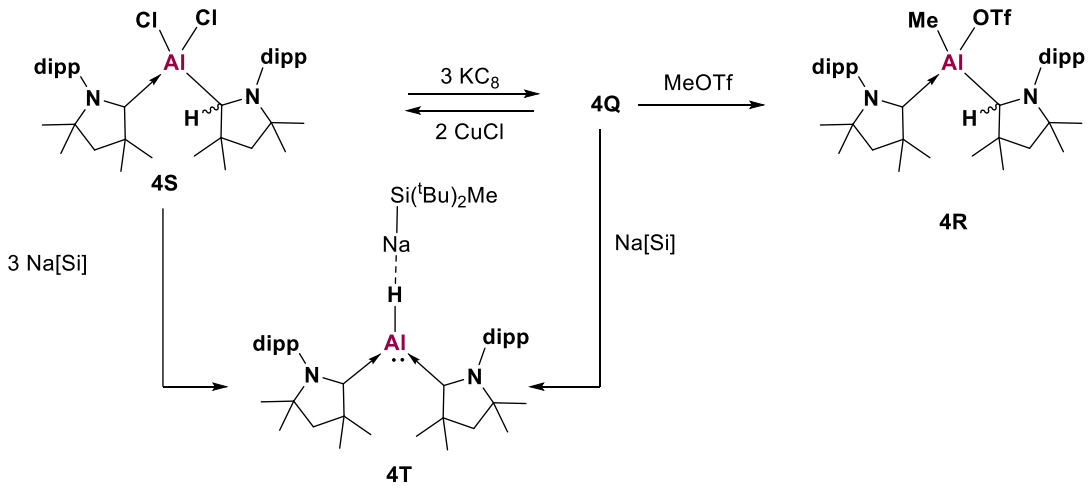

Scheme 4.3: Summary of reactivity of **4Q**.

Complex **4Q** did not react cleanly with typical small molecules (e.g., CO_2, H_2) and instead led to the formation of an intractable mixture of products. Instead, methyl triflate was found to undergo nucleophilic substitution at the aluminium centre (**4R**). Mechanistically, the nucleophilic attack of the methyl group was said to destabilise the aluminium centre, forming an Al(III) cation with concomitant migration of the hydride to the cAAC centre. The formation of **4Q** from the analogous aluminium(III) dichloride (**4S**) was found to be reversible in the presence of copper(I) chloride, and the 1:1 complex **4T** could be obtained *via* the reaction of one or three equivalents of sodium silane with **4Q** or **4S**, respectively. Interestingly, dissolution of **4T** yielded only free **4Q** and Na[Si^{t}BuMe$_2$], and thus **4T** was said to form *via* the co-crystallisation of **4Q** and the sodium silane

Thus far, all examples of Al(I) compounds discussed have featured aluminium as a formally two-coordinate metal centre. The isolation of one-coordinate monovalent group 13 complexes (M = Ga, In, Tl) was reported by the Power group between 1997-2009 (**4U**, **Figure 4.5**), but the analogous aluminium species remained elusive until 2020.[160–162] The monovalent aluminium(I) compound **4V** was initially targeted *via* the traditional reduction of aryl aluminium dihalides, but the extreme reactivity of the reduced aluminium species precluded its isolation. Instead, a super-bulky terphenyl ligand was employed, and **4V** was successfully synthesised *via* the reduction of the precursor aluminium diiodide with Na/NaCl (**Scheme 4.4**).

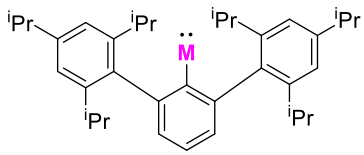

4U
M = *Ga, In, Th*

Figure 4.5: Previously reported one-coordinate group 13(I) complexes.

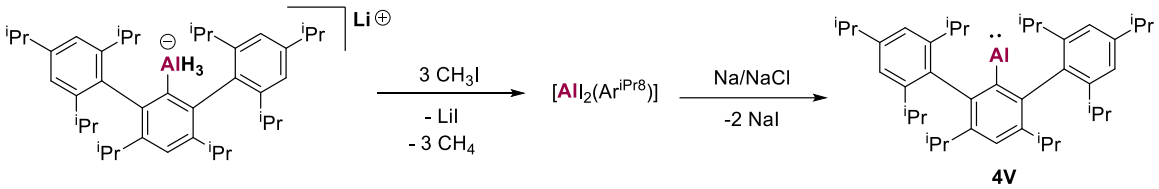

Scheme 4.4: Synthesis of monovalent aluminium(I) compound **4V**.

Yellow crystals of **4V** were isolated in a ca. 8% yield and characterised crystallographically; it crystallised in the Pc space group and contained two independent molecules of **4V**, with both aluminium centres bound only to one carbon atom. The Al-C distances (1.988(4) and 2.003(4) Å) were shorter than their calculated value (2.023 Å) and only slightly longer than the Al-C distances in the parent diiodide (1.965(57) Å). DFT analysis found that the HOMO was occupied by the non-bonding lone pair on aluminium, whilst the LUMO and LUMO+1 orbitals were comprised of the aluminium 3p orbitals. Early reactivity studies with **4V** revealed that reaction with dihydrogen yielded the known aluminium hydride-bridged dimer [AlH(μ-H)Ar^{iPr8}]$_2$ and was surprising considering the analogous gallium species exhibited no reactivity.[163] Further reactivity studies are said to be in progress.

4.1.3 Anionic Aluminium(I) Compounds

Low oxidation state aluminium chemistry was long dominated by the synthesis and reactivity of neutral aluminium(I) compounds owing to its intrinsic Lewis acidity. In 2018, the first example of an anionic aluminium(I) nucleophile **4W** (**Figure 4.6**) was reported by Aldridge and co-workers, with later examples **4X**-**4AB** reported in a relatively short amount of time since then.[164–169] The alumanyl complexes **4W**-**4Y** were all synthesised *via* the reduction of the parent diiodide compounds with KC_8 and exhibited many identical properties. All products formed as centrosymmetric dimers, with two anionic [Al]$^-$ units bound by two potassium counterions, with stabilising potassium-phenyl interactions (**4W**: 3.226(3)-3.474(3) Å; **4X**: 3.161(2)-3.565(2) Å; **4Y**: 2.945(1)-3.026(1) Å). An assessment of the molecular orbitals revealed the HOMO of **4W**-**4Y** to be the aluminium-centred lone pair, and the LUMO in all

instances was a ligand-based orbital. The reactivity of these complexes is dictated by the energy separation between the aluminium lone pair and the vacant aluminium p-orbital, which was found to be the LUMO+3 in all complexes.[170] The HOMO-LUMO gaps of **4W**-**4Y** were calculated to be 3.50, 4.06 and 3.90 eV, respectively.[164,171,172]

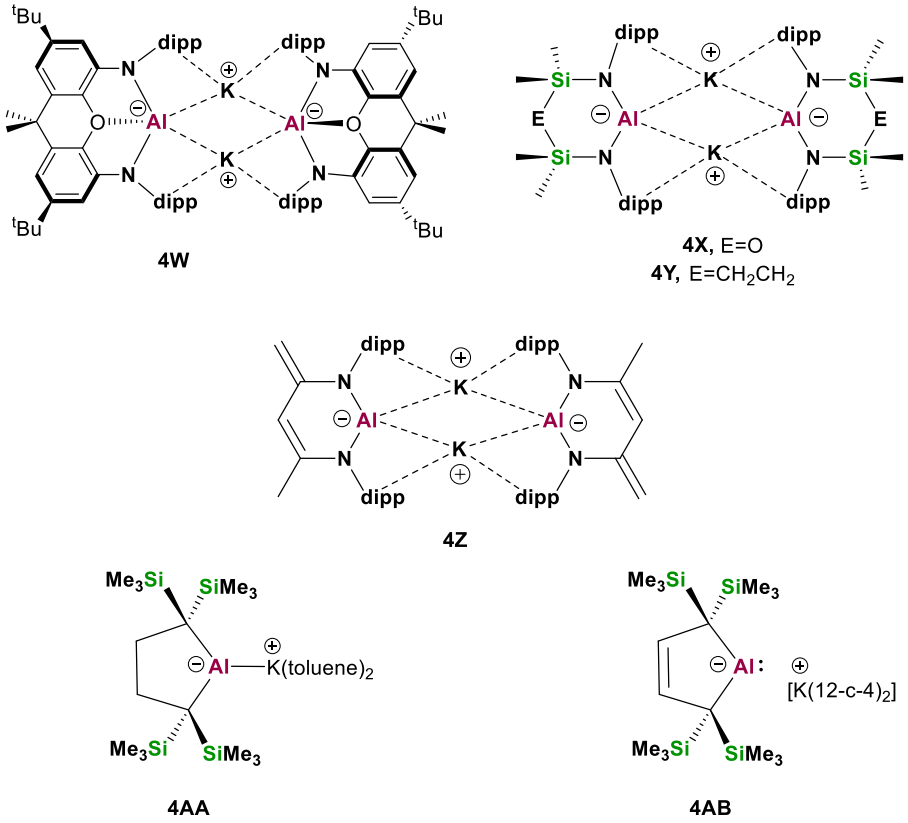

Figure 4.6: Alumanyl complexes **4W**-**4AB**.

The dimeric alumanyl **4Z** was synthesised *via* an alternative synthetic route; compound **4B** (**Figure 4.1**) was reacted with [KCH(SiMe$_3$)$_2$] ("RK"). Interestingly, RK deprotonated one of the methyl groups on the backbone of **4B**, which implies the use of RK as a base instead of as a nucleophile. As with **4W**-**4Y**, **4Z** forms a centrosymmetric dimer in the solid-state. The ligand backbone in **4Z** was formally classified as a dianionic *bis*-amide and the presence of alternating C-C and C=C bonds was confirmed by X-ray crystallography. Compound **4Z** was found to possess the shortest Al-N (1.865(4)-1.868(4) Å), Al-K (3.499(1)-3.588(1) Å) and Al--Al (long range) (5.236(5) Å) distances of all dimers **4W**-**4Y** and thus the dimeric structure of **4Z** was described as tightly bound.

The monomeric alumanyl alkyl-substituted structures **4AA-4AB** (**Figure 4.6**) were reported by Yamashita and Kinjo, respectively.[167,169] Compounds **4AA-4AB** were synthesised by the reduction of the parent dialumane compounds (**4AA**: Na/K alloy; **4AB**: KC_8). Combined crystallographic and computational analyses of **4AA** indicated high p- and s-character of the aluminium centre in the C-Al and Al-K bonds, respectively, owing to the longer Al-C bonds (2.084(9) Å) compared to the dialumane complex (2.005(3)-20.11(3) Å); natural bond orbital (NBO) analysis indicated 80.78% p-character on Al for C-Al and 78.98% s-character on Al for Al-K. The HOMO of **4AA** contained the lone pair of electrons at the aluminium centre, whilst the LUMO was comprised of the π* orbitals of the toluene molecule coordinated to the potassium atom.[167] The HOMO-LUMO gap (2.564 eV) was much narrower than for **4W-4Y**, attributed to the absence of both electronegative nitrogen atoms and Al-N πp-πp interactions, as well as the presence of the low lying π* toluene orbital. Complex **4AB** was characterised in the solid-state as a charge-separated ion pair. The large interatomic distance between aluminium and potassium (6.66 Å) indicated a lack of interaction between these two atoms. In contrast to **4AA**, the aluminium centre of **4AB** was two-coordinate with the carbon and nitrogen atoms, and the atoms of the five-membered ring were nearly coplanar. The aluminium atom in the Al-C and Al-N bonds exhibited high p-character, as was observed for **4AA**. Probing the electronic structure computationally revealed the aluminium lone pair to be the HOMO whilst the LUMO+1 was comprised of the vacant aluminium p-orbital and confirmed that **4AB** is isoelectronic to a cyclic (alkyl)(amino) carbene.

The reactivity of alumanyl compounds has been widely explored since they were first reported in 2018 and they have been shown to act as aluminium-centred nucleophiles in nucleophilic substitution, oxidative addition, cycloaddition, and oxidation reactions. This reactivity is beyond the scope of this thesis, but for a more extensive summary see detailed reviews by Bakewell *et al.* and Aldridge *et al.*.[156,170]

4.1.5 Dialumane and Dialumene Chemistry

4.1.5.1 Dialumanes and Dihydrodialanes

Dialumanes are compounds containing an aluminium-aluminium single bond (bond distances reported in the range 2.5-2.95 Å) with both metal centres in the +2 oxidation state.[70] The isolation of these compounds was said to be impossible based on calculations for Al_2H_4, which stated that facile isomerisation of these compounds would trigger thermal decomposition.[173]

This assumption was debunked in 1988, with the reported synthesis of **4AC**-*dis* by Uhl *et al.* (**Figure 4.7**) *via* the reduction of the relevant *bis*-(trimethylsilyl)aluminium chloride with potassium. The high steric shielding of the bulky ligands, in conjunction with the electron donating effects of the $CH(SiMe_3)_2$ group, prevented disproportionation.[174] The related compounds **4AC**-*tipp* and **4AC**-*Si* (**Figure 4.7**) have also been reported with variation in steric bulk at the R positions.[175,176] 1,2-Dihalodialumanes are a more synthetically challenging target due to the difficulty in stabilising X-Al-Al-X moieties, but the groups of Power and Tokitoh reported the synthesis of the 1,2-diiodo- and 1,2-dibromodialumanes **4AD** and **4AD'**, respectively (**Figure Figure 4.***7*).[173,177] Attempts to reduce **4AD** with KC_8 in toluene to obtain the related dialumene complex (aluminium-aluminium double bonded) instead yielded the product **4AE**. Whilst the dialumene complex was not isolated or characterised, it was proposed to form *in situ*, as it was hypothesised that **4AE** formed *via* the reductive dehalogenation of **4AD** with a subsequent formal [4+2] cycloaddition with the toluene solvent. Thus, **4AE** was deemed to be a masked dialumene.[177] Related Cp*-substituted complexes **4AF** and **4AF'** (**Figure 4.7**), differing in their halogen substituent, were reported by Arnold and Braunschweig, respectively, and were synthesised *via* the reductive dehalogenation of the corresponding Cp^*AlX_2 species. Their reactivity with electron-rich substrates was explored, and both compounds were found to react with dimethylacetylene, as well as phenyl- and mes-azide.[178,179] The first examples of asymmetric dialumanes (**4AG/4AG'**, **Figure 4.7**) were reported by Roesky *et al.*, synthesised *via* the disproportionation reaction of **4B** (**Figure 4.1**) with ligand-stabilised cyclic (alkyl)(amino) carbenes. X-ray analysis revealed aluminium-aluminium bond lengths of 2.595(2) Å (**4AG**) and 2.633(1) Å (**4AG'**) and both aluminium centres adopted a distorted tetrahedral geometry.[180]

The reactivity of dialumane complexes remains relatively under explored, owing in part to their propensity to disproportionate to aluminium(I) and aluminiun(III) compounds. The family of dialumane complexes can be expanded to include dihydrodialanes, with Al(H)-Al(H) single bonds and aluminium in the +2 oxidation state. In 2010, Jones *et al.* reported the remarkable synthesis of the parent dihydrodialane compound, Al_2H_4 (**4AH**, **Figure 4.8**), as a *bis*-carbene adduct stabilised by bulky di-*iso*-propylphenyl groups. The isolation of a series of amidinate and guanidinate (**4AI**, **Figure 4.8**) dihydrodialane complexes synthesised from the parent aluminium dihydride compounds was also reported, and all compounds were synthesised *via* the reduction of bridged aluminium(III) hydride dimers with a magnesium(I) reducing agent. The reaction proceeded *via* the transfer of hydrogen from aluminium(III) to magnesium(I), to

yield the alumiunium(II) and magnesium(II) products. These complexes were all characterised crystallographically and exhibited high thermal stability, but their reactivity was not explored.[70,97]

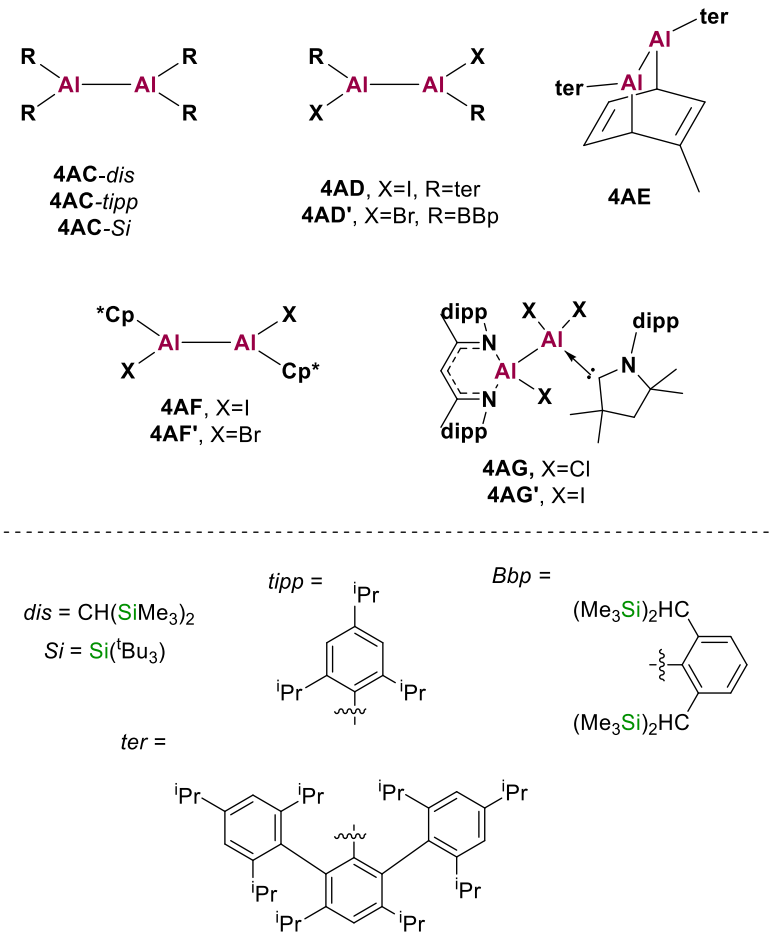

Figure 4.7: Dialumane complexes **4AC**-**4AG** and their corresponding substituents.

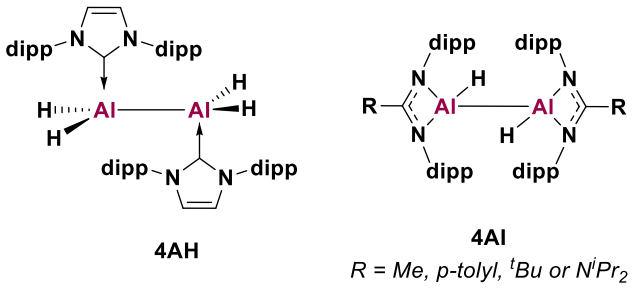

Figure 4.8: 1,2-Dihydrodialane complexes **4AH**-**4AI**.

In 2020, Cowley and co-workers reported the synthesis of the dipp- and mes-substituted dihydrodialane complexes **4AJ**-**4AK** (**Figure 4.9**), respectively, supported by amidophosphine ligands. They were synthesised analogously to **4AH**-**4AI** *via* the hydrogen transfer reaction of the parent aluminium dihydrides with a magnesium(I) reducing agent. The coordination of basic amidophosphine ligands facilitated the formation of the dihydrodialane as opposed to a hydride-bridged dimer. Generally, the mes-substituted dihydrodialanes were isolated in higher yields (**4AK**, 81%; **4AK'**, 37%) than their respective dipp counterparts (**4AJ**, 20%; **4AJ'**, 43%) and all complexes adopted a tetrahedral geometry at the aluminium centre with κ^2-coordination by the amidophosphine ligands. The Al-Al bond distances were remarkably long (2.6586(16)-2.886(2) Å), and the longer bond lengths of the mes-substituted compounds were attributed to intermolecular dispersion interactions in the crystal structures.

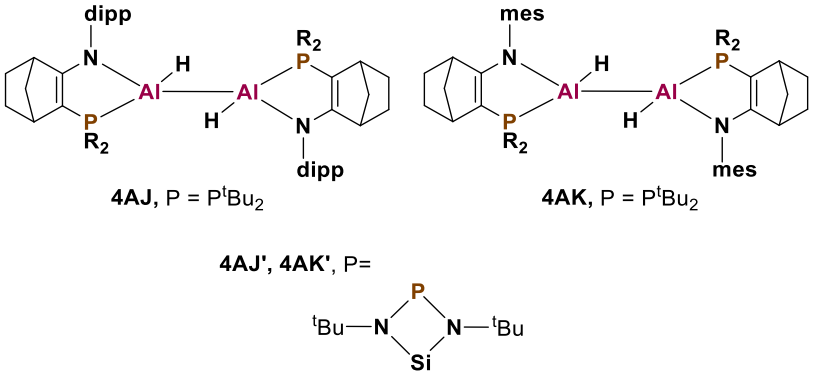

Figure 4.9: 1,2-Dihydrodialane complexes **4AJ** and **4AK** supported by amidophosphine ligands.

The amidophosphine ligands induce complex stereochemistry into these compounds and there were six possible diastereomers for each one. Monitoring the reduction by $^{13}P\{^1H\}$ NMR spectroscopy (**Figure 4.10**, **4AK** used as a select example) revealed interconversion between the stereoisomers **4AK-1** to **4AK-2**. In stereoisomer **4AK-1**, the phosphorus ligands were located *syn* across the Al-Al bond and both phosphorus centres were equivalent. For **4AK-2**, the phosphorus ligands were located *anti* across the Al-Al bond, and the interconversion between **4AK-1** to **4AK-2** must proceed *via* inversion of stereochemistry at the aluminium centre. This was proposed to proceed *via* reductive elimination at the aluminium-hydrogen bond and was verified computationally. Alternative mechanisms of action were considered but ruled out owing to unfavourable energy profiles (reversible phosphine dissociation) or through observed lack of experimental evidence (photolytic dissociation). Preliminary investigations into the reactivity of **4AK** revealed conversion to the diiodo complex upon reaction with iodine,

with potentially significant applications when targeting the reduction of dihydrodialanes to dialumene complexes.[181]

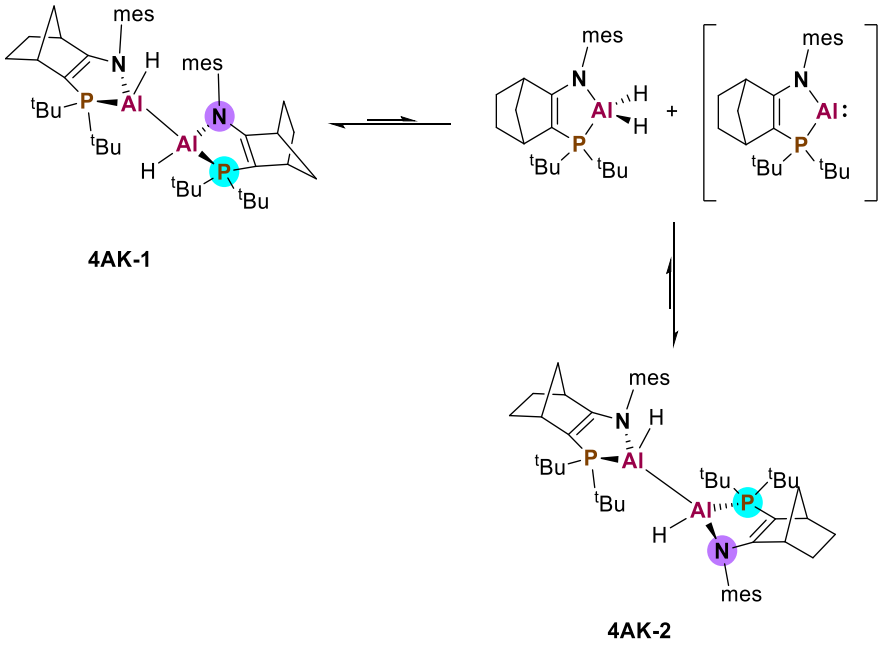

Figure 4.10: Reversible reductive elimination at aluminium using **4AK** as a select example.

4.1.5.2 Dialumene Compounds

There are now multiple reports of dialumane compounds in the literature and whilst their reactivity has been somewhat explored, this is often hampered by their propensity to disproportionate (*vide supra*). Dialumenes are neutral compounds featuring an aluminium-aluminium double bond with both aluminium centres in the +1oxidation state. Retention of partial double bond character during catalytic processes, mimicking the reactivity of transition metals, could have huge implications in terms of chemical industry sustainability and thus dialumenes have been a long sought-after synthetic target. The difficulty in synthesising these compounds arises from their inherent Lewis acidity as well as finding sufficiently bulky substituents. Main group double bonds also contain significant diradical character, facilitating their enhanced reactivity and decreased stability.[182] Whilst it was inferred that **4AE** (**Figure 4.7**) formed *via* a dialumene intermediate, it was not until 2017 that the first example was isolated and characterised by Inoue and co-workers (**4AL**, **Scheme 4.5**). Compound **4AL** was synthesised *via* the reaction of an NHC-stabilised aluminium hydride with a slight excess of boron trihalide (BX_3, X=I or Br) and di-*tert*-butyl(methyl)silyl sodium ($^tBu_2MeSiNa$) to yield the corresponding NHC-stablised aluminium(III) dihalides, which were then reduced by three

equivalents of KC_8 to yield **4AL** (X=I, 53%; X=Br, 35%) (**Scheme 4.5**). In the solid-state, **4AL** possesses a *trans*-planar geometry to minimise interactions between the sterically hindered NHC substituents and each aluminium centre exhibits an almost trigonal planar geometry (sum of angles = 359.99 °).

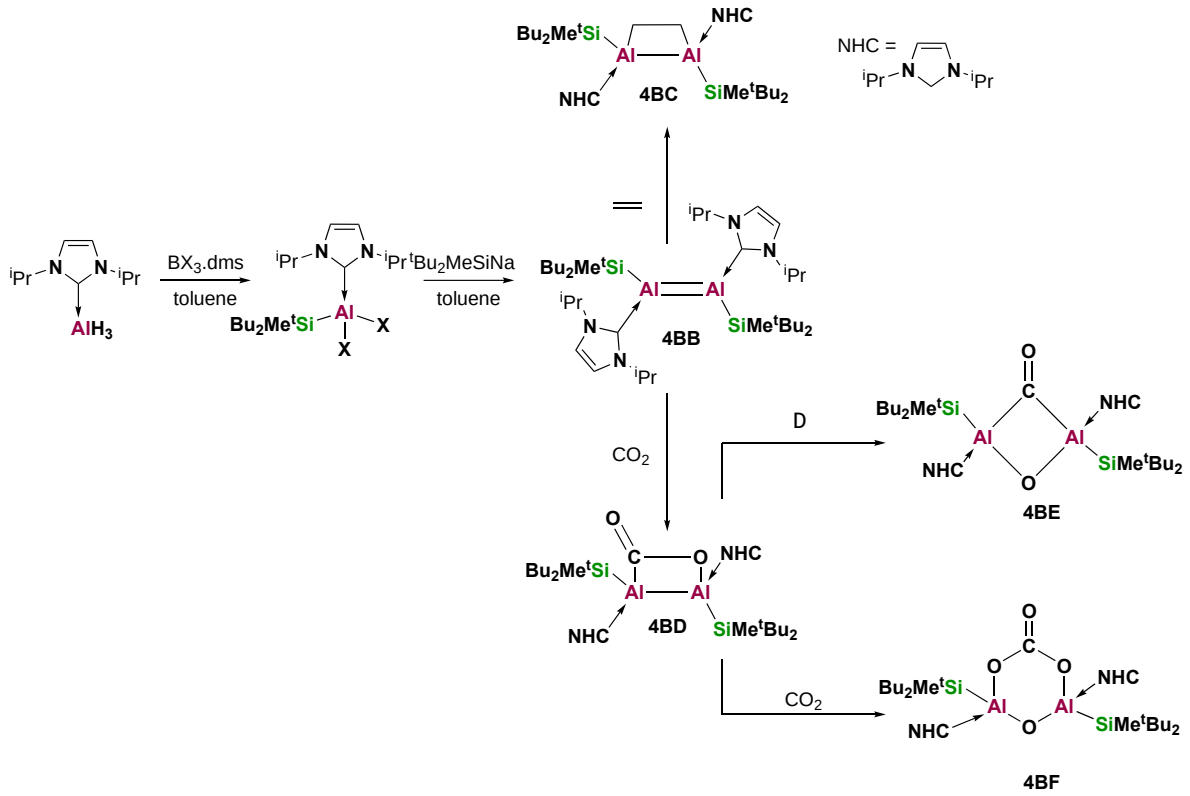

Scheme 4.5: Synthesis of dialumene compound **4AL** and a summary of its reactivity.

The Al=Al bond length was shorter than the range of known single bond lengths (2.3943(16) Å) and its bonding profile was probed using DFT analysis. The HOMO and HOMO-1 were comprised of the out of plane Al-Al π-bond and σ-bonds, respectively, with a calculated HOMO-LUMO gap of 2.24 eV. Natural bond orbital analysis (NBO) revealed the electron occupancies of each aluminium centre to be 1.91 for the σ-bond and 1.78 for the π-bond. Its double bonding character was further examined upon reaction with small molecules and a summary of the reactivity of **4AL** is shown in **Scheme 4.5**. Compound **4AL** reacted with ethylene gas *via* a formal [2+2] cycloaddition reaction to form **4AM**, whilst reaction with phenylacetylene yielded a mixture of both the analogous [2+2] cycloaddition and C-H insertion products. Single crystal X-ray analysis of these products revealed significant elongation of the Al-Al bond lengths (2.6503(10), 2.6363(11) and 2.6411(9) Å, respectively) and are in the known range of aluminium-aluminium single bond lengths.[183] In an analogous fashion, **4AL**

can also facilitate CO_2 fixation to yield **4AN**, with a planar four-membered Al-Al-C-O ring and exocylic carbon-oxygen bond, again *via* a formal [2+2] cycloaddition reaction. The formation of **4AN** was irreversible, however heating it under an inert atmosphere for 1 hour (323 K) formed the co-planar isomerisation product **4AO** whilst further heating under an atmosphere of CO_2 resulted in the formation of **4AP** (**Scheme 4.5**). The two aluminium centres in the six-membered ring were separated by one bridging carbonate group and one oxygen atom, and bond length measurements indicated a degree of electron delocalisation across the structure. Computational insights into the mechanism of formation indicated that **4AL** reacts with one equivalent of oxygen to form a four-membered Al-O-O-Al ring. Breaking of this ring facilitates recombination at each aluminium centre and this mechanism was confirmed experimentally with the formation of a mixture of *cis* and *trans* isomers.

Inoue and co-workers also reported the synthesis of dialumene **4AQ** (**Scheme 4.6**), synthesised in an analogous fashion to **4AL** with substitution of the $^{t}Bu_2MeSi$ group for the more sterically encumbered 1,3,5-tri-*iso*-propylphenyl (Tipp) ligand (**Figure 4.7**). This allowed for direct comparison of the ligand influence on resulting structural geometry and reactivity. Compound **4AQ** possessed a *trans*-bent geometry, in contrast to the planar geometry of **4AL**, with an almost-perpendicular (85°) arrangement of NHC groups (parallel in **4AL**) and a slightly longer Al=Al bond length (2.4039(8) Å), though again this was still shorter than known aluminium-aluminium single bonds. Key differences were noted in the electronic structure of **4AQ** compared to **4AL**, including a loss of uniformity of the HOMO of the aluminium centres and a decreased HOMO-LUMO gap (**4AL**, 2.24 eV; **4AQ**, 1.86 eV) which were attributed to the change in orientation of the NHC groups facilitating increased overlap with the p-orbital of the NHC-carbon atom. These changes in the sterics and electronics facilitated divergent reactivity compared to **4AL** (**Scheme 4.6**). With ethylene, the analogous [2+2] cycloaddition product **4AR** was formed, though the enhanced reactivity of **4AQ** was demonstrated by its propensity to undergo the same reaction with diphenylacetylene (**4AS**), which was not observed with **4AL**. Similarly, reaction with phenylacetylene formed the [2+2] cycloaddition product **4AT** as a single isomer, in contrast to a mixture of both the [2+2] cycloaddition and C-H insertion products observed with **4AL**. However, **4AT** decomposed over the course of three days to form styrene *via* an intramolecular C-H activation process.

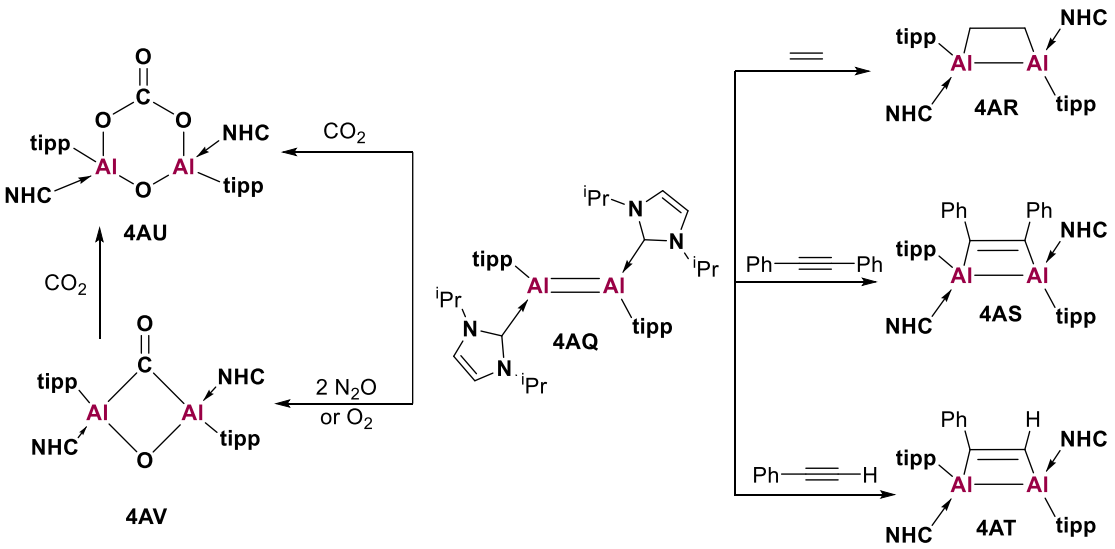

Scheme 4.6: Dialumene compound **4AQ** and a summary of its reactivity.

As with **4AL**, **4AQ** reacted with CO_2 to form **4AU** as the [2+2] cycloaddition product and reaction with one equivalent of oxygen (or N_2O) yielded the dioxo product **4AM** (and exposure of **4AM** to CO_2 formed **4AU**). The catalytic activity of **4AP** and **4AU** towards the hydroboration of CO_2 is summarised in Chapter 1. Compounds **4AL** and **4AQ** are both examples of base-coordinated dialumene compounds. In 2021, Cowley and co-workers expanded their family of amidophosphine-supported 1,2-dihydrodialanes to include the first example of reversible dissociation of a dialumene compound. The 1,2-dihydrodialane compound **4AK** (**Figure 4.9**) was reacted with iodine and the resultant diiododialane (**4AW**) was reduced using a Na/K alloy in THF (**Scheme 4.7**) to yield dialumene **4AX**.[184]

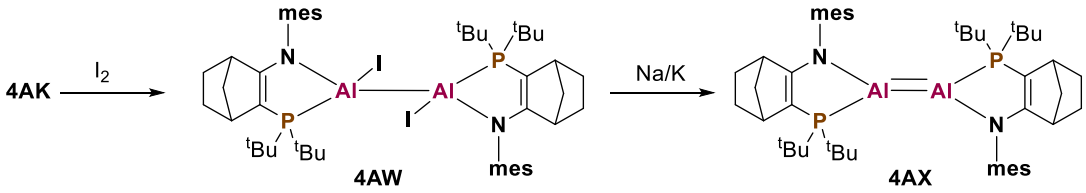

Scheme 4.7: Synthesis of dialumene **4AX**.

Compound **4AX** adopted a *trans*-bent geometry akin to **4AQ** (**Scheme 4.6**) with an Al=Al bond length of 2.5190(14) Å, however NBO analysis revealed a distinct bonding profile, with natural localised molecular orbitals (NLMOs) representing Al-Al σ- and π-bonds. The NLMOs were localised on the aluminium centres (with some retention of π-bond character) whilst **4AL** and

4AQ more closely resembled classical π-bonds. The Al-Al bond of **4AX** exhibited increased s-character, which was attributed to the mixing of Al-Al σ*-orbitals, in contrast to **4AL**/**4AQ** where the π-bond was comprised of p-orbitals only. This is reflected in the Wiberg Bond Indices of each compound (**4AL**, 1.67; **4AQ**, 1.54; **4AX**, 1.31). Quantum theory of atoms in molecules (QTAIM) analysis revealed that the Al-Al bond was weak, with weak shared-shell covalent character. In conjunction with the longer bond length of **4AX**, it was concluded that this species exhibited intermediate double bond order (~1.5). The marked contrast in bonding between these dialumene compounds was investigated computationally. It was found that electropositive substituents ($SiMe_3$) invoke structures that are more planar and possess shorter Al=Al bonds, whereas electronegative or π-donating substituents (including phosphorus substituents) result in *trans*-bent structures with longer Al=Al bonds. The stronger/more planar bonds of NHC-stabilised dialumenes were therefore attributed to the strong donor abilities of the NHC substituent, which was said to raise the HOMO of the monomeric low valent constituent and reduce the singlet-triplet energy gap ($\Delta E_{S\text{-}T}$). The complex stereochemistry observed for dihydrodialane complexes **4AJ** and **4AK** (**Figure 4.8**) was also observed in dialumene complex **4AX**. At 300 K, monitoring the reaction by $^{31}P\{^{1}H\}$ NMR spectroscopy revealed an exchange between the three possible stereoisomers. Only intramolecular exchange processes were observed below 300 K, whilst elevated temperatures (>300 K) facilitated the dissociation of **4AX** and subsequent recombination of the monomeric components to invert the stereocentres. Thus, the dissociation of dialumene **4AX** was said to be reversible.

As with **4AL** and **4AQ**, **4AX** reacted with ethylene gas and diphenylacetylene to yield the [2+2] cycloaddition products **4AY** and **4AZ**, respectively (**Scheme 4.8**). Interestingly, increasing the steric encumbrance of the alkyne further ($Me_3SiC{=}CSiMe_3$) resulted in the formation of aluminacyclopropane **4BA**, which was instead formed *via* the reaction of the monomeric constituent as opposed to a cycloaddition reaction with dialumene **4AX**.

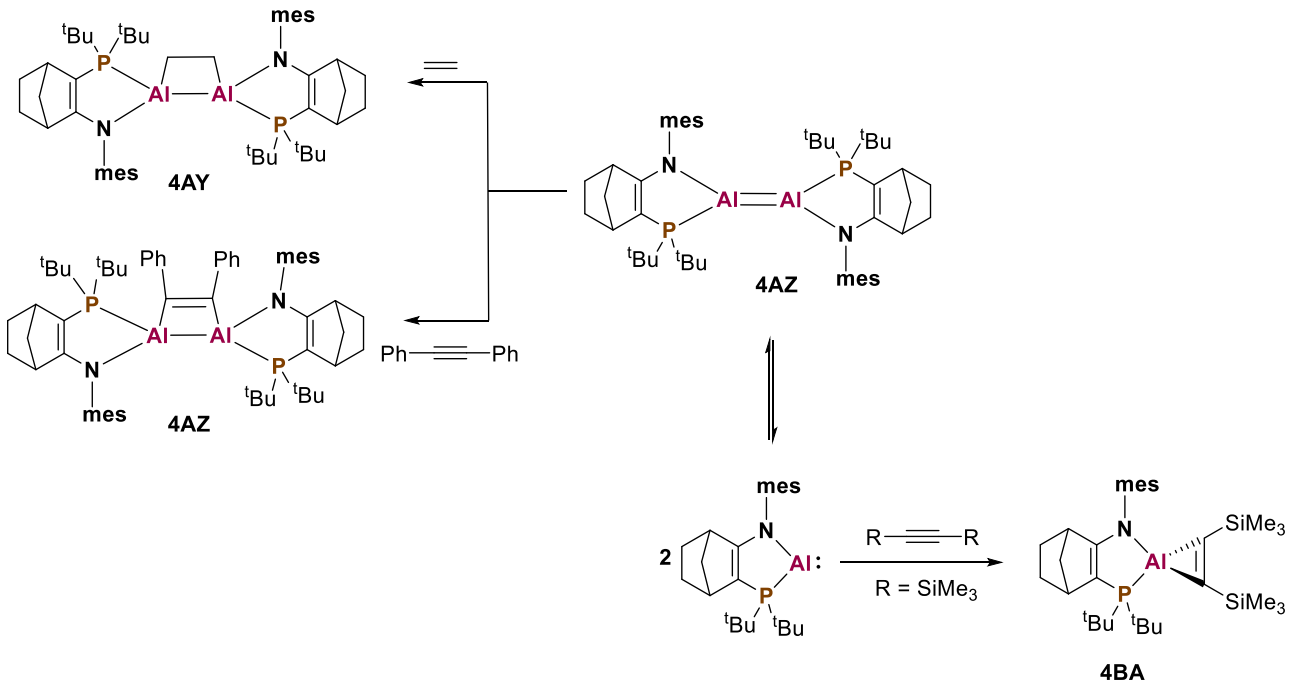

Scheme 4.8: Summary of reactivity of **4AX**.

Developments in the field of low oxidation state aluminium chemistry remained stagnant for many years, whilst numerous advances were made with heavier group 13, and other main group, elements. Aluminium chemistry has seen a renaissance in interest in recent years, with landmark discoveries continually demonstrating that main group compounds can exhibit transition-metal like reactivity if stabilised by sufficiently bulky or basic substituents. It was hypothesised that the 2,6-diphenylmethyl-4-methylphenyl substituent employed in the synthesis of the aluminium amidinate hydride and alkyl complexes reported in this thesis would be sufficiently sterically encumbered to facilitate the isolation of low oxidation state aluminium compounds, and the attempts to isolate these is described within.

4.2 Routes to Low Oxidation State Aluminium Complexes

Encouraged by the reports of a new class of super-bulky amidinate complex bearing the 2,6-diphenylmethyl-4-*iso*-propylphenyl substituent (chapter 2, section 2.1.3) and the recent advances in low oxidation state aluminium chemistry (section 4.1), the synthesis of the low valent analogues of the amidine ligands detailed in this thesis was investigated. Two reaction pathways were used to target the low valent species, which are summarised in **Scheme 4.9**. Pathway A followed synthetic methods first reported by Roesky *et al*. for the isolation of **4B**, with the reduction of an appropriate aluminium diiodide precursor with a strong reducing agent such as potassium metal.[20]

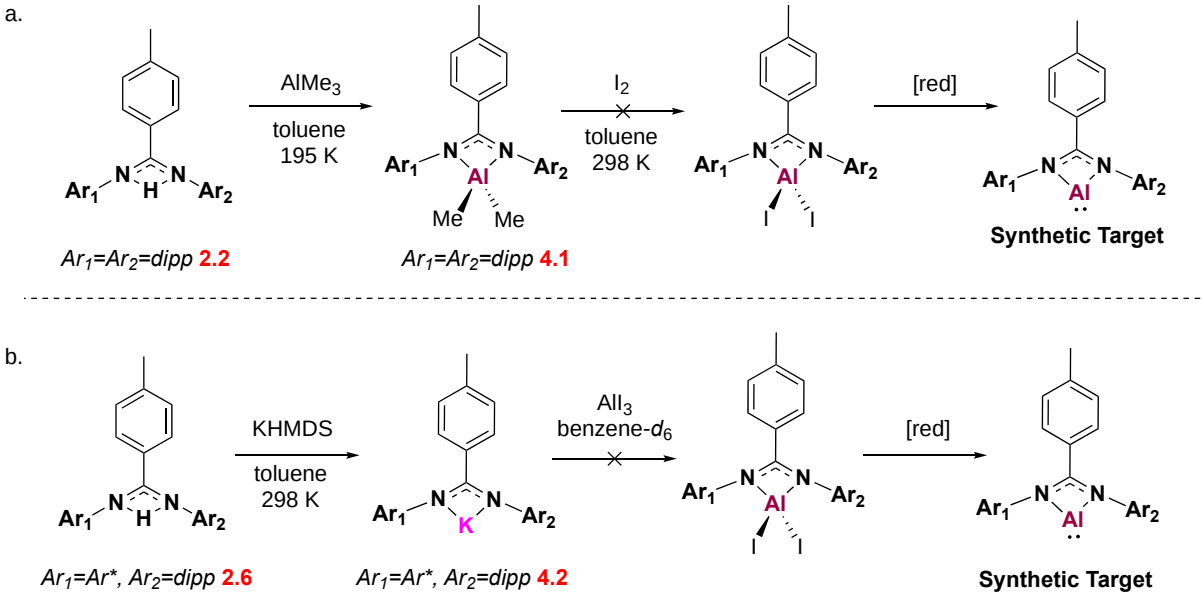

Scheme 4.9: Synthetic routes attempted to target a novel low valent aluminium species.

Complex **2.14** was reacted with two equivalents of iodine in toluene and stirred at room temperature overnight. The solvent was removed *in vacuo* and the resultant ^{1}H NMR spectrum looked promising: the alkyl resonance below 0 ppm disappeared, suggesting the desired product had formed. Yellow crystals formed after recrystallisation in toluene, and preliminary X-ray screening experiments revealed the formation of the deprotonated form of the ligand with an AlI_4^+ counterion (**Figure 4.11**).

To ascertain whether the Ar* substituent induced divergent reactivity, the diiodide species was targeted *via* the smaller, symmetrical ligand **2.2** (Ar_1=Ar_2=dipp). Ligand **2.2** was reacted with trimethyl aluminium at 195 K in toluene (**Scheme 4.9a**), the solvent was removed *in vacuo* and the aluminium alkyl compound **4.1** was isolated. The ^{1}H NMR spectrum revealed key features

that were also observed for **2.14** and **2.15** (chapter 2, section 2.5), including the disappearance of the N**H** proton and a characteristic alkyl resonance below 0 ppm (-0.05 ppm) integrating to six protons. The solvent was removed *in vacuo* and the ^{1}H NMR spectrum was consistent with the dealkylation of **4.1**. Two sets of crystals were obtained after recrystallisation in toluene. Larger, orange crystals formed initially, followed by smaller, colourless crystals; this is summarised in **Scheme 4.10**. Preliminary single crystal X-ray diffraction studies revealed the orange crystals to be the protonated form of the ligand with an I_3^- counter ion. The colourless crystals were found to be the ligand datively bound to aluminium triiodide. Full data sets were not collected and alternative routes to the target compound were sought.

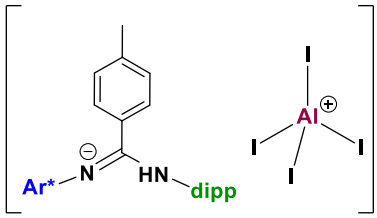

Figure 4.11: Reactivity of **2.14** with iodine.

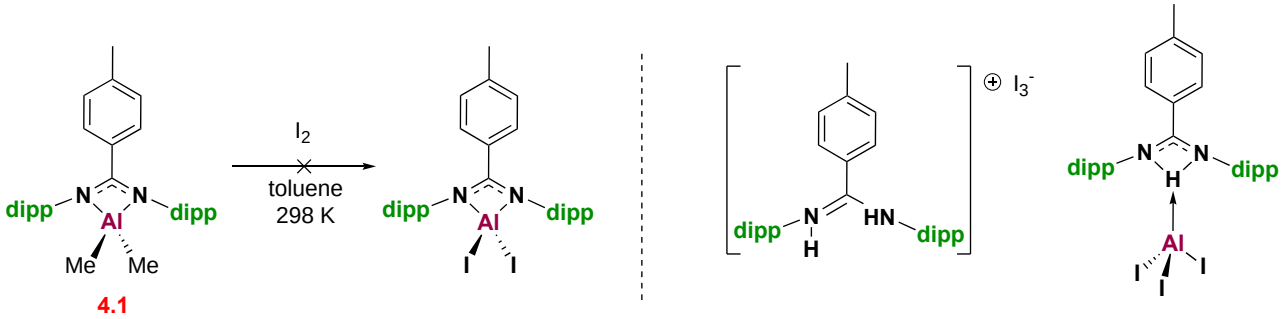

Scheme 4.10: Reactivity of **4.1** with iodine.

Ligand **2.6** was reacted with 1.6 equivalents of KHMDS (KHMDS = potassium *bis*-(trimethylsilyl)amide) in toluene and stirred at 298 K overnight. The resultant ^{1}H NMR spectrum showed complete consumption of the starting ligand and conversion to the potassium salt of the ligand, **4.2**, was proposed (**Scheme 4.9b**). The ^{1}H NMR spectrum revealed the disappearance of the N**H** resonance, with two new resonances at 0.07 and 0.12 ppm assigned as liberated HMDS and excess KHMDS. The potassium salt **4.2** was then reacted with aluminium triiodide (AlI_3) on an NMR scale to investigate its reactivity and this is summarised in **Scheme 4.11**.

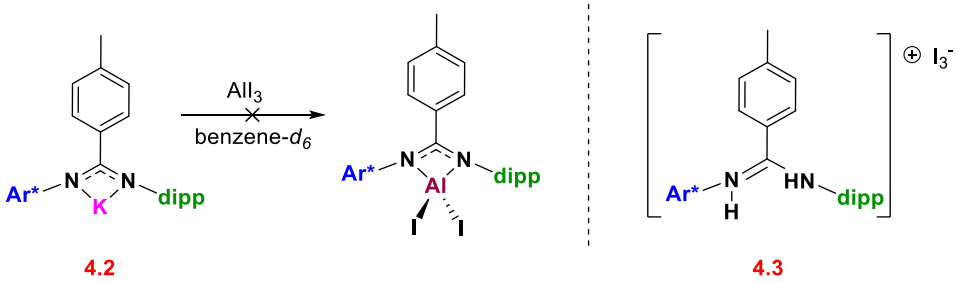

4.2 4.3

Scheme 4.11: Reactivity of **4.2** with aluminium triiodide.

The reaction of **4.2** with AlI_3 in benzene-d_6 was monitored by ^{1}H NMR spectroscopy and after 15 minutes at room temperature a mixture of products had formed. It was possible to isolate a single product after recrystallisation in benzene-d_6/hexane. The resultant ^{1}H NMR spectrum revealed two resonances at 11.97 and 12.83 ppm integrating to approximately one proton each, neither of which correspond to the starting ligand **2.6**, and these would not be expected for the formation of a diiodide complex. Single crystals suitable for X-ray analysis were grown from benzene-d_6/hexane and revealed the solid-state structure of **4.3** (**Figure 4.12**).

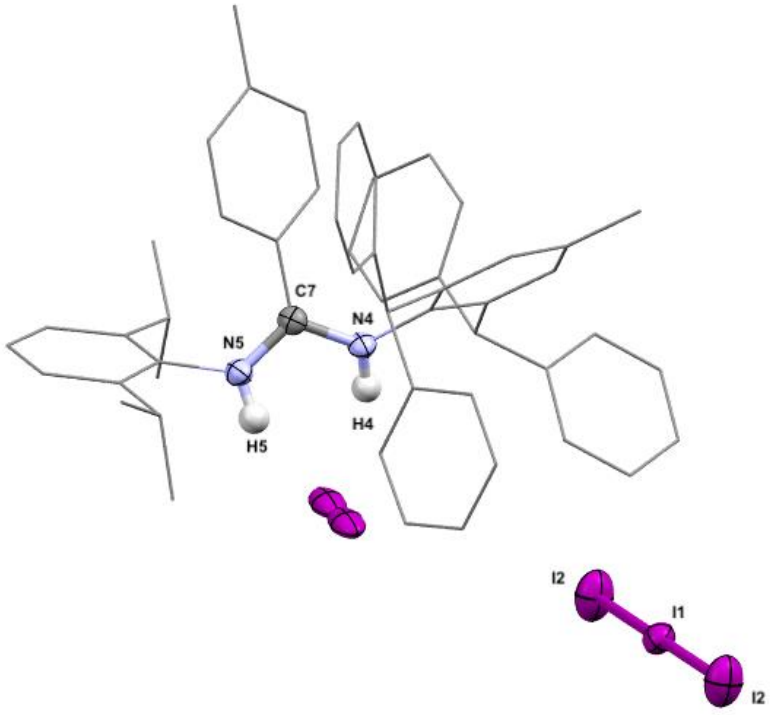

Figure 4.12: X-ray crystal structure of **4.3**.

Compound **4.3** formed as the protonated form of ligand **2.6** with an I_3^- counterion and crystallised in the $P\bar{1}$ space group with three molecules in the unit cell. The N-C-N core was

planar with a bond angle of 115.8° and the C-N bond lengths were nearly identical (C7-N4, 1.330(3) Å; C7-N5 1.331(3) Å). These are in good agreement with average amide bond lengths, demonstrating that **4.3** exhibits partial double bond character.[185] The iodide counterion had equal bond lengths of 2.903(2) Å.

The isolation of the protonated forms of **2.2** and **2.6** from different synthetic pathways indicates that the formation of the amidinate diiodide complexes is both kinetically and thermodynamically unfavourable. As a result, further investigations into the isolation of low oxidation state aluminium complexes focused on the reaction of aluminium hydride complexes with known low valent aluminium reagents, to target the formation of complexes with aluminium-aluminium multiple bonds. There exist relatively few examples of isolated dialumane and dialumene compounds, with even fewer reported examples of their reactivity. However, recent advances in this field (section 4.1.5) have demonstrated the capacity of these compounds to undergo reductive elimination processes, and the dialumene derivative **4AP** was proven to catalyse the reduction of CO_2 in an analogous fashion to transition metal compounds. The literature examples detailed in section 4.1.5 are all dimers comprised of the same monomeric unit. A series of amidinateAl-AlBDI and asymmetric BDIAl-AlBDI dialumane compounds was targeted to ascertain whether the asymmetry induced any interesting or divergent properties compared to current literature examples, and whether these compounds undergo further derivatisation, either to form reversibly, activate small molecules, or to reduce the Al-Al single bond. A summary of targeted reactivity is shown in **Scheme 4.12**.

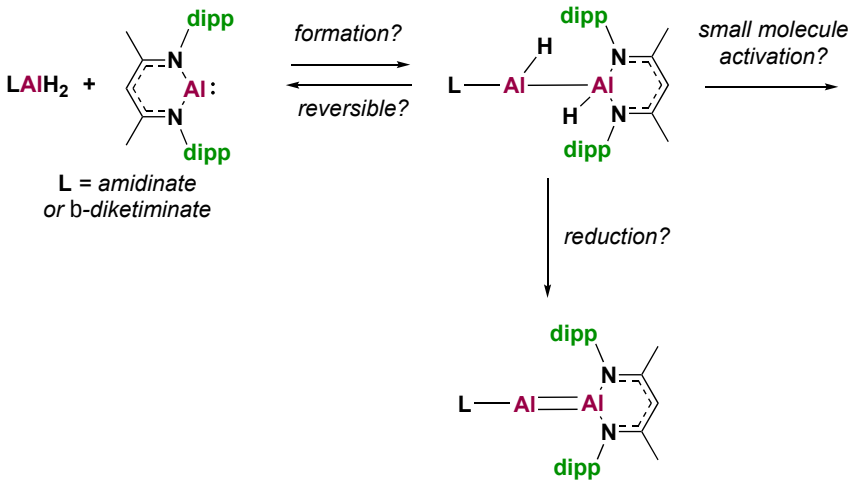

Scheme 4.12: Targeted scheme of reactivity with known aluminium(I) reagents.

4.3 Routes to Complexes with Aluminium-Aluminium Bonds

4.3.1 Reactions with Amidinate Complexes

Inspired by recent developments in the literature, and particularly the reversible reductive elimination of **4F** to the corresponding aluminium(I) and aluminium(III) reagents (section 4.1.2, **Figure 4.2**), the aluminium hydride complex **2.8** was reacted with the low valent aluminium reagent **4.4**, with the proposed scheme of reactivity shown in **Scheme 4.13a** and the observed scheme of reactivity shown in **Scheme 4.13b**.‡‡ All reactions were conducted on an NMR scale.

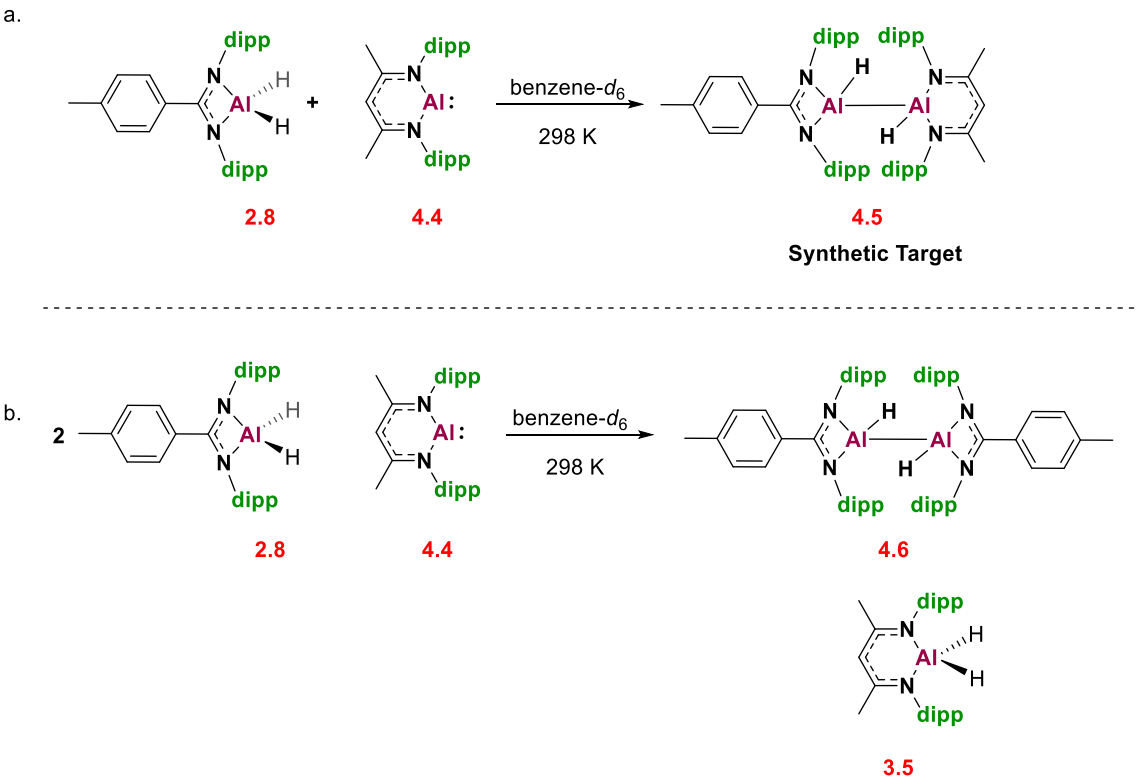

Scheme 4.13: a. Proposed reactivity of aluminium amidinate complex **2.8** with **4.4**; b. Observed reactivity of aluminium amidinate complex **2.8** with **4.4**.

Complexes **2.8** and **4.4** were reacted in a 1:1 ratio in benzene-d_6 and monitored by ^{1}H NMR spectroscopy. The resultant ^{1}H NMR spectrum after 15 minutes at room temperature (**Scheme 4.13**, top) appeared to show multiple species in solution. There were two singlets at 4.87 and 5.01 ppm; sharp singlets in this region are characteristic of the backbone methine proton in β-diketiminate complexes, whilst the doublets at 6.35 and 6.40 ppm are characteristic of the *ortho*

‡‡ See experimental section for full details and for synthesis of **4.4**.

or *meta* protons of the amidinate backbone ligand. There were three broad singlets at 4.54, 5.05 and 5.66 ppm (in a 2:2:1 ratio, respectively), indicative of chemically inequivalent aluminium hydrides. To aid in elucidating the products of this reaction, it was compared to ^{1}H NMR spectra of the starting materials **2.8**/**4.4** and **3.5**, [AlH_2(^{dipp}BDI)], a plausible product from the reaction **(Figure Figure 4.*13***). Assessment of the ^{1}H NMR spectra revealed complete consumption of the starting reagents **2.8** and **4.4**, whilst the β-diketiminate aluminium hydride complex **3.5** was found to be present in the reaction mixture (accounting for resonances at 1.14, 1.39, 1.55, 3.43 and 4.87 ppm). Although not included in this figure, the formation of the parent amidine and β-diketimine ligands (**2.2** and **3.3**, respectively) was also ruled out.

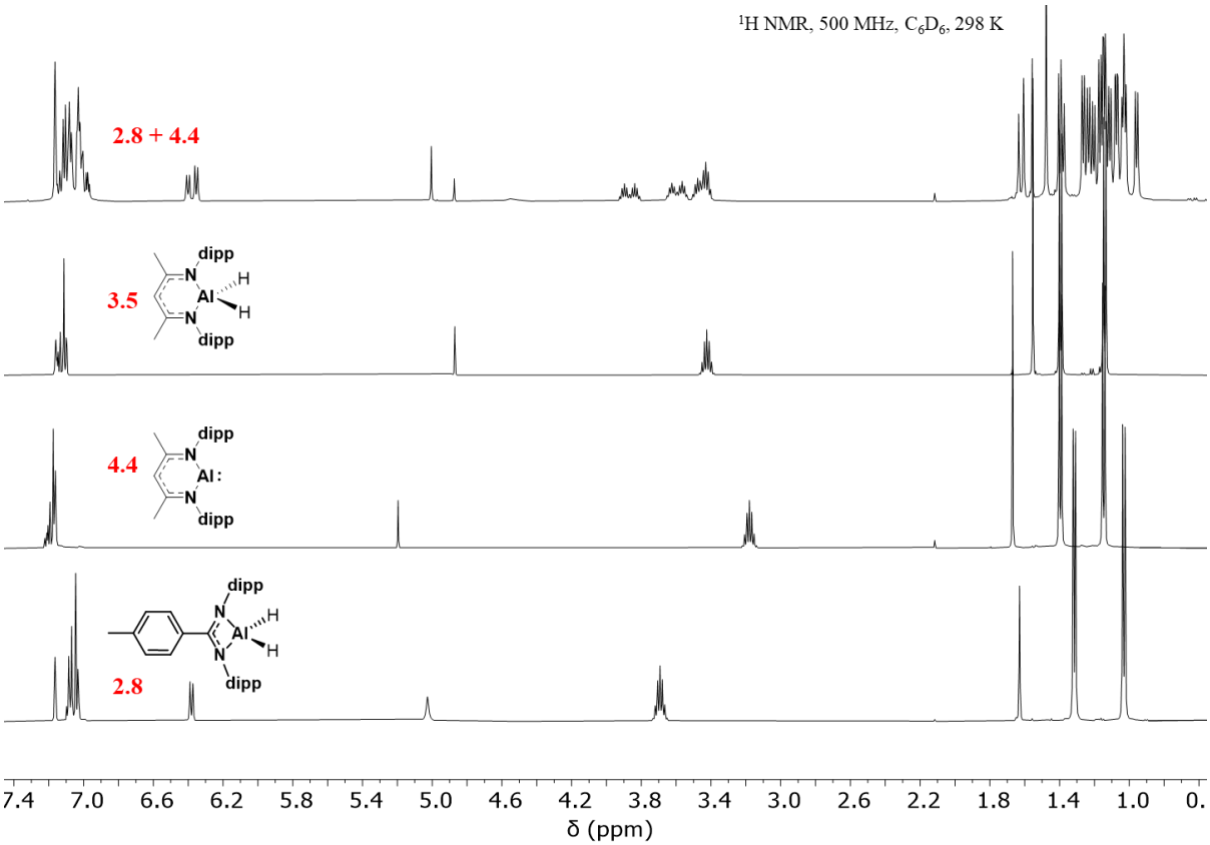

Figure 4.13: ^{1}H NMR stack of the reaction of **2.8** and **4.4**, stacked with **3.5**, **4.4** and **2.8** for comparison.

The formation of the β-diketiminate species **3.5** was surprising based on the formation of the symmetric dimer **4F** reported by Nikonov *et al.* (**Figure 4.2**).[33] This must occur *via* hydrogen abstraction from **2.8** and initially led to the proposal of *in situ* formation of a low valent aluminium amidinate species (**Scheme 4.14**).

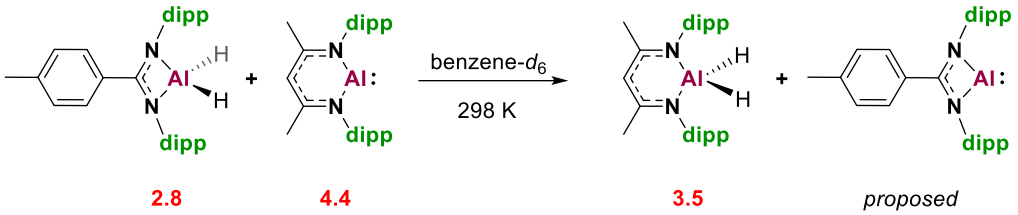

Scheme 4.14: Proposed scheme of reactivity based on initial ^{1}H NMR observations.

However, the presence of three aluminium hydride resonances discounted this suggestion, and instead the formation of **4.6** (**Scheme 4.13b**) was proposed. Complex **4.6** is a known literature compound, and the reported ^{1}H NMR resonances in benzene-d_6 confirm that this is present (most notably, resonances at 6.40, 5.67 and 3.84/3.91 ppm); the reaction must therefore be formally 2:1 with respect to **2.8** and the mechanism of formation of **4.6** was investigated.[97]

Related work has shown the dimeric species **4F** to be in equilibrium with its monomeric constituents **4B** and **4E** (**Figure 4.2c**). It was rationalised that by adjusting the stoichiometry of the reaction it might be able to disfavour product formation and isolate the intermediate. Reacting one equivalent of **2.8** with an excess (1.5 equivalents) of [Al:(^{dipp}BDI)] (**4.4**) at 298 K in benzene-d_6 circumvented the formation of the complex mixture of products seen in the 1:1 reaction and led to one major product as well as residual aluminium(I) (**Figure 4.14**). The absence of key resonances at 6.40 and 5.66 ppm ruled out the formation of **4.6**. The β-diketiminate singlet at 5.01 ppm and the amidinate doublet at 6.35 ppm were present in a 1:2 ratio. In conjunction with the broad aluminium hydride resonances, this suggests they belong to the same compound and the formation of the synthetic target **4.5** (**Scheme 4.13a**) was proposed. Analysing the reaction mixture after three days at room temperature revealed a small increase in the concentration of **3.5** and a decrease in the concentration of **4.4**, and the emergence of **4.6** was identified in the ^{1}H NMR spectrum.

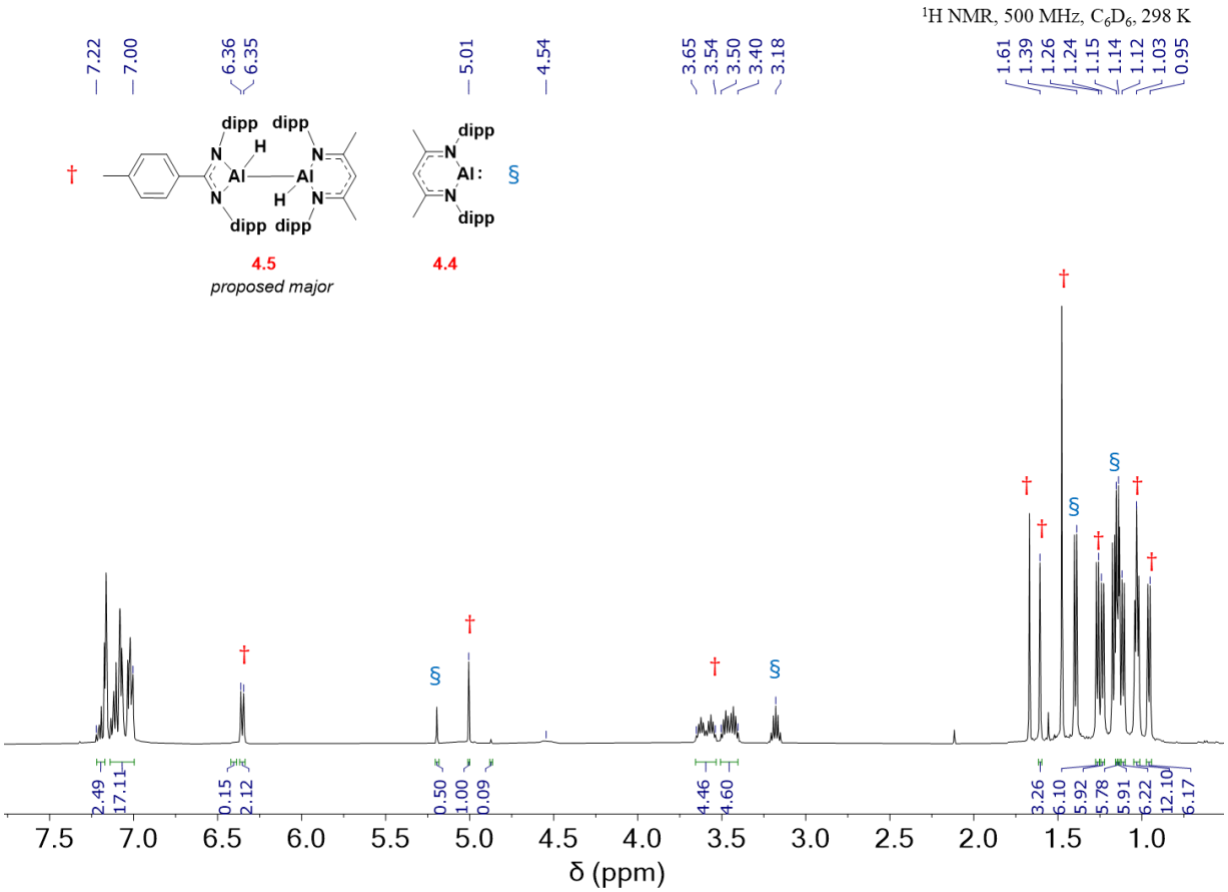

Figure 4.14: ^{1}H NMR spectrum of the reaction of **2.8** with an excess of **4.4**.

When this reaction was repeated with an excess of **2.8** (1.3 equivalents), recording a ^{1}H NMR spectrum after 15 minutes at room temperature revealed the presence of excess [$AlH_2(Ar^{dipp}Ar^{dipp}Am)$] (**2.8**), a small amount of [$AlH_2(^{dipp}BDI)$] (**3.5**), and both the asymmetric and symmetric dimers **4.5** and **4.6**, respectively (**Figure 4.15**). Monitoring the reaction by ^{1}H NMR spectroscopy revealed that, after 16 hours at room temperature, the reaction composition had changed, and the aluminium dihydride **2.8** had been completely consumed; this was unsurprising given the established 2:1 nature of the reaction. The consumption of **4.5** (as evidenced by a decrease in intensity of the resonances at 5.01/6.35 ppm) occurred with concomitant formation of **4.6** and aluminium dihydride **3.5**. Thus, this led to the proposal that **4.5** forms as a reaction intermediate, before undergoing transformation to **4.6** and **3.5** as the final products and that conducting the reaction with an excess of **2.8** forces the equilibrium to the right. This directly contrasted the observed reactivity when an excess of **4.4** was used, which favoured the formation of the intermediate species **4.5**, with very slow conversion to **3.5** and **4.6**.

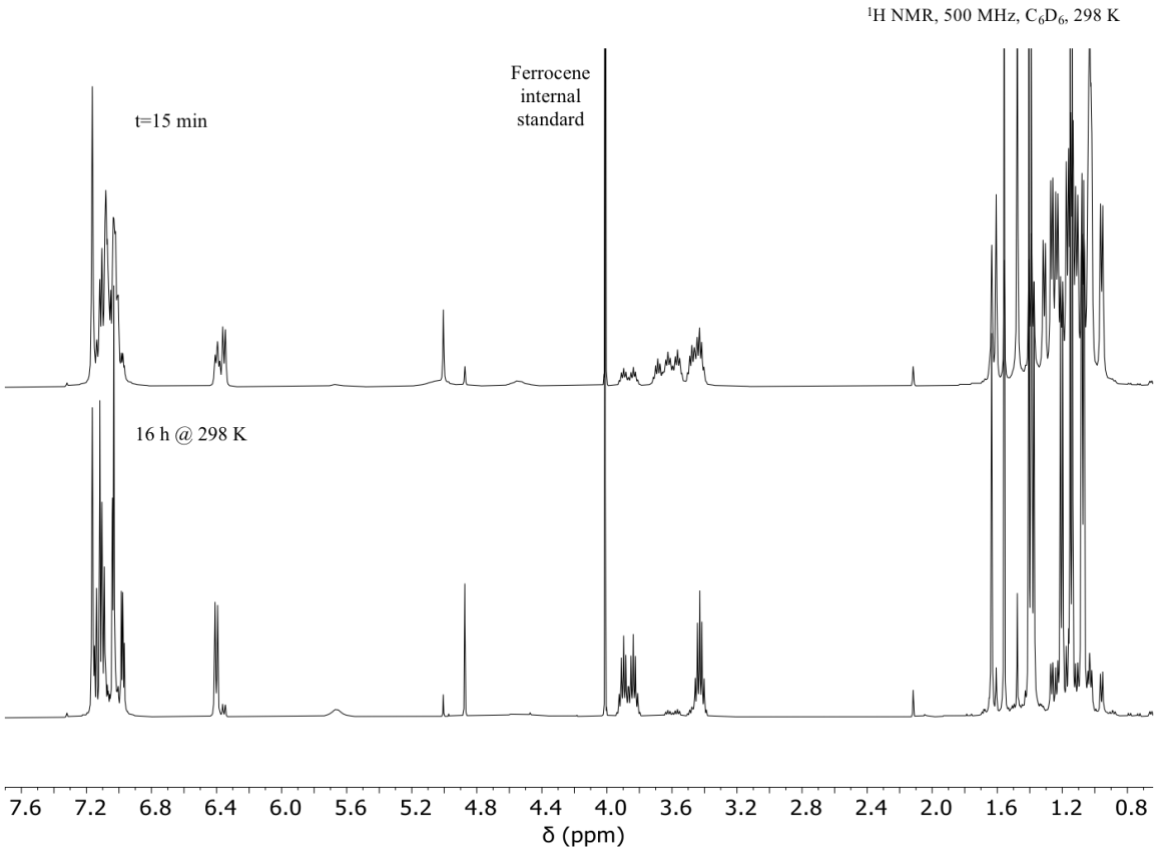

Figure 4.15: ^{1}H NMR stack of the reaction of an excess of **2.8** with **4.4** after 15 minutes (top) and after 16 hours at 298 K (bottom).

Based on the experimental observations detailed in this section, a more accurate scheme of reactivity is shown in **Scheme 4.15**. The low valent aluminium amidinate species was not observed on the NMR timescale, but its formation (and consumption) is inferred based on the identity of the products formed. Preliminary investigations into the reversibility of this reaction using variable temperature NMR (VT-NMR) experiments were largely inconclusive. This could however be investigated *via* the addition of a second aluminium dihydride into the reaction mixture and monitoring by ^{1}H NMR spectroscopy to observe the formation of additional dialumane compounds. Similar experiments were reported by Cowley *et al.* to provide further evidence of reductive elimination of **4AK**. In all of the experiments detailed thus far it was not possible to recrystallise the reaction mixtures to either isolate single products or obtain X-ray analysis on the structures. Conducting the reactions on a small scale and the formation of mixtures of products undoubtedly contributed to this, and future work would focus on characterising the proposed structures in the solid state. Repeating the reaction with the bulkier amidinate dihydrides **2.9** and **2.10** led to the formation of the aluminium dihydride **3.5**,

but the reaction mixtures were unstable and showed high levels of decomposition. Presumably, the increased steric encumbrance of the Ar* substituent disfavoured the formation of the analogous aluminium dimers. With the reactivity of the amidinate complexes **2.8-2.10** with **4.4** established, the reactivity of a series of β-diketiminate aluminium hydride complexes with **4.4** was next explored.

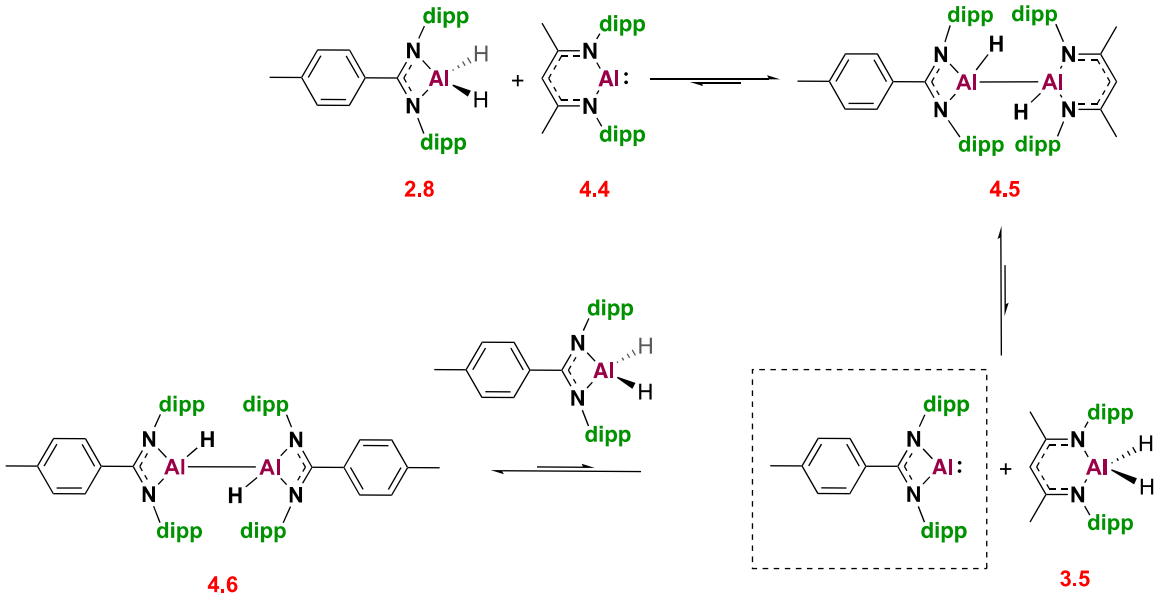

Scheme 4.15: Proposed scheme of reactivity for **2.8** with **4.4** based on experimental observations.

4.3.2 Reactions with β-Diketiminate Complexes

Based on the initial results with aluminium amidinate complexes, the formation of additional asymmetric dihydrodialane complexes was investigated. Specifically, mes- and Ph-substituted (**4.9** and **4.10**, respectively) BDI complexes were investigated for their reactivity with **4.4** to ascertain whether the induction of asymmetry into the products would affect the reversibility of the reaction, and secondly to establish whether the steric encumbrance of the flanking ligand affects the position of the reaction equilibrium. The aluminium hydride complexes **4.9** and **4.10** were synthesised *via* the reaction of the parent ligand with trimethylamine alane (**Scheme 4.16**) and reacted with one equivalent of **4.4**.[§§]

[§§] See experimental section for synthetic details of ligands **4.7**-**4.8** and aluminium hydrides **4.9**-**4.10**.

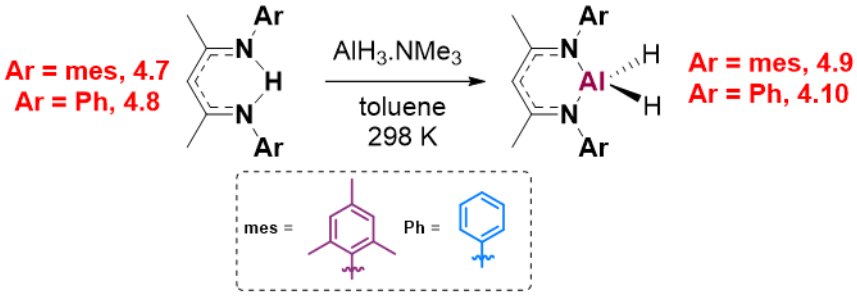

Scheme 4.16: Synthesis of known b-diketiminate complexes **3.4**, **4.9**-**4.10**.

Aluminium dihydride **4.9** was reacted with one equivalent of the aluminium(I) reagent **4.4** and monitored by ^{1}H NMR spectroscopy with the findings summarised in **Scheme 4.17**. **Figure 4.16** shows the ^{1}H NMR spectrum recorded after 15 minutes at room temperature, with select resonances peak picked and integrated. Inspection of the ^{1}H NMR spectrum revealed complete consumption of the aluminium dihydride **4.9** with a small amount of **4.4** remaining. As observed with **2.8**, the reaction yielded the formation of **3.5** as evidenced by the multiplet at 3.43 ppm and the singlet at 4.87 ppm. Four new singlets in the alkyl region were observed at 1.48, 2.09, 2.17 and 2.42 ppm (remaining resonances at 1.14, 1.39 and 1.55 ppm are assigned to **3.5**) and all integrated to approximately twelve protons each. These were assigned as the methyl groups in the *ortho* and *meta* positions of the mes substituent, as well as the methyl groups of the ligand backbone. This, in conjunction with the absence of any additional major methine resonances, led to the proposal that the symmetric dimer **4.11** formed as the major product. The presence of four singlets with equal integration suggests that the *ortho* protons of the mes substituent are chemically inequivalent.

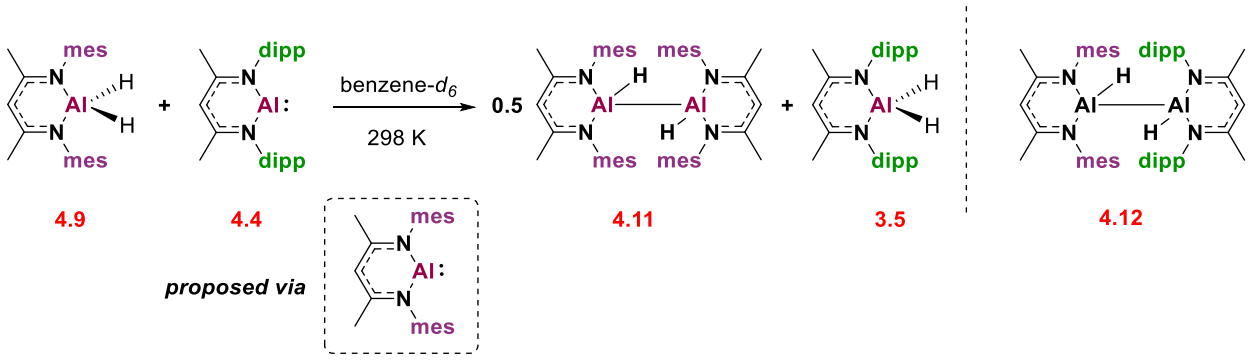

Scheme 4.17: Scheme to show proposed reactivity of **4.9** with **4.4** *via* **4.12**.

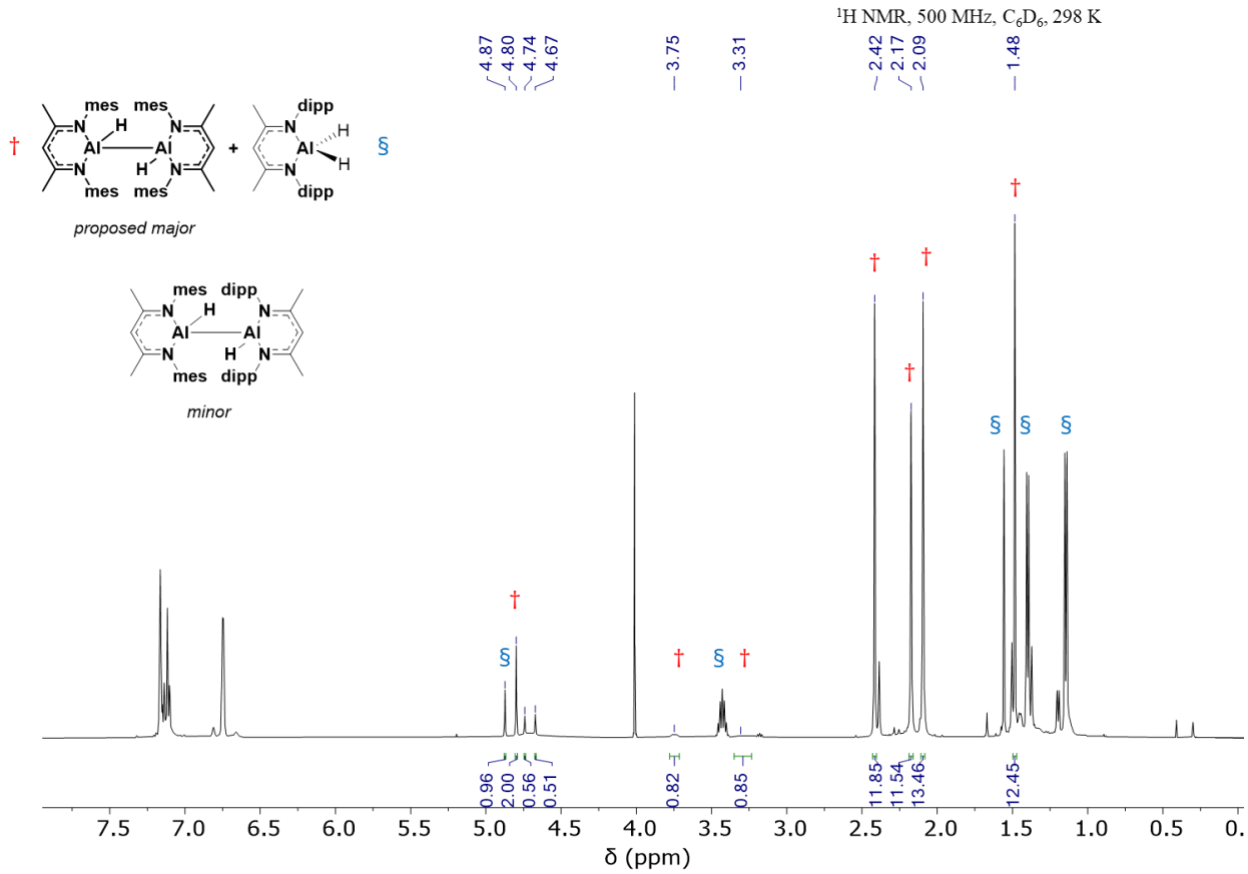

Figure 4.16: ^{1}H NMR spectrum after 15 minutes of the 1:1 reaction of **4.9** and **4.4**.

Further inspection of the ^{1}H NMR spectrum showed the presence of a third, minor product in solution. Two singlets at 4.67 and 4.74 ppm in a 1:1 ratio indicated the presence of one asymmetric β-diketiminate complex or two different β-diketiminate complexes formed in the same ratio. Based on experimental observations for **2.8**, the asymmetric aluminium dimer **4.12** was proposed to form as a reaction intermediate (**Scheme 4.17**). It is interesting to note that, whilst the products of this reaction appear analogous to compound **2.8**, the ratio in which they form from a 1:1 reaction of reagents was different. The asymmetric intermediate **4.5** and the symmetric dimer **4.6** were present in an almost equal ratio when formed *via* the reaction of **2.8** (0.45:0.55) and required heating, excess **2.8** or long reaction times to convert to a mixture with **4.6**/**3.5** as the major products. In contrast, the symmetric dimer **4.11** forms as the major product after 15 minutes at room temperature, and the reaction mixtures showed **4.11** and **4.12** were present in an approximate 0.4:0.1 ratio. This initially suggests that the formation of **4.11** has a lower energy barrier than **4.6**, and therefore could be reversible in solution. Overall, **4.12** appears to be less stable in solution, and the reactivity of this was later compared to that of aluminium dihydride **4.10**.

To establish whether the formation of **4.11** was reversible, the reaction mixture was heated at 323 K for 3 hours. A small grease peak at 0.30 ppm was normalised and all resonances were integrated with respect to this. Heating to 323 K for 3 hours revealed an increase in the integration of **4.4** (298 K: 0.19 with respect to grease, 3 hours at 323 K: 0.42 with respect to grease). The precise integrations of the product and intermediate resonances were harder to establish as the broad aluminium hydride sits under this region. However, this was an early sign that the reaction is reversible, and future experiments could explore this concept further.

Finally, one equivalent of the aluminium hydride **4.10** was reacted with one equivalent of **4.4** and the reactivity is summarised in **Scheme 4.18**. After 15 minutes at room temperature, the ^{1}H NMR spectrum (**Figure 4.17**) showed the formation of one major product. The presence of two resonances at 5.03 and 5.14 ppm in a 1:1 ratio was indicative of the formation of an asymmetric aluminium dimer, and thus **4.13** was proposed as the product of this reaction based on previous reactivity for **2.8** and **4.9**. The reaction mixture was stable at room temperature and the formation of the symmetric dimer analogous to **4.6** or **4.11** was not observed. Intermediate **4.13** is therefore more persistent in solution and could be attributed to the decreased steric encumbrance of the phenyl substituents preventing dissociation of the species formed. It is difficult to compare this phenomenon to the literature examples of the dipp analogue, as any dissociation and recombination reactions between intermediate and product dimers are masked by the identical nature of both species. Attempts to recrystallise **4.13** were unsuccessful and, due to time constraints of the project, no further reactivity has been explored.

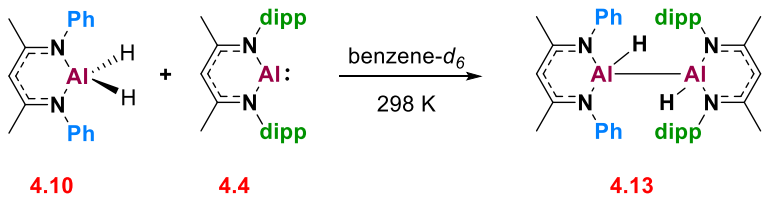

Scheme 4.18: Reaction of **4.10** with **4.4** in a 1:1 ratio.

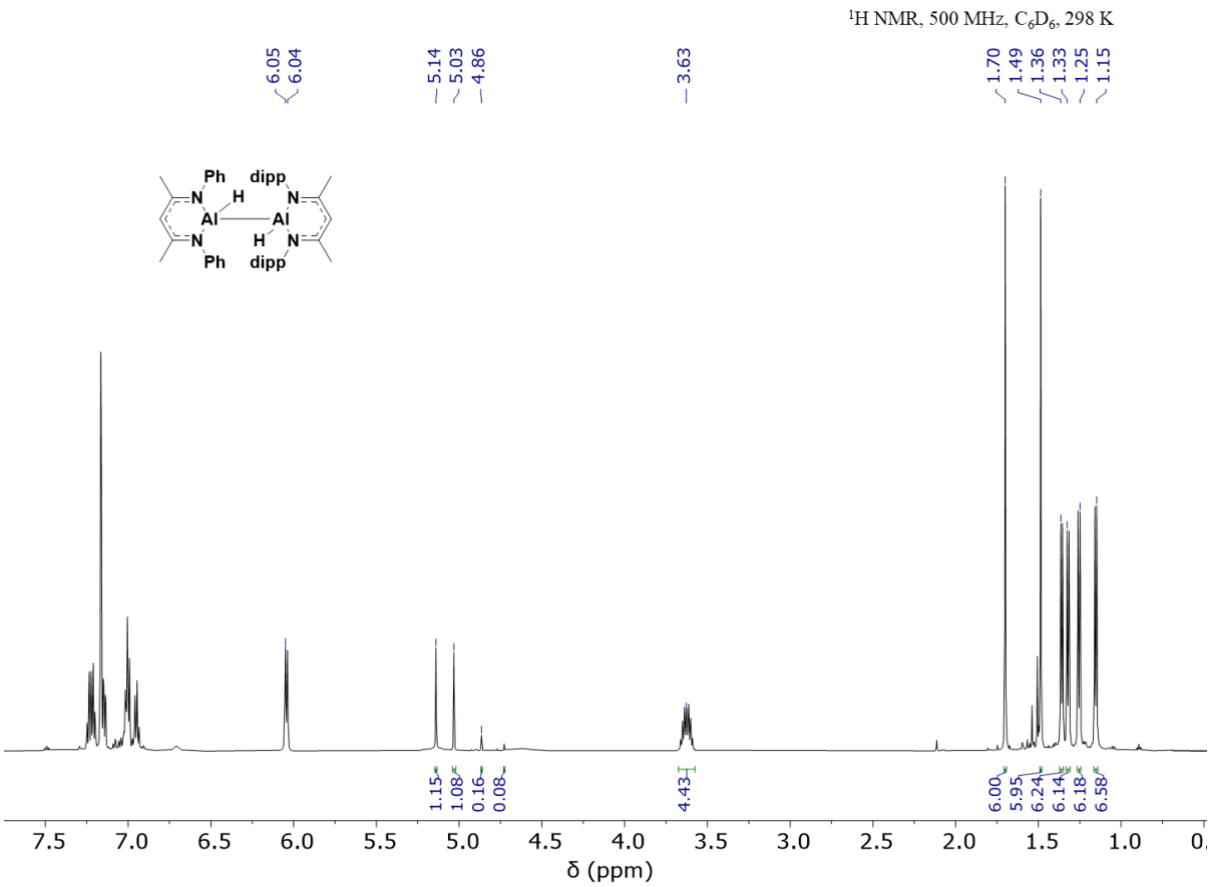

Figure 4.17: ^{1}H NMR spectrum after 15 minutes of the 1:1 reaction of **4.9** and **4.4**.

4.4 Summary and Outlook

4.4.1 Summary

The aluminium amidinate hydride **2.8** reacted with **4.4** to overall form the previously-reported dihydrodialane species **4.6** and known aluminium dihydride **3.5**, *via* a mixed BDI-amidinate intermediate **4.5**. Whilst these species were not characterised crystallographically, by varying the stoichiometries of the starting reagents the intermediate or the products could be selectively favoured, with an excess of **4.4** facilitating the formation of intermediate **4.6**. Future work will focus on exploring whether this process is reversible and whether further functionalisation of this bond is possible.

Within this series of reactions using β-diketiminate aluminium hydride complexes, the reaction outcomes of the 1:1 reaction with the aluminium(I) reagent **4.4** varied. For example, the reaction with **4.9** proceeded rapidly at room temperature to form the symmetric dimer **4.11** and the aluminium hydride **3.5** with only a small amount of the intermediate **4.12** present in solution. The opposite was observed with **4.10**, with clean formation of the asymmetric

intermediate species **4.13**. Early investigations into the reversibility of these BDI reactions looked positive, though further evidence is needed to support this claim.

4.4.1 Outlook

These experiments revealed an alternative synthetic route to the literature aluminium(II) dihydrodialane species **4.6** and thus their reactivity can be further explored. The observation of the intermediate species in the reaction mixture, with further experiments, could provide detailed mechanistic insight into the formation of dihydrodialanes, and further functionalisation may facilitate the formation of dialumene compounds, which at present are isolated to a select few examples. In all instances the symmetric dihydrodialane compounds form *via* the *in situ* formation of aluminium(I) reagents, and further experiments should focus on trapping these *via* exposure to small molecules (e.g. CO_2).

This work should be complemented by density functional theory calculations. Specifically, the activation enthalpies for the formation of the intermediate and symmetric products should be calculated. This could provide some rationale for the formation of symmetric dimers with **2.8** and **4.9** contrasted to the stable formation of the asymmetric intermediate **4.10**. Further derivatives of amidinate- and BDI-hydride complexes could be further investigated.

4.5 Chapter 4 Experimental Section

The work described in this chapter is the subject of ongoing lab work, and thus full characterisation of the compounds formed (X-ray analysis) is currently unavailable. The products that have been proposed to form have been inferred based only on NMR experiments, and thus the proposed structures of these compounds may be subject to change based on the results of future experiments.

4.5.1 Synthesis of [$AlMe_2(Ar^{dipp}Ar^{dipp}Am)$] (4.1)

$Ar^{dipp}Ar^{dipp}AmH$ (**2.2**, 0.44 mmol, 200 mg) was dried under vacuum for 1 h, dissolved in toluene (10 mL) and cooled to 195 K. Trimethyl aluminium (0.53 mmol, 0.26 mL) was added dropwise, methane gas was seen to evolve, and the reaction was stirred at 298 K overnight. The solvent was removed *in vacuo* and the resultant product was washed with hexane to yield a white solid after filtration (126 mg, 53%).

^{1}H NMR (500 MHz, C_6D_6, 298 K) δ ppm: -0.05 (s, 6H, Al(C**H**$_3$)$_2$) 0.97 (d, 12H, CH(C**H**$_3$)$_2$ $^3J_{HH}$ = 6 Hz), 1.28 (d, 12H, CH(C**H**$_3$)$_2$, $^3J_{HH}$ = 6 Hz), 1.64 (s, 3H, ^{L}C**H**$_3$), 3.64 (sept, 4H, C**H**(CH$_3$)$_2$, $^3J_{HH}$ = 5.5 Hz), 6.40 (d, 2H, ^{L}C**H**, $^3J_{HH}$ = 6.5 Hz), 7.03-7.10 (m, 8H, ^{Ph}C**H**).

4.5.2 Synthetic Procedure for Iodination of 2.14 and 4.1

Aluminium alkyl (**2.14** (170 mg)/**4.1** (117 mg), 23 mmol) was dissolved in toluene and added dropwise at room temperature to a solution of I_2 (50 mmol, 126 mg) dissolved in toluene and stirred at 298 K overnight. The solvent was removed *in vacuo* before recrystallising in toluene. Synthetic target not isolated.

4.1: ^{1}H NMR (600 MHz, C_6D_6, 298K) δ ppm: 0.99 (d, 12H, CH(C**H**$_3$)$_2$, $^3J_{HH}$ = 6.6 Hz), 1.39 (d, 12H, CH(C**H**$_3$)$_2$, $^3J_{HH}$ = 6.6 Hz), 1.45 (s, 3H, ^{Ar*}C**H**$_3$), 3.49 (sept, 4H, C**H**(CH$_3$)$_2$, $^3J_{HH}$ = 6.6 Hz), 6.25 (d, 2H, ^{Ar*}C**H**, $^3J_{HH}$ = 8.4 Hz), 6.84 – 6.99 (m, 8H, ^{Ph}C**H**).

4.5.3 Synthesis of [K(Ar*Ar^{dipp}Am)] (4.2)

Ar*ArdippAmH (**2.6**, 0.28 mmol, 200 mg) and KHMDS (45 mmol, 89 mg) were dissolved in toluene and stirred at 298 K overnight. The solvent was removed *in vacuo*, washed with hexane, filtered, dried, and isolated. (84 mg, 38%).

^{1}H NMR (500 MHz, C_6D_6, 298K) δ ppm: 1.18 (d, 6H, CH(C**H**$_3$)$_2$, $^{3}J_{HH}$ = 7.0 Hz), 1.33 (d, 6H, CH(C**H**$_3$)$_2$, $^{3}J_{HH}$ = 7.0 Hz), 1.85 (s, 3H, ^{Ar*}C**H**$_3$), 1.88 (s, 3H, ^{L}C**H**$_3$), 3.83 (sept, 2H, C**H**(CH$_3$), $^{3}J_{HH}$ = 7.2 Hz), 6.10 (s, 2H, C**H**(Ph$_2$)), 6.64 (s, 2H, ^{Ar*}C**H**), 6.77 (d, 2H, ^{L}*o*-C**H**), 6.65 – 7.13 (m, 25H, ^{Ar}**H**), 7.43 (d, 2H, ^{L}*m*-C**H**, $^{3}J_{HH}$ = 8 Hz); ^{13}C{^{1}H} NMR (500 MHz, C_6D_6, 298K): 21.1 (^{L}**C**H$_3$), 21.4 (^{Ar*}**C**H$_3$), 22.7 (CH(**C**H$_3$)$_2$), 25.3 (CH(**C**H$_3$)$_2$), 28.3 (**C**H(CH$_3$)$_2$), 54.0 (**C**H(Ph)$_2$), 119.9 (C^{IV}), 122.7 (C^{IV}), 126.4 (C^{IV}), 126.9 (C^{IV}), 127.4 (C^{IV}), 128.6 (^{Ar*}**C**H), 128.7 (C^{IV}), 129.3 (^{L}*m*-**C**H), 129.7 (^{L}*o*-**C**H), 130.4 (C^{IV}), 130.5 (C^{IV}), 136.5 (C^{IV}), 136.8 (C^{IV}).

4.5.4 Synthesis of [Ar*Ar^{dipp}AmH$_2$]$^{+}$ I$_3^{-}$ (4.3)

[K(Ar*Ar^{dipp}Am)] (**4.2**, 0.021 mmol, 15 mg) and aluminium triiodide (0.021 mmol, 8.5 mg) were dissolved in benzene-*d*$_6$ and monitored by ^{1}H NMR spectroscopy.

^{1}H NMR (600 MHz, C_6D_6, 298K) δ ppm: 0.72 (d, 6H, CH(C**H**$_3$)$_2$, $^{3}J_{HH}$ = 6.6 Hz), 1.38 (d, 6H, CH(C**H**$_3$)$_2$, $^{3}J_{HH}$ = 7.2 Hz), 1.54 (s, 3H, C**H**$_3$), 1.64 (s, 3H, C**H**$_3$), 3.10 (sept, 2H, C**H**(CH$_3$)$_2$, $^{3}J_{HH}$ = 7.2 Hz), 6.03 (d, 2H, ^{Ph}C**H**, $^{3}J_{HH}$ = 7.8 Hz), 6.39 (d, 2H, ^{Ph}C**H**, $^{3}J_{HH}$ = 8.4 Hz), 6.42 (s, 2H, , ^{Ph}C**H**), 6.82 (d, 2H, ^{Ph}C**H**, $^{3}J_{HH}$ = 7.8 Hz), 6.90 (s, 2H, ^{Ph}C**H**), 6.95-7.08 (m, 16 H, ^{Ph}C**H**), 7.23 (t, 4H, ^{Ph}C**H**, $^{3}J_{HH}$ = 7.8 Hz), 11.97 (s, 1H, N**H**), 12.83 (s, 1H, N**H**).

4.5.5 Multistep Synthesis of [Al:(^{dipp}BDI)] (4.4)

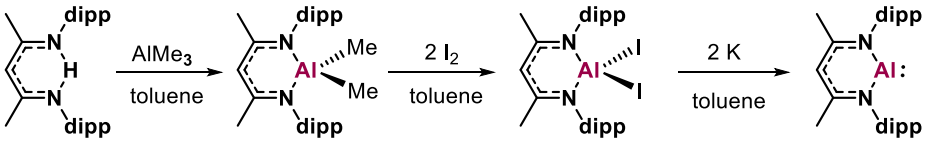

4.4A 4.4B 4.4

4.4A: ^{dipp}BDIH (**3.3**, 19.1 mmol, 8.0 g) was dried under vacuum for 1 h and dissolved in toluene (30 mL) and trimethyl aluminium (2M in toluene, 22 mmol, 11.5 mL) was added dropwise with vigorous stirring and the reaction was stirred at 298 K overnight. The solvent was removed

in vacuo. The crude product was recrystallised in a minimum amount of hot toluene at 255 K. (7.10 g, 78%). NMR matches that reported in the literature.[20]

^{1}H NMR (500 MHz, C_6D_6, 298K) δ ppm: -0.50 (s, 6H, Al(C**H**$_3$)$_2$), 1.14 (d, 12H, CH(C**H**$_3$)$_2$, $^{3}J_{HH}$ = 7 Hz), 1.33 (d, 12H, CH(C**H**$_3$)$_2$, $^{3}J_{HH}$ = 6.5 Hz), 1.56 (s, 3H, C**H**$_3$), 3.42 (sept, 4H, 6H, C**H**(CH$_3$)$_2$, $^{3}J_{HH}$ = 6.5 Hz), 4.96 (s, 1H, C**H**), 7.10-7.16 (m, 6H, ^{Ph}C**H**).

4.4B: [AlMe$_2$(^{dipp}BDI)] (**4.4A**, 10.5 mmol, 5.0 g) was dissolved in toluene and added dropwise with vigorous stirring to a solution of iodine (22.1 mmol, 5.61 g) dissolved in toluene at 298 K. The reaction was stirred at room temperature overnight before the solvent was removed *in vacuo* and heated under vacuum at 318 K for 2 hours. The crude product was recrystallised from hot toluene at 255 K. (6.09 g, 83%). NMR matches that reported in the literature.[20]

^{1}H NMR (500 MHz, C_6D_6, 298K) δ ppm: 1.08 (d, 12H, CH(C**H**$_3$)$_2$, $^{3}J_{HH}$ = 7 Hz), 1.43 (d, 12H, CH(C**H**$_3$)$_2$, $^{3}J_{HH}$ = 7 Hz), 1.49 (s, 3H, C**H**$_3$), 3.59 (sept, 4H, 6H, C**H**(CH$_3$)$_2$, $^{3}J_{HH}$ = 7 Hz), 5.06 (s, 1H, C**H**), 7.09-7.14 (m, 6H, ^{Ph}C**H**).

4.4: [AlI$_2$(^{dipp}BDI)] (**4.4B**, 1.4 mmol, 100 mg) was dissolved in toluene (10 mL) and potassium pieces (3.0 mmol, 118 mg) were added. The solution was stirred vigorously for 72 hours. The precipitate was settled, the solution filtered, and the solvent removed *in vacuo*. The residue was redissolved in a minimum amount of toluene (3-5 mL) and filtered in a glass fibre filter/pipette into an ampoule. The reaction mixture was recrystallised at 268 K. (73 mg, 12%). NMR matches that reported in the literature.[20]

^{1}H NMR (500 MHz, C_6D_6, 298K) δ ppm: 1.14 (d, 12H, CH(C**H**$_3$)$_2$, $^{3}J_{HH}$ = 7 Hz), 1.38 (d, 12H, CH(C**H**$_3$)$_2$, $^{3}J_{HH}$ = 7 Hz), 1.67 (s, 3H, C**H**$_3$), 3.18 (sept, 4H, 6H, C**H**(CH$_3$)$_2$, $^{3}J_{HH}$ = 7 Hz), 5.20 (s, 1H, C**H**), 7.16-7.22 (m, 6H, ^{Ph}C**H**).

4.5.6 Synthesis of [(Ar^{dipp}Ar^{dipp}Am)Al(H)Al(H)(^{dipp}BDI)] (4.5)

[AlH$_2$(Ar^{dipp}Ar^{dipp}Am)] (**2.8**, 0.015 mmol, 8 mg) and [Al:(^{dipp}BDI)] **(4.4**, 0.023 mmol, 10 mg) were dissolved in benzene-d_6 and reacted for 15 minutes at 298 K. Reaction was monitored by ^{1}H NMR spectroscopy.

^{1}H NMR (500 MHz, C_6D_6, 298 K) δ ppm: 0.95 (d, 2H, CH(C**H**$_3$)$_2$, $^{3}J_{HH}$ = 7 Hz), 1.03 (m, 12H, CH(C**H**$_3$)$_2$, $^{3}J_{HH}$ = 7 Hz), 1.11 (d, 6H, CH(C**H**$_3$)$_2$, $^{3}J_{HH}$ = 6.5 Hz), 1.13 (d, 6H, CH(C**H**$_3$)$_2$, $^{3}J_{HH}$ = 3 Hz), 1.16 (d, 6H, CH(C**H**$_3$)$_2$, $^{3}J_{HH}$ = 6.5 Hz), 1.23 (d, 6H, CH(C**H**$_3$)$_2$, $^{3}J_{HH}$ = 7 Hz), 1.25 (d, 6H, CH(C**H**$_3$)$_2$, $^{3}J_{HH}$ = 6.5 Hz), 1.48 (s, 6H, (C**H**$_3$)$_2$), 1.61 (s, 3H, ^{L}C**H**$_3$), $^{3}J_{HH}$ = 6.5 Hz), 3.40-3.50 (m, 4H, C**H**(CH$_3$)$_2$), 3.54-3.61 (m, 4H C**H**(CH$_3$)$_2$), 5.01 (s, 1H, **C**H), 6.34 (d, 2H, ^{L}*o*-**C**H $^{3}J_{HH}$ = 8.5 Hz), 7.00-7.22 (m, 14 H, ^{Ph}C**H**). Carbon data is not assigned due to accidental omission of HSQC data collection, but ^{13}C and HMBC spectra are included in the appendix.

4.5.7 Synthesis of [Al(H)(Ar^{dipp}Ar^{dipp}Am)]$_2$ (4.6)

[AlH$_2$(Ar^{dipp}Ar^{dipp}Am)] (**2.8**, 0.018 mmol, 9 mg) and [Al:(^{dipp}BDI)] **(4.4**, 0.013 mmol, 6 mg) were dissolved in benzene-*d*$_6$ and reacted for 16 hours at 298 K. Reaction was monitored by ^{1}H NMR spectroscopy. NMR matches that reported in the literature.[97]

^{1}H NMR (500 MHz, C_6D_6, 298 K) δ ppm: 1.06 (d, 12H, CH(C**H**$_3$)$_2$, $^{3}J_{HH}$ = 6.5 Hz), 1.07 (d, 12H, CH(C**H**$_3$)$_2$, $^{3}J_{HH}$ = 6.5 Hz), 1.20 (d, 12H, CH(C**H**$_3$)$_2$, $^{3}J_{HH}$ = 6.5 Hz), 1.38 (d, 12H, $^{3}J_{HH}$ = 2.5 Hz), 1.63 (s, 6H, C**H**$_3$), 3.79-3.92 (m, 8H, C**H**(CH$_3$)$_2$), 5.66 (s, 2H, Al**H**), 6.40 (d, 4H, ^{L}C**H** $^{3}J_{HH}$ = 8.5 Hz), 6.96-7.13 (m, 16H, ^{Ph}C**H**).

4.5.8 Synthesis of ^{mes}BDIH (4.7)

Concentrated HCl (12 M, 33.6 mmol, 3.8 mL) was added dropwise to a solution of acetylacetonate (33.6 mmol, 3.3 mL) and 2,4,6-trimethylaniline (74 mmol, 10.4 mL) in ethanol. The reaction was stirred at 363 K for 3 days before the solvent was concentrated *in vacuo*. Dichloromethane (DCM, 20 mL) and saturated Na_2CO_3 were added to the mixture and stirred for 2 hours at 298 K to extract the ligand into DCM. The organic layer was washed with distilled H_2O (2 x 20 mL), dried ($MgSO_4$) and concentrated *in vacuo*. The crude reaction mixture was recrystallised in methanol. (6.5 g, 57%). NMR matches that reported in the literature.[186]

^{1}H NMR (500 MHz, $CDCl_3$, 298 K) δ ppm: 1.69 (s, 6H, C**H**$_3$), 2.13 (s, 12H, ^{mes}*o*-C**H**$_3$), 2.27 (s, 6H, C**H**$_3$), 4.86 (s, 1H, C**H**), 6.86 (s, 4H, ^{Ph}C**H**), 12.14 (s, 1H, N**H**).

4.5.9 Synthesis of ^{Ph}BDIH (4.8)

Concentrated HCl (12 M, 107 mmol, 9.0 mL) was added dropwise to aniline (214 mmol, 19.5 mL and 273 K, allowed to warm to room temperature and stirred overnight. The resultant solid was dissolved in DCM (4 mL) and H_2O (50 mL), neutralised (NEt_3, 15 mL) and extracted into pet. ether (2 x 150 mL). The solvent was removed *in vacuo* and the resultant oil was recrystallised in ethanol at 255 K. (8.72 g, 36%). NMR matches that reported in the literature.[187]

^{1}H NMR (500 MHz, $CDCl_3$, 298 K) δ ppm: 2.03 (s, 6H, C**H**$_3$), 4.90 (s, 1H, C**H**), 6.99 (d, 4H, ^{Ph}*o*-C**H**, $^3J_{HH}$ = 8 Hz), 7.07 (t, 2H, ^{Ph}*p*-C**H**, $^3J_{HH}$ = 7.5 Hz), 7.31 (t, 4H, ^{Ph}*m*-C**H**, $^3J_{HH}$ = 8 Hz).

4.5.10 Synthesis of [AlH$_2$(^{mes}BDI)] (4.9)

^{mes}BDIH (**4.7**, 0.60 mmol, 200 mg) was dissolved in hexane and added dropwise to a solution of trimethylamine alane (0.72 mmol, 63 mg) dissolved in hexane at room temperature. The reaction was stirred at 298 K overnight, before the solvent was removed *in vacuo*. The crude mixture was recrystallised in hot hexane at 278 K. The reaction was filtered, dried *in vacuo* and isolated as clear and colourless crystals. (120 mg, 54.5%).

^{1}H NMR (500 MHz, C_6D_6, 298 K) δ ppm: 1.49 (s, 6H, (C**H**$_3$)$_2$, 2.10 (s, 6H, ^{mes}*p*-C**H**$_3$), 2.32 (s, 12H, ^{mes}*o*-C**H**$_3$), 4.80 (s, 1H, C**H**), 6.76 (s, 4H, ^{mes}*m*-C**H**); ^{13}C{^{1}H} NMR (500 MHz, C_6D_6, 298K): 18.1 (^{mes}*o*-**C**H), 20.8 (^{mes}*p*-**C**H), 22.0 ((**C**H$_3$)$_2$), 95.8 (**C**H), 127.9 (^{mes}*m*-**C**H), 129.9 (C^{IV}), 133.5 (C^{IV}), 135.8 (C^{IV}), 139.8 (C^{IV}), 169.7 (C^{IV}).

4.5.11 Synthesis of [AlH$_2$(^{Ph}BDI)] (4.10)

^{Ph}BDIH (**4.8**, 120 mmol, 300 mg) was dissolved in toluene and added dropwise to a solution of trimethylamine alane (144 mmol, 128 mg) dissolved in toluene at room temperature. The reaction was stirred at 298 K overnight, before the solvent was removed *in vacuo*. The crude mixture was recrystallised in hot hexane at 278 K. (140 mg, 42%).

^{1}H NMR (500 MHz, C_6D_6, 298 K) δ ppm: 1.54 (s, 6H, C**H**$_3$), 4.73 (s, 1H, C**H**), 6.91 (t, 2H, ^{Ph}*p*-C**H**), 7.02-7.09 (m, 8H, ^{Ph}C**H**).

4.5.12 Synthesis of [AlH(^{mes}BDI)]$_2$ (4.11) and [(^{mes}BDI)Al(H)Al(H)(^{dipp}BDI)] (4.12)

[AlH$_2$(^{mes}BDI)] (**4.9**, 0.013 mmol, 5 mg) and [Al:(^{dipp}BDI)] (**4.4**, 0.013 mmol, 6 mg) were dissolved in benzene-*d*$_6$ and reacted for 15 minutes at room temperature. The reaction was heated to 353 K and regular ^{1}H NMR spectra were recorded over the course of 3 hours. It was not possible to assign resonances for **4.12**, other than the backbone methine protons at 4.67 and 4.74 ppm.

4.11: ^{1}H NMR (500 MHz, C$_6$D$_6$, 298 K) δ ppm: 1.48 (s, 12H, C**H**$_3$), 2.09 (s, 12H, C**H**$_3$), 2.17 (s, 12H, C**H**$_3$), 2.42 (s, 12H, C**H**$_3$), 4.80 (s, 2H, C**H**); further assignments were not possible.

4.5.15 Synthesis of [(^{Ph}BDI)Al(H)Al(H)(^{dipp}BDI)] (4.13)

[AlH$_2$(^{dep}BDI)] (**4,10**, 0.015 mmol, 4 mg) and [Al:(^{dipp}BDI)] (**4.4**, 0.015 mmol, 7 mg) were dissolved in benzene-*d*$_6$ and reacted for 15 minutes at room temperature. The reaction was monitored by ^{1}H NMR spectroscopy and no change in the reaction composition was observed at longer reaction times (>24 hours).

^{1}H NMR (500 MHz, C$_6$D$_6$, 298 K) δ ppm: 1.15 (d, 6H, CH(C**H**$_3$)$_2$, $^3J_{HH}$ = 6.6 Hz), 1.25 (d, 6H, CH(C**H**$_3$)$_2$, $^3J_{HH}$ = 6.6 Hz), 1.32 (d, 6H, CH(C**H**$_3$)$_2$, $^3J_{HH}$ = 7.2 Hz), 1.35 (d, 6H, CH(C**H**$_3$)$_2$, $^3J_{HH}$ = 6.6 Hz), 1.49 (s, 6H, C**H**$_3$), 1.70 (s, 6H, C**H**$_3$), 3.63 (sept, 4H, C**H**(CH$_3$)$_2$, $^3J_{HH}$ = 9 Hz), 5.03 (s, 1H, C**H**), 5.14 (s, 1H, C**H**), 6.04 (d, 4H, ^{Ph}C**H**), 6.93-7.25 (m, 14 H, ^{Ph}C**H**); ^{13}C{^{1}H} NMR (150 MHz, C$_6$D$_6$, 298K) δ ppm: 22.9 (CH(**C**H$_3$)$_2$), 23.5 (**C**H$_3$), 23.6 (**C**H$_3$), 24.4 (CH(**C**H$_3$)$_2$), 24.7 (CH(**C**H$_3$)$_2$), 27.1 (CH(**C**H$_3$)$_2$), 28.0 (**C**H(CH$_3$)$_2$), 98.4 (**C**H), 103.2 (**C**H), 124.2 (^{Ph}**C**H), 124.5 (^{Ph}**C**H), 124.7 (^{Ph}**C**H), 125.8 (^{Ph}**C**H), 127.0 (^{Ph}**C**H), 129.0 (^{Ph}**C**H), 146.1 (**C**^{IV}), 146.9 (**C**^{IV}), 170.0 (**C**^{IV}).

Chapter 5:

Conclusions and Future Work

5.1 Conclusions

This thesis describes the synthesis of a series of sterically encumbered amidine ligands bearing the 2,6-diphenylmethyl-4-methylphenyl substituent. These ligands were reacted with trimethylamine alane and trimethyl aluminium to synthesise a range of aluminium hydride and alkyl complexes, respectively. All complexes were characterised spectroscopically (^{1}H, ^{13}C{^{1}H} NMR), and in some cases by single crystal X-ray and elemental analyses. These complexes were investigated as catalysts for the hydroboration of phenylacetylene and a mechanistic study was undertaken.

The aluminium hydride complexes **2.8**-**2.10**, **2.12** and the aluminium alkyl complexes **2.14**-**2.15** were found to be catalysts and pre-catalysts, respectively, for the hydroboration of phenylacetylene. Reaction times varied across the series of catalysts which could be tentatively linked to catalyst size, structure, or stability. The kinetic profiles of the aluminium hydride catalysts were complex and indicate that competing reaction pathways were in operation at high conversions (>75%). In contrast, the aluminium alkyl complexes exhibited an induction period before becoming catalytically active and were found to be in good agreement with a first-order reaction profile throughout. The mechanism of action was probed through a series of stoichiometric experiments and uncovered a reaction pathway that likely proceeds *via* the coordination of a molecule of HBpin to the aluminium centre before undergoing transmetallation with phenylacetylene. Previously reported literature mechanisms were ruled out owing to an observed lack of reactivity with phenylacetylene or disubstituted alkynes. The steric encumbrance of the ligand influenced stability and reactivity. The mes-substituted aluminium hydride **2.12** retained its dimeric character in solution, and in the presence of HBpin formed borane as a decomposition product. To add to the complexity of these reactions, borane is a known hydroboration catalyst and thus it is difficult to elucidate the true mechanism of action for this species. A mixed hydride-alkyl species was said to form as the active catalyst from the alkyl complexes **2.14**-**2.15**, based on both experimental observations and previous literature reports.

The known dialumane (aluminium-aluminium single bond) compound **4.6** was formed *via* the 1:1 reaction of aluminium hydride **2.8** with a known low valent aluminium(I) reagent *via* a mixed amidinateAl-AlBDI intermediate. Conducting the reaction with an excess of aluminium(I) favoured the formation of intermediate **4.5**, whilst repeating the reaction with

excess aluminium hydride favoured the formation of products. The known aluminium hydride [$AlH_2(^{dipp}BDI)$] **3.5** formed as a product of these reactions. Repeating these reactions with β-diketiminate complexes revealed a distinct preference for the formation of the symmetrical dimer with a mes-substituted dihydride, however decreasing the steric encumbrance to phenyl-substituted aluminium dihydrides favoured the formation of the asymmetric intermediate. Complete characterisation and investigations into the reactivity of these complexes are the subject of further experimentation.

5.2 Future Work

5.2.1 Chapter 2 Future Work

The family of amidine ligands and aluminium amidinate complexes could be expanded by increase the steric encumbrance of the Ar* substituent further. For example, complexes of this type bearing the 2,6-diphenylmethyl-4-*iso*-propylphenyl substituent were reported by Jones *et al*. in the isolation of sterically encumbered group 2 complexes but they were not investigated for their catalytic capabilities. Similarly, synthesis of the smaller, symmetrical mes/mes-substituted complex could further highlight differences in the solid- and solution-state properties of these compounds.

5.2.2 Chapter 3 Future Work

The research in chapter 3 details comprehensive investigations undertaken to explore the mechanism of action for the reaction of the aluminium-catalysed hydroboration of phenylacetylene. As this work was conducted using representative substrates (phenylacetylene, HBpin) future efforts will focus on uncovering the substrate scope of these catalysts. The influence of electron-donating or withdrawing substituents on the rate of reaction will be investigated, in conjunction with the effects of alkyl *versus* aryl substituents. Similarly, the hydroalumination pathway first proposed by Cowley *et al*. should not be ruled out based on experiments for diphenylacetylene alone. This substrate is particularly large, and this mechanism should be investigated using smaller disubstituted alkynes. Finally, the precise nature of the HBpin adduct should be investigated *via* computational analyses with further investigations into the remaining steps of the catalytic cycle.

5.2.3 Chapter 4 Future Work

The reactions in chapter 4 were conducted on a small (~5 mg) scale. Future work should target the solid-state characterisation of the intermediate products by conducting these reactions on a larger scale. These reactions are formally 2:1 with respect to the aluminium hydride and thus should be repeated in this ratio to gain better insight into the overall reactivity. A generic scheme of future work is shown in **Scheme 5.1** based on the current literature.

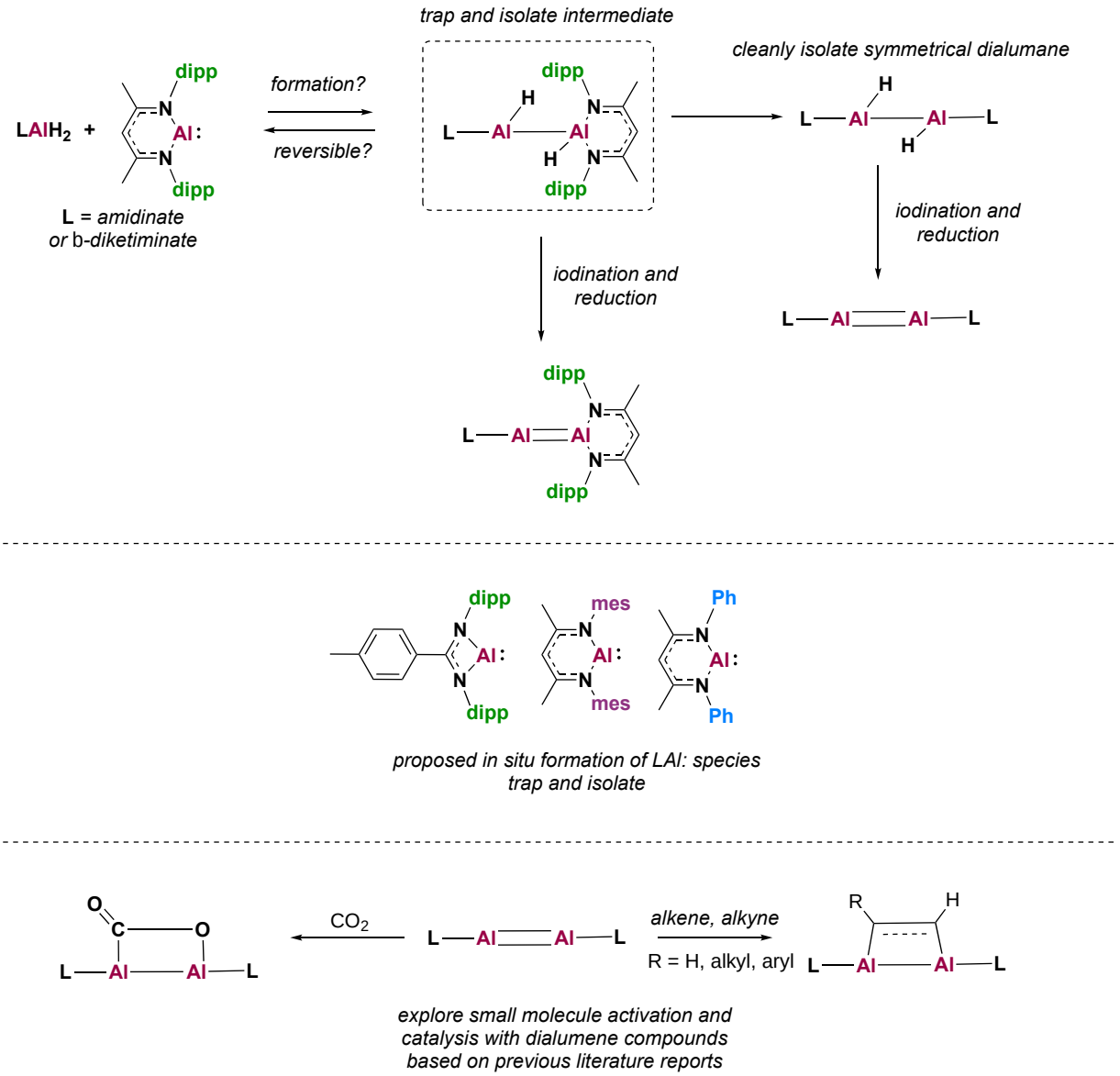

Scheme 5.1: Scheme of reactivity to highlight Chapter 4 future work.

In all instances the symmetric dihydrodialane (aluminium-aluminium single bond with both aluminium centres bonded to hydrogen) products are proposed to form *via* the *in situ* generation of aluminium(I) complexes, and future experiments should focus on trapping these. Examples

of these experiments include exposure of the reaction mixture to small molecules (e.g. CO_2, H-F) in order to trap the corresponding oxidative addition products. Similarly, clean isolation of the symmetric dihydrodilane complexes should be targeted and explored for their propensity to undergo iodination and reduction to yield the analogous dialumene species. Small molecule activation and catalytic reactions using dialumene complexes will be targeted. β-diketiminate complexes with more sterically encumbered substituents (e.g. 2,6-diethylphenyl "dep") should be used to investigate the influence of sterics on the reaction profile: does increasing steric encumbrance favour trapping of the reaction intermediate or direct formation of the symmetric dimer product? Initial investigations suggest that the reaction of [$AlH_2(^{mes}BDI)$] **4.9** with [Al:(^{dipp}BDI)] is reversible and this concept should be further explored. Similarly, reactions with [$AlH_2(^{Ph}BDI)$] **4.10** should be repeated and the reaction stoichiometries varied to investigate the formation of the intermediate *versus* the symmetric dimer product. This work should be complemented by DFT studies to investigate transition states, enthalpies of formation and mechanistic processes.

Chapter 6:

References

1 Q. L. Zhou, *Angew. Chem. Int. Ed.*, 2016, **55**, 5352–5353.
2 D. M. Beller and C. Bolm, *Transition Metals for Organic Synthesis*, Wiley, Weinheim, 2004.
3 G. J. Leigh, *Haber-Bosch and Other Industrial Processes*, Springer, Dordrecht, 1st edn., 2004, vol. 1.
4 O. A. Bereketidou and M. A. Goula, *Biogas reforming for syngas production over nickel supported on ceria–alumina catalysts*, Elsevier, Amsterdam, 2012.
5 R. Martin and S. L. Buchwald, *Acc. Chem. Res.*, 2008, **41**, 1461–1473.
6 N. Miyaura and A. Suzuki, *Chem. Rev*, 1995, **95**, 2457–2483.
7 J. R. Ludwig and C. S. Schindler, *Chem*, 2017, **2**, 313–316.
8 L. Souillart and N. Cramer, *Chem. Rev.*, 2015, **115**, 9410–9464.
9 M. García-Melchor, A. A. C. Braga, A. Lledós, G. Ujaque and F. Maseras, *Acc. Chem. Res.*, 2013, **46**, 2626–2634.
10 The Nobel Prize in Chemistry 2010, https://www.nobelprize.org/prizes/chemistry/2010/summary/, (21 September 2021).
11 T. P. Umile, *Catalysis for sustainability : goals, challenges, and impacts*, CRC Press, Florida, 2011.
12 What Is Palladium? It's Suddenly the Most Precious Metal - Bloomberg, https://www.bloomberg.com/news/articles/2019-10-28/why-palladium-is-suddenly-a-more-precious-metal-quicktake-k2ap4ryc, (accessed 21 September 2021).
13 Elements in danger, https://www.rsc.org/new-perspectives/sustainability/elements-in-danger/#surveyfindings, (accessed 21 September 2021).
14 C. Weetman and S. Inoue, *ChemCatChem*, 2018, **10**, 4213–4228.
15 P. P. Power, *Nature*, 2010, **463**, 171–177.
16 M. Yoshifuji, I. Shima and N. Inamoto, *J. Am. Chem. Soc.*, 1981, **103**, 4587–4589.
17 R. West, M. J. Fink and J. Michl, *Science*, 1981, **214**, 1343–1344.
18 P. P. Power, *J. Chem. Soc. Dalton. Trans.*, 1998, **18**, 2939–2951.
19 S. P. Green, C. Jones and A. Stasch, *Science*, 2007, **318**, 1754–1757.
20 C. Cui, H. W. Roesky, H. Schmidt and M. Noltemeyer, *Angew. Chem. Int. Ed.*, 2000, **39**, 4274–4276.
21 G. Jin, C. Jones, P. C. Junk, A. Stasch and W. D. Woodul, *New J. Chem.*, 2008, **32**, 835–842.
22 A. V. Protchenko, K. H. Birjkumar, D. Dange, A. D. Schwarz, D. Vidovic, C. Jones, N. Kaltsoyannis, P. Mountford and S. Aldridge, *J. Am. Chem. Soc.*, 2012, **134**, 6500–6503.
23 T. J. Hadlington, M. Hermann, J. Li, G. Frenking and C. Jones, *Angew. Chem. Int. Ed.*, 2013, **52**, 10199–10203.
24 R. C. Fischer and P. P. Power, *Chem. Rev.*, 2010, **110**, 3877–3923.
25 R. L. Melen, *Science*, 2019, **363**, 479–484.
26 L. D. Tuck, *J. Pharm. Sci.*, 1966, **55**, 993–993.
27 L. Pu, A. D. Phillips, A. F. Richards, M. Stender, R. S. Simons, and M. M. Olmstead and P. P. Power*, *J. Am. Chem. Soc.*, 2003, **125**, 11626–11636.
28 A. Sekiguchi, R. Kinjo and M. Ichinohe, *Science*, 2004, **305**, 1755–1757.
29 M. Stender, A. D. Phillips, R. J. Wright and P. P. Power, *Angew. Chem. Int. Ed*, 2002, **41**, 1785-1788.
30 L. Pu, and B. Twamley and P. P. Power, *J. Am. Chem. Soc.*, 2000, **122**, 3524–3525.
31 Geoffrey H. Spikes, and James C. Fettinger and P. P. Power, *J. Am. Chem. Soc.*, 2005, **127**, 12232–12233.
32 M. Arrowsmith, J. Bohne, H. Braunschweig, M. Celik Ali, T. Dellerman and K. Hammond, *Chem. Eur. J*, 2016, **22**, 17169–17172.

33 T. Chu, I. Korobkov and G. I. Nikonov, *J. Am. Chem. Soc.*, 2014, **136**, 9195–9202.
34 J. D. Erickson, P. Vasko, R. D. Riparetti, J. C. Fettinger, H. M. Tuononen and P. P. Power, *Organometallics*, 2015, **34**, 5785–5791.
35 Y. Peng, J. D. Guo, B. D. Ellis, Z. Zhu, J. C. Fettinger, S. Nagase and P. P. Power, *J. Am. Chem. Soc.*, 2009, **131**, 16272–16282.
36 C. Bakewell, A. J. P. White and M. R. Crimmin, *J. Am. Chem. Soc.*, 2016, **138**, 12763–12766.
37 T. Chu, Y. Boyko, I. Korobkov and G. I. Nikonov, *Organometallics*, 2015, **34**, 5363–5365.
38 C. Bakewell, A. J. P. White and M. R. Crimmin, *Angew. Chem. Int. Ed.*, 2018, **57**, 6638–6642.
39 Y. Xiong, S. Yao and M. Driess, *Chem. A Eur. J.*, 2012, **18**, 3316–3320.
40 G. D. Frey, J. D. Masuda, B. Donnadieu and G. Bertrand, *Angew. Chem.*, 2010, **122**, 9634–9637.
41 B. Gehrhus, P. B. Hitchcock, M. F. Lappert, J. Heinicke, R. Boese and D. Bläser, *J. Organomet. Chem.*, 1996, **521**, 211–220.
42 T. Chu and G. I. Nikonov, *Chem. Rev.*, 2018, 118, 3608–3680.
43 P. L. Timms, *Inorg. Chem.*, 1968, **7**, 387–389.
44 P. Jutzi and A. Möhrke, *Angew. Chem. Int. Ed.*, 1989, **28**, 762–763.
45 C. Ganesamoorthy, S. Loerke, C. Gemel, P. Jerabek, M. Winter, G. Frenking and R. A. Fischer, *Chem. Commun.*, 2013, **49**, 2858–2860.
46 S. J. Urwin, D. M. Rogers, G. S. Nichol and M. J. Cowley, *Dalton. Trans.*, 2016, **45**, 13695–13699.
47 C. P. Sindlinger and L. Wesemann, *Chem. Sci.*, 2014, **5**, 2739–2746.
48 Y. Peng, B. D. Ellis, X. Wang, J. C. Fettinger and P. P. Power, *Science*, 2010, **1668**, 2–3.
49 P. Šimon, F. de Proft, R. Jambor, A. Růžička and L. Dostál, *Angew. Chem. Int. Ed.*, 2010, **49**, 5468–5471.
50 C. Weetman, *Chem. Eur. J.*, 2021, **27**, 1941–1954.
51 T. Sugahara, J. D. Guo, T. Sasamori, S. Nagase and N. Tokitoh, *Angew. Chem. Int. Ed.*, 2018, **57**, 3499–3503.
52 M. S. Hill, D. J. Liptrot and C. Weetman, *Chem. Soc. Rev.*, 2016, **45**, 972–988.
53 S. H. and and T. J. Marks, *Acc. Chem. Res.*, 2004, **37**, 673–686.
54 L. C. Wilkins and R. L. Melen, *Coord. Chem. Rev.*, 2016, **324**, 123–139.
55 M. R. Crimmin, and I. J. Casely and M. S. Hill, *J. Am. Chem. Soc.*, 2005, **127**, 2042–2043.
56 F. Hild and S. Dagorne, *Organometallics*, 2012, **31**, 1189–1194.
57 J. Koller and R. G. Bergman, *Chem. Commun.*, 2010, **46**, 4577–4579.
58 C. C. Chong and R. Kinjo, *ACS Catal.*, 2015, **5**, 3238–3259.
59 M. Arrowsmith, T. J. Hadlington, M. S. Hill and G. Kociok-Köhn, *Chem. Commun.*, 2012, **48**, 4567–4569.
60 T. J. Hadlington, M. Hermann, G. Frenking and C. Jones, *J. Am. Chem. Soc.*, 2014, **136**, 3028–3031.
61 C. C. Chong, H. Hirao and R. Kinjo, *Angew. Chem. Int. Ed.*, 2015, **54**, 190–194.
62 R. L. Melen, *Chem. Soc. Rev.*, 2016, 45, 775–788.
63 Z. Yang, M. Zhong, X. Ma, K. Nijesh, S. De, P. Parameswaran and H. W. Roesky, *J. Am. Chem. Soc.*, 2016, **138**, 2548–2551.
64 G. C. Welch, R. R. San Juan, J. D. Masuda and D. W. Stephan, *Science*, 2006, **314**, 1124–1126.
65 P. Spies, G. Erker, G. Kehr, K. Bergander, R. Fröhlich, S. Grimme and D. W. Stephan,

Chem. Commun., 2007, **0**, 5072–5074.
66 G. C. W. and and D. W. Stephan, *J. Am. Chem. Soc.*, 2007, **129**, 1880–1881.
67 D. W. Stephan, *Dalton. Trans.*, 2009, **0**, 3129–3136.
68 A. L. Travis, S. C. Binding, H. Zaher, T. A. Q. Arnold, J. C. Buffet and D. O'Hare, *Dalton. Trans.*, 2013, **42**, 2431–2437.
69 Aluminium - Element information, properties and uses | Periodic Table, http://www.rsc.org/periodic-table/element/13/aluminium, (accessed 8 September 2021).
70 P. Bag, C. Weetman and S. Inoue, *Angew. Chem. Int. Ed.*, 2018, **57**, 14394–14413.
71 H. Pines and W. O. Haag, *J. Am. Chem. Soc.*, 2002, **82**, 2471–2483.
72 D. A. Atwood and B. C. Yearwood, *J. Organomet. Chem.*, 2000, **600**, 186–197.
73 K. Ziegler, *Angew. Chem. Int. Ed.*, 1952, **64**, 323–329.
74 S. S. Karpiniec, D. S. McGuinness, M. G. Gardiner, B. F. Yates and J. Patel, *Organometallics*, 2011, **30**, 1569–1576.
75 R. L. Shriner and F. W. Neumann, *Chem. Rev.*, 2002, **35**, 351–425.
76 J. Barker and M. Kilner, *Coord. Chem. Rev.*, 1994, **133**, 219–300.
77 R. J. Schwamm and M. P. Coles, *Organometallics*, 2013, **32**, 5277–5280.
78 M. Bayram, D. Bläser, C. Wölper and S. Schulz, *Organometallics*, 2014, **33**, 2080–2087.
79 T. Elkin, M. Botoshansky, R. M. Waymouth and M. S. Eisen, *Organometallics*, 2014, **33**, 840–843.
80 T. Chlupatý and A. Růžička, *Coord. Chem. Rev.*, 2016, 314, 103–113.
81 D. M. Grove, G. van Koten, H. J. C. Ubbels, K. Vrieze, L. C. Niemann and C. H. Stam, *J. Chem. Soc. Dalton. Trans.*, 1986, 717–724.
82 J. A. R. Schmidt and J. Arnold, *J. Chem. Soc. Dalton. Trans.*, 2002, 2890–2899.
83 M. P. Coles, D. C. Swenson, R. F. Jordan and J. V. G. Young, *Organometallics*, 1997, **16**, 5183–5194.
84 K. B. Aubrecht, and M. A. Hillmyer and W. B. Tolman, *Macromolecules*, 2002, **35**, 644–650.
85 D. Doyle, Y. K. Gunko, P. B. Hitchcock and M. F. Lappert, *J. Chem. Soc. Dalton. Trans.*, 2000, 4093–4097.
86 H. Hu and C. Cui, *Organometallics*, 2012, **31**, 1208–1211.
87 K. Kincaid, C. P. Gerlach, G. R. Giesbrecht, J. R. Hagadorn, G. D. Whitener, A. Shafir and J. Arnold, *Organometallics*, 1999, **18**, 5360–5366.
88 V. Y. Radkov, G. G. Skvortsov, G. K. Fukin, K. A. Lyssenko, M. Y. Antipin and A. A. Trifonov, *Russ. Chem. Bull.*, 2011 **60**, 803–808.
89 R. Lechler, H. D. Hausen and U. Weidlein, *J. Organomet. Chem.*, 1989, **359**, 1–12.
90 D. Kottmair-Maieron, R. Lechler and J. Weidlein, *Z. Anorg. Allg. Chem.*, 1991, **593**, 111–123.
91 G. Talarico and P H. M. Budzelaar, *Organometallics*, 2000, **19**, 5691–5695.
92 B. Clare, N. Sarker, R. Shoemaker and J. R. Hagadorn, *Inorg. Chem.*, 2004, **43**, 1159–1166.
93 Y. Lei, F. Chen, Y. Luo, P. Xu, Y. Wang and Y. Zhang, *Inorganica Chim. Acta*, 2011, **368**, 179–186.
94 F. Qian, K. Liu and H. Ma, *Dalton. Trans.*, 2010, **39**, 8071–8083.
95 A. Rösch, F. Seifert, V. Vass, H. Görls and R. Kretschmer, *New J. Chem.*, 2021, **45**, 972–981.
96 C. Jones, P. C. Junk, M. Kloth, K. M. Proctor and A. Stasch, *Polyhedron*, 2006, **25**, 1592–1600.
97 S. J. Bonyhady, D. Collis, G. Frenking, N. Holzmann, C. Jones and A. Stasch, *Nat.*

Chem., 2010, **2**, 865–869.
98 T. Peddarao, A. Baishya, S. K. Hota and S. Nembenna, *J. Chem. Sci.* 2018, **130**, 1-7.
99 D. O. Meléndez, J. A. Castro-Osma, A. Lara-Sánchez, R. S. Rojas and A. Otero, *J. Polym. Sci. Part A*, 2017, **55**, 2397–2407.
100 D. O. Meléndez, A. Lara-Sánchez, J. Martínez, X. Wu, A. Otero, J. A. Castro-Osma, M. North and R. S. Rojas, *ChemCatChem*, 2018, **10**, 2271–2277.
101 A. K. Maity, S. Fortier, L. Griego and A. J. Metta-Magaña, *Inorg. Chem.*, 2014, **53**, 8155–8164.
102 A. K. Maity, J. Murillo, A. J. Metta-Magaña, B. Pinter and S. Fortier, *J. Am. Chem. Soc.*, 2017, **139**, 15691–15700.
103 C. N. De Bruin-Dickason, T. Sutcliffe, C. Alvarez Lamsfus, G. B. Deacon, L. Maron and C. Jones, *Chem. Commun.*, 2018, **54**, 786–789.
104 K. F. Kalz, A. Brinkmeier, S. Dechert, R. A. Mata and F. Meyer, *J. Am. Chem. Soc.*, 2014, **136**, 16626–16634.
105 R. T. Boeré, V. Klassen and G. Wolmershäuser, *J. Chem. Soc. Dalton. Trans.*, 1998, **24**, 4147–4154.
106 M. L. Cole, C. Jones, P. C. Junk, M. Kloth and A. Stasch, *Chem. Eur. J.*, 2005, **11**, 4482–4491.
107 M. L. Cole, A. J. Davies, C. Jones, P. C. Junk, A. I. McKay and A. Stasch, *Z. Anorg. Allg. Chem.*, 2015, **641**, 2233–2244.
108 A. L. Brazeau, Z. Wang, C. N. Rowley and S. T. Barry, *Inorg. Chem.*, 2006, **45**, 2276–2281.
109 M. L. Cole, A. I. McKay and N. S. Ping, *Polyhedron*, 2019, **170**, 424–430.
110 R. Duchateau, A. Meetsma and J. H. Teuben, *Chem. Commun.*, 1996, 223–224.
111 M. Zhong, Y. Liu, S. Kundu, N. Graw, J. Li, Z. Yang, R. Herbst-Irmer, D. Stalke and H. W. Roesky, *Inorg. Chem.*, 2019, **58**, 10625–10628.
112 H. Nagashima, H. Kondo, T. Hayashida, Y. Yamaguchi, M. Gondo, S. Masuda, K. Miyazaki, K. Matsubara and K. Kirchner, *Coord. Chem. Rev.*, 2003, **245**, 177–190.
113 H. A. Jenkins, D. Abeysekera, D. A. Dickie and J. A. C. Clyburne, *J. Chem. Soc. Dalton. Trans.*, 2002, **20**, 3919–3922.
114 F. Qian, K. Liu and H. Ma, *Dalton. Trans.*, 2010, **39**, 8071–8083.
115 T. D. W. Claridge, *High Resolution Techniques in Organic Chemistry*, Elsevier, Amsterdam, 2009.
116 J. A. R. Schmidt and J. Arnold, *Organometallics*, 2002, **21**, 2306–2313.
117 J. Koller and R. G. Bergman, *Organometallics*, 2010, **29**, 5946–5952.
118 L. Kong, J. Morvan, D. Pichon, M. Jean, M. Albalat, T. Vives, S. Colombel-Rouen, M. Giorgi, V. Dorcet, T. Roisnel, C. Crévisy, D. Nuel, P. Nava, S. Humbel, N. Vanthuyne, M. Mauduit and H. Clavier, *J. Am. Chem. Soc.*, 2020, **142**, 93–98.
119 H. C. BROWN, presented in part at *25th International Congress of Pure and Applied Chemistry*, Jerusalem, 1977.
120 A. J. J. Lennox and G. C. Lloyd-Jones, *Chem. Soc. Rev.*, 2013, **43**, 412–443.
121 N. Miyaura and Y. Yamamoto, in *Comprehensive Organometallic Chemistry III*, eds. P. M. Mingos and H. R. Crabtree, Elsevier, Amsterdam, 3rd edn., 2007, ch 9, pp. 145–244.
122 Z. Yang, M. Zhong, X. Ma, S. De, C. Anusha, P. Parameswaran and H. W. Roesky, *Angew. Chem. Int. Ed.*, 2015, **54**, 10225–10229.
123 N. Sarkar, S. Bera and S. Nembenna, *J. Org. Chem.*, 2020, **85**, 4999–5009.
124 D. Franz, L. Sirtl, A. Pöthig and S. Inoue, *Z. Anorg. Allg. Chem.*, 2016, **642**, 1245–1250.
125 A. Harinath, J. Bhattacharjee and T. K. Panda, *Adv. Synth. Catal.*, 2019, **361**, 850–857.

126 W. Liu, Y. Ding, D. Jin, Q. Shen, B. Yan, X. Ma and Z. Yang, *Green Chem.*, 2019, **21**, 3812–3815.
127 V. B. Saptal, R. Wang and S. Park, *RSC Adv.*, 2020, **10**, 43539–43565.
128 Y. Ding, X. Liu, X. Ma, Y. Liu, M. Zhong, W. Li, Z. Yang and Y. Yang, *J. Organomet. Chem.*, 2018, **868**, 55–60.
129 W. Uhl, E. A. Hepp, J. Kösters, M. Layh, M. Rohling, A. Vinogradov, E. U. Würthwein and N. Ghavtadze, *Eur. J. Inorg. Chem.*, 2009, 3307–3316.
130 A. Bismuto, S. P. Thomas and M. J. Cowley, *Angew. Chem. Int. Ed.*, 2016, **55**, 15356–15359.
131 A. Bismuto, M. J. Cowley and S. P. Thomas, *ACS Catal.*, 2018, **8**, 2001–2005.
132 V. A. Pollard, S. A. Orr, Ross McLellan, A. R. Kennedy, E. Hevia and R. E. Mulvey, *Chem. Commun.*, 2018, **54**, 1233–1236.
133 R. L. Falconer, G. S. Nichol and M. J. Cowley, *Inorg. Chem.*, 2019, **58**, 11439–11448.
134 A. Harinath, I. Banerjee, J. Bhattacharjee and T. K. Panda, *New J. Chem.*, 2019, **43**, 10531–10536.
135 N. Sarkar, S. Bera and S. Nembenna, *J. Org. Chem.*, 2020, **85**, 4999–5009.
136 T. Peddarao, N. Sarkar and S. Nembenna, *Inorg. Chem.*, 2020, **59**, 4693–4702.
137 C. Cui, S. Köpke, R. Herbst-Irmer, H. W. Roesky, M. Noltemeyer, H. G. Schmidt and B. Wrackmeyer, *J. Am. Chem. Soc.*, 2001, **123**, 9091–9098.
138 C. M. Zinser, F. Nahra, L. Falivene, M. Brill, D. B. Cordes, A. M. Z. Slawin, L. Cavallo, C. S. J. Cazin and S. P. Nolan, *Chem. Commun.*, 2019, **55**, 6799–6802.
139 A. D. Bage, T. A. Hunt and S. P. Thomas, *Org. Lett.*, 2020, **22**, 4107–4112.
140 A. Bismuto, S. P. Thomas and M. J. Cowley, *Angew. Chem. Int. Ed.*, 2016, **55**, 15356–15359.
141 Z. Huang, S. Wang, X. Zhu, Q. Yuan, Y. Wei, S. Zhou and X. Mu, *Inorg. Chem.*, 2018, **57**, 15069–15078.
142 D. Männig and H. Nöth, *Angew. Chem. Int. Ed.*, 1985, **24**, 878–879.
143 K. Burgess and M. Jaspars, *Tetrahedron Lett.*, 1993, **34**, 6813–6816.
144 A. D. Bage, K. Nicholson, T. Langer and S. P. Thomas, *ACS Catal.*, 2020, **10**, 13479–13486.
145 Q. Yin, S. Kemper, H. F. T. Klare and M. Oestreich, *Chem. Eur. J.*, 2016, **22**, 13840–13844.
146 M. Magre, B. Maity, A. Falconnet, L. Cavallo and M. Rueping, *Angew. Chem. Int. Ed.*, 2019, **58**, 7025–7029.
147 Y. M. Variani, C. W. Lopes, B. P. Nicola, D. M. Meira, S. B. C. Pergher and K. Bernardo-Gusmão, *New J. Chem.*, 2020, **44**, 15100–15108.
148 J. Li, X. Ma, Y. Peng, X. He, Z. Du and Z. Yang, *J. Mol. Liq.*, 2021, **337**, 116423.
149 C. Cui, H. W. Roesky, H. Hao, H. G. Schmidt and M. Noltemeyer, *Angew. Chem. Int. Ed.*, 2000, **39**, 1815–1817.
150 K. W. Klinkhammer, W. Uhl, J. Wagner and W. Hiller, *Angew. Chem. Int. Ed.*, 1991, **30**, 179–180.
151 C. Dohmeier, C. Robl, M. Tacke and H. Schnöckel, *Angew. Chem. Int. Ed.*, 1991, **30**, 564–565.
152 S. Nagendran and H. W. Roesky, *Organometallics*, 2008, **27**, 457–492.
153 H. W. Roesky, *Inorg. Chem.*, 2004, **43**, 7284–7293.
154 R. Y. Kong and M. R. Crimmin, *Chem. Commun.*, 2019, **9095**, 15–18.
155 A. Hofmann, T. Tröster, T. Kupfer and H. Braunschweig, *Chem. Sci.*, 2019, **10**, 3421–3428.
156 K. Hobson, C. J. Carmalt and C. Bakewell, *Chem. Sci.*, 2020, **11**, 6942–6956.
157 S. J. Bonyhady, D. Collis, N. Holzmann, A. J. Edwards, R. O. Piltz, G. Frenking, A.

Stasch and C. Jones, *Nat. Commun.* 2018, **9**, 1–6.
158 S. K. Mellerup, Y. Cui, F. Fantuzzi, P. Schmid, J. T. Goettel, G. Bélanger-Chabot, M. Arrowsmith, I. Krummenacher, Q. Ye, V. Engel, B. Engels and H. Braunschweig, *J. Am. Chem. Soc.*, 2019, **141**, 16954–16960.
159 H. B. Wedler, P. Wendelboe and P. P. Power, *Organometallics*, 2018, **37**, 2929–2936.
160 Z. Zhu, R. C. Fischer, B. D. Ellis, E. Rivard, W. A. Merrill, M. M. Olmstead, P. P. Power, J. D. Guo, S. Nagase and L. Pu, *Chem. Eur. J.*, 2009, **15**, 5263–5272.
161 S. T. H. and and P. P. Power*, *J. Am. Chem. Soc.*, 1998, **120**, 2202–2203.
162 M. Niemeyer and P. P. Power, *Angew. Chem. Int. Ed*, 1998, **37**, 1277-1279.
163 C. A. Caputo, J. Koivistoinen, J. Moilanen, J. N. Boynton, H. M. Tuononen and P. P. Power, *J. Am. Chem. Soc.*, 2013, **135**, 1952–1960.
164 J. Hicks, P. Vasko, J. M. Goicoechea and S. Aldridge, *Nature*, 2018, **557**, 92–95.
165 R. J. Schwamm, M. D. Anker, M. Lein and M. P. Coles, *Angew. Chem. Int. Ed.*, 2019, **58**, 1489–1493.
166 R. J. Schwamm, M. P. Coles, M. S. Hill, M. F. Mahon, C. L. McMullin, N. A. Rajabi and A. S. S. Wilson, *Angew. Chem. Int. Ed.*, 2020, **59**, 3928–3932.
167 S. Kurumada, S. Takamori and M. Yamashita, *Nat. Chem.*, 2020, **12**, 36–39.
168 S. Grams, J. Eyselein, J. Langer, C. Färber and S. Harder, *Angew. Chem. Int. Ed.*, 2020, **59**, 15982–15986.
169 K. Koshino and R. Kinjo, *J. Am. Chem. Soc.*, 2020, **142**, 9057–9062.
170 J. Hicks, P. Vasko, J. M. Goicoechea and S. Aldridge, *Angew. Chem. Int. Ed.*, 2021, **60**, 1702–1713.
171 R. J. Schwamm, M. P. Coles, M. S. Hill, M. F. Mahon, C. L. McMullin, N. A. Rajabi and A. S. S. Wilson, *Angew. Chem. Int. Ed.*, 2020, **59**, 3928–3932.
172 R. J. Schwamm, M. D. Anker, M. Lein and M. P. Coles, *Angew. Chem. Int. Ed.*, 2019, **58**, 1489–1493.
173 T. Agou, K. Nagata, H. Sakai, Y. Furukawa and N. Tokitoh, *Organometallics*, 2012, **31**, 3806–3809.
174 W. Uhl, *Angew. Chem. Int. Ed.*, 1993, **32**, 1386–1397.
175 R. J. Wehmschulte, K. Ruhlandt-Senge, M. M. Olmstead, H. Hope, B. E. Sturgeon and P. P. Power, *Inorg. Chem.*, 2002, **32**, 2983–2984.
176 N. Wiberg, K. Amelunxen, T. Blank, H. Nöth and J. Knizek, *Organometallics*, 1998, **17**, 5431–5433.
177 R. J. Wright, and A. D. Phillips and P. P. Power, *J. Am. Chem. Soc.*, 2003, **125**, 10784–10785.
178 A. Hofmann, A. Lamprecht, O. F. González-Belman, R. D. Dewhurst, J. O. C. Jiménez-Halla, S. Kachel and H. Braunschweig, *Chem. Commun.*, 2018, **54**, 1639–1642.
179 S. G. Minasian and J. Arnold, *Chem. Commun.*, 2008, 4043–4045.
180 B. Li, S. Kundu, H. Zhu, H. Keil, R. Herbst-Irmer, D. Stalke, G. Frenking, D. M. Andrada and H. W. Roesky, *Chem. Commun.*, 2017, **53**, 2543–2546.
181 R. L. Falconer, K. M. Byrne, G. S. Nichol, T. Krämer and M. J. Cowley, *Angew. Chem. Int. Ed.*, 2021, **60**, 24702–24708.
182 J. Moilanen, P. P. Power and H. M. Tuononen, *Inorg. Chem.*, 2010, **49**, 10992–11000.
183 P. Bag, A. Porzelt, P. J. Altmann and S. Inoue, *J. Am. Chem. Soc.*, 2017, **139**, 14384–14387.
184 R. L. Falconer, K. M. Byrne, G. S. Nichol, T. Krämer and M. J. Cowley, *Angew. Chem. Int. Ed.*, 2021, **60**, 24702-24708.
185 Standard Bond Lengths and Bond Angles, http://hydra.vcp.monash.edu.au/modules/mod2/bondlen.html, (accessed 13 September

2021).
186 J. Feldman, S. J. McLain, A. Parthasarathy, W. J. Marshall, J. C. Calabrese and S. D. Arthur, *Organometallics*, 1997, **16**, 1514–1516.
187 J. Riedhammer, J. R. Aguilar-Calderón, M. Miehlich, D. P. Halter, D. Munz, F. W. Heinemann, S. Fortier, K. Meyer and D. J. Mindiola, *Inorg. Chem.*, 2020, **59**, 2443–2449.

Chapter 7:

Appendices

Crystallographic Data

All crystals were ran on a Agilent Oxford Diffraction SuperNova equipped with a microfocus Cu Kα X-ray source and an Atlas CCD detector. Full spheres of data were collected to 0.84 Å resolution with each 1° scan frame in ω collected twice. Total collection time varied depending on size and quality of crystal, and sample temperature. The Cryojet5® used for these measurements is the original prototype device developed by Oxford Instruments and the Pt-resistance sensor is located in the copper-block heat exchanger and not in the nozzle of the instrument close to the sample (in contrast to the CryojetHT® used in the PXRD experiments). Thus the temperatures quoted in these SXD experiments should be treated as nominal (despite stability to much better than 0.1 °C). Using Olex2,[1] the structure was solved with the ShelXT[2] structure solution program using Intrinsic Phasing and refined with the ShelXL[3] refinement package using Least Squares minimisation.

Crystal Data for 2.9

$C_{130}H_{130}Al_2N_4$, M =1802.33, orthorhombic, *Aea2*, a = 27.8353(8) Å, b = 20.6582(6) Å, c = 18.2376(5) Å, V = 10487.1(5) Å^3, Z = 4, T = 151(1) K, μ(CuKα) = 0.645 mm^{-1}, r_{calc}g/cm^3 = 1.142, 38212 reflections measured (7.204° ≤ 2Θ ≤ 145.436°), 10133 unique (R_{int} = 0.0188, R_{sigma} = 0.0150) which were used in all calculations. The final R_1 was 0.0287 (I > 2σ(I)) and wR_2 was 0.0750 (all data), 627 parameters. CCDC: 2054527.

Crystal Data for 2.10

$C_{74}H_{63}AlN_2$, M =1007.24, triclinic, *P-1*, a = 11.7022(2) Å, b = 13.6375(3) Å, c = 19.3373(4) Å, α = 74.497(2)°, β = 78.438(2)°, γ = 76.750(2)°, V = 2862.54(11) Å^3, Z = 2, T = 158.5(9) K, μ(CuKα) = 0.647 mm^{-1}, r_{calc}g/cm^3 = 1.169, 51500 reflections measured (6.846° ≤ 2Θ ≤ 145.582°), 11136 unique (R_{int} = 0.0294, R_{sigma} = 0.0191) which were used in all calculations. The final R_1 was 0.0377 (I > 2σ(I)) and wR_2 was 0.1451 (all data), 913 parameters. CCDC: 2054529.

Crystal Data for 2.11

$C_{53}H_{56}AlN_3$, M =761.98, triclinic, P-1, a = 9.7344(2) Å, b = 12.4989(3) Å, c = 18.3934(4) Å, α = 80.575(2)°, β = 86.868(2)°, γ = 85.991(2)°, V = 2200.18(9) Å^3, Z = 2, T = 150.2(7) K, μ(CuKα) = 0.685 mm^{-1}, r_{calc}g/cm^3 = 1.150, 33455 reflections measured (7.184° ≤

2Θ ≤ 145.424°), 8526 unique (R_{int} = 0.0291, R_{sigma} = 0.0225) which were used in all calculations. The final R_1 was 0.0395 (I > 2σ(I)) and wR_2 was 0.1469 (all data), 727 parameters. CCDC: 2054528.

Crystal Data for 2.12

$C_{100}H_{94}Al_2N_4$ *M* =1405.75, monoclinic, *C2/c*, *a* = 22.8043(2) Å, *b* = 12.75660(10) Å, *c* = 32.3911(3) Å, *β* = 104.1670(10)°, *V* = 9136.16(14) Å^3, *Z* = 4, *T* = 150.00(10) K, μ(CuKα) = 0.621 mm^{-1}, $r_{calc}g/cm^3$ = 1.022, 70840 reflections measured (8.002° ≤ 2Θ ≤ 145.398°), 9021 unique (R_{int} = 0.0821, R_{sigma} = 0.0342) which were used in all calculations. The final R_1 was 0.0512 (I > 2σ(I)) and wR_2 was 0.1505 (all data), 507 parameters. CCDC: 2054525.

The structure of **2.12** was found to be disordered, with the mesityl group split over two positions which had both major (78.8%) and minor occupancy (21.2%). The thermal parameters of adjacent atoms in the major and minor components of the disordered fragment were then restrained to be similar. The atoms in the minor component were refined isotropically and the atoms in the major component were refined anisotropically. The asymmetric unit also contained a disordered molecule of hexane and one of benzene, which were modelled using a solvent mask (SQUEEZE).

Crystal Data for 2.13

$C_{100}H_{91}AlN_4$ (*M* =1375.74 g/mol): monoclinic *C2/c*, *a* = 22.7932(3) Å, *b* = 22.7393(3) Å, *c* = 17.2859(2) Å, *β* = 92.9790(10)°, *V* = 8947.2(2) Å^3, *Z* = 4, *T* = 149.97(10) K, μ(CuKα) = 0.535 mm^{-1}, r_{calc}g/cm^3 = 1.021, 17676 reflections measured (7.648° ≤ 2Θ ≤ 145.338°), 8611 unique (R_{int} = 0.0228, R_{sigma} = 0.0261) which were used in all calculations. The final R_1 was 0.0397 (I > 2σ(I)) and wR_2 was 0.1117 (all data), 481 parameters. CCDC: 2054524.

2.13 was found to crystallise in a *C2/c* space group. The asymmetric unit also contained two disordered molecules of hexane and one of benzene, which were modelled using a solvent mask (SQUEEZE).

Crystal Data for 2.14

$C_{61}H_{71}AlN_2$ (M =859.17 g/mol): triclinic P-1, *a* = 11.8634(2) Å, *b* = 15.3910(4) Å, *c* = 15.5263(4) Å, *α* = 102.162(2)°, *β* = 109.645(2)°, *γ* = 92.471(2)°, *V* = 2589.94(11) Å^3, *Z* = 2, T = 149.9(4) K, μ(CuKα) = 0.625 mm^{-1}, r_{calc} g/cm^3 = 1.102, 41510 reflections measured (7.496° ≤ 2Θ ≤ 147.048°), 10269 unique (R_{int} = 0.0285, R_{sigma} = 0.0212) which were used in all

calculations. The final R1 was 0.0513 (I > 2σ(I)) and wR2 was 0.1533 (all data), 587 parameters. CCDC: 2054526.

Crystal Data for 3.6

$C_{80}H_{73}AlN_2O_2$, M =1121.38, monoclinic, $P2_1/c$, a = 13.2305(2) Å, b = 22.8842(3) Å, c = 23.8160(3) Å, β = 103.2350(10) °, V = 7019.23(17) Å^3, Z = 4, T = 149.8(4) K, μ(CuKα) = 0.593 mm^{-1}, $r_{calc}g/cm^3$ = 1.061, 51376 reflections measured (7.626° ≤ 2Θ ≤ 145.446°), 13771 unique (R_{int} = 0.0375, R_{sigma} = 0.0287) which were used in all calculations. The final R_1 was 0.0565 (I > 2σ(I)) and wR_2 was 0.1644 (all data), 773 parameters. CCDC: 2054530.

The asymmetric unit also contained three disordered molecules of benzene, which were modelled using a solvent mask (SQUEEZE).

Crystal Data for 4.3

$C_{40}H_{41}I_3N_2$, M =1064.9, triclinic, P-1, a = 13.2502(3) Å, b = 14.1830(4) Å, c = 14.4330(3) Å, α = 87.447(2)°, β = 87.322(2)°, γ = 73.617(2) °, V = 2598.00(11) Å^3, Z = 3, T = 151(1) K, μ(CuKα) = 9.791 mm^{-1}, $r_{calc}g/cm^3$ = 1.361, 42178 reflections measured (6.958° ≤ 2Θ ≤ 145.89°), 10181 unique (R_{int} = 0.0465, R_{sigma} = 0.0313) which were used in all calculations. The final R_1 was 0.0405 (I > 2σ(I)) and wR_2 was 0.1147 (all data).

References

1. O. V. Dolomanov, L. J. Bourhis, R. J. Gildea, J. A. K. Howard and H. Puschmann, *J. Appl. Crystallogr.*, 2009, **42**, 339–341.
2. S. G. M., *Acta Cryst. A*, **64**, 112–122.
3. G. M. Sheldrick, *Acta Cryst*, 2015, **A71**, 3–8.

Chapter 2 Appendix

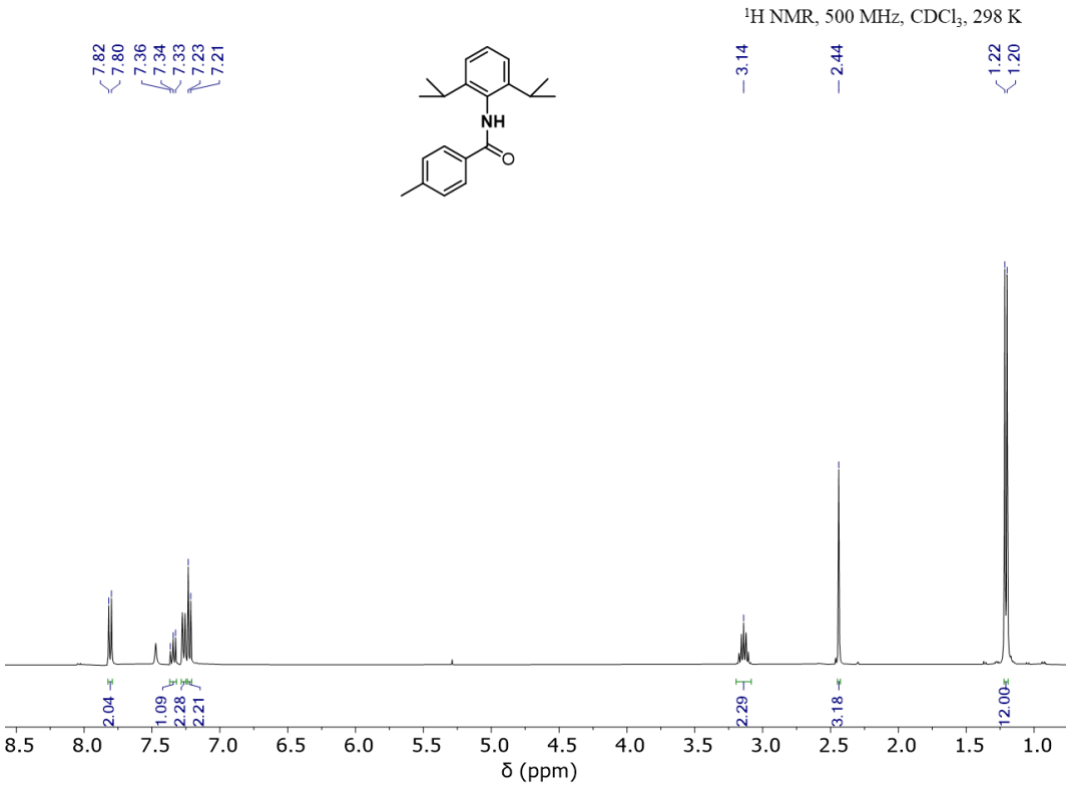

Figure A.1: ^{1}H NMR spectrum of **2.1**.

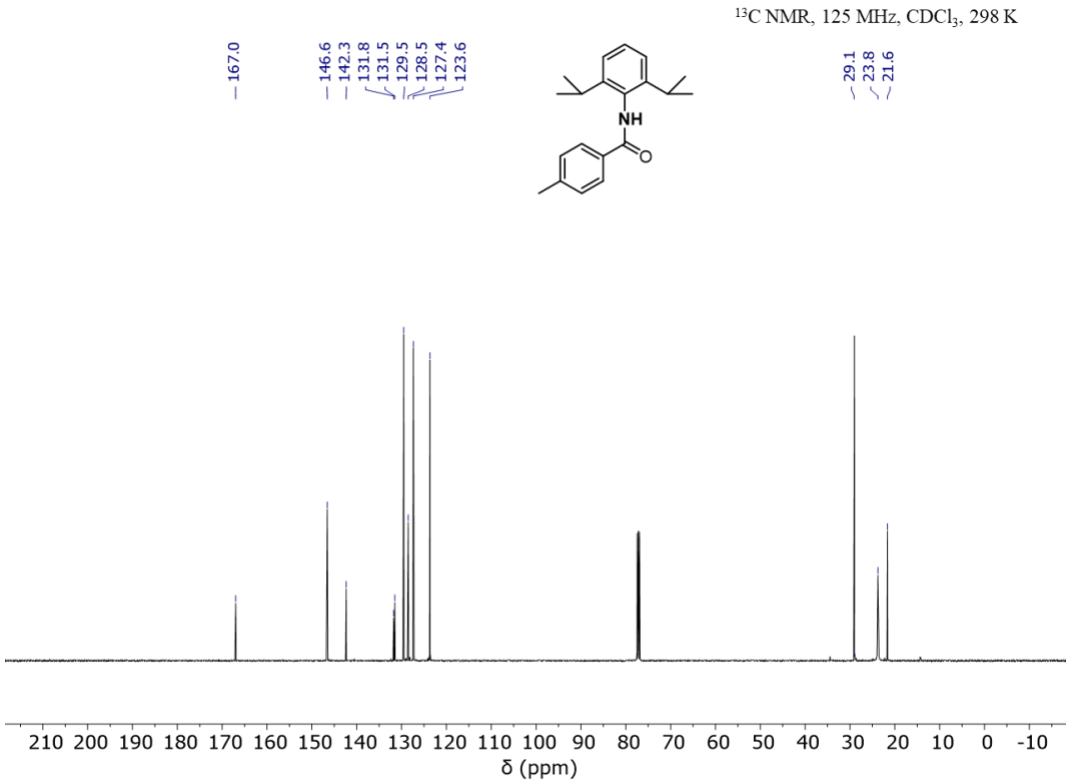

Figure A.2: ^{13}C NMR spectrum of **2.1**.

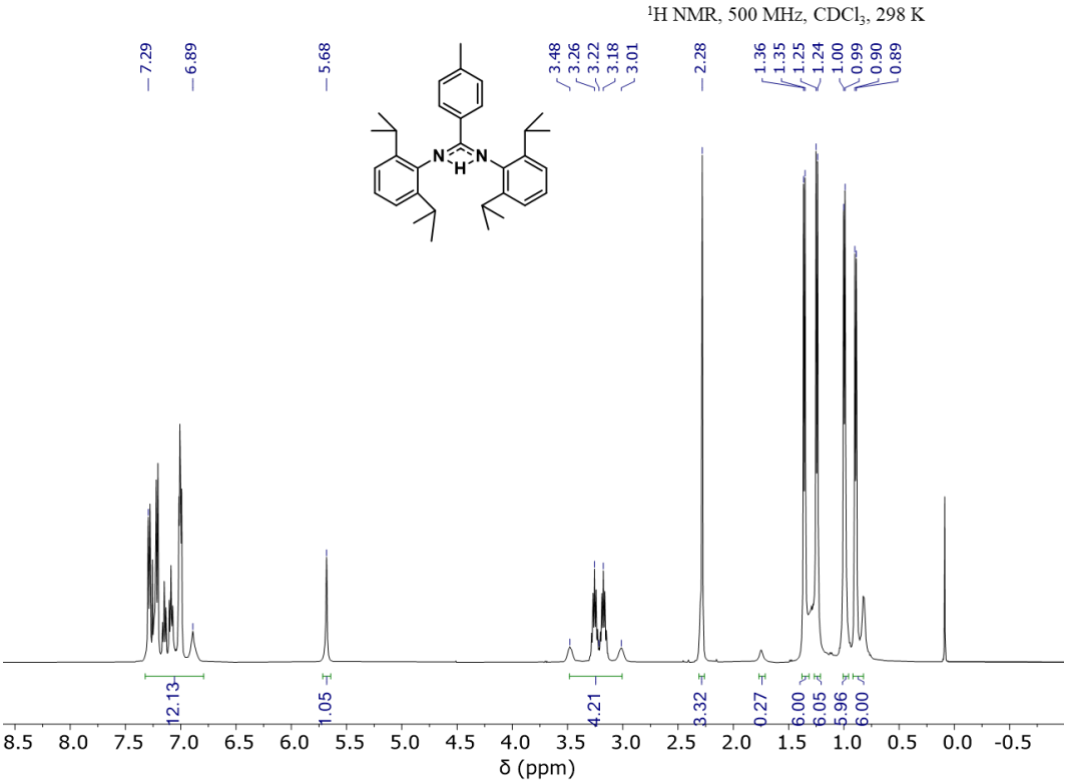

Figure A.3: ^{1}H NMR spectrum of **2.2**.

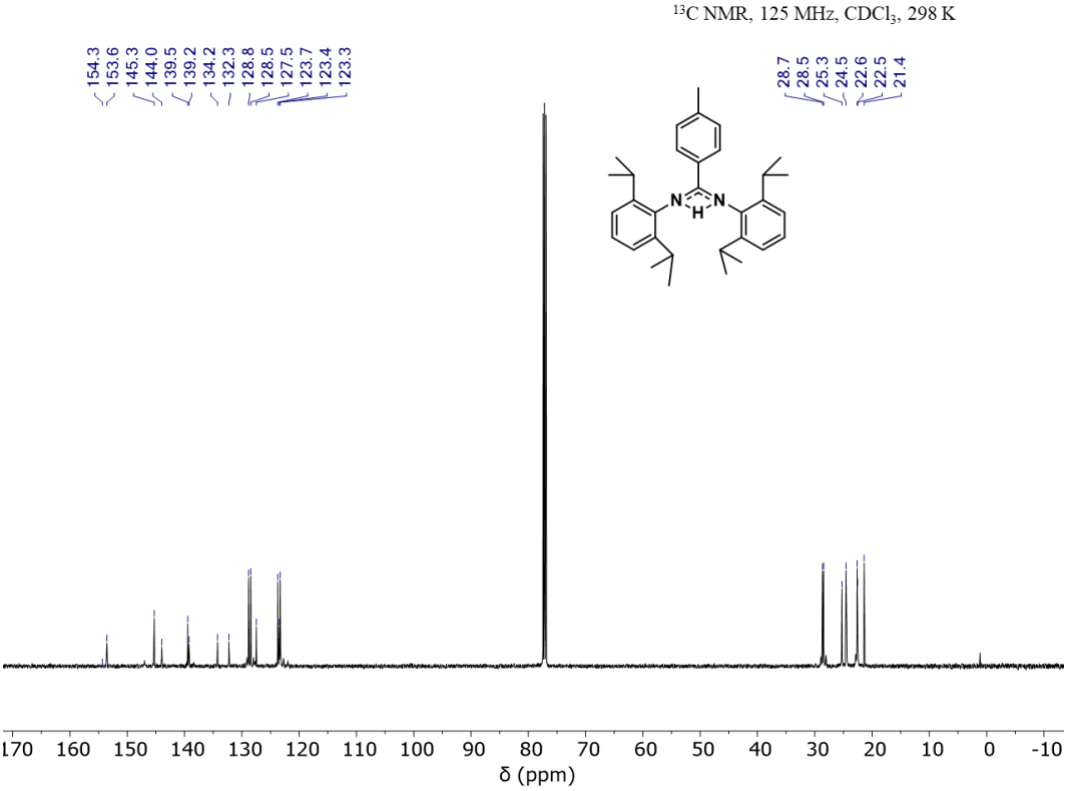

Figure A.4: ^{13}C NMR spectrum of **2.2**.

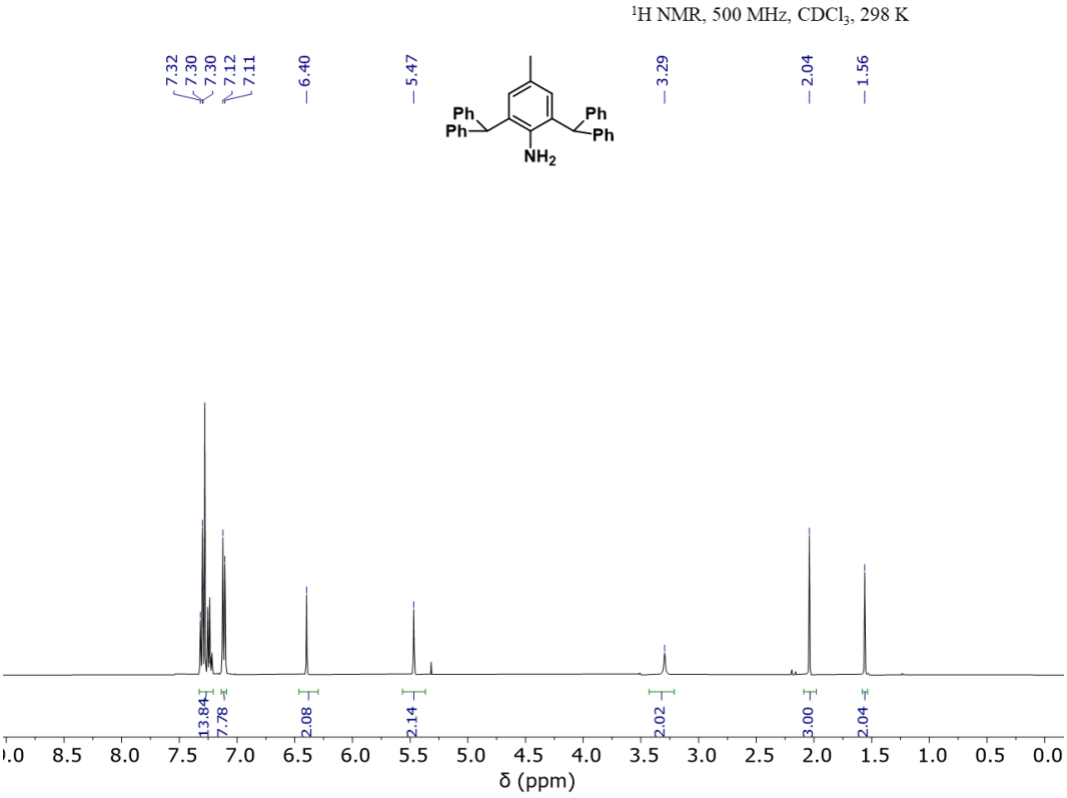

Figure A.5: ^{1}H NMR spectrum of **2.3**.

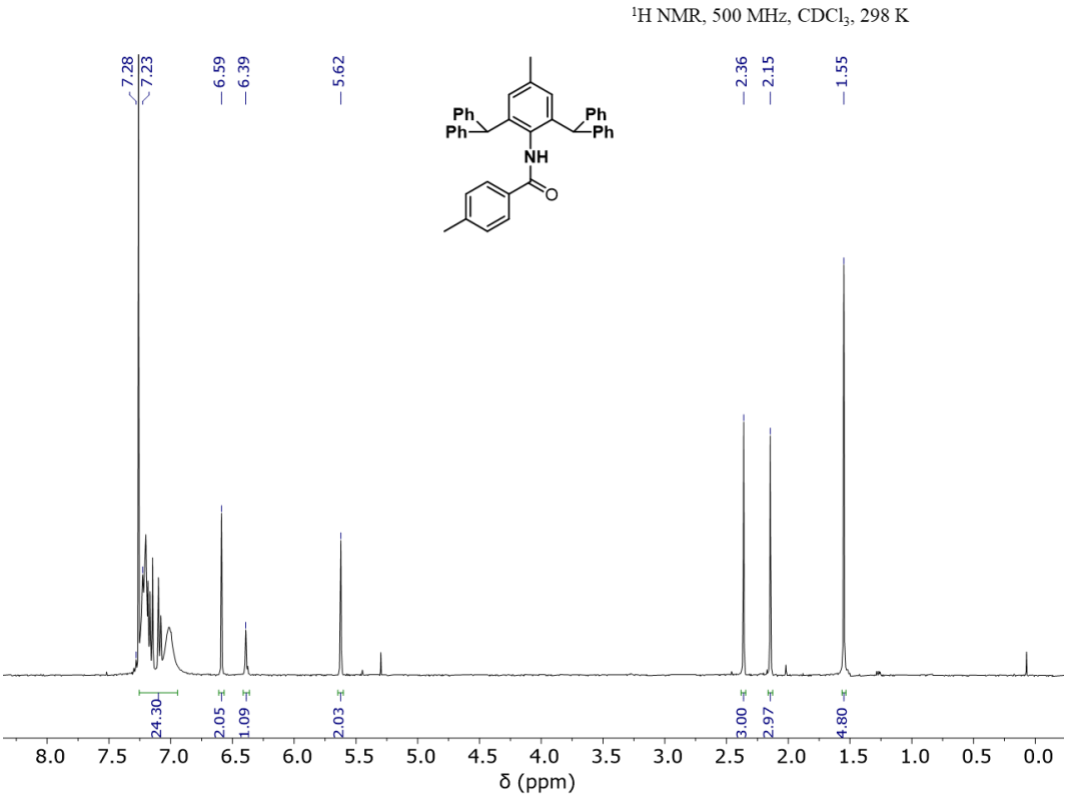

Figure A.6: ^{1}H NMR spectrum of **2.4**.

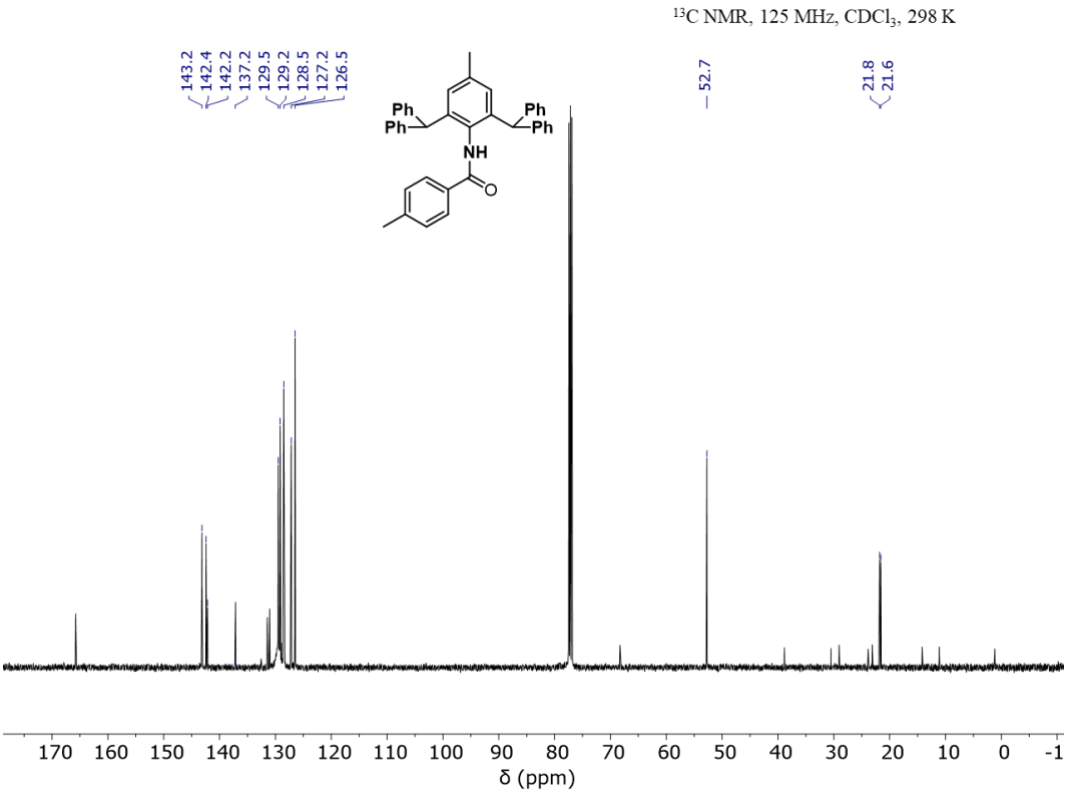

Figure A.7: ^{13}C NMR spectrum of **2.4**.

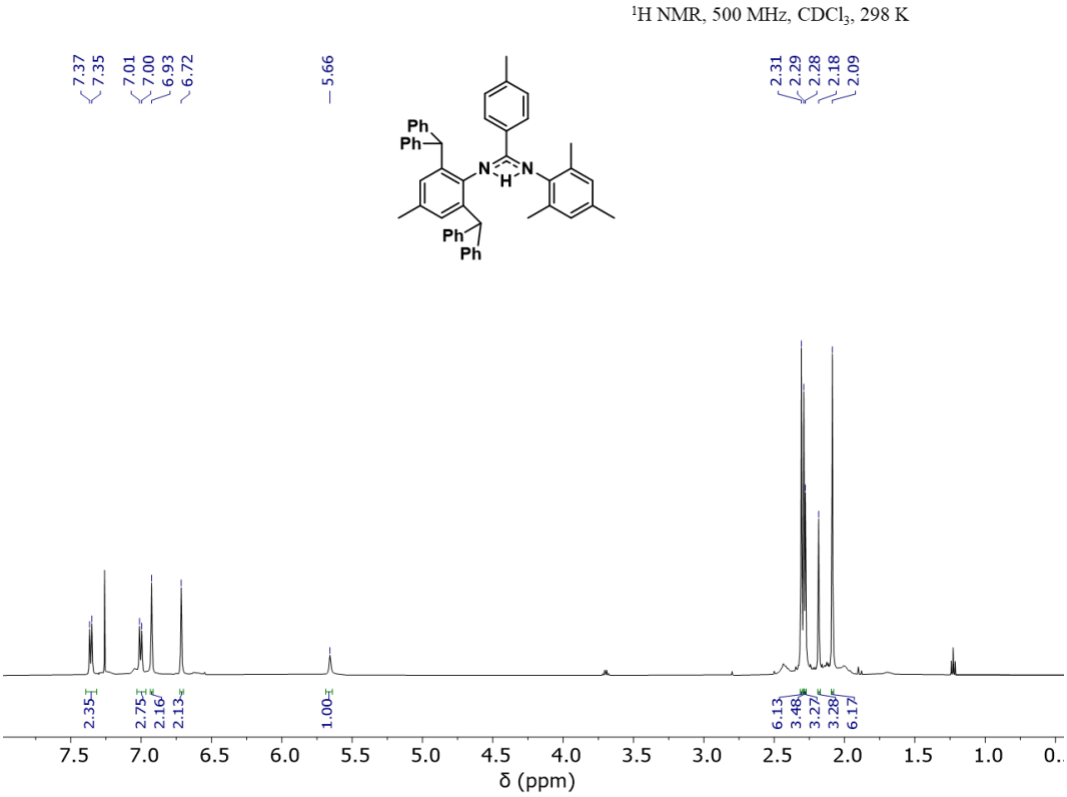

Figure A.8: ^{1}H NMR spectrum of **2.5**.

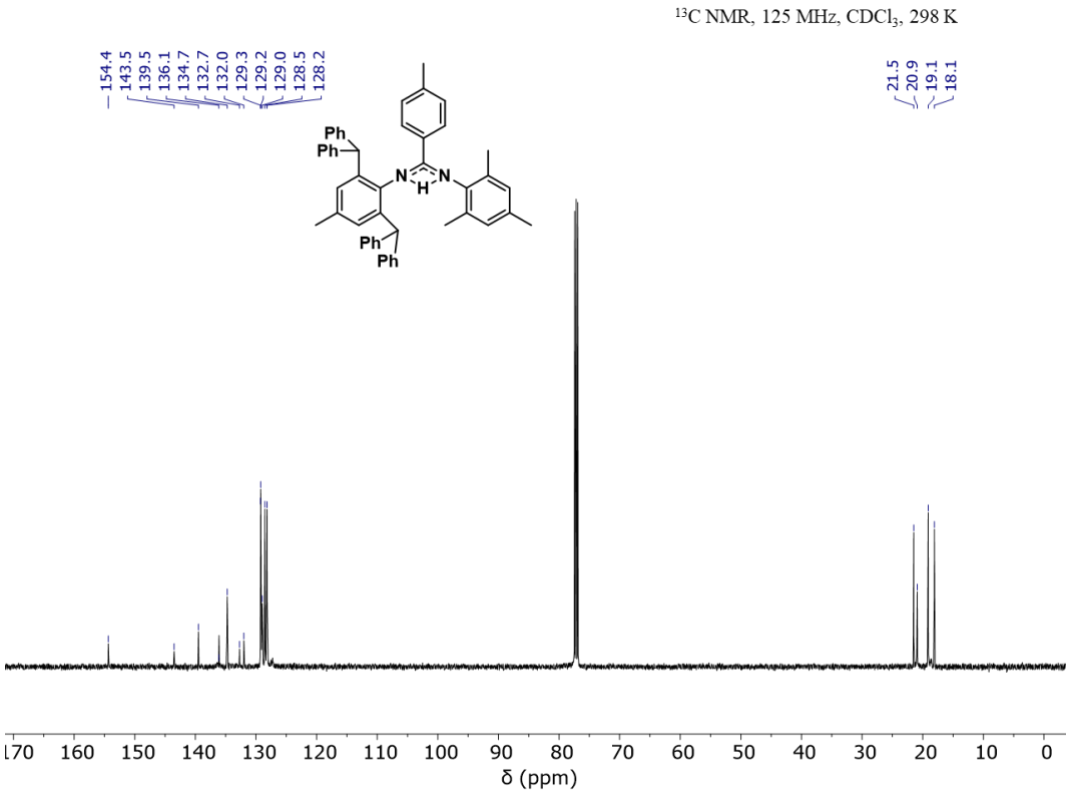

Figure A.9: ^{13}C NMR spectrum of **2.5**.

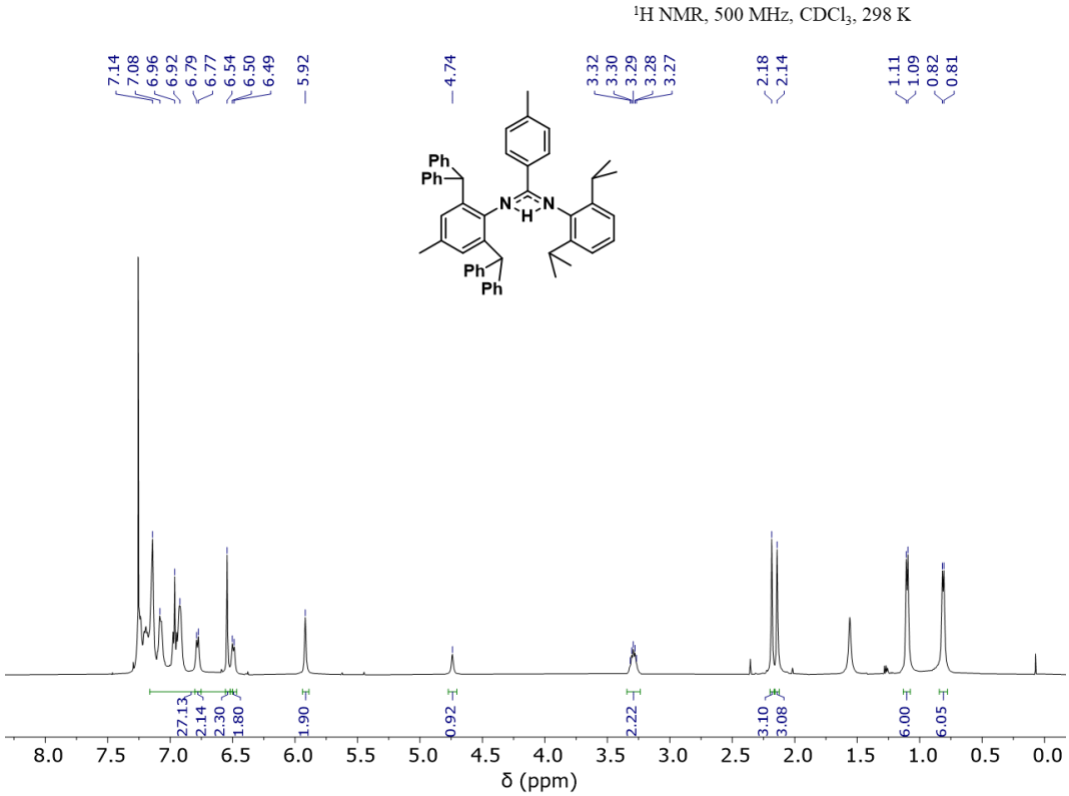

Figure A.10: ^{1}H NMR spectrum of **2.6**.

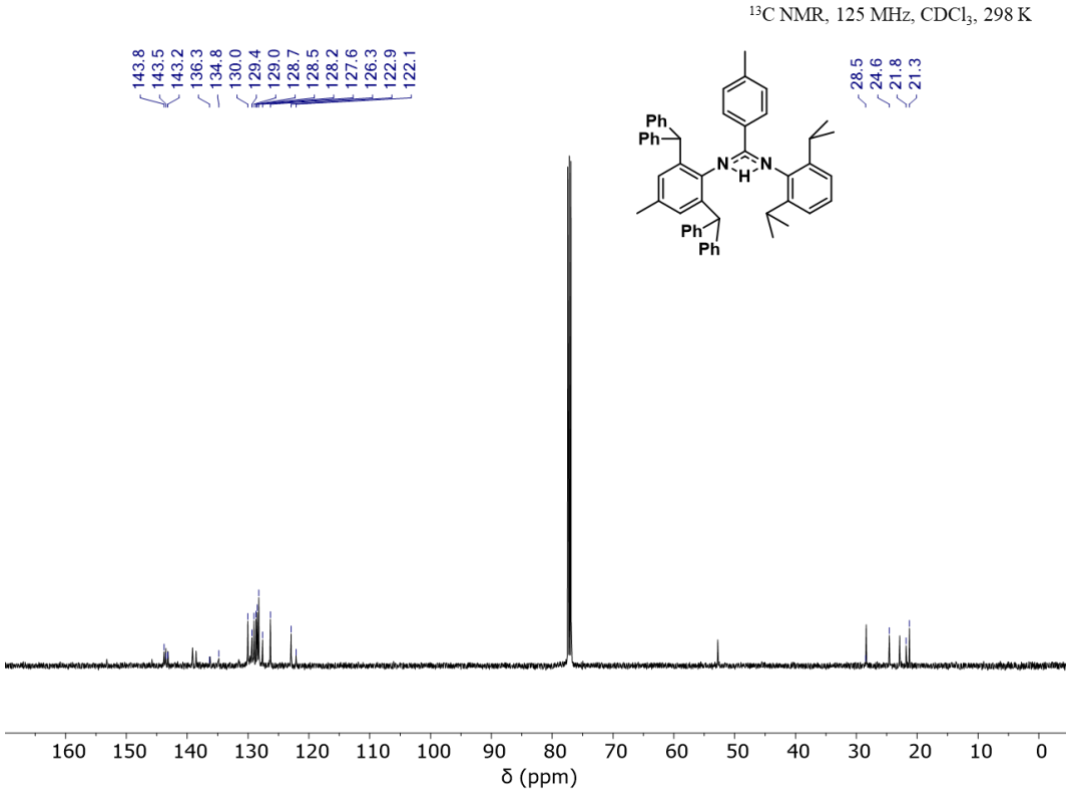

Figure A.11: ^{13}C NMR spectrum of **2.6**.

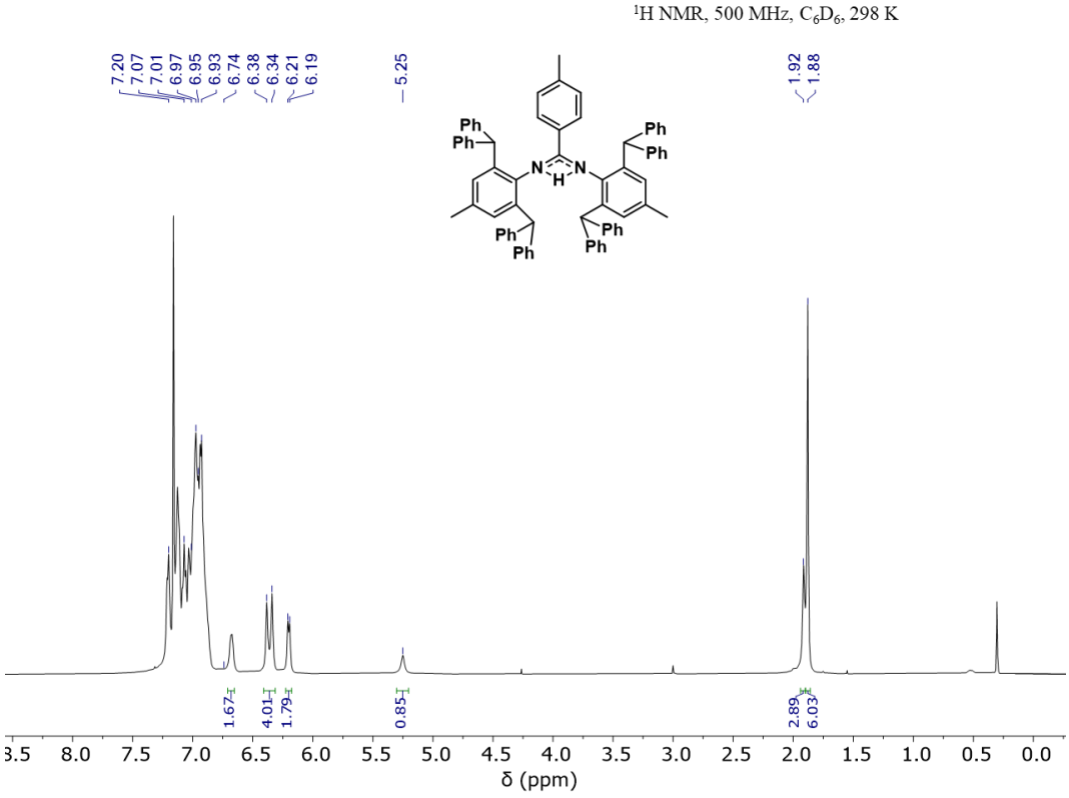

Figure A.12: ^{1}H NMR spectrum of **2.7**.

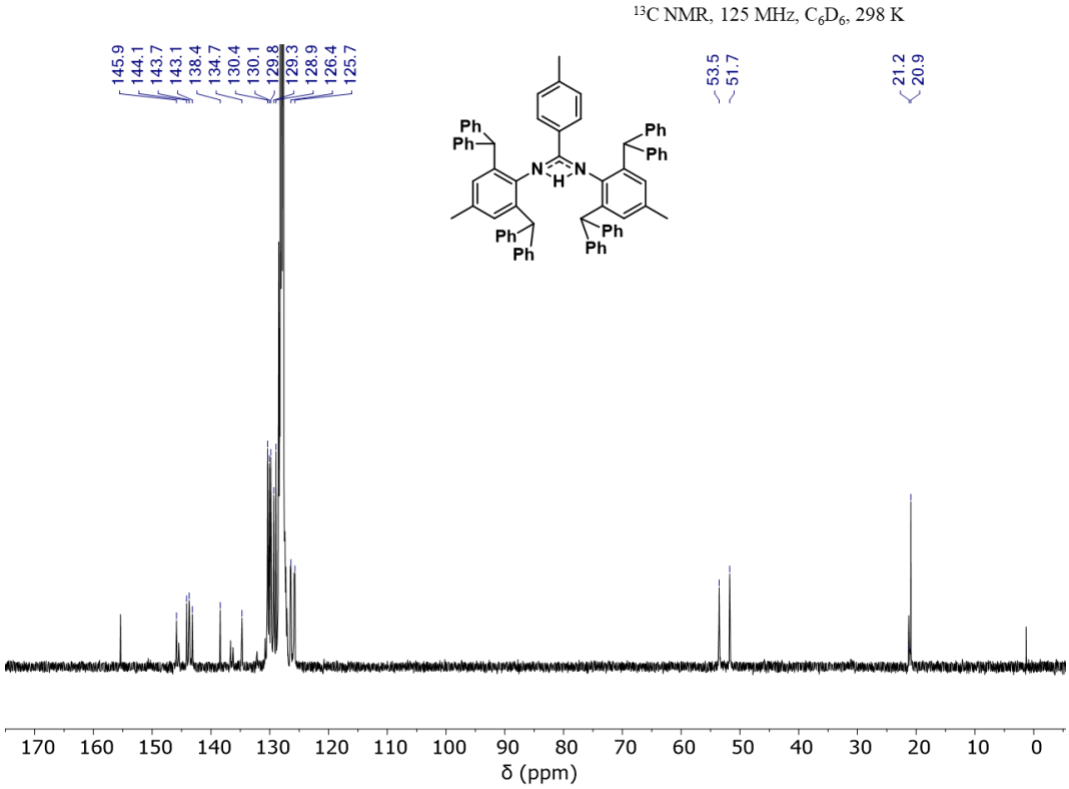

Figure A.13: ^{13}C NMR spectrum of **2.7**.

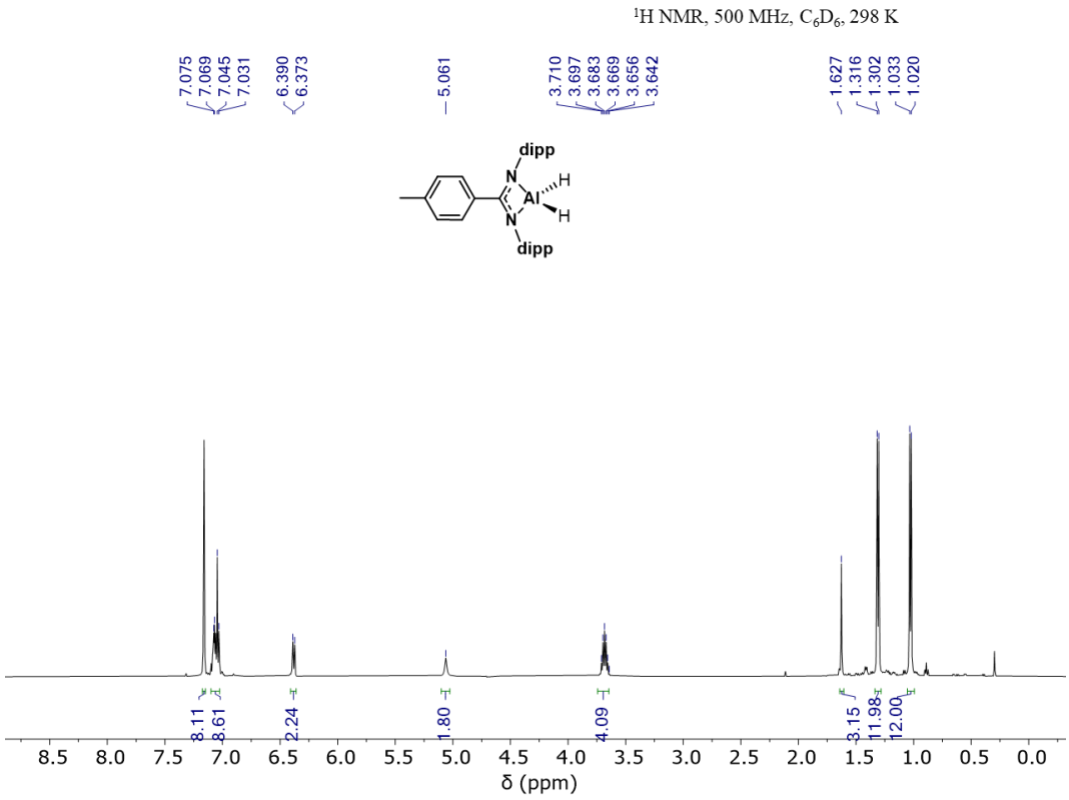

Figure A.14: ^{1}H NMR spectrum of **2.8**.

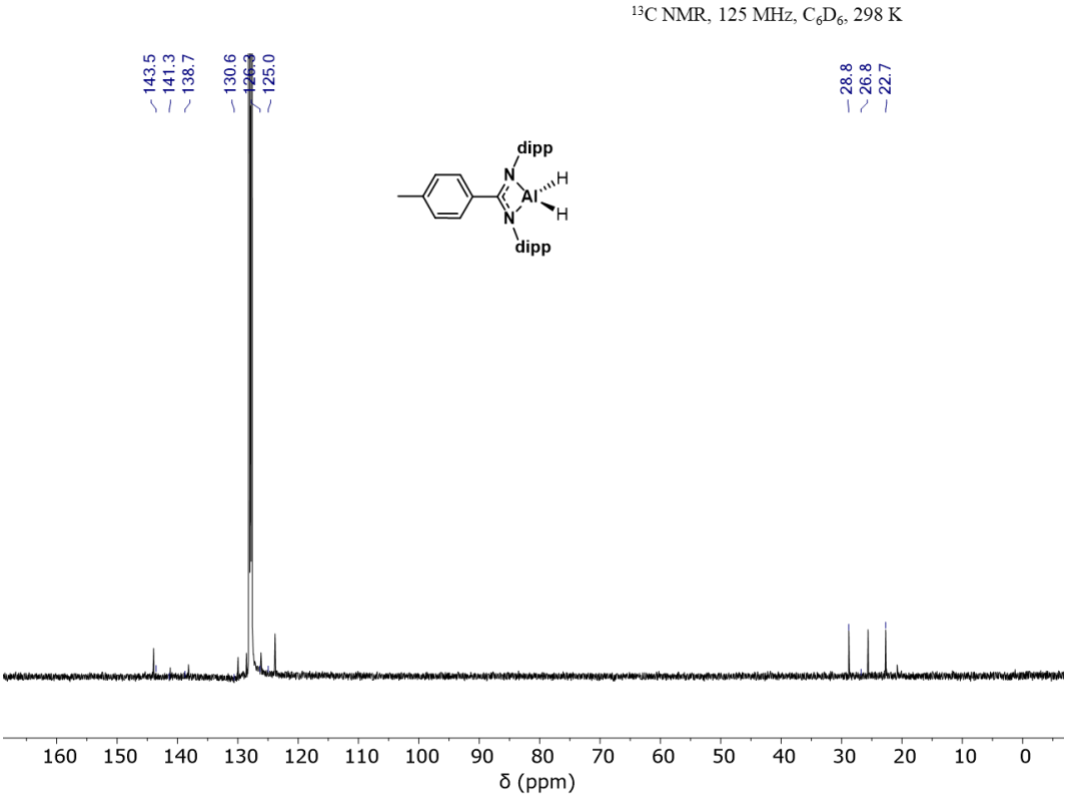

Figure A.15: ^{13}C NMR spectrum of **2.8**.

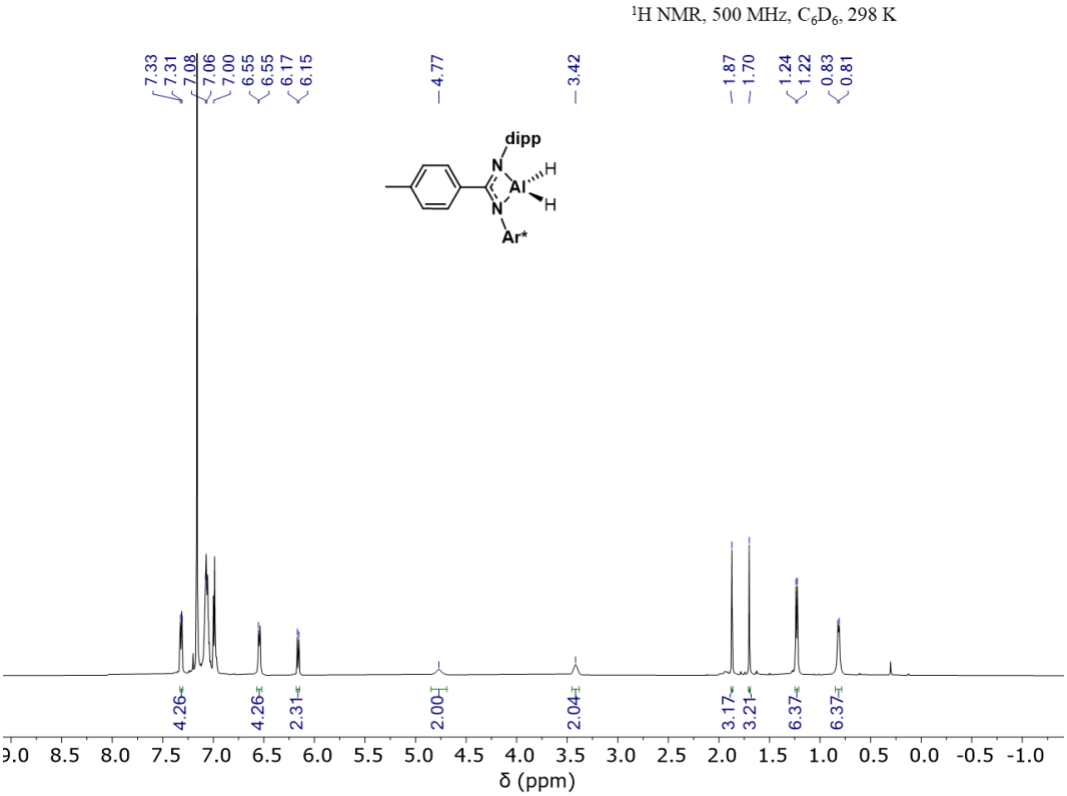

Figure A.16: ^{1}H NMR spectrum of **2.9**.

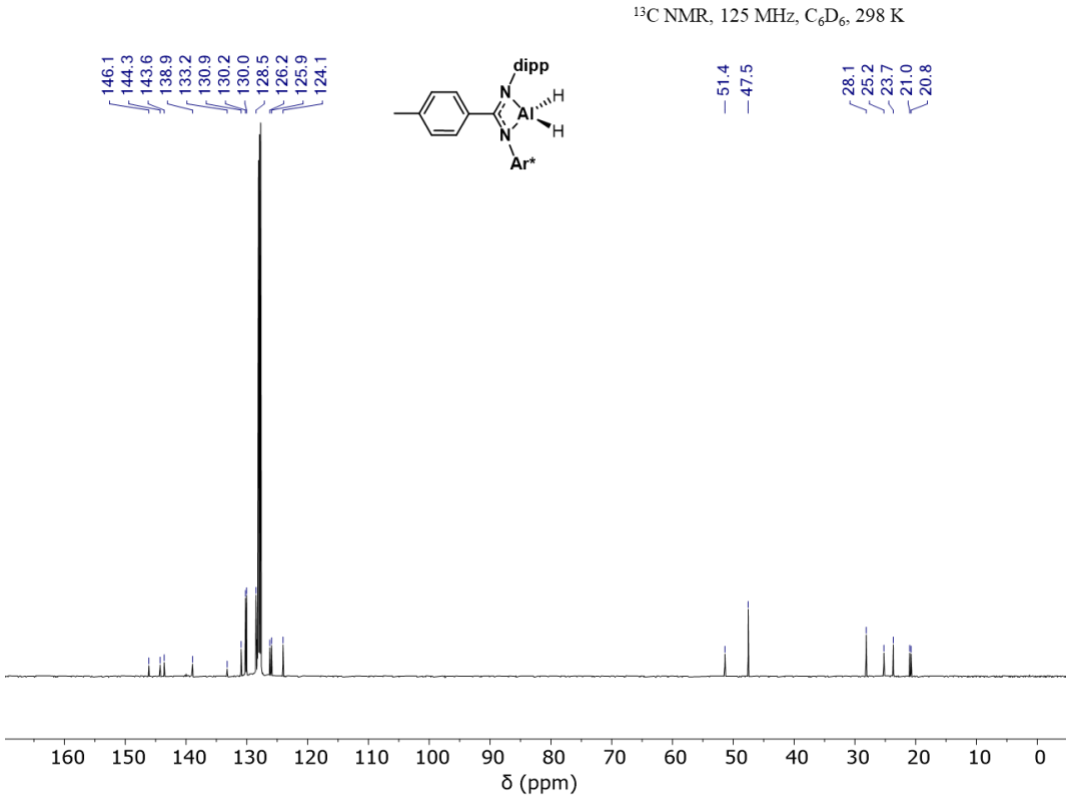

Figure A.17: ^{13}C NMR spectrum of **2.9**.

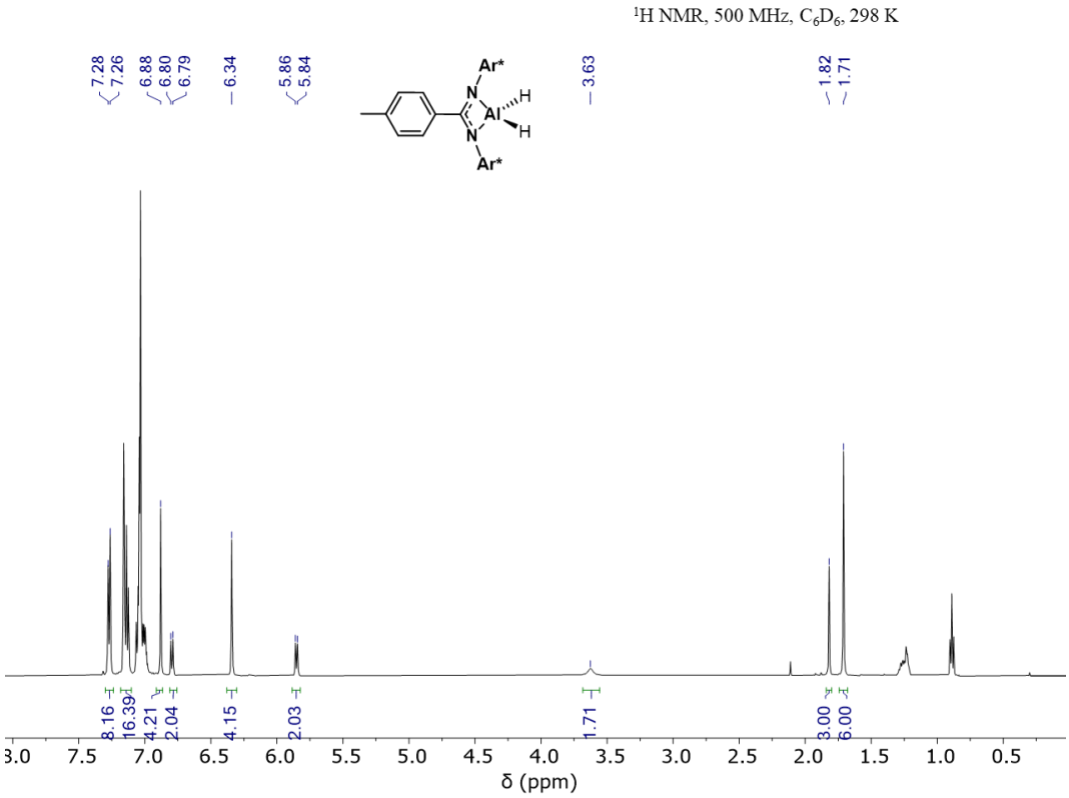

Figure A.18: ^{1}H NMR spectrum of **2.10**.

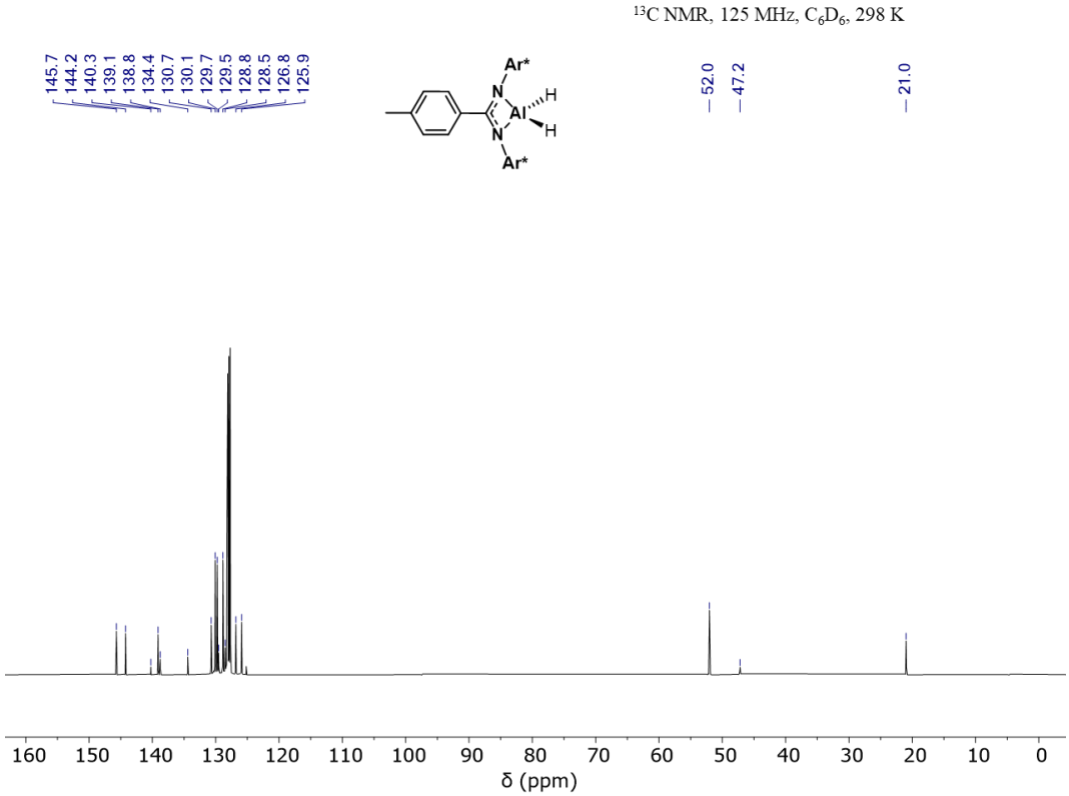

Figure A.19: ^{13}C NMR spectrum of **2.10**.

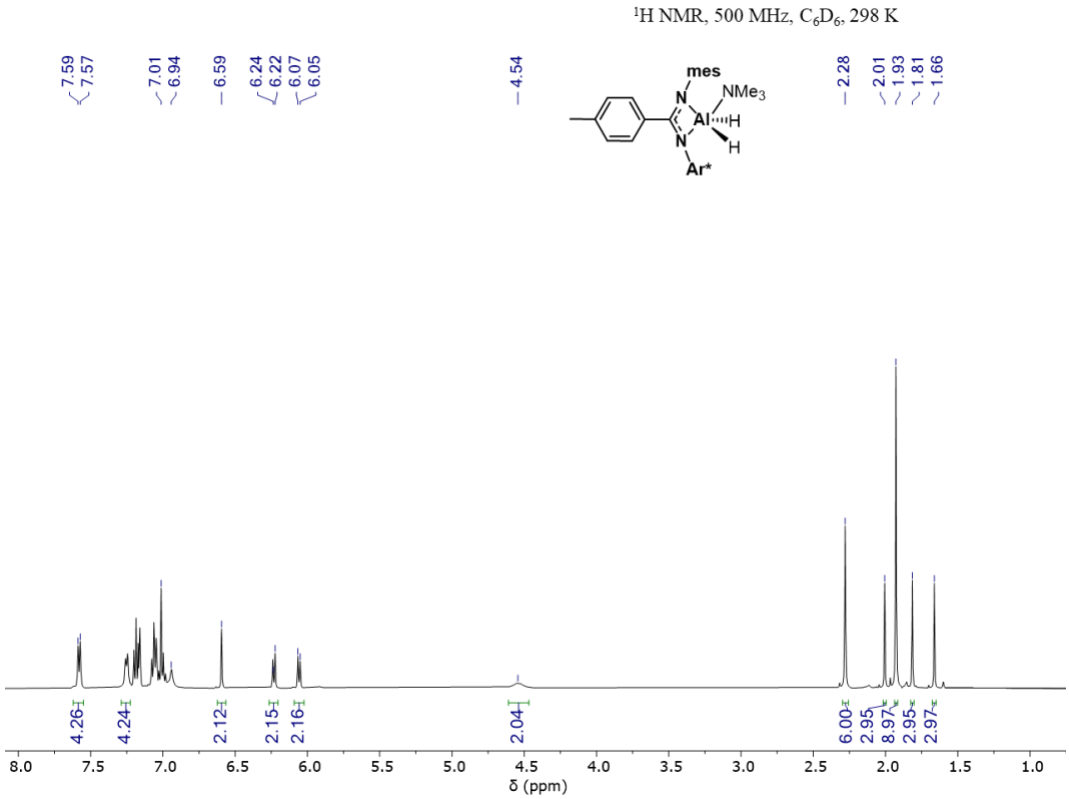

Figure A.20: ^{1}H NMR spectrum of **2.11**.

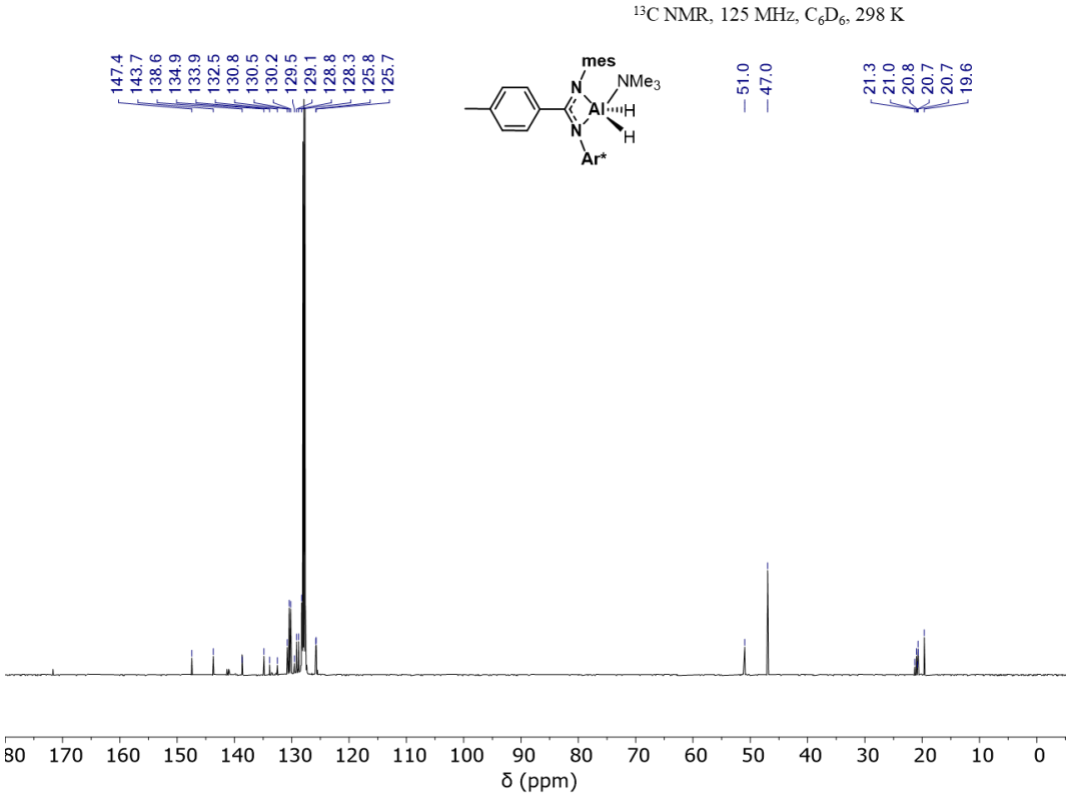

Figure A.21: ^{13}C NMR spectrum of **2.11**.

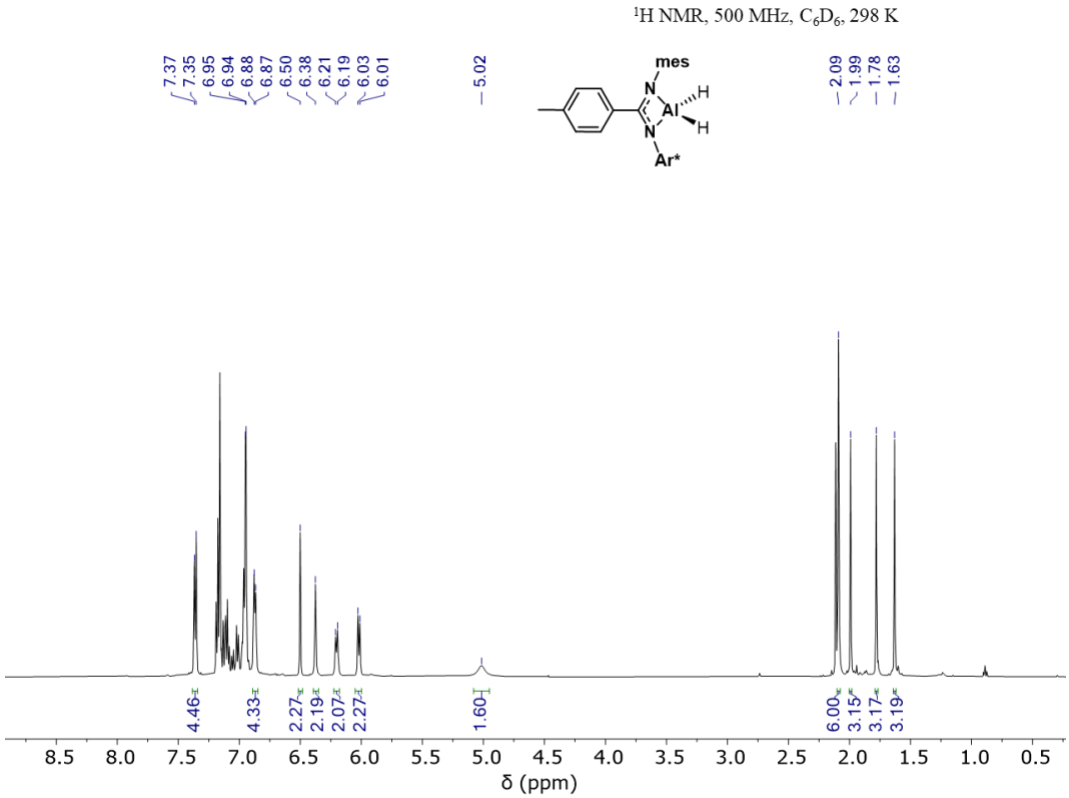

Figure A.22: ^{1}H NMR spectrum of **2.12**.

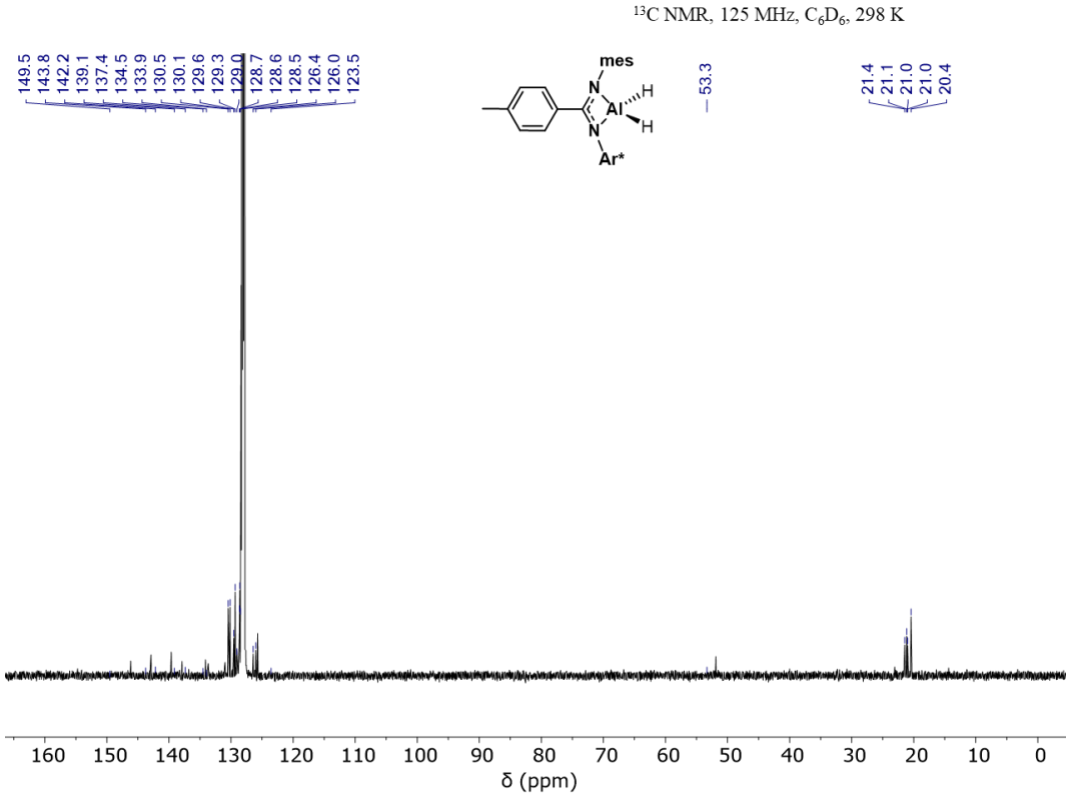

Figure A.23: ^{13}C NMR spectrum of **2.12**.

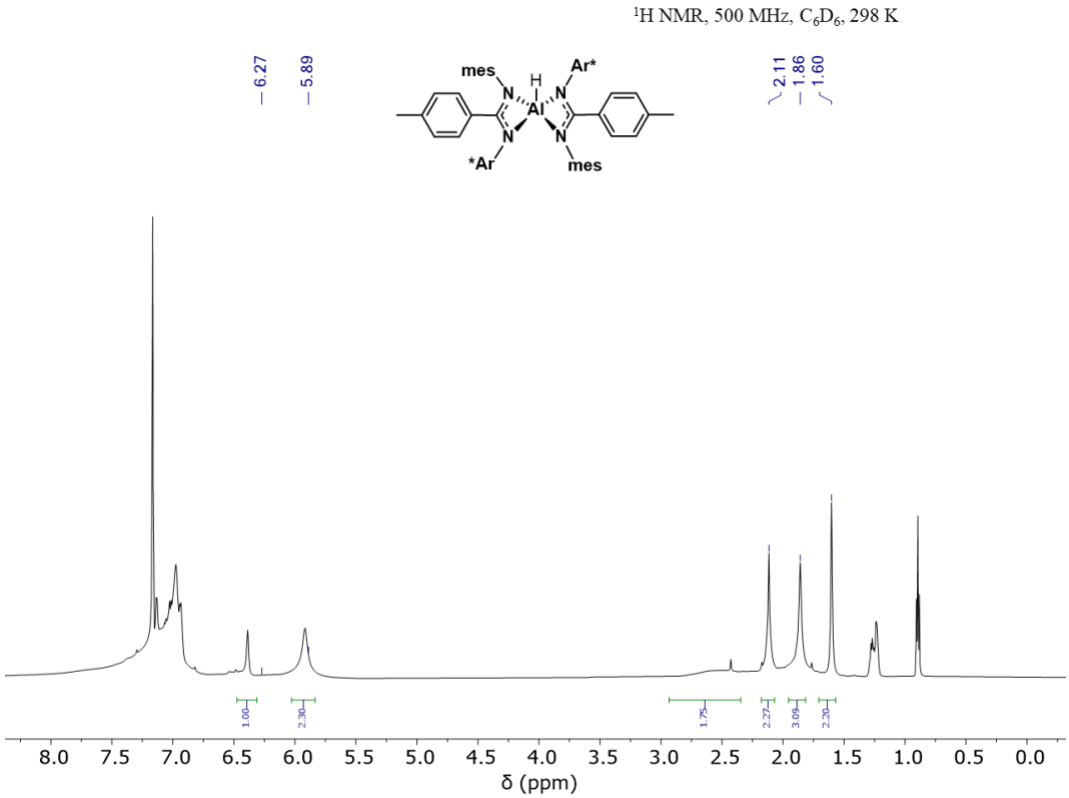

Figure A.24: ^{1}H NMR spectrum of **2.13**.

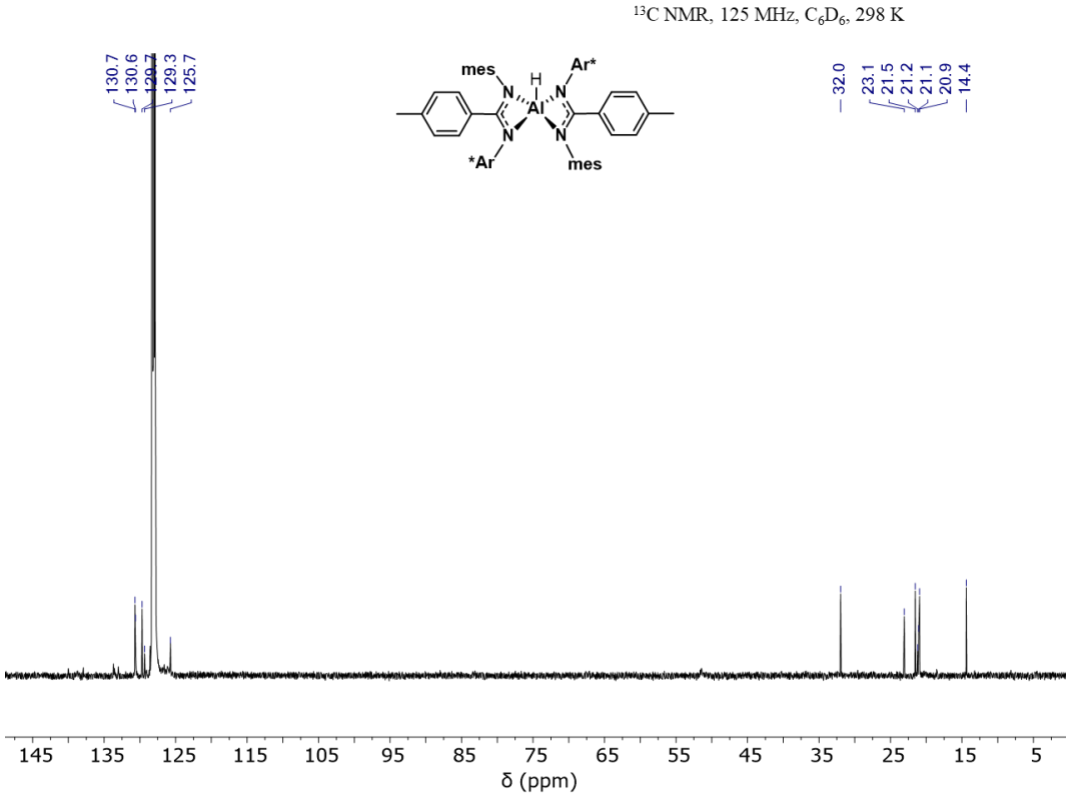

Figure A.25: ^{13}C NMR spectrum of **2.13**.

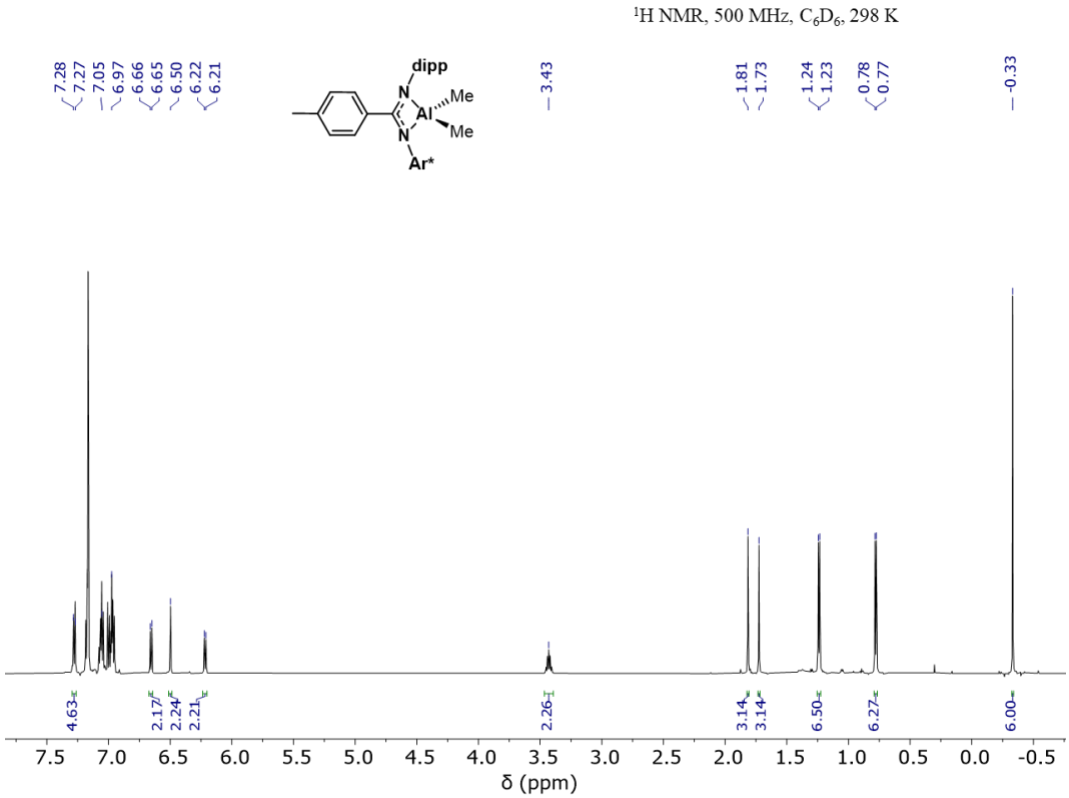

Figure A.26: ^{1}H NMR spectrum of **2.14**.

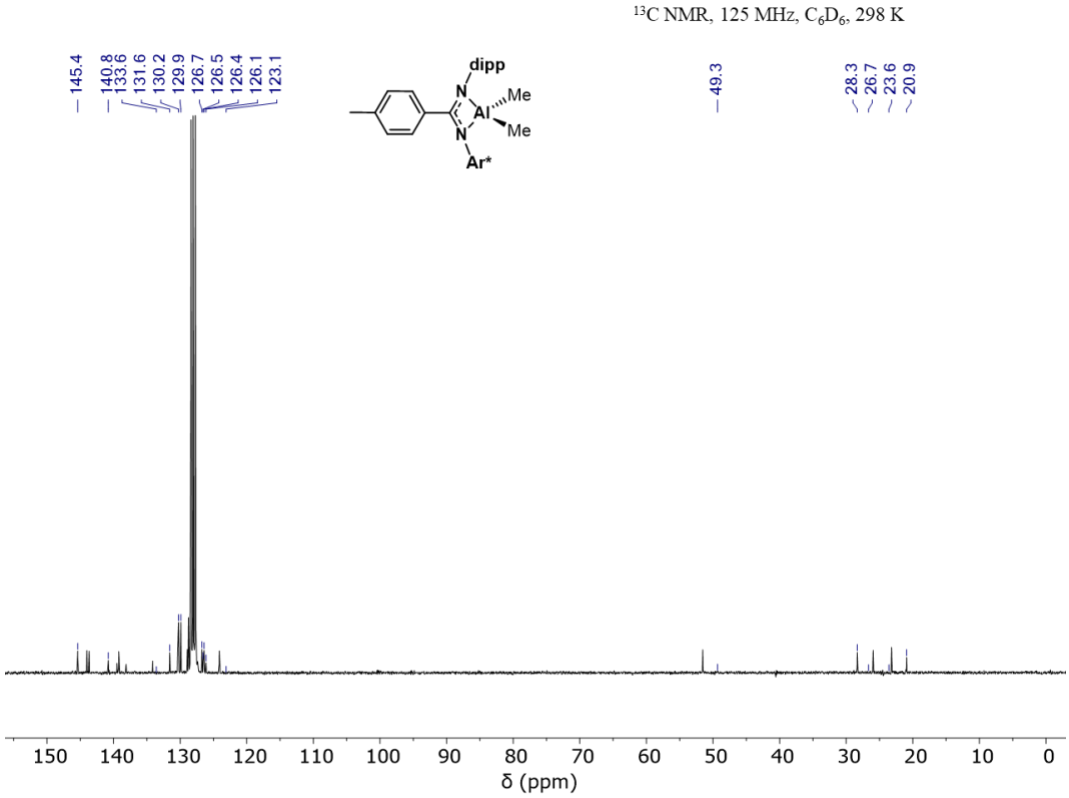

Figure A.27: ^{13}C NMR spectrum of **2.14**.

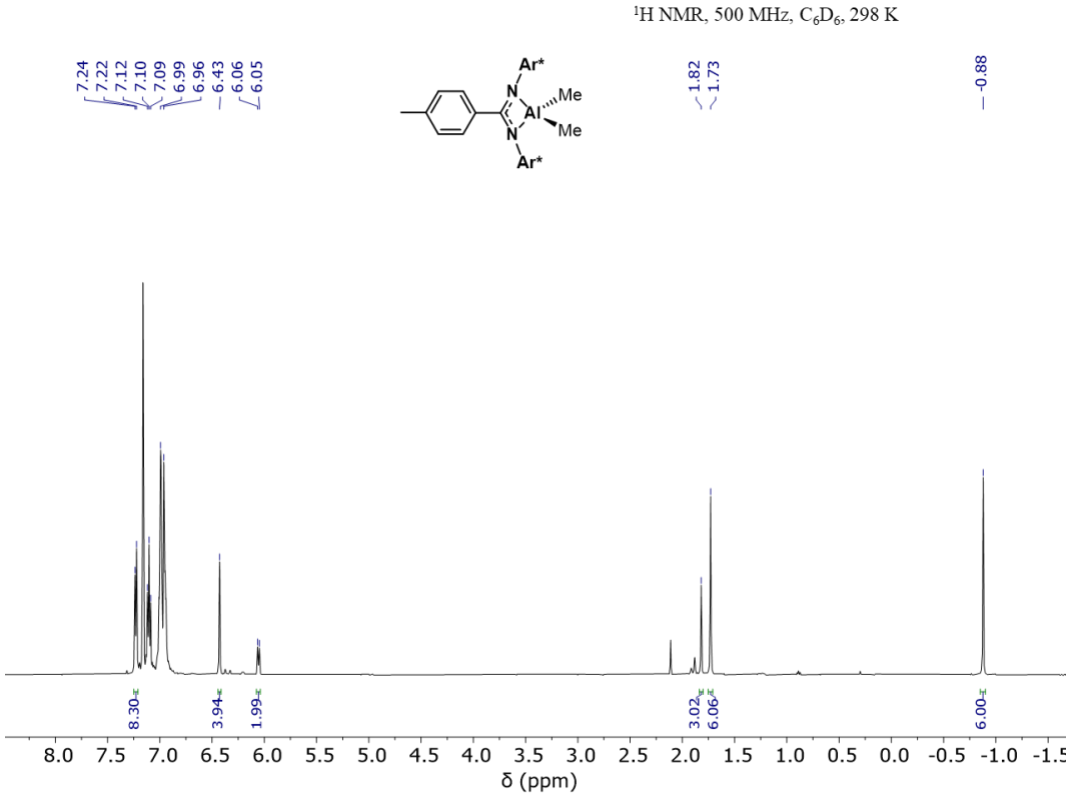

Figure A.28: ^{1}H NMR spectrum of **2.15**.

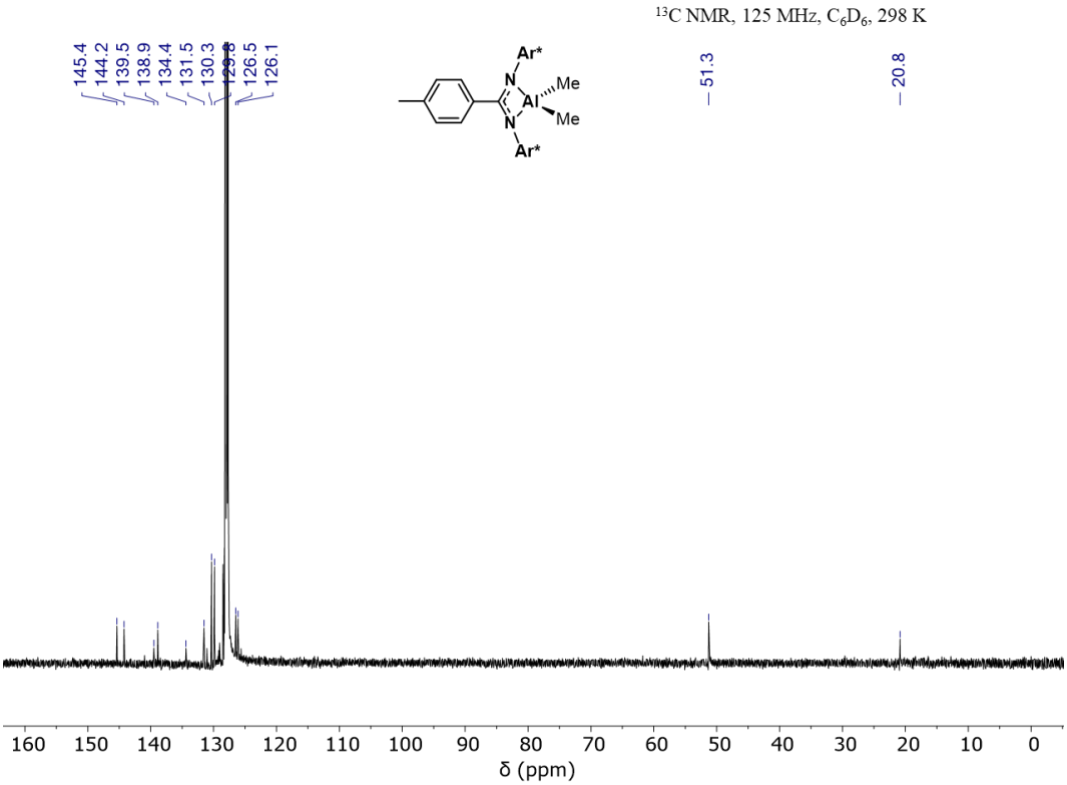

Figure A.29: ^{13}C NMR spectrum of **2.15**.

Chapter 3 Appendix

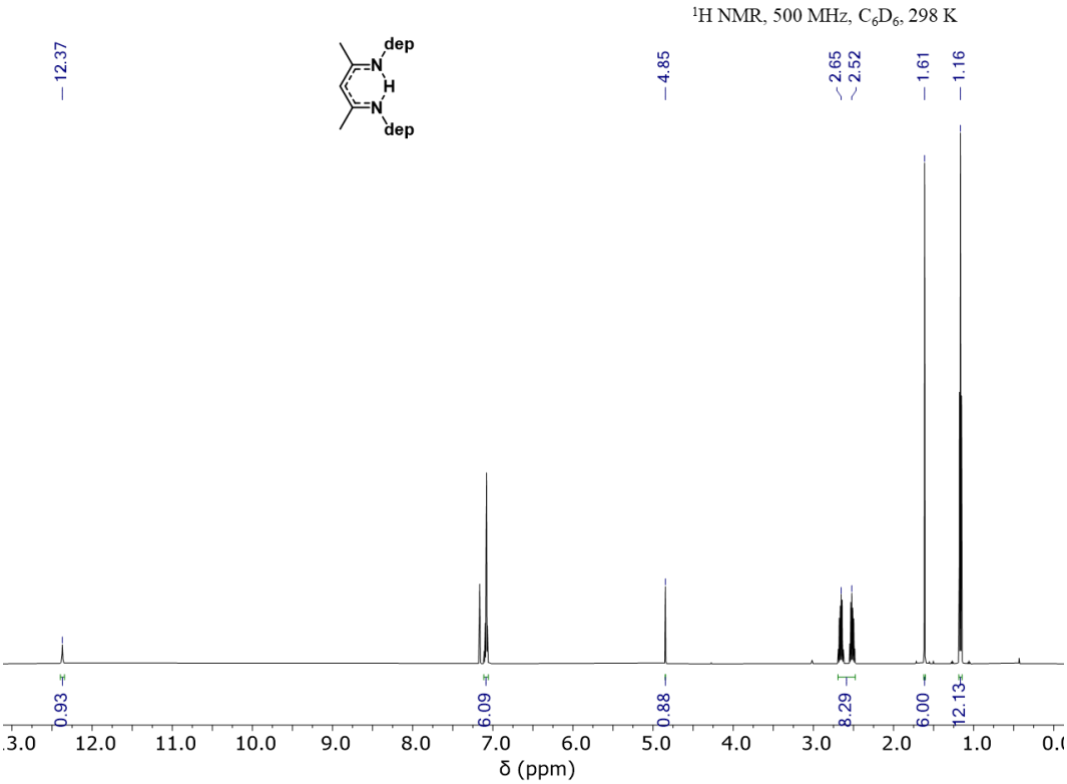

Figure A.30: ^{1}H NMR spectrum of **3.2**.

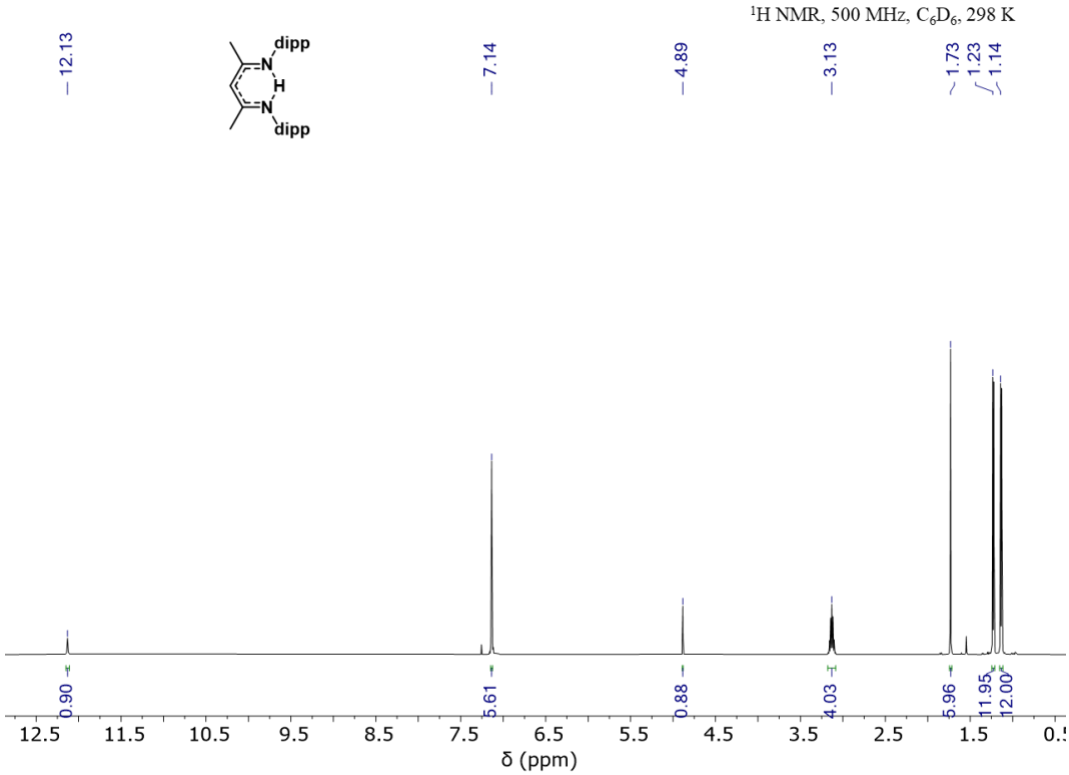

Figure A.31: ^{1}H NMR spectrum of **3.3**.

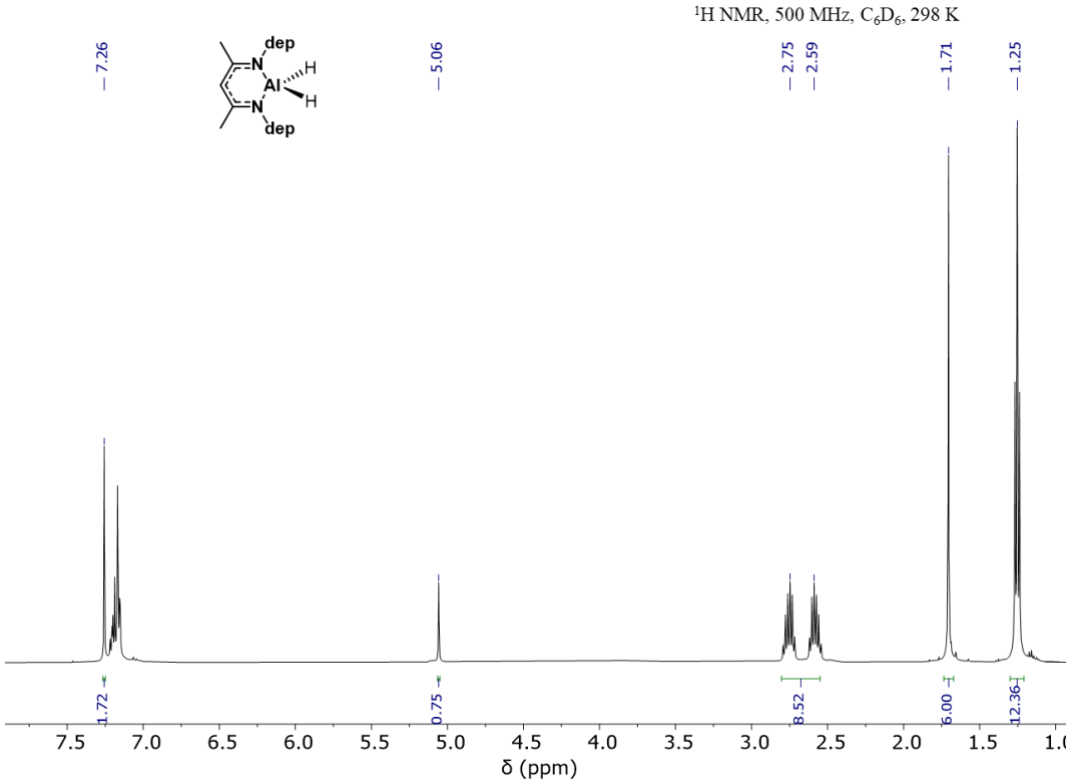

Figure A.32: ^{1}H NMR spectrum of **3.4**.

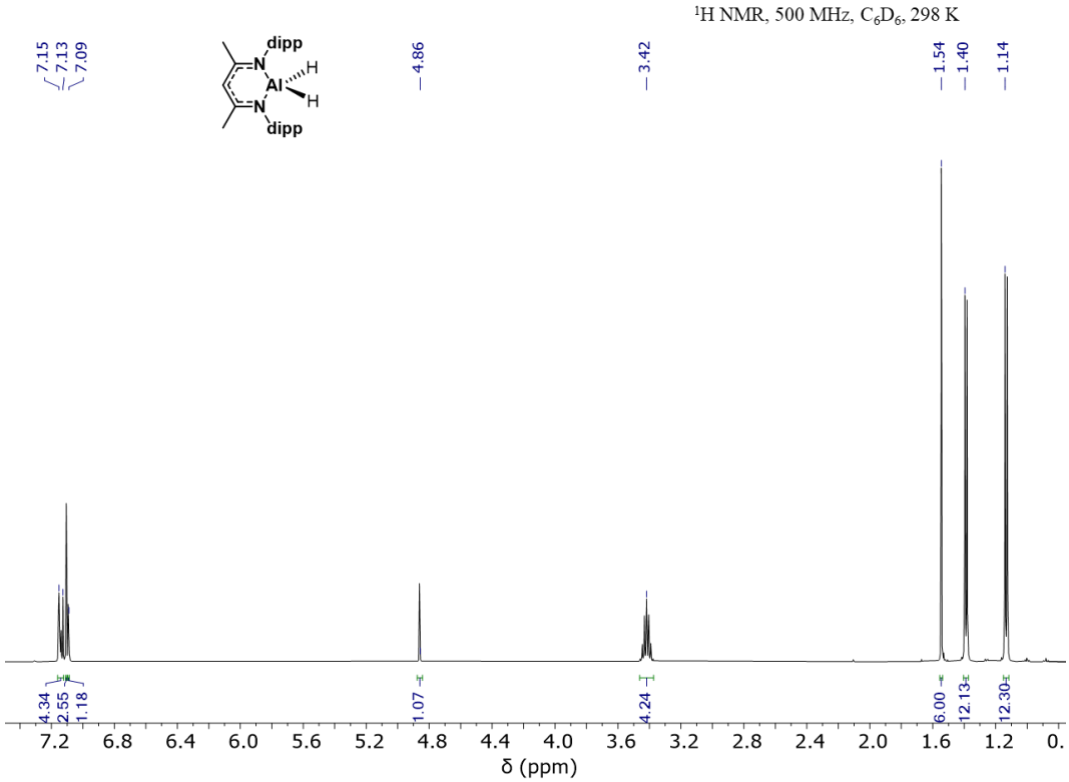

Figure A.33: ^{1}H NMR spectrum of **3.5**.

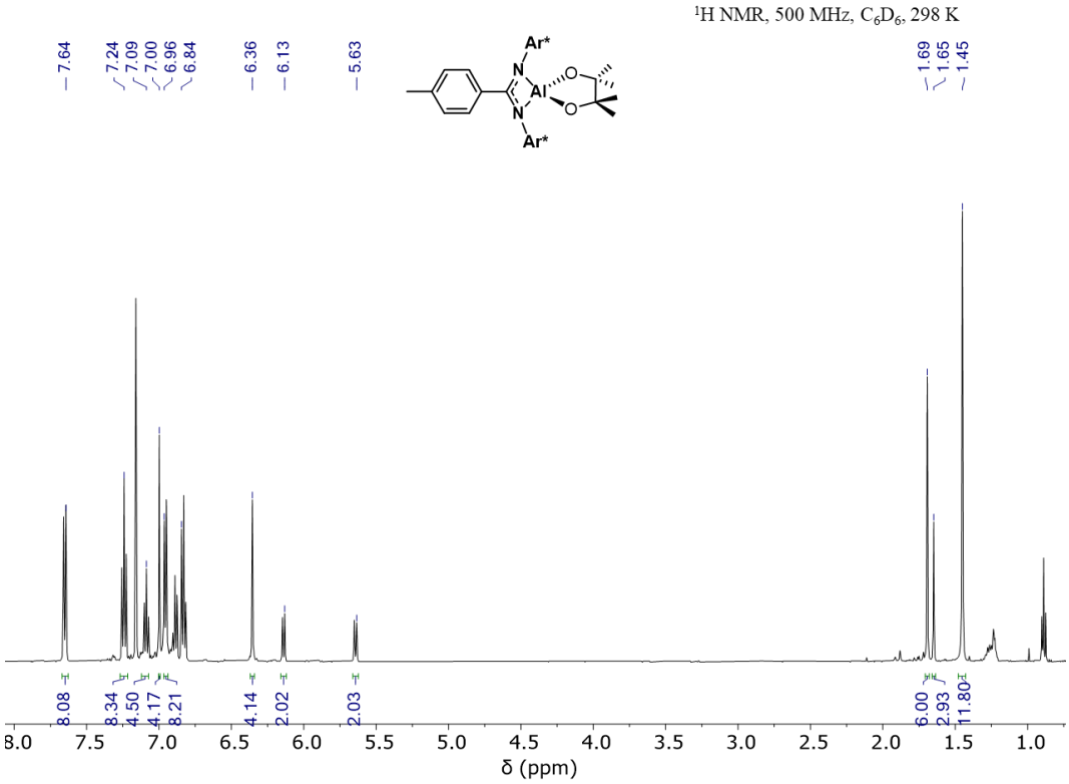

Figure A.34: ^{1}H NMR spectrum of **3.6**.

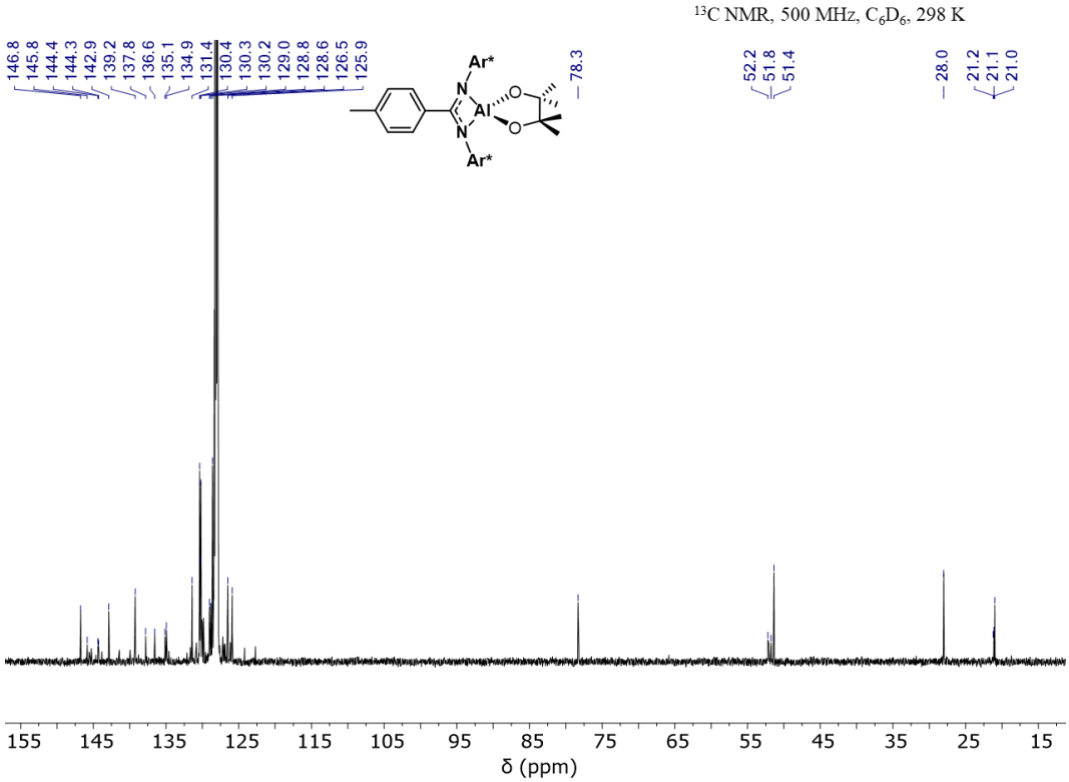

Figure A.35: ^{13}C NMR spectrum of **3.6**.

Stoichiometric Reaction NMR Stacks

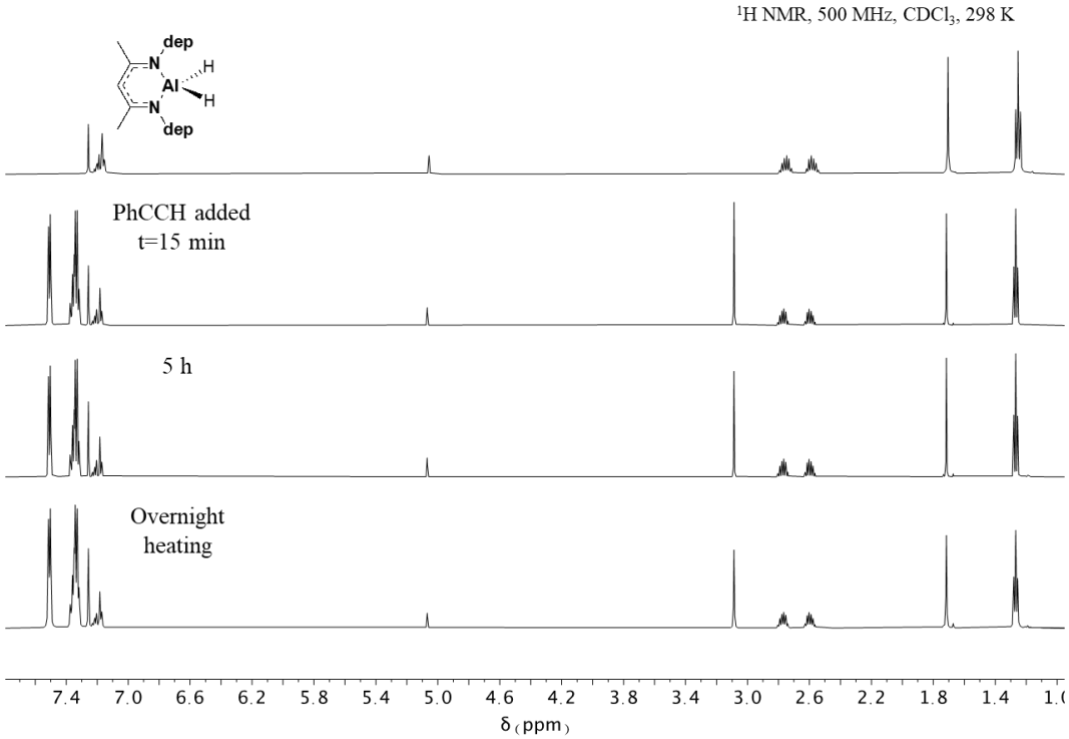

Figure A.36: ^{1}H NMR stack of the reaction of **3.4** with phenylacetylene in chloroform-*d*.

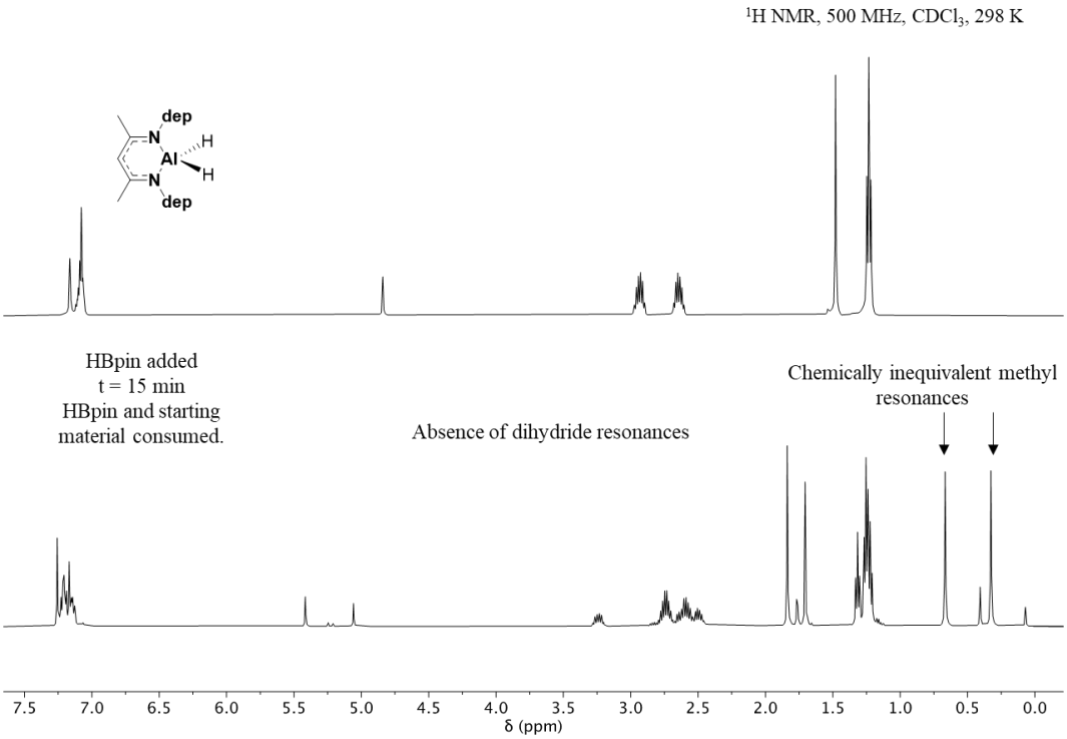

Figure A.37: ^{1}H NMR stack of the reaction of **3.4** with HBpin in chloroform-*d*.

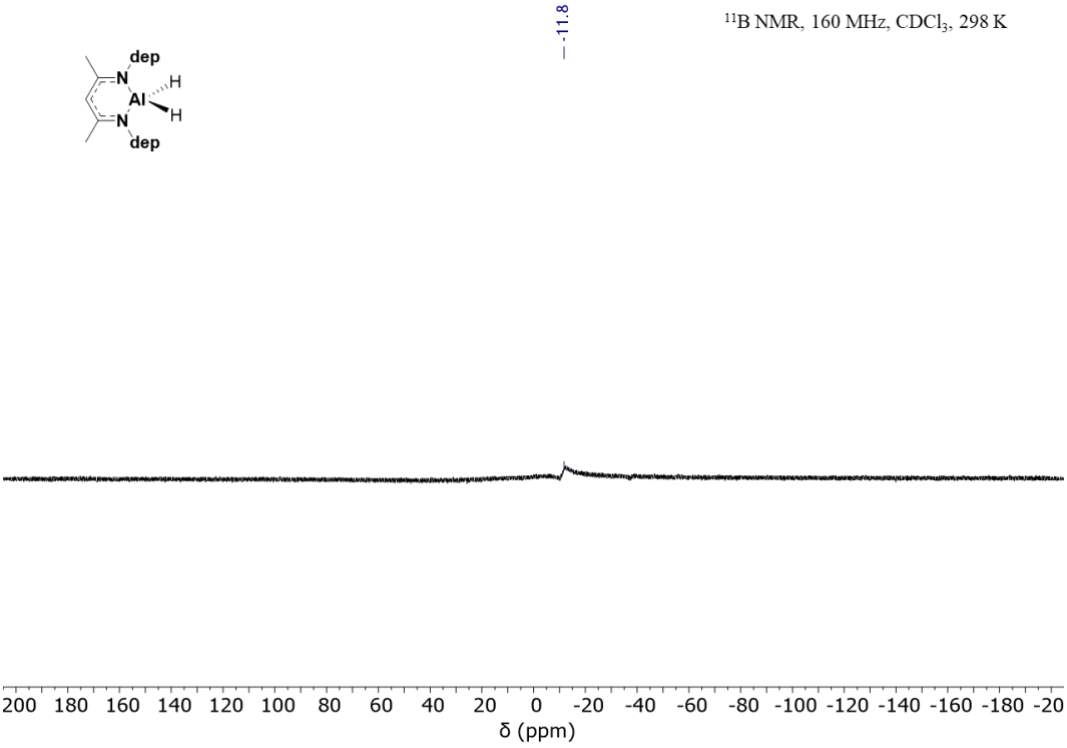

Figure A.38: ^{11}B NMR spectrum of the reaction of **3.4** with HBpin.

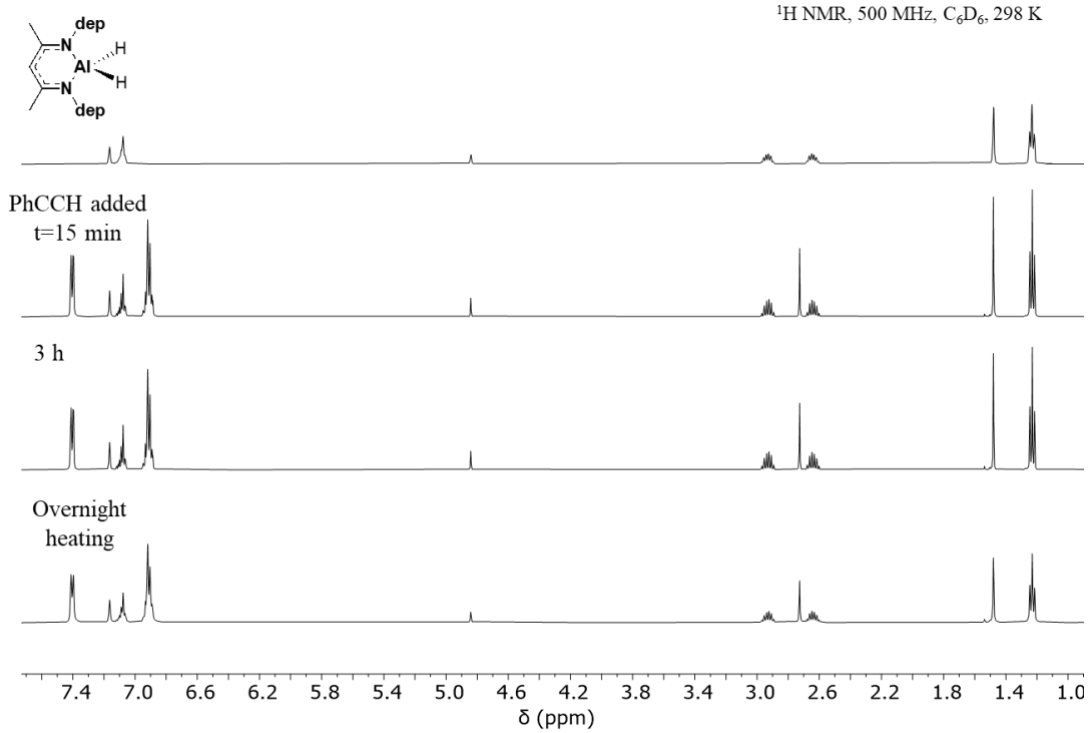

Figure A.39: ^{1}H NMR stack of the reaction of **3.4** with phenylacetylene in benzene-d_6.

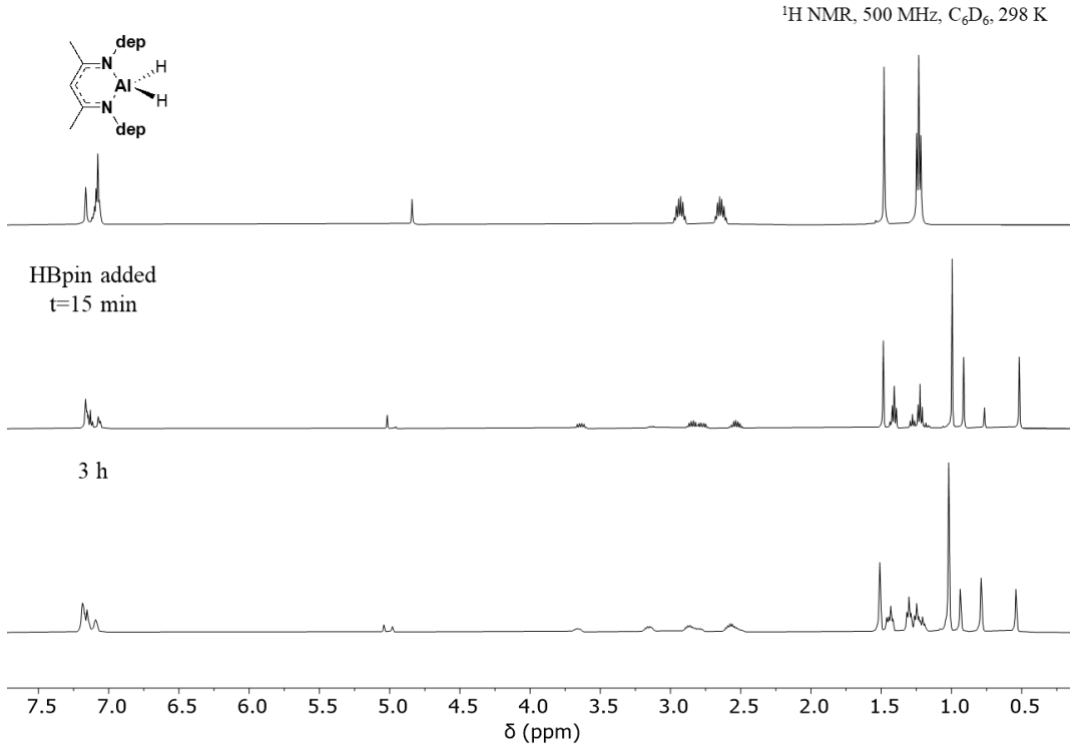

Figure A.40: ^{1}H NMR stack of the reaction of **3.4** with HBpin in benzene-d_6.

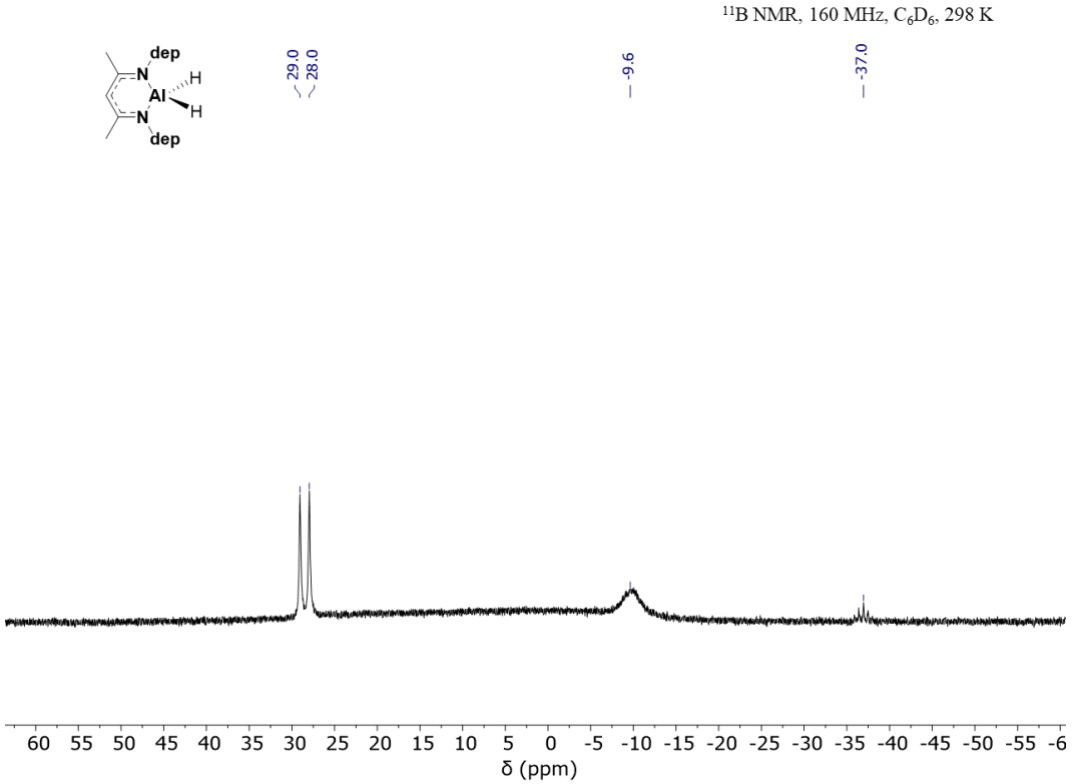

Figure A.41: ^{11}B NMR spectrum of the reaction of **3.4** with HBpin in benzene-d_6.

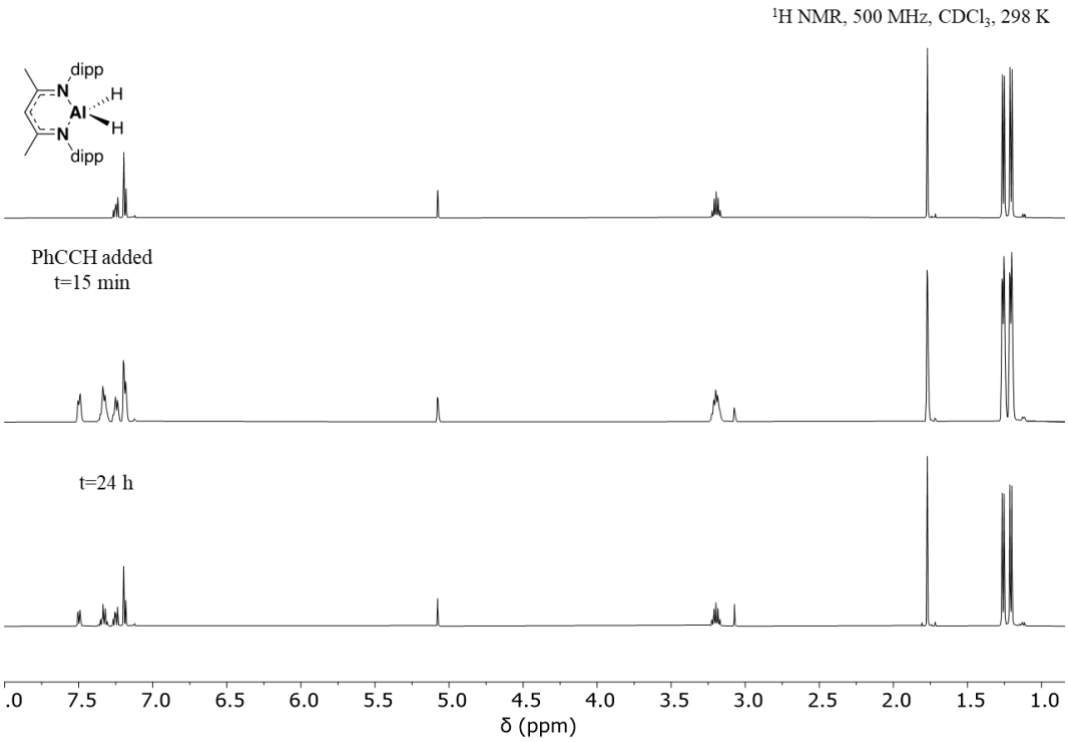

Figure A.42: ^{1}H NMR spectrum of the reaction of **3.5** with phenylacetylene in chloroform-*d*.

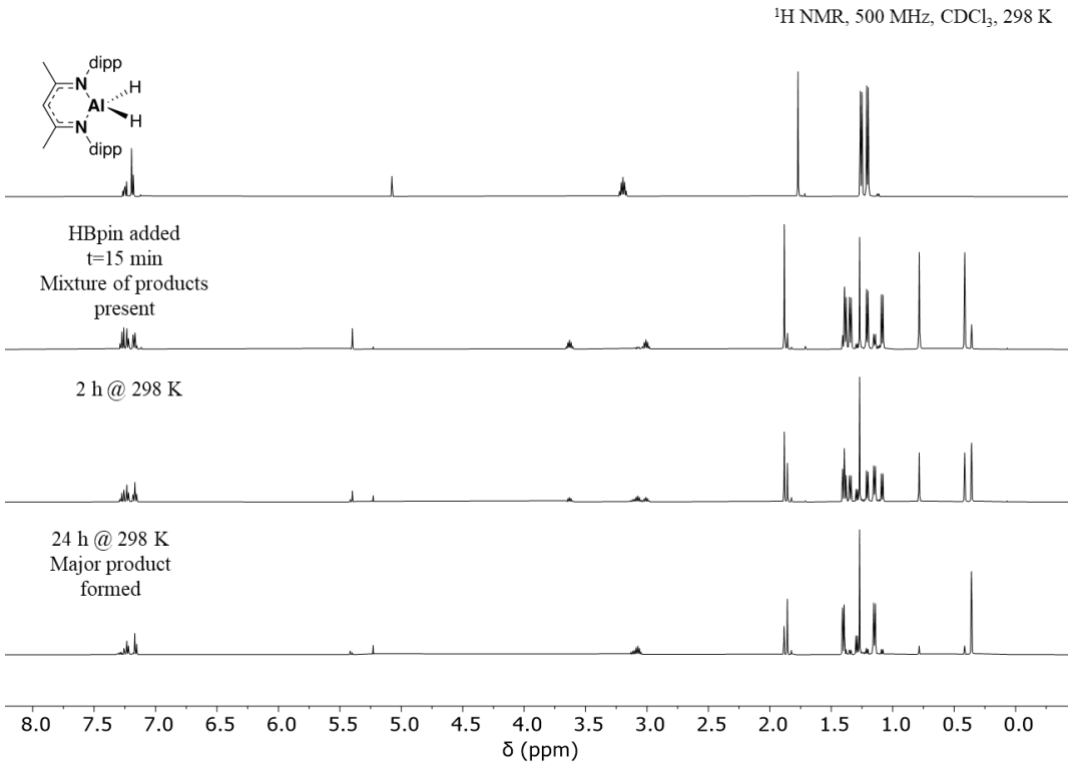

Figure A.43: ^{1}H NMR stack of the reaction of **3.5** with HBpin in chloroform-*d*.

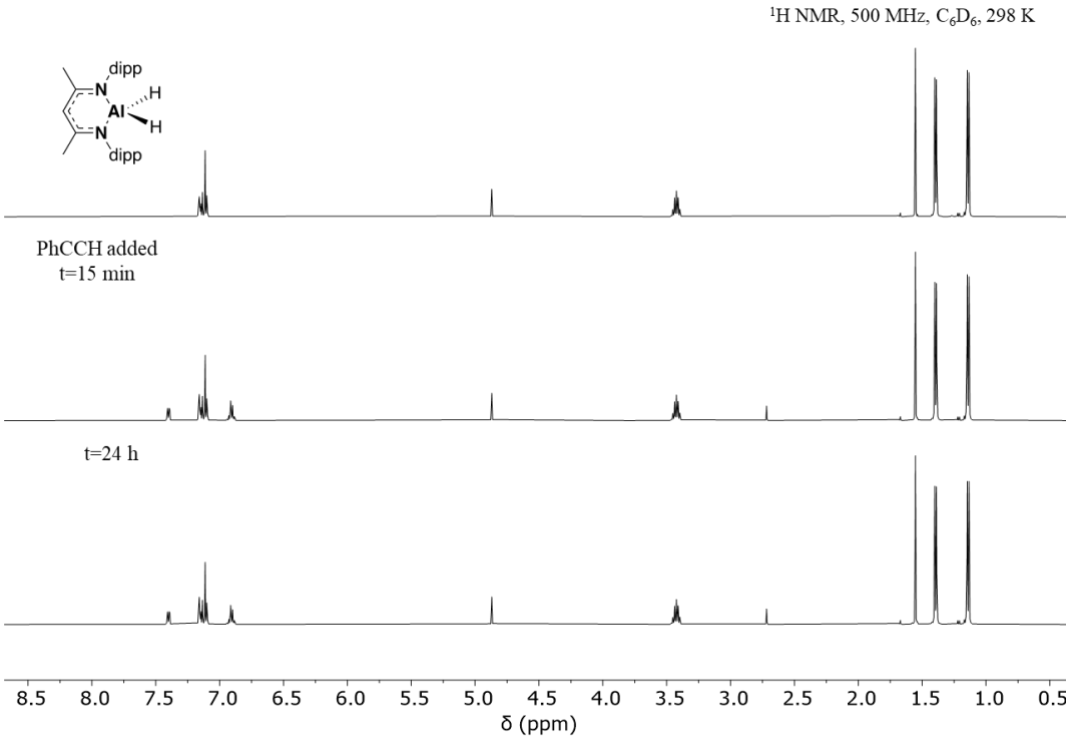

Figure A.44: ^{1}H NMR stack of the reaction of **3.5** with phenylacetylene in benzene-d_6.

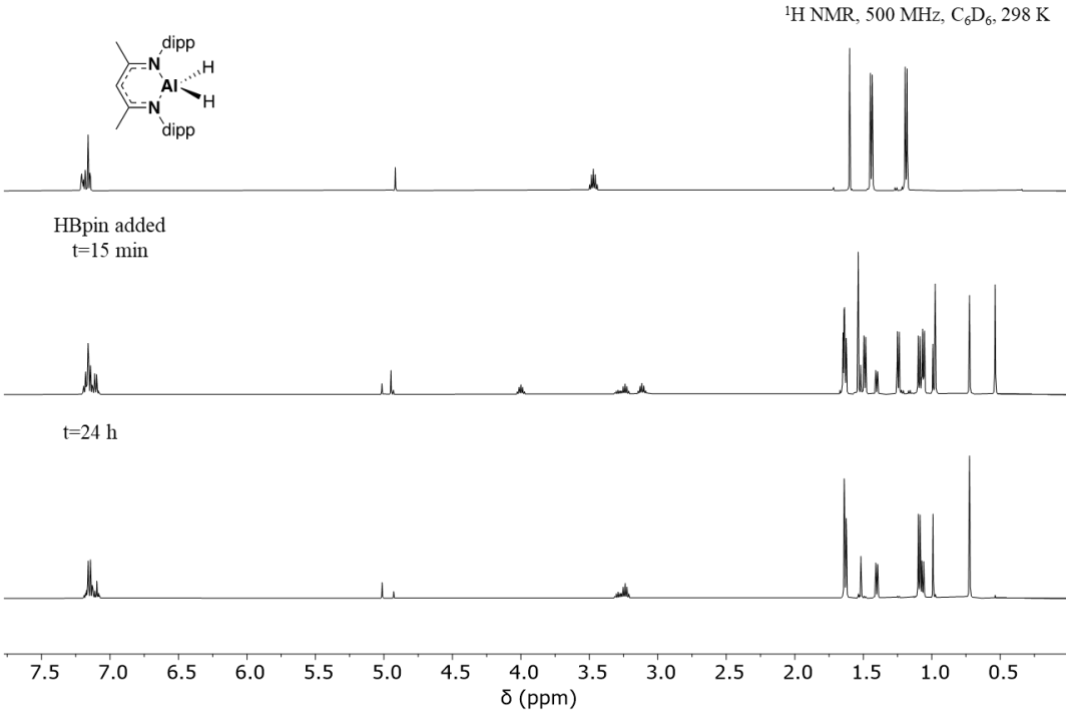

Figure A.45: ^{1}H NMR stack of the reaction of **3.5** with HBpin in benzene-d_6.

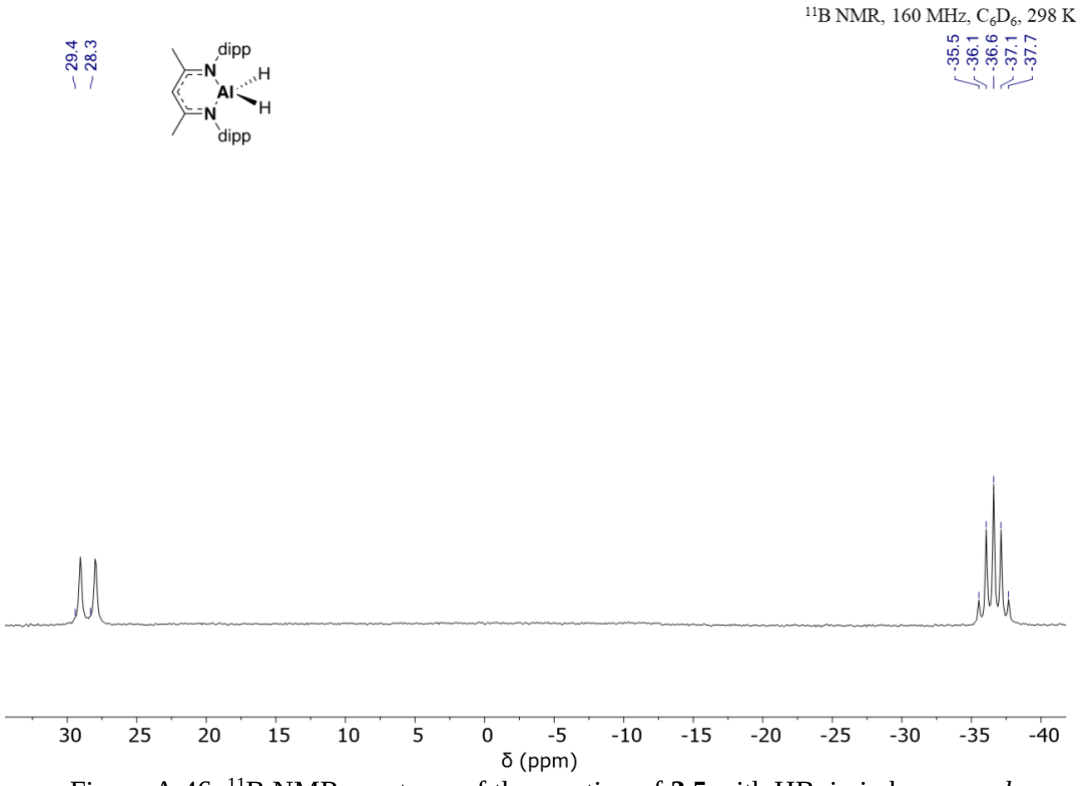

Figure A.46: ^{11}B NMR spectrum of the reaction of **3.5** with HBpin in benzene-d_6.

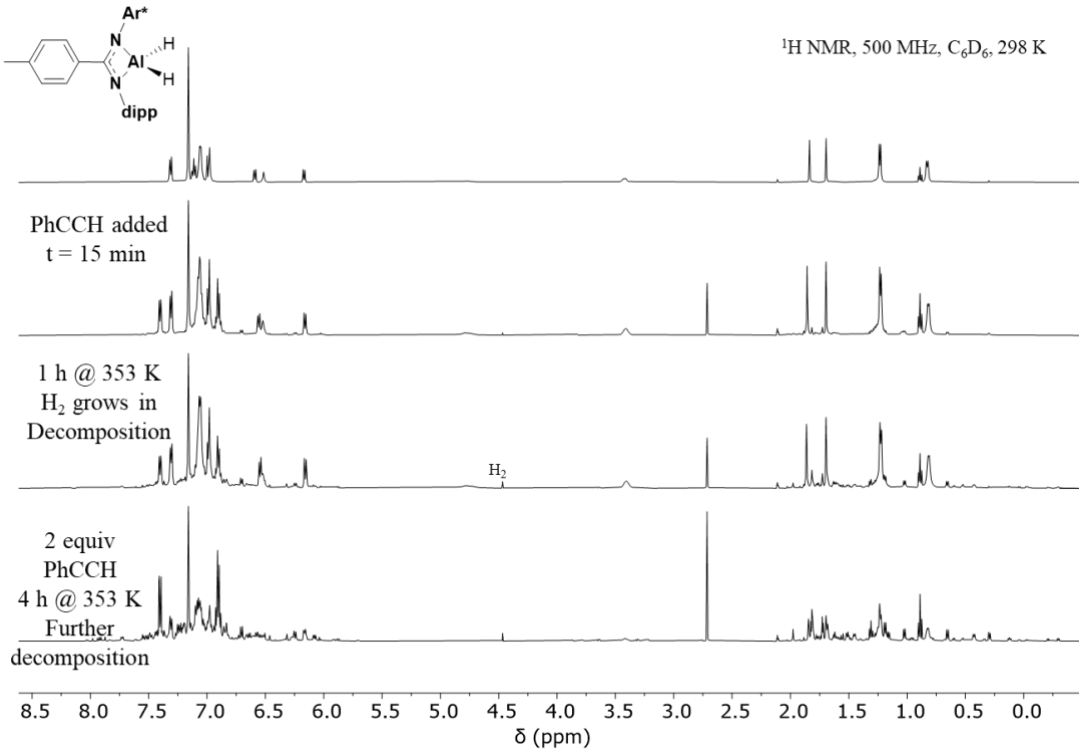

Figure A.47: ^{1}H NMR spectrum of the reaction of **2.9** with phenylacetylene in benzene-d_6.

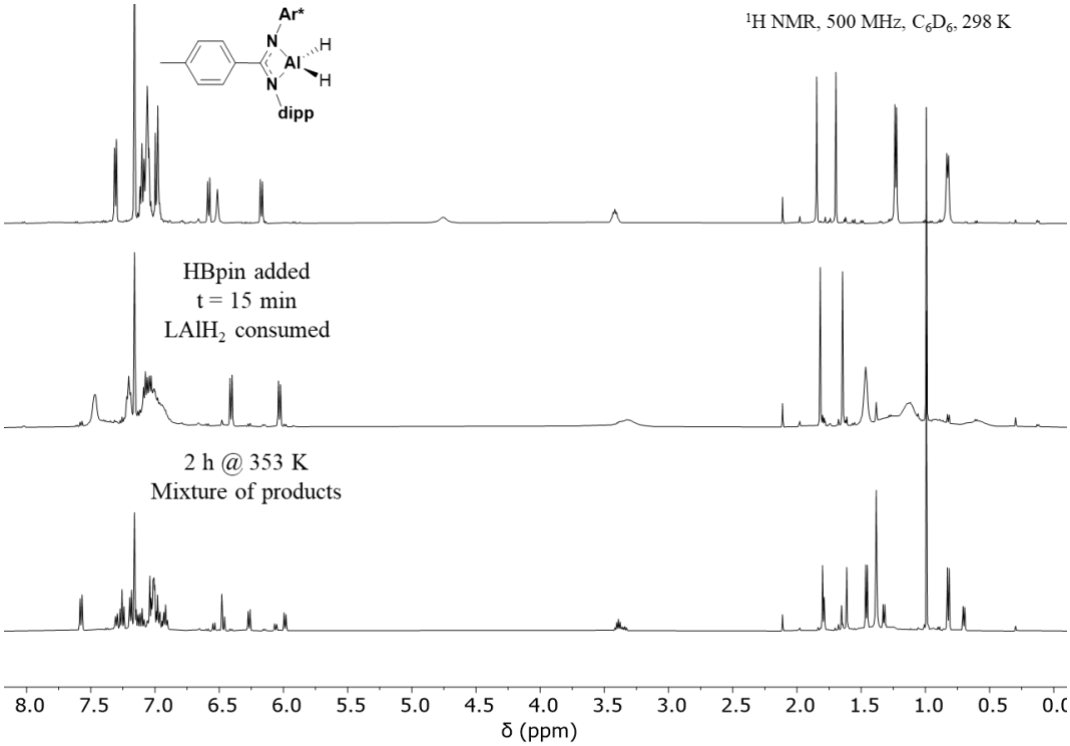

Figure A.48: ^{1}H NMR stack of the reaction of **2.9** with HBpin in benzene-d_6.

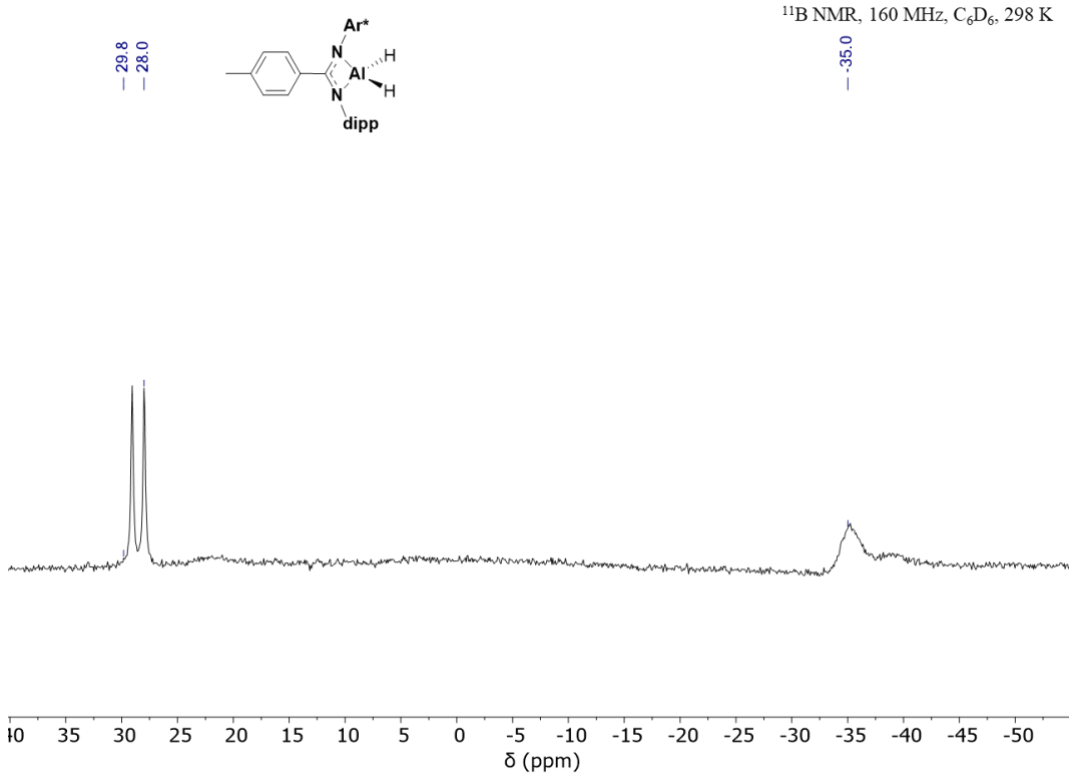

Figure A.49: ^{11}B NMR spectrum of the reaction of **2.9** with HBpin in benzene-d_6.

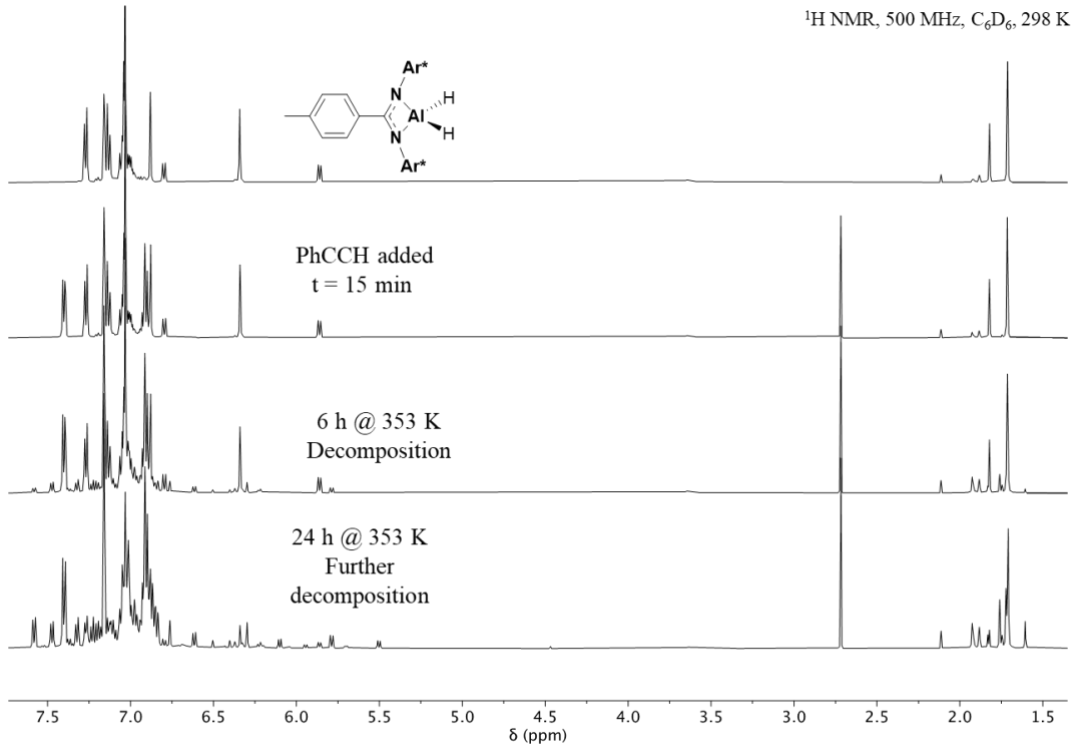

Figure A.50: ^{1}H NMR stack of the reaction of **2.10** with phenylacetylene in benzene-d_6.

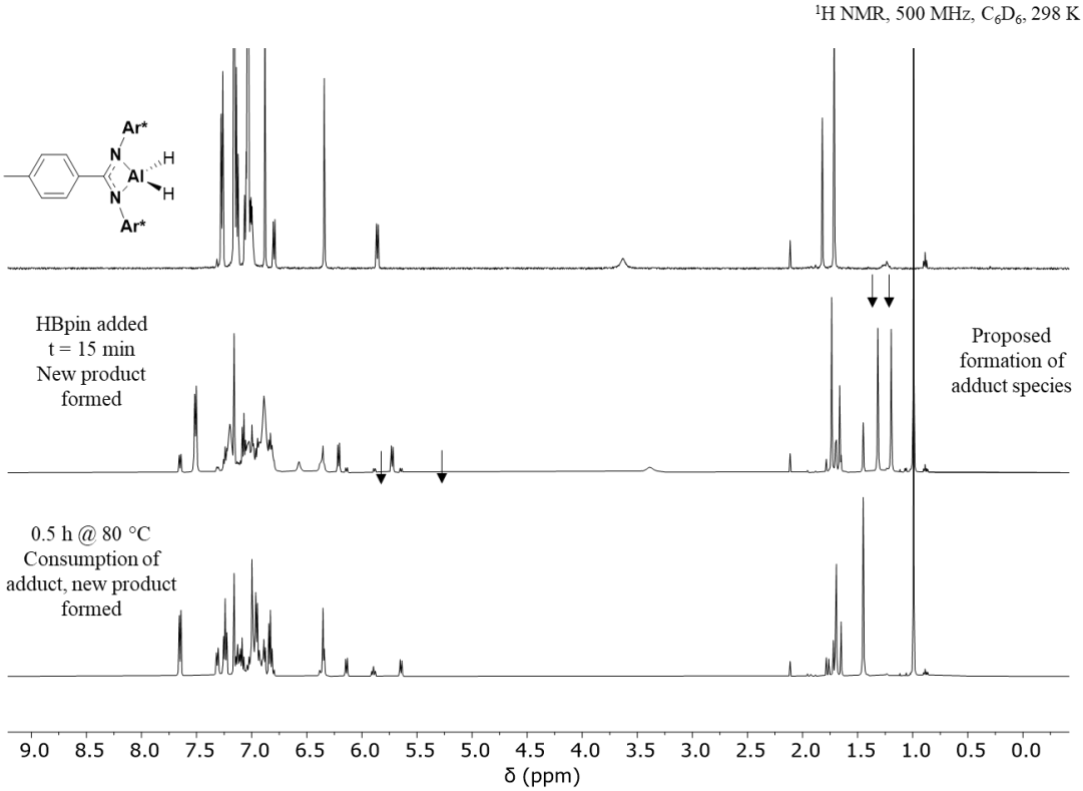

Figure A.51: ^{1}H NMR stack of the reaction of **2.10** with HBpin in benzene-d_6.

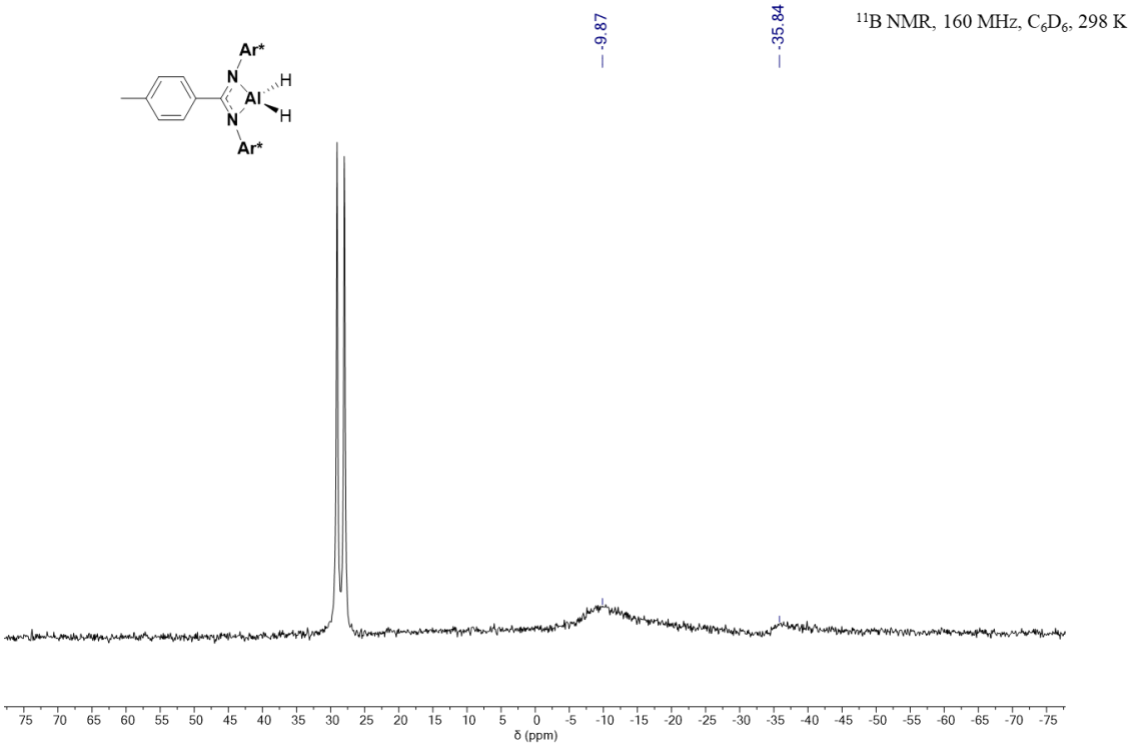

Figure A.52: ^{11}B NMR spectrum of the reaction of **2.10** with HBpin in benzene-d_6.

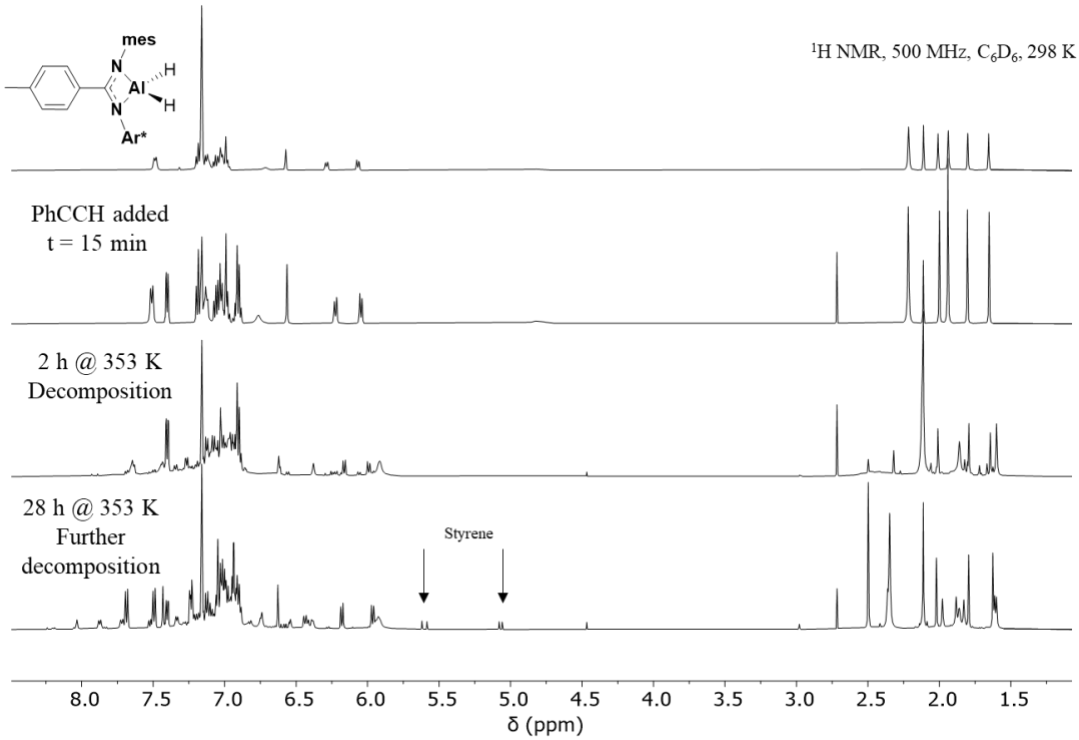

Figure A.53: ^{1}H NMR spectrum of the reaction of **2.12** with phenylacetylene in benzene-d_6.

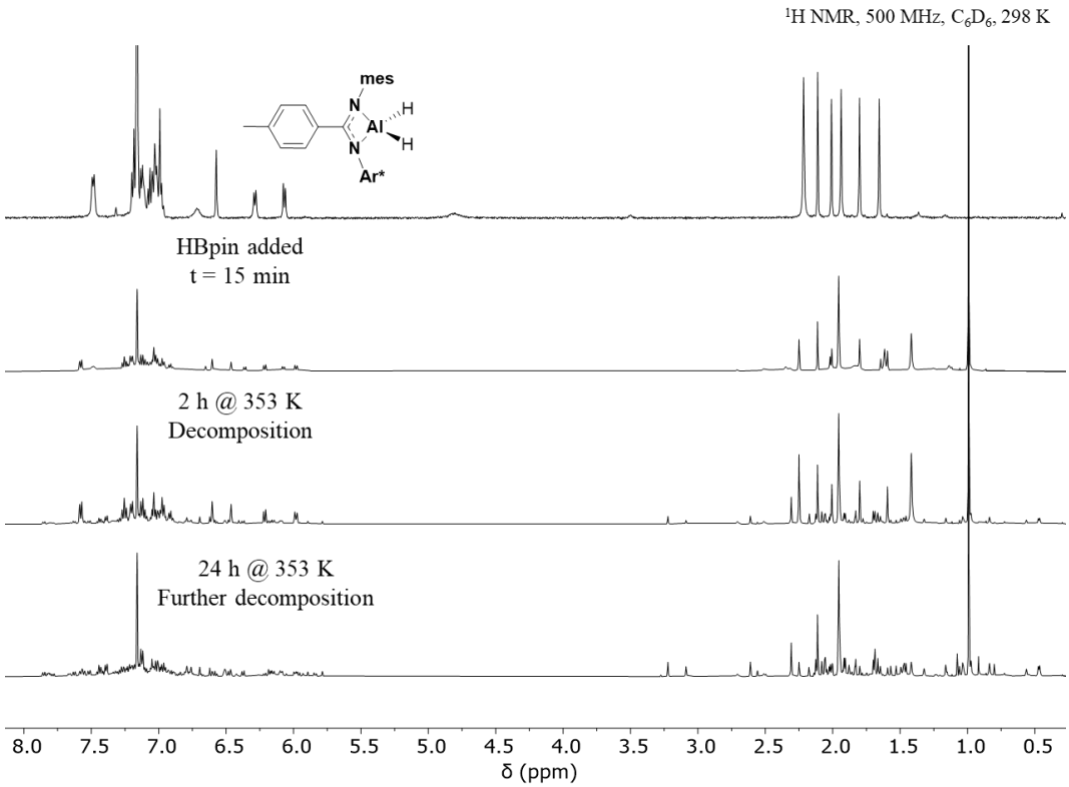

Figure A.54: ^{1}H NMR spectrum of the reaction of **2.12** with HBpin in benzene-d_6.

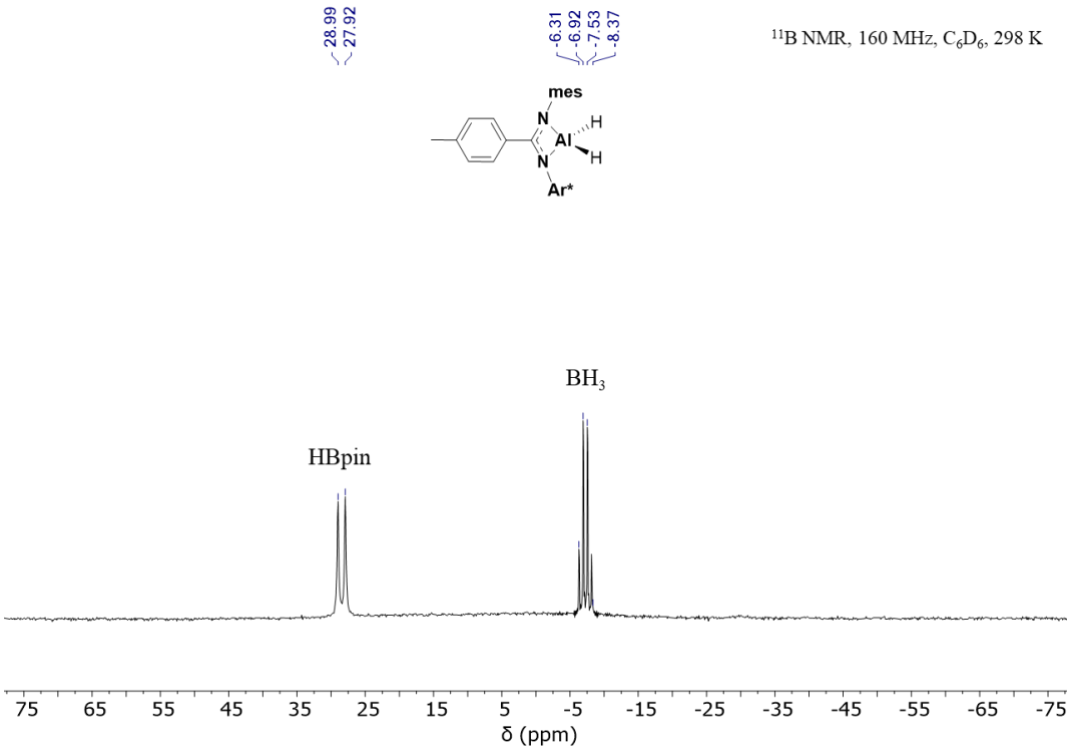

Figure A.55: ^{11}B NMR spectrum of the reaction of **2.12** with HBpin in benzene-d_6.

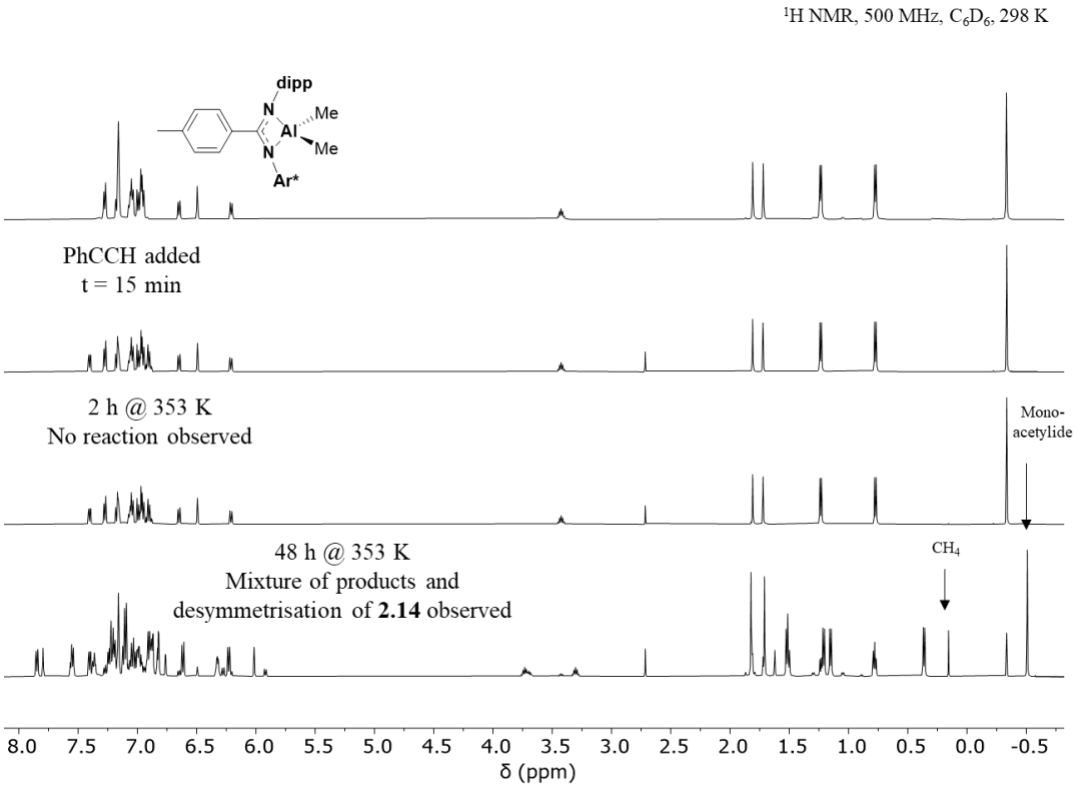

Figure A.56: ^{1}H NMR stack of the reaction of **2.14** with phenylacetylene in benzene-d_6.

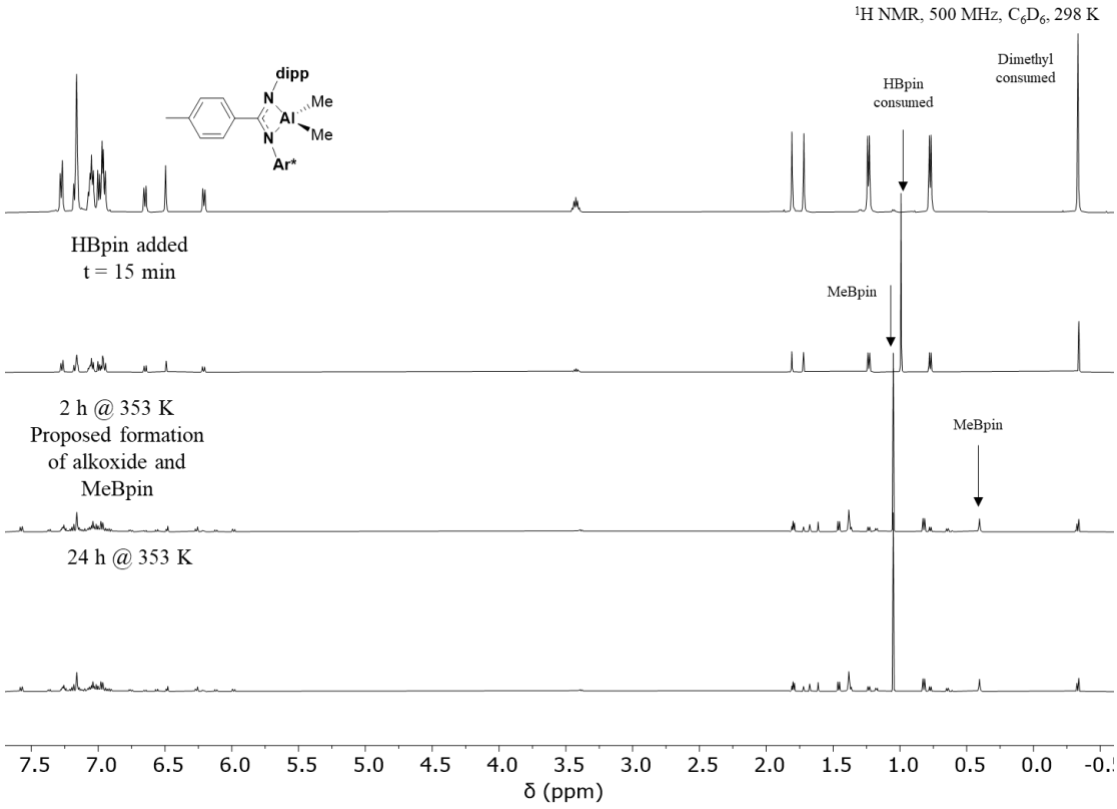

Figure A.57: ^{1}H NMR spectrum of the reaction of **2.14** with HBpin in benzene-d_6.

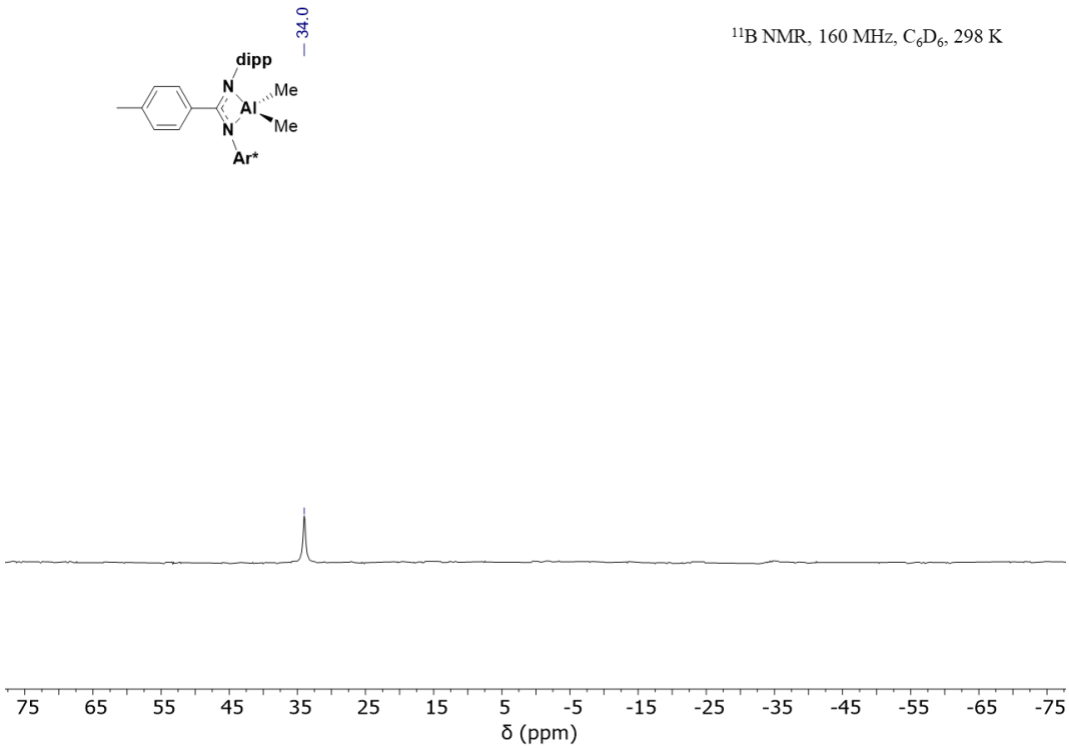

Figure A.58: ^{11}B NMR spectrum of the reaction of **2.14** with HBpin in benzene-d_6.

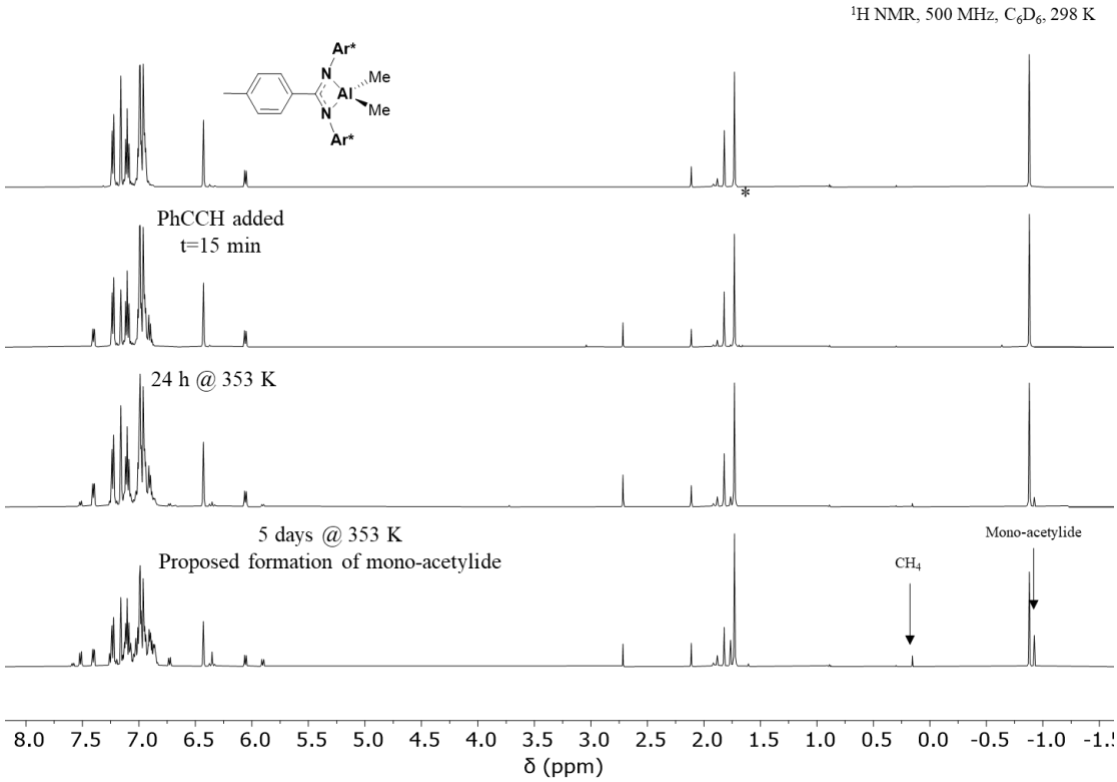

Figure A.59: ^{1}H NMR stack of the reaction of **2.15** with phenylacetylene in benzene-d_6.

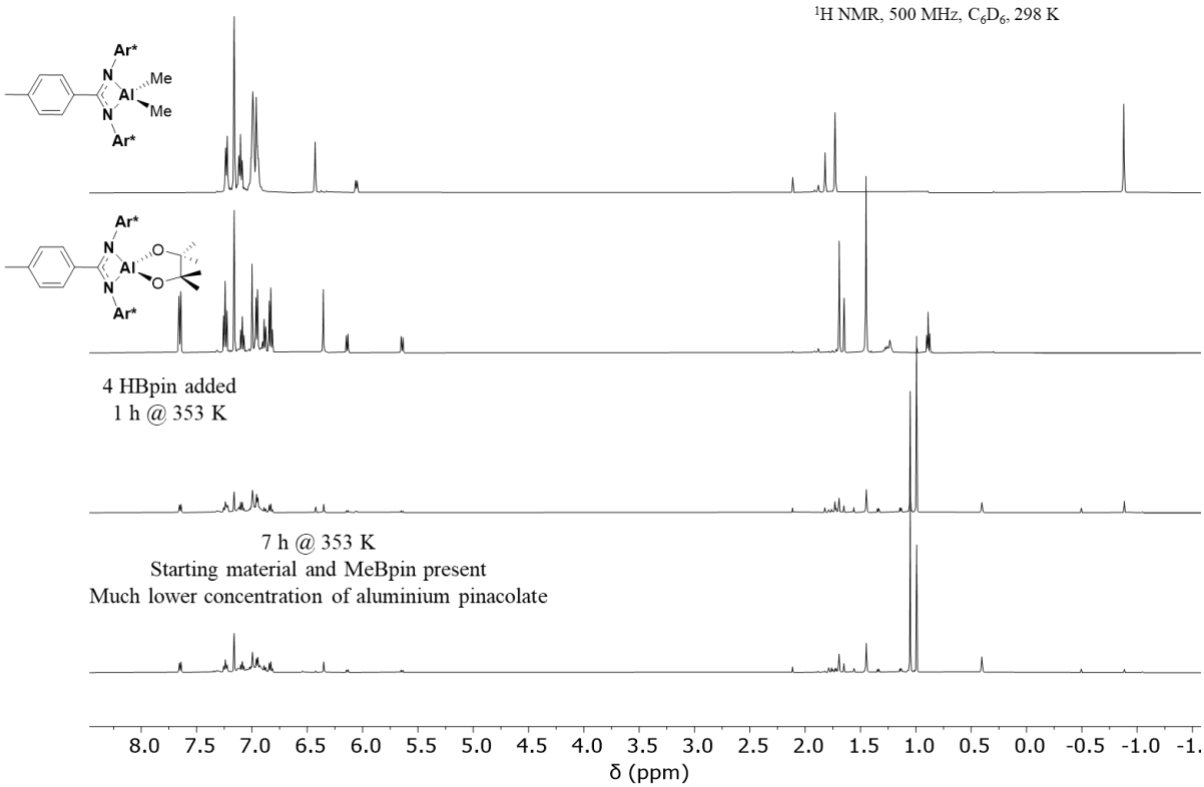

Figure A.60: ^{1}H NMR stack of the reaction of **2.15** with HBpin in benzene-d_6.

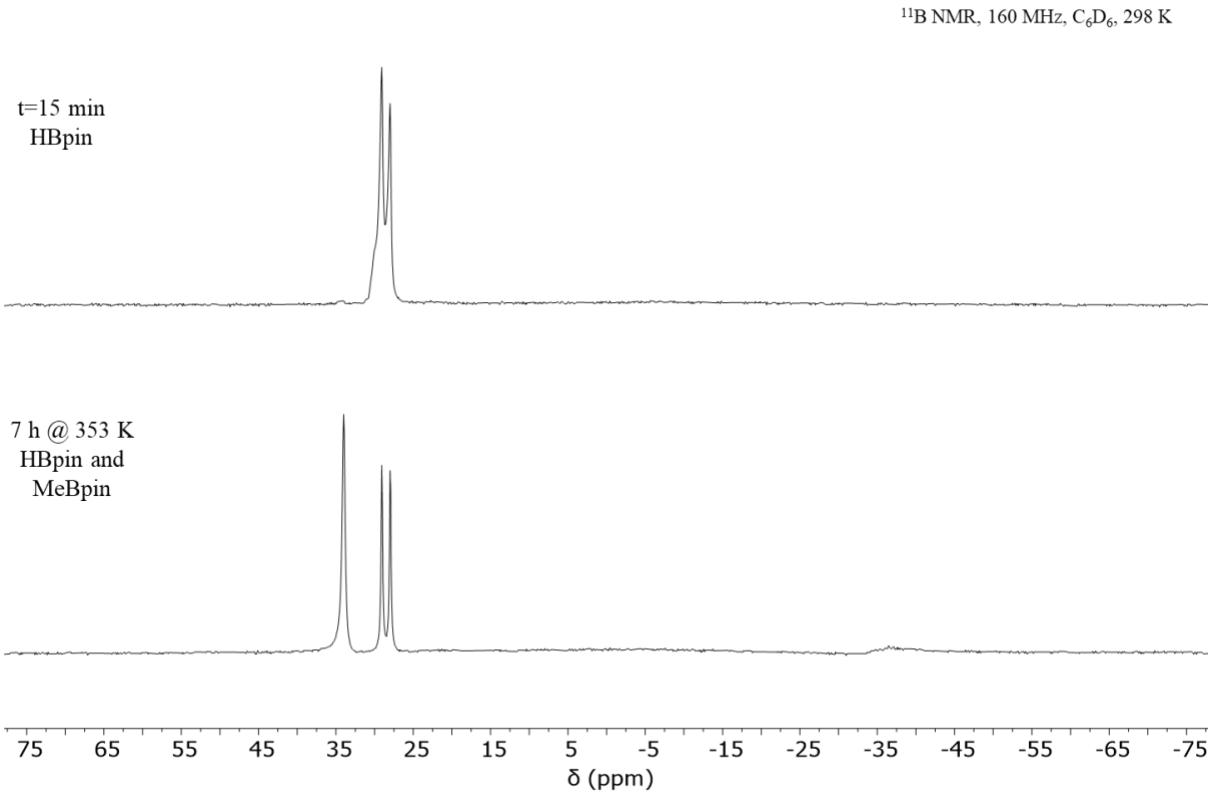

Figure A.61: ^{11}B NMR stack of the reaction of **2.15** with HBpin in benzene-d_6.

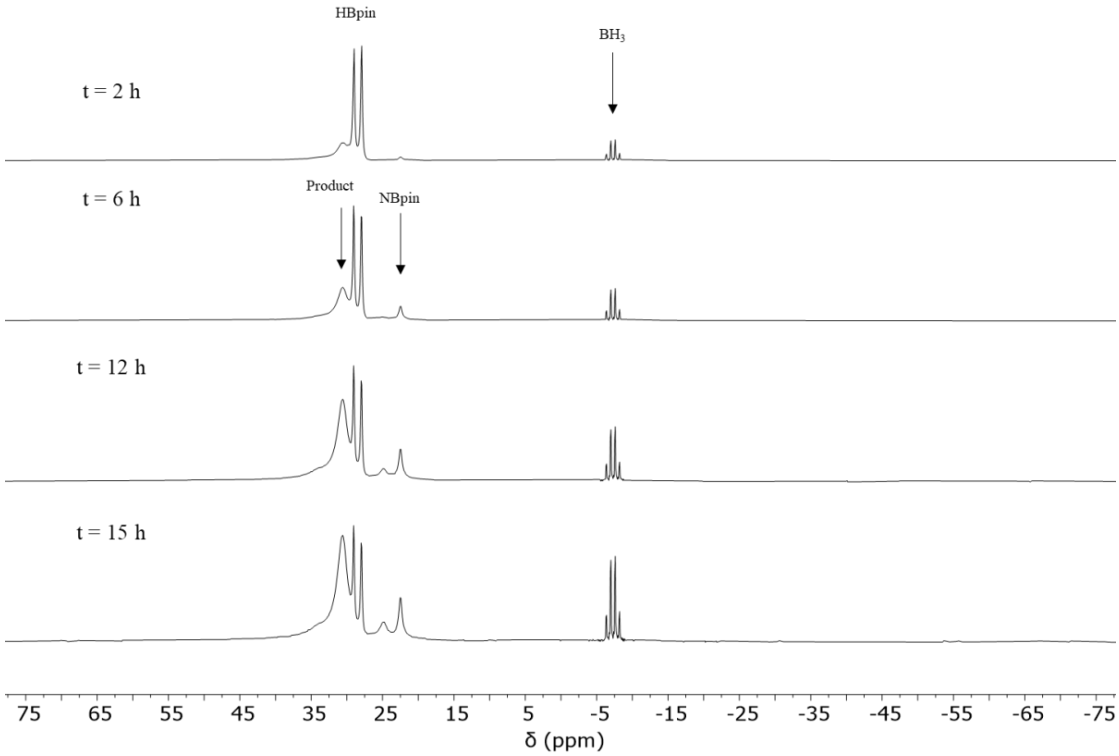

Figure A.62: ^{11}B NMR stack of the catalytic reaction of **2.12** with phenylacetylene and HBpin in benzene-d_6.

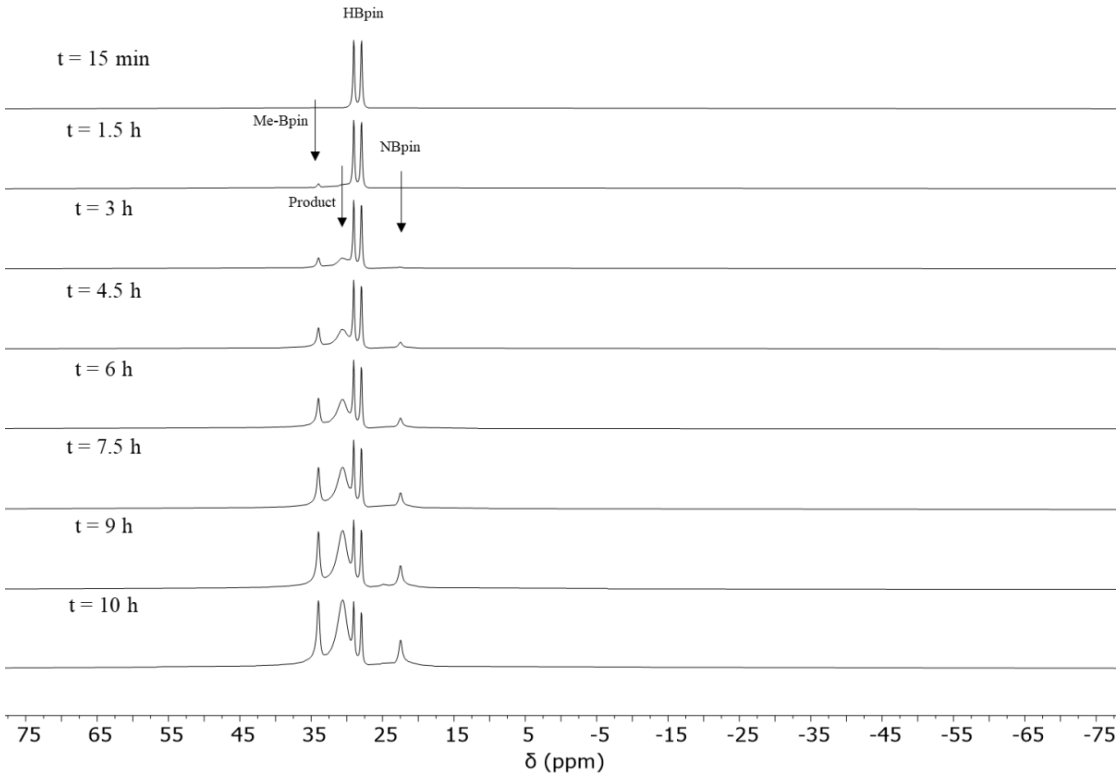

Figure A.63: ^{11}B NMR stack of the catalytic reaction of **2.14** with phenylacetylene and HBpin in benzene-d_6.

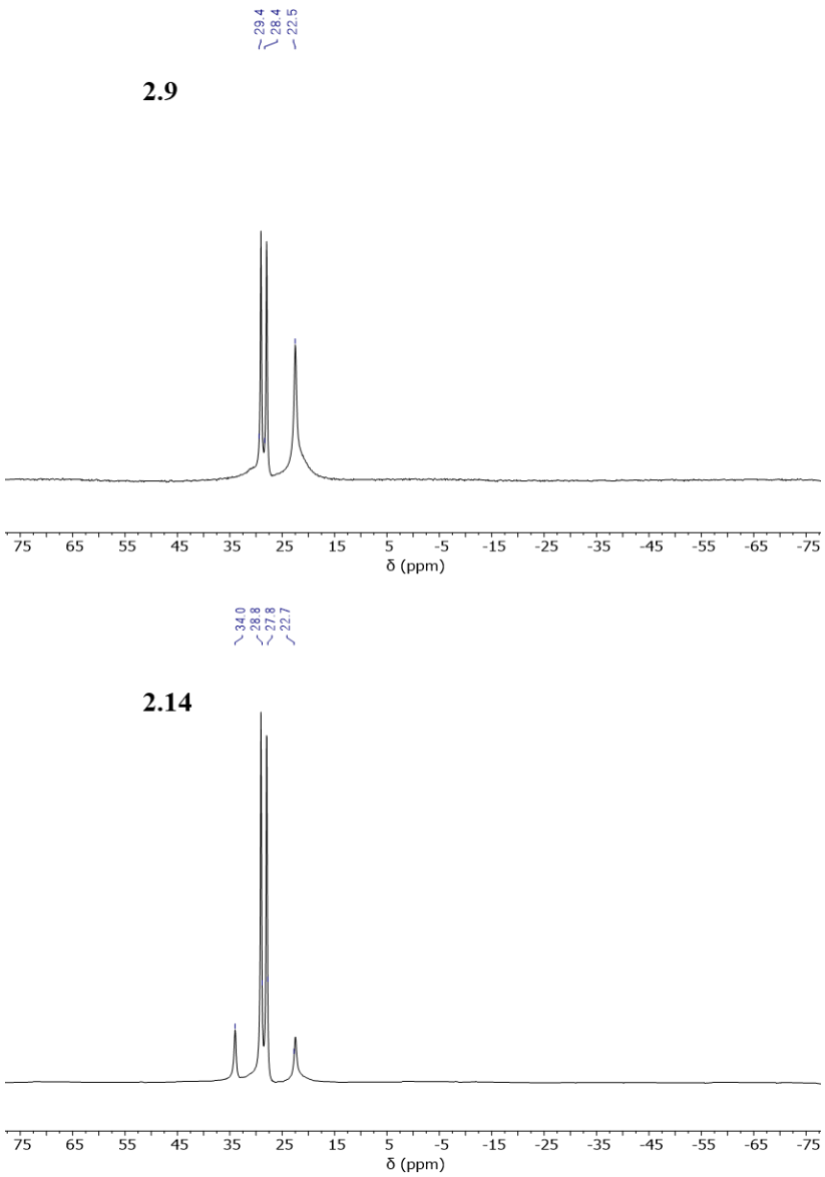

Figure A.64: ^{11}B NMR spectrum of the non-catalytic reactions of **2.9** and **2.14** with diphenylacetylene and HBpin in benzene-d_6.

Chapter 4 Appendix

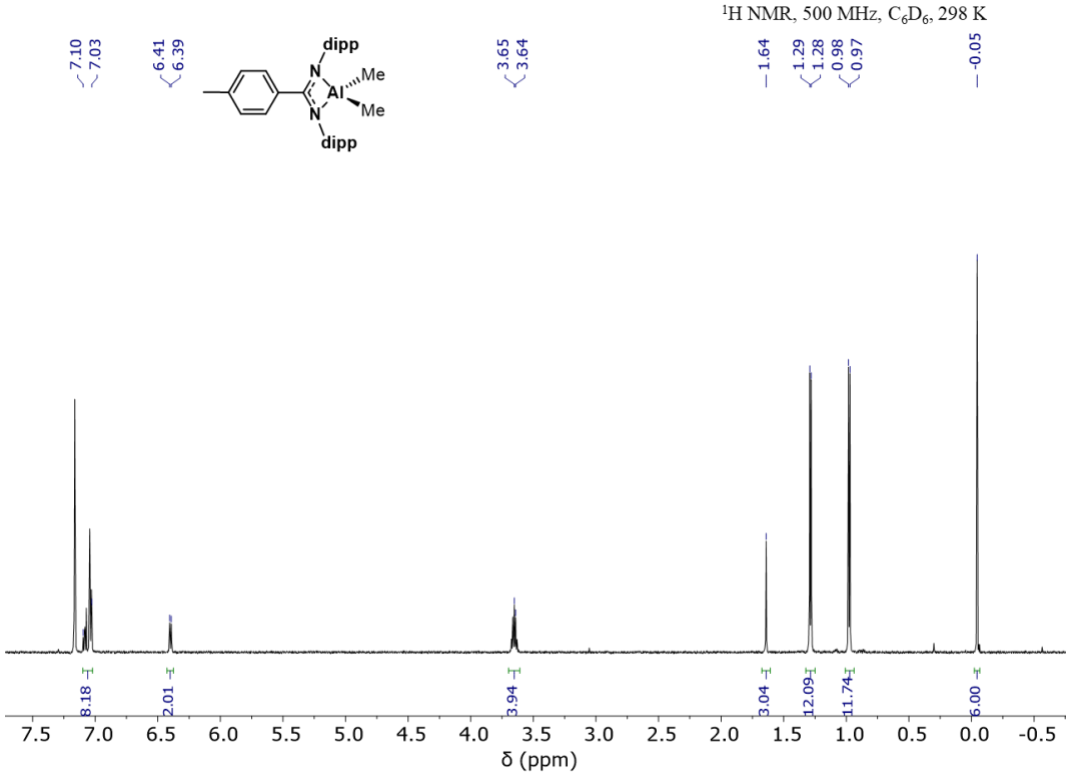

Figure A.65: ^{1}H NMR spectrum of **4.1**.

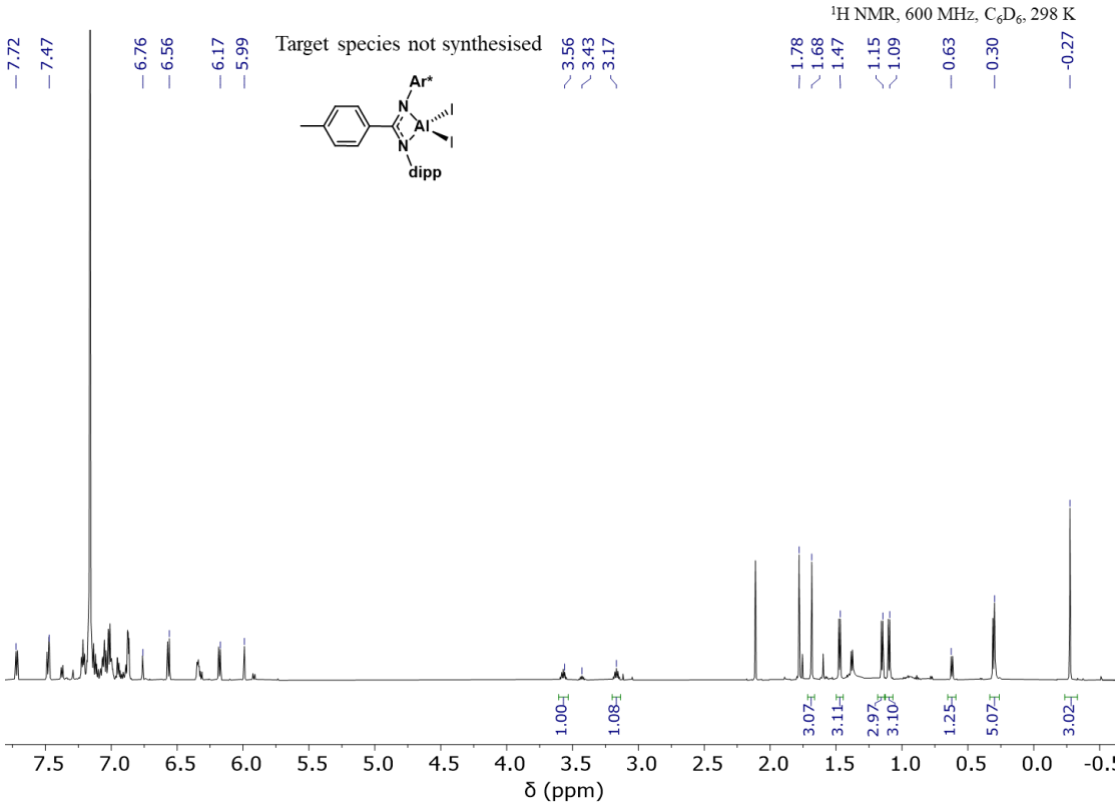

Figure A.66: ^{1}H NMR spectrum of the reaction of **2.14** with iodine.

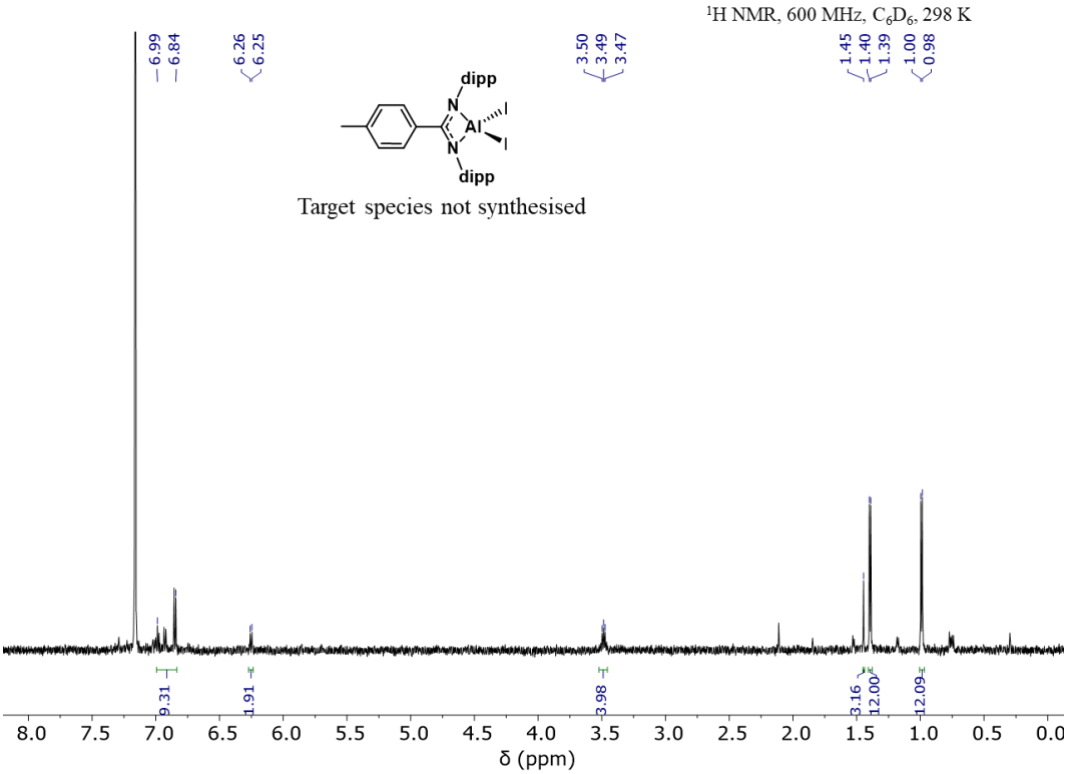

Figure A.67: ^{1}H NMR spectrum of the reaction of **4.1** with iodine.

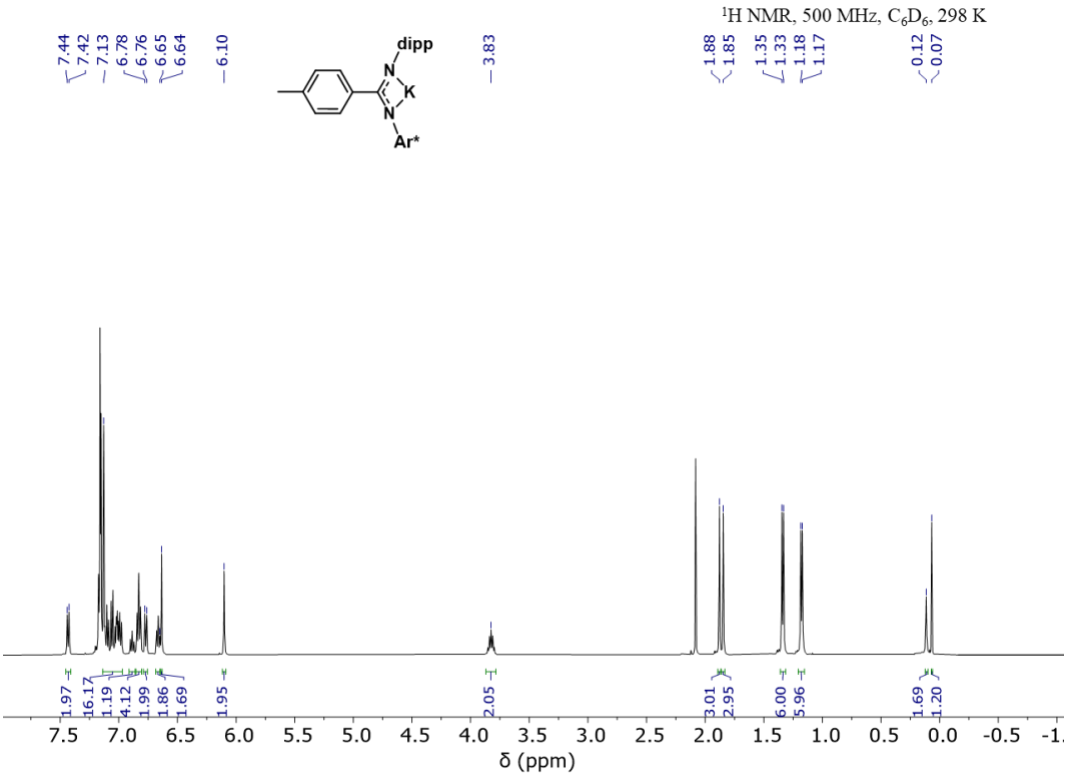

Figure A.68: ^{1}H NMR spectrum of **4.2**.

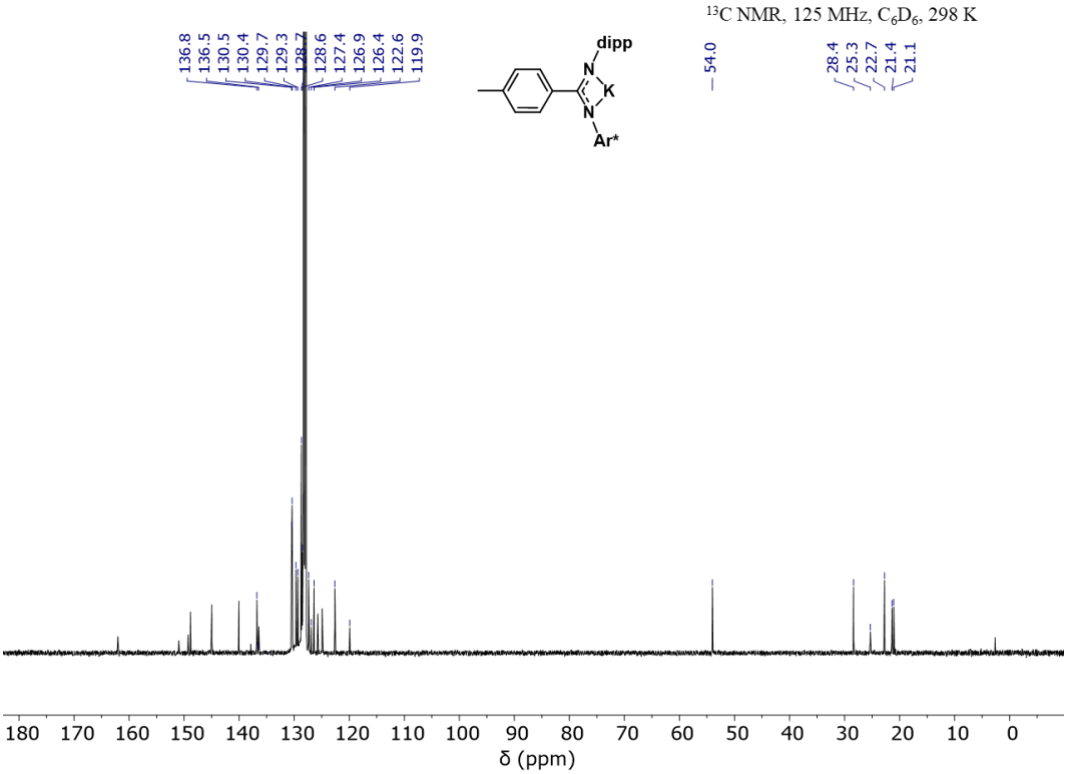

Figure A.69: ^{13}C NMR spectrum of **4.2**.

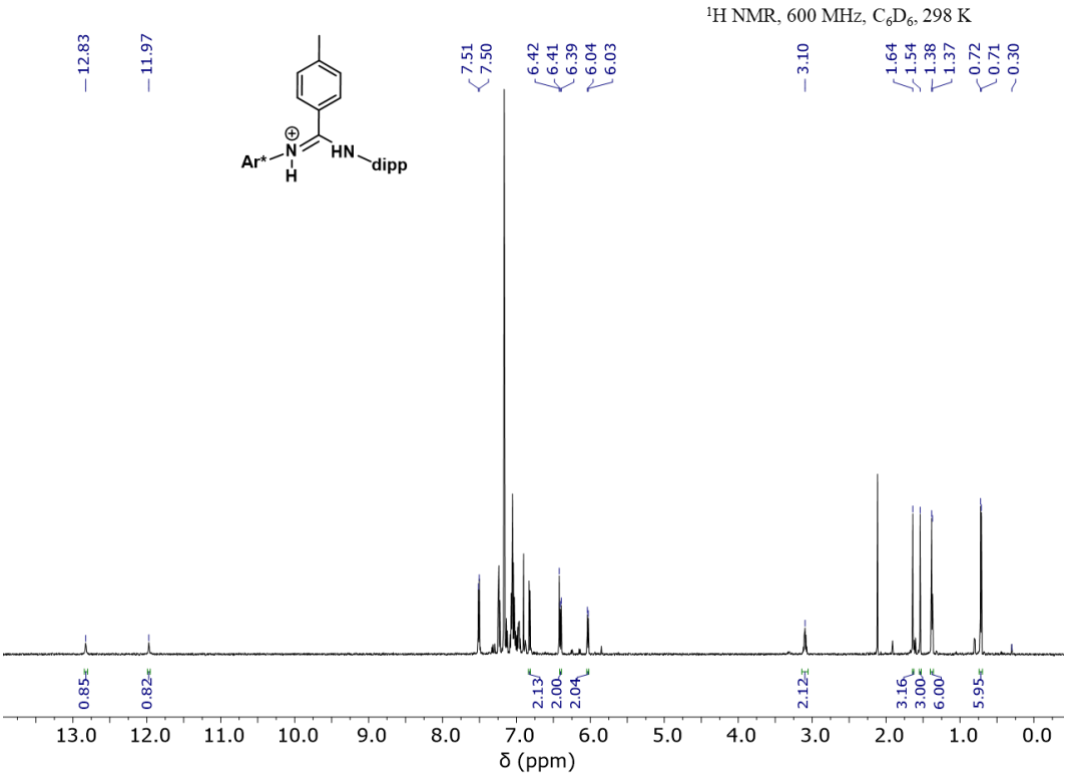

Figure A.70: ^{1}H NMR spectrum of **4.3**.

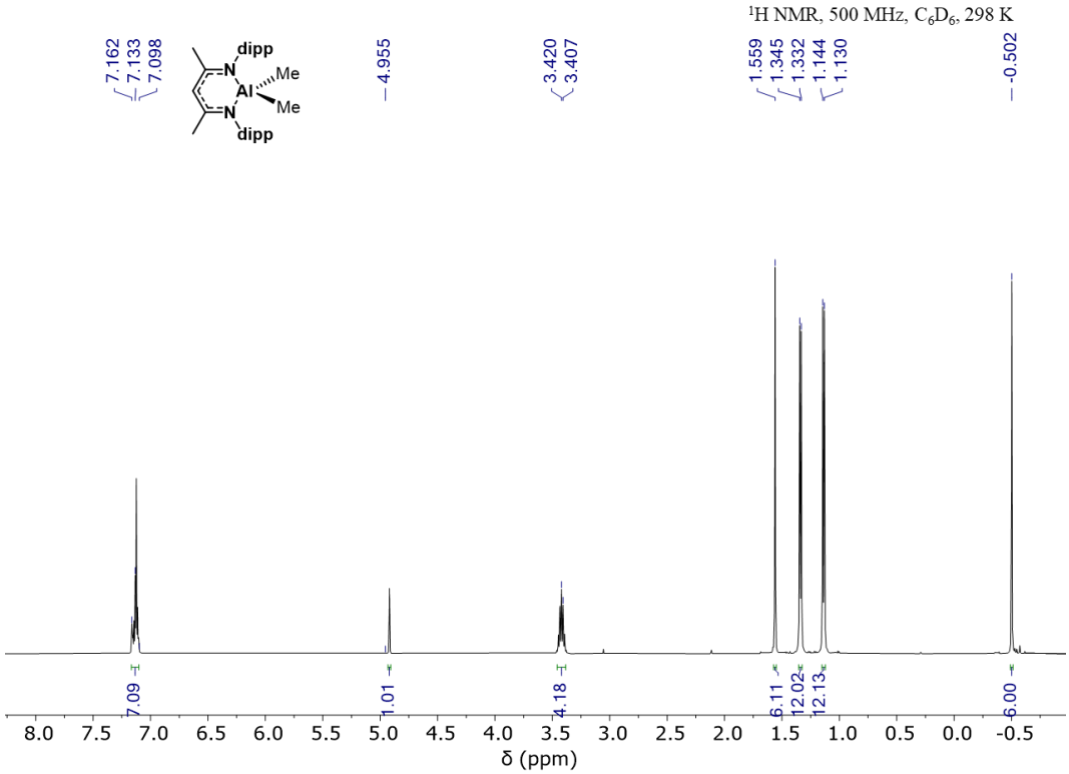

Figure A.71: ^{1}H NMR spectrum of **4.4A**.

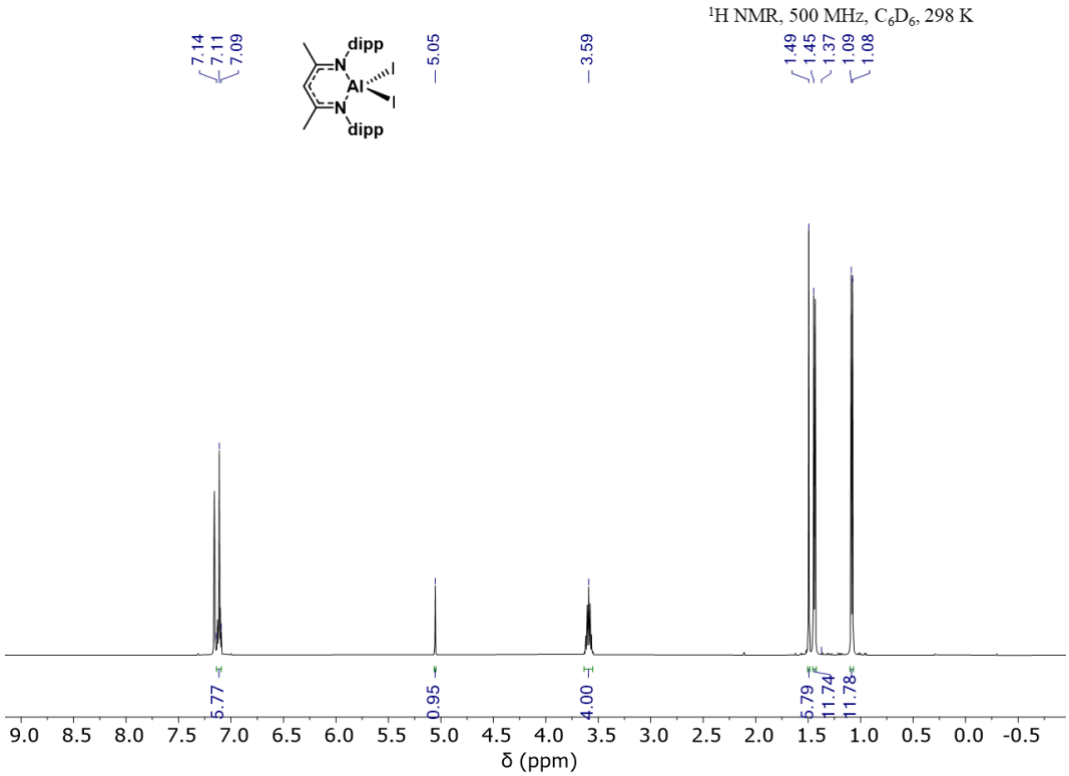

Figure A.72: ^{1}H NMR spectrum of **4.4B**.

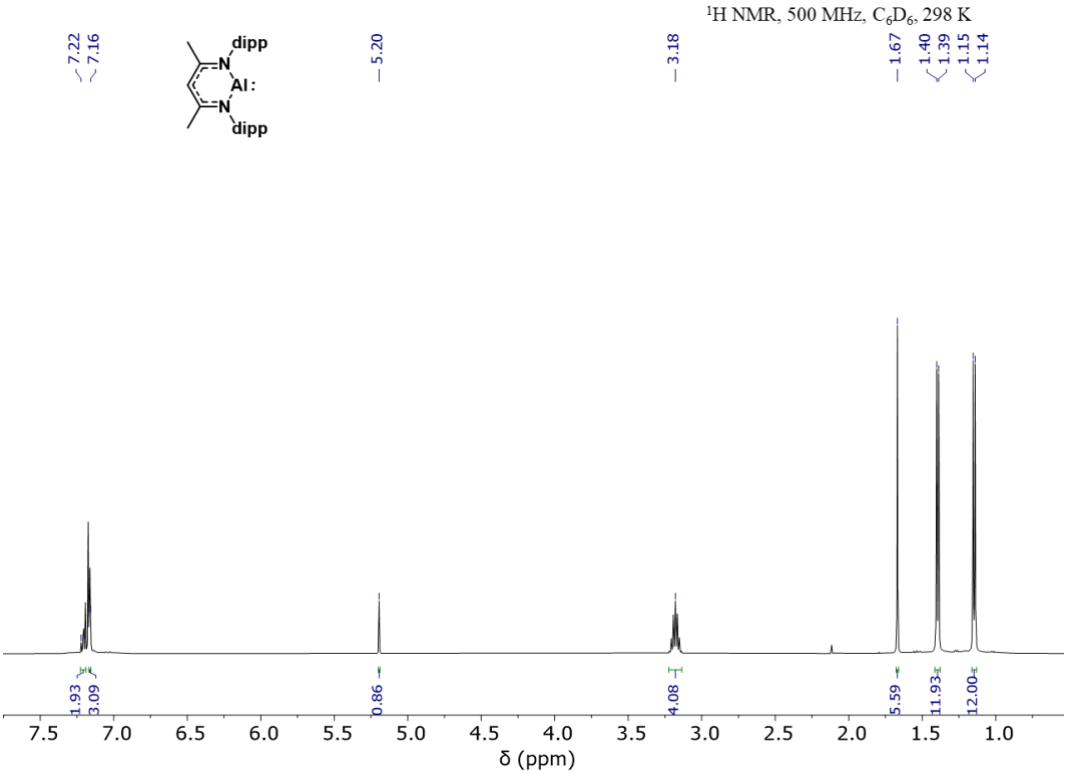

Figure A.73: ^{1}H NMR spectrum of **4.4**.

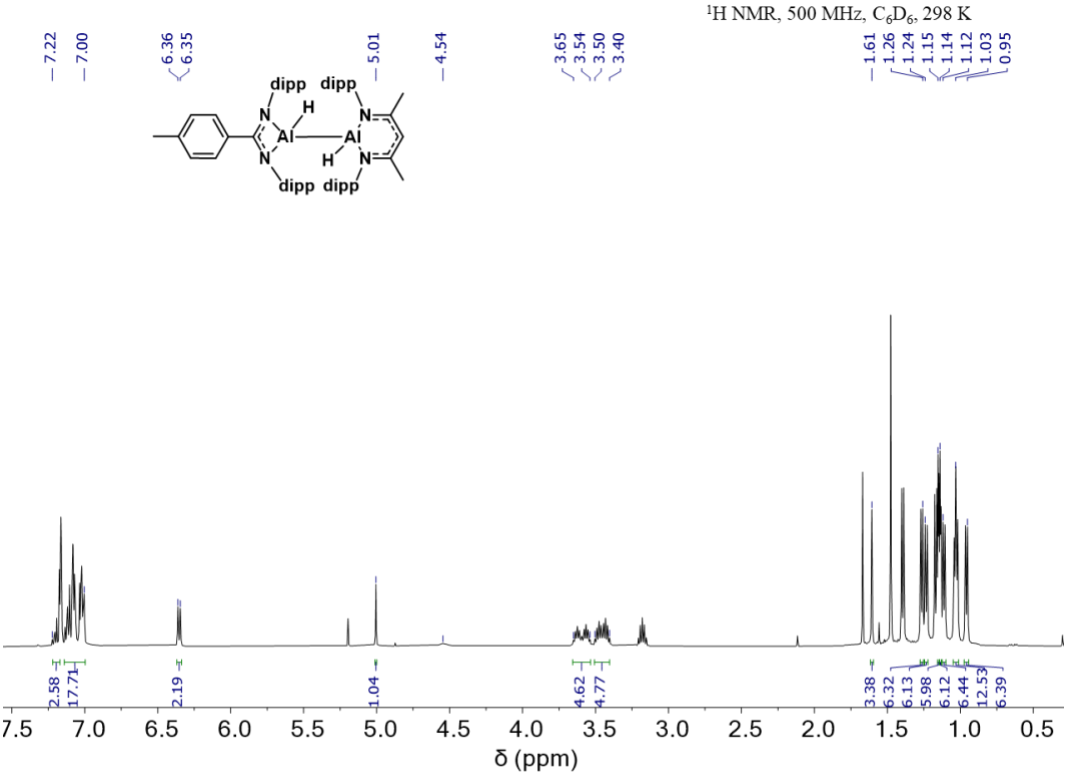

*** Non-picked/integrated peaks assigned to [Al:(^{dipp}BDI)], 4.4**

Figure A.74: ^{1}H NMR spectrum of **4.5**.

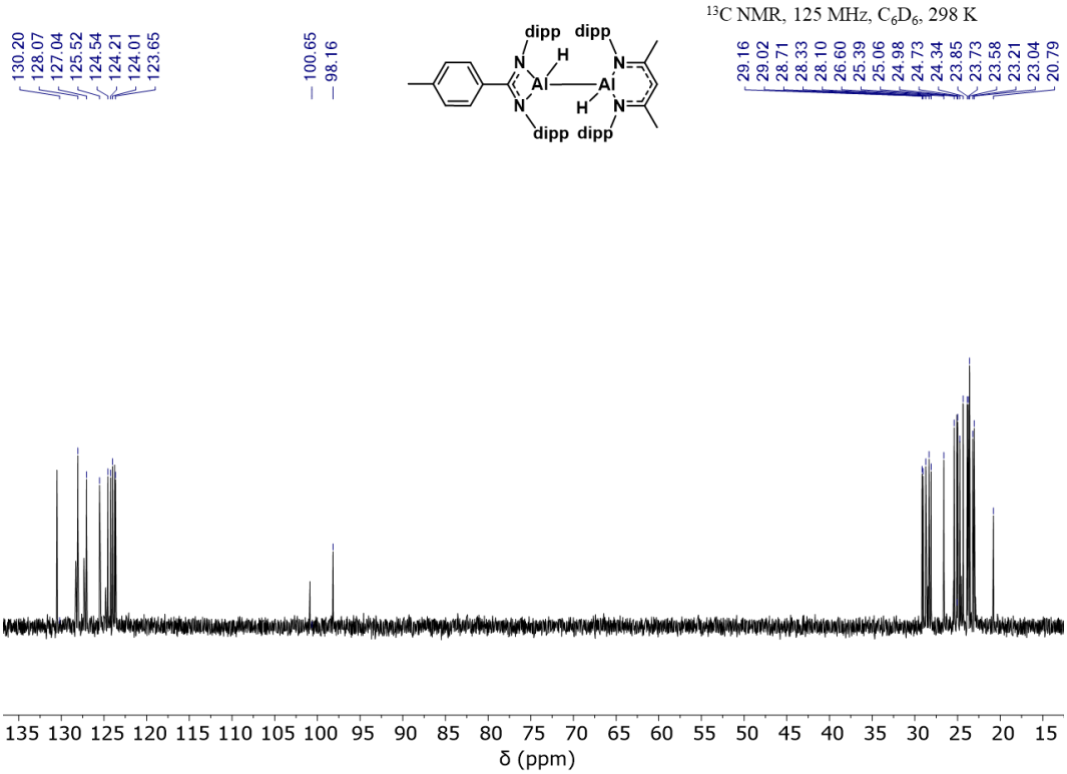

Figure A.75: ^{13}C NMR spectrum of **4.5**.

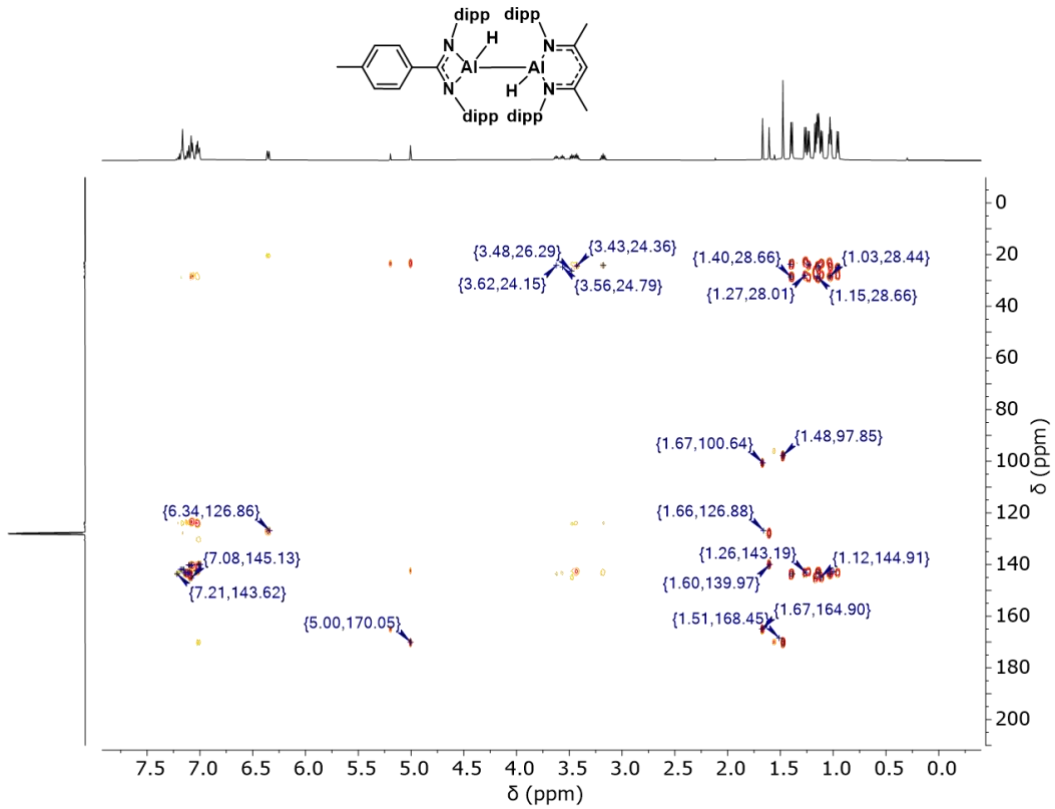

Figure A.76: HMBC spectrum of **4.5**.

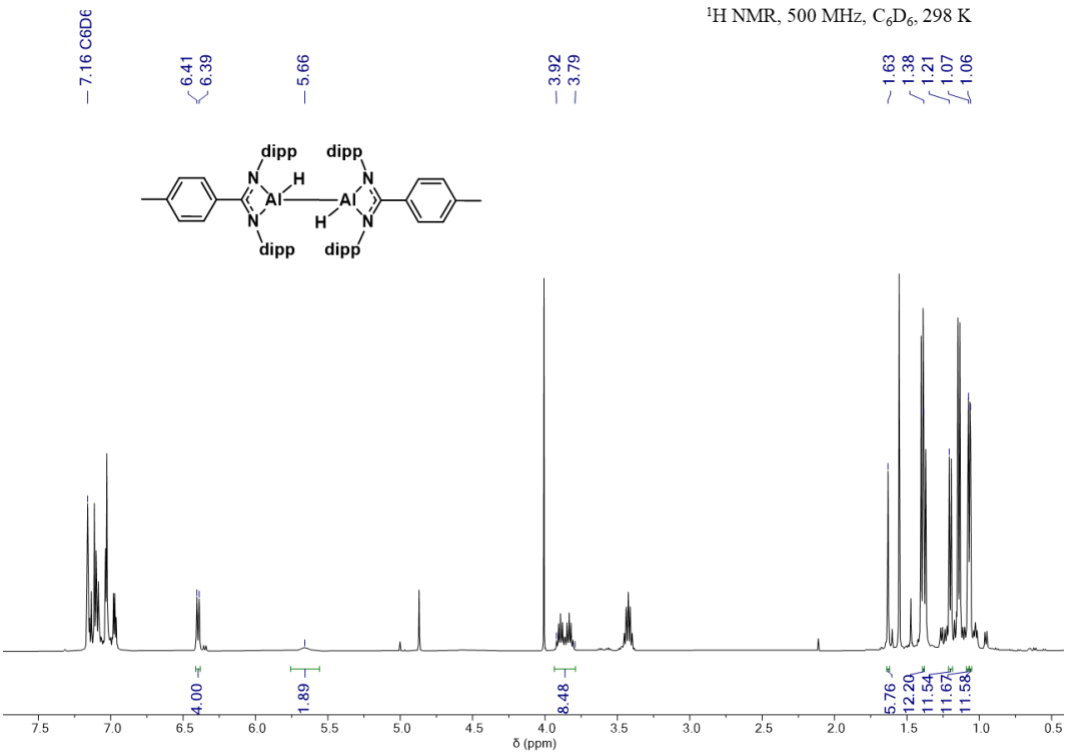

*** Non-picked/integrated peaks assigned to [AlH_2(^{dipp}BDI)], 3.5**

Figure A.77: ^{1}H NMR spectrum of **4.6**.

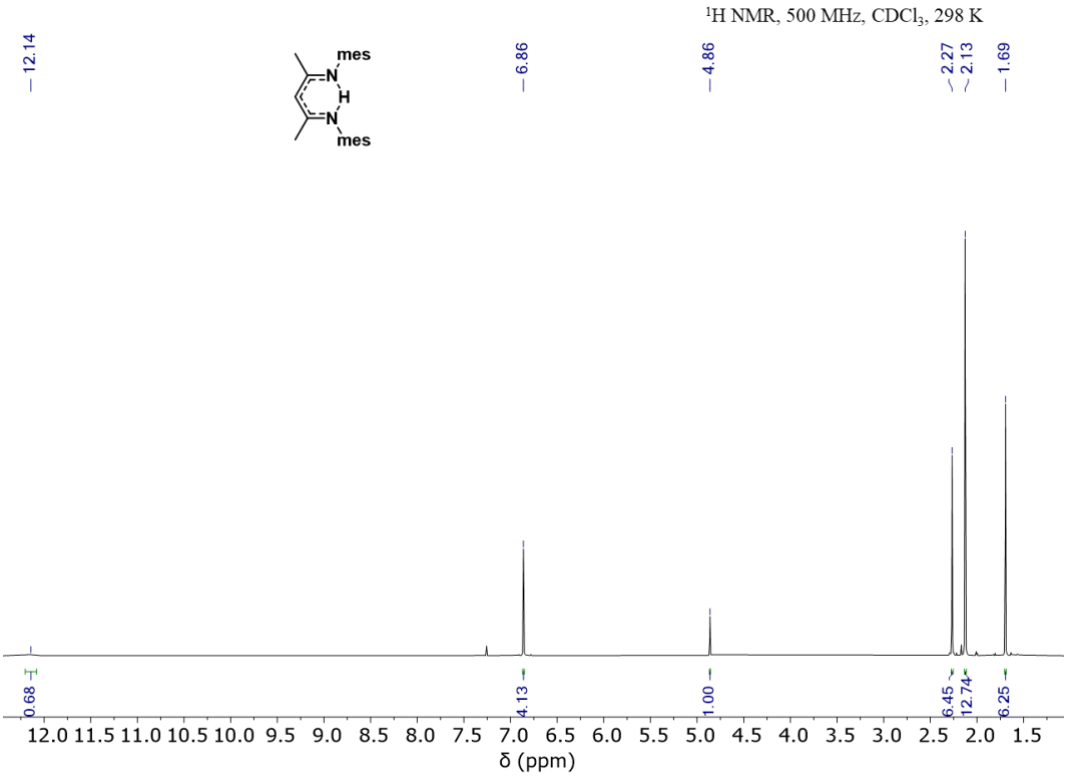

Figure A.78: ^{1}H NMR spectrum of **4.7**.

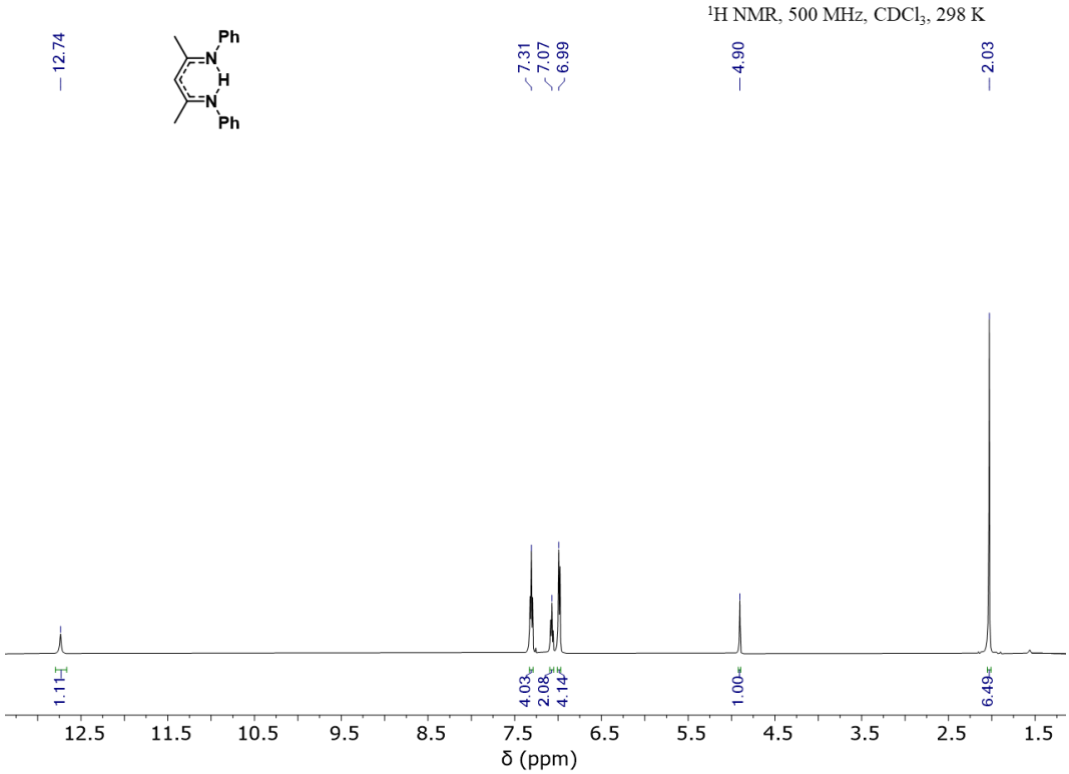

Figure A.79: ^{1}H NMR spectrum of **4.8**.

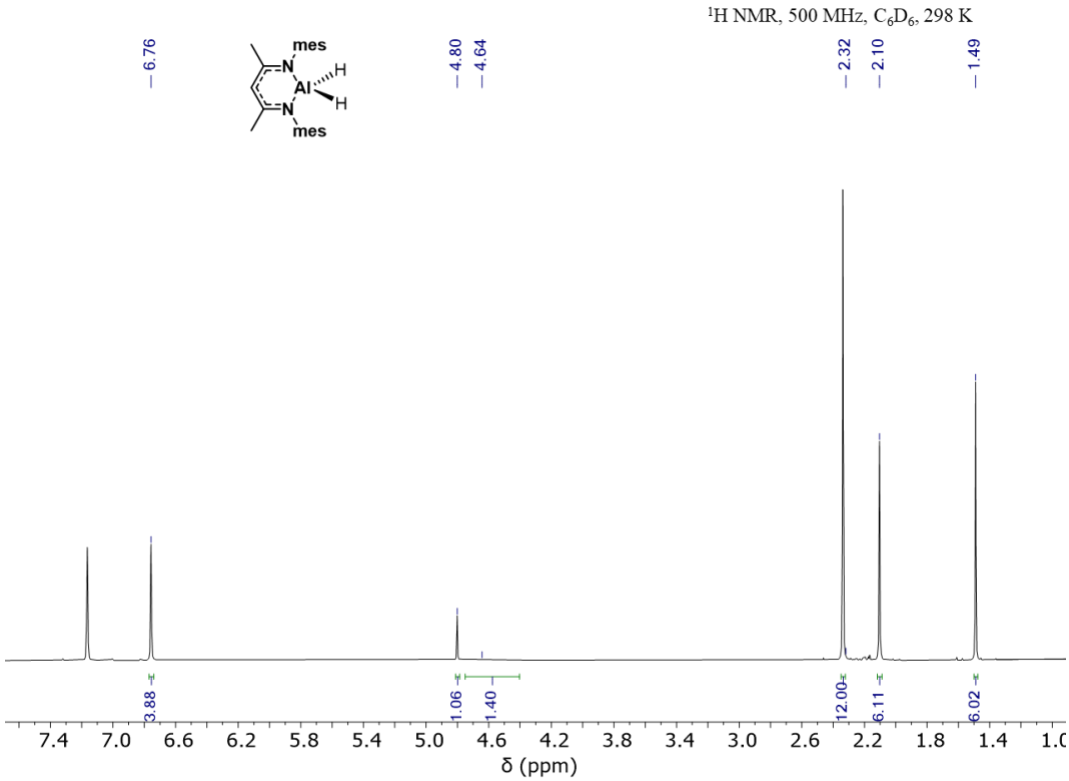

Figure A.80: ^{1}H NMR spectrum of **4.9**.

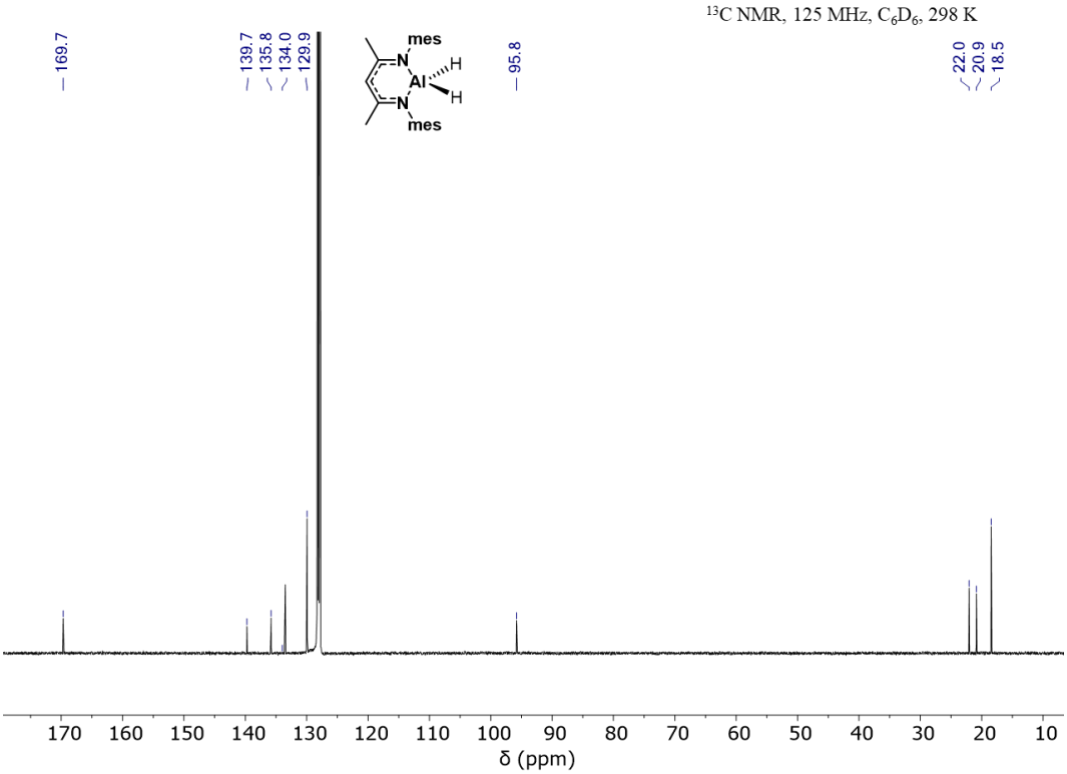

Figure A.81: ^{13}C NMR spectrum of **4.9**.

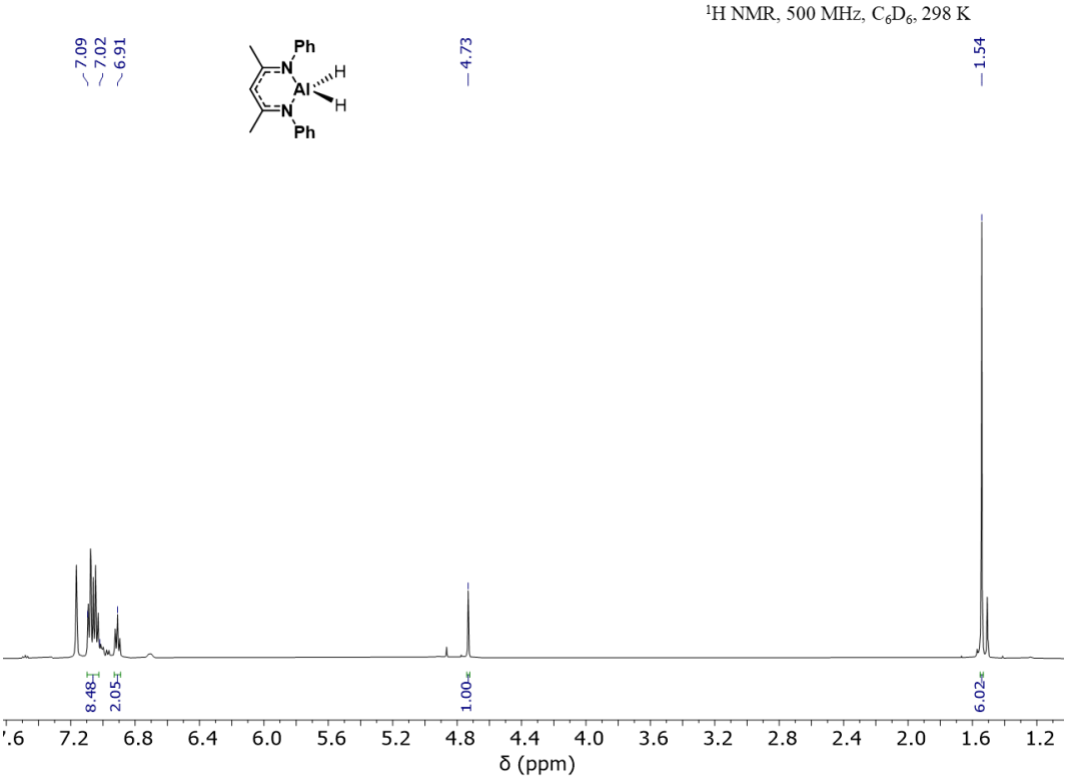

Figure A.82: ^{1}H NMR spectrum of **4.10**.

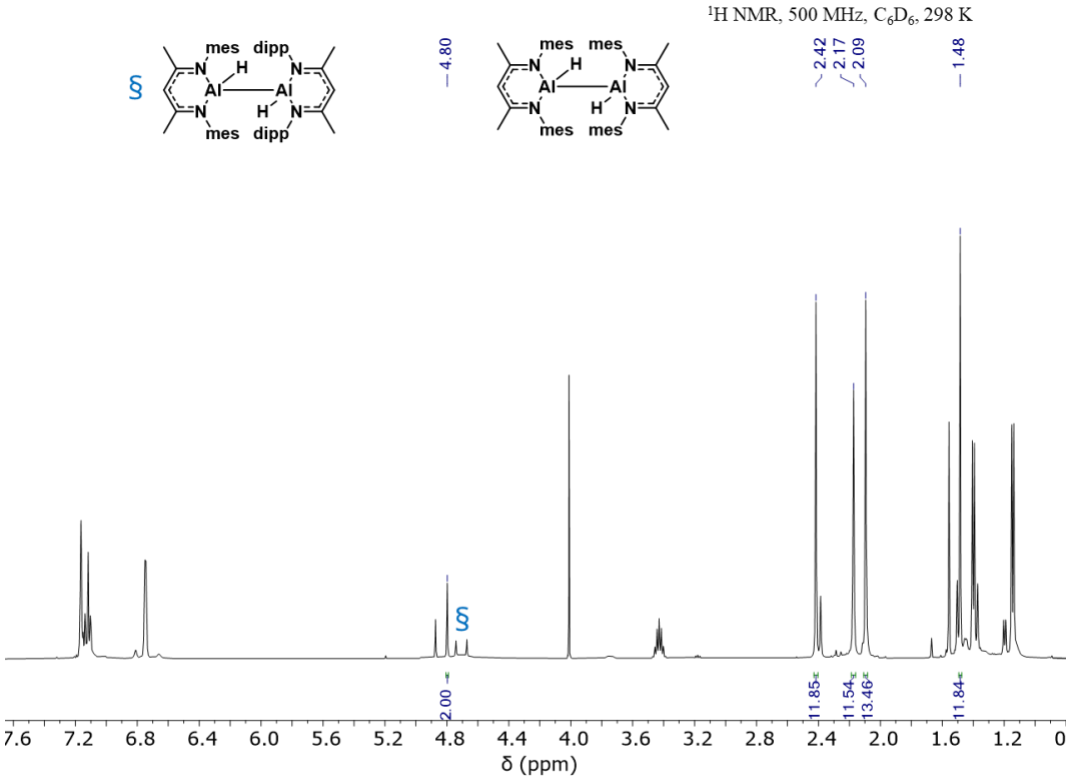

Integrated peaks assigned to 4.11, peaks assigned with symbols assigned to 4.12.

Figure A.83: ^{1}H NMR spectrum of **4.11** and **4.12**.

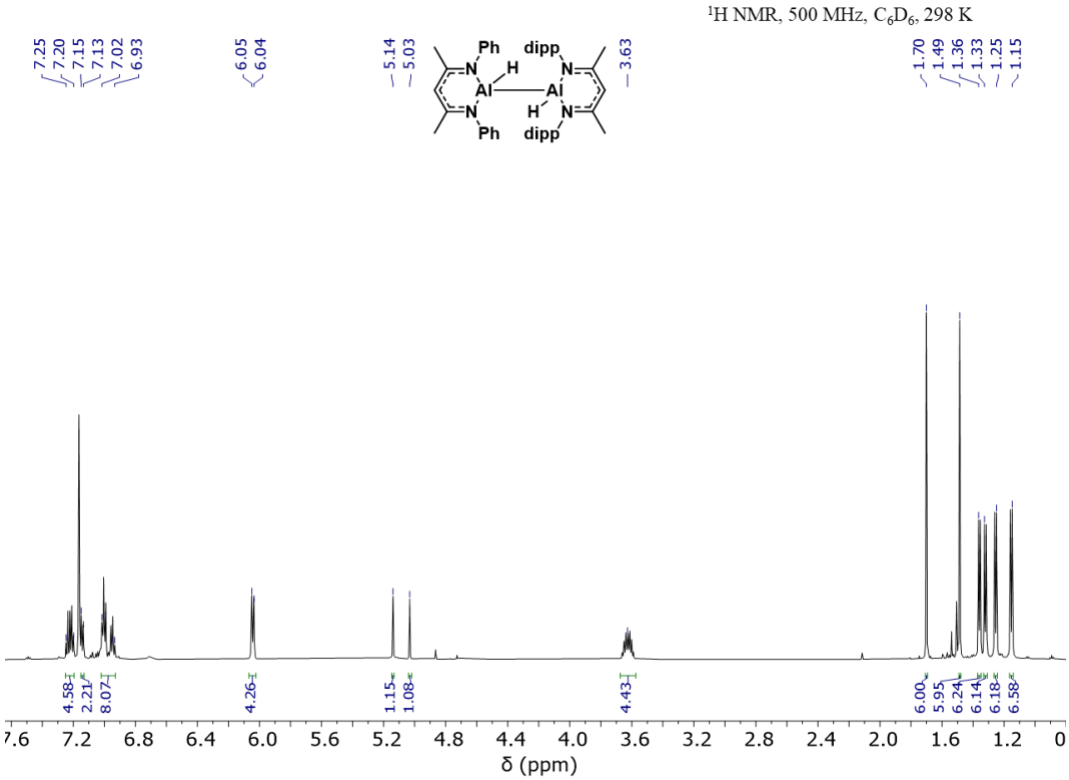

Figure A.84: ^{1}H NMR spectrum of **2.13**.

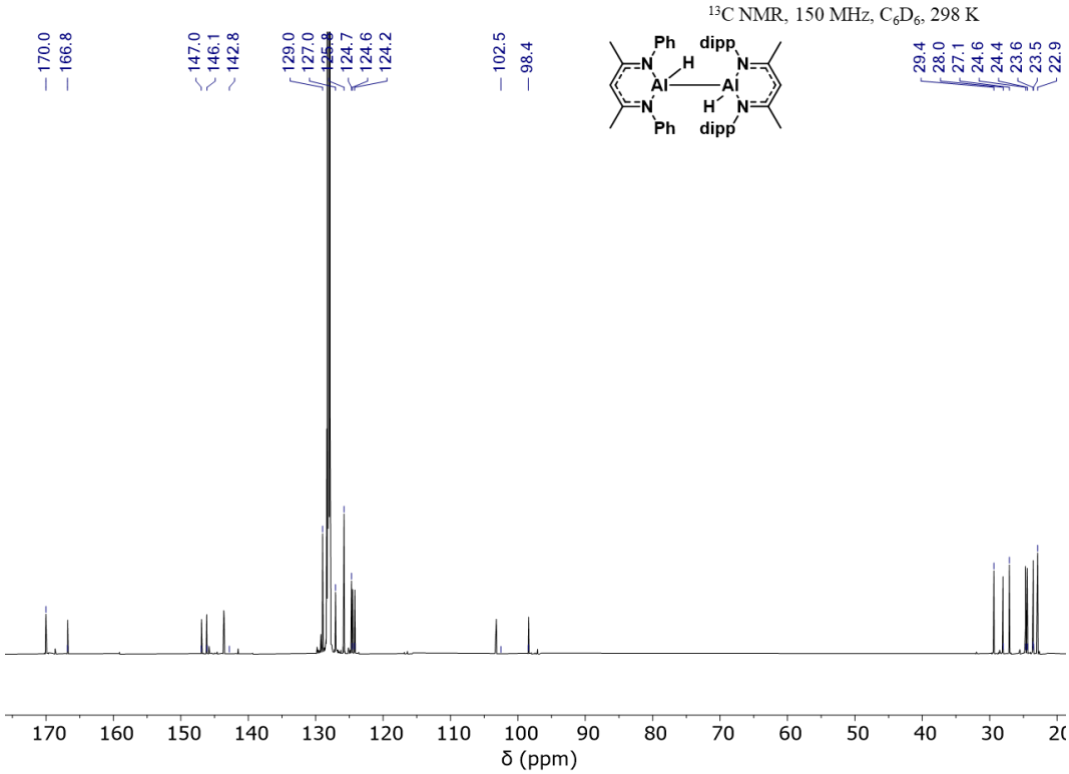

Figure A.85: ^{13}C NMR spectrum of **4.13**.